INVESTIGATING POLYMER OPTICAL FIBRE BRAGG GRATING TECHNOLOGY FOR FREEZE DRYING APPLICATIONS

SANDRA BERNADETTE DONOHOE

Doctor of Philosophy

ASTON UNIVERSITY

June 2017

Aston University

Investigating Polymer Optical Fibre Bragg Grating technology for freeze drying applications

Sandra Bernadette Donohoe

Doctor of Philosophy
June 2017

Thesis Summary

Pharmaceuticals and biologics that are unstable in aqueous form but liable to thermal degradation are generally freeze dried or lyophilised to extend their shelf life.

Primary drying is the most expensive and longest stage of the freeze drying process, prompting extensive research to reduce production costs and increase productivity. This work investigated current commercially available technologies used to detect sublimation of water vapour and determine the end of primary drying time. The investigation identified the potential cost benefits of using polymer optical fibre Bragg gratings (POFBGs), as non-invasive sensors that monitor batch sublimation of water vapour during primary drying.

The thesis initially discusses the fabrication of POFBG sensors, the protocols and housing structure developed to protect the sensors in this extreme environment. This was achieved by studying the behaviour of custom-built anemometers, temperature data loggers and sensors that detect changes in gas composition.

The next stage involved the characterisation of PMMA and TOPAS POFBGs to changes in temperature and pressure within the chamber. This provided information on the sensitivity of the sensors to these parameters at dry sub-atmospheric pressures. The studies revealed red shifts in the Bragg wavelengths as temperature decreased from an inlet shelf temperature of $20^{\circ}C$ to $-20^{\circ}C$ and temperature drifts from radiative heat effects. The pressure studies revealed non-linear Bragg wavelength sensitivity within the region of $200\mu bar$ to $2500\mu bar$, several orders of magnitude greater than reported within literature in high pressure chambers.

The POFBGs were exposed to water vapour subliming from samples of water, mannitol and native collagen, which were frozen and attached to the access port or placed onto the shelf and freeze dried. The studies reveal the potential for POFBG technology to be used to detect sublimation and end of primary drying, with future work focusing on modifications to the design and temperature compensation techniques.

Keywords: PMMA POFBG, TOPAS POFBG, temperature, sublimation, pressure

Dedication

This thesis is dedicated to my parents Mr Martin Donohoe and Mrs Alicja Donohoe, who have always supported and motivated me throughout my life. I also wish to thank all of my family, loved ones and friends for their continued support throughout this journey.

Acknowledgement

Contents

List of Tables

List of Figures

14

1   Abbreviations and Definitions

(Atm)	Atmospheric pressure
(ADCs)	Analogue to Digital Converters
(API)	Active Pharmaceutical Ingredient
(BP)	British Pharmacopoeia
(T_C)	Collapse temperature
(CIP)	Clean in Place
(CIV)	Chamber Isolation Valves
(CPP)	Critical Process Parameter
(Ph. Eur.)	European Pharmacopoeia
(Teu)	Eutectic temperature
(FBG)	Fibre Bragg Grating
(FC/PC)	Ferrule connector/Physical contact
(FC/APC)	Ferrule connector/Angled physical contact
(FDA)	Food and Drug Administration
(FM)	Few mode
(FWHM)	Full width half maximum
(Tg')	Glass transition temperature of the maximally freeze-concentrated phase
(HeCd)	Helium cadmium
(MM)	Multimode
(mPOF)	Microstructured polymer optical fibre
(MTM)	Manometric Temperature Measurement
(NA)	Numerical aperture
(OSA)	Optical spectrum analyser
(PC)	Polycarbonate
(PID)	Proportional-Integral-Derivative
(PLC)	Programmable Logic Controller
PMMA	Poly (methyl methacrylate)
(POF)	Polymer Optical Fibre
(POFBG)	Polymer Optical Fibre Bragg Grating
(PS)	Polystyrene
(%RH)	%Relative Humidity

(RPM)	Revolutions Per Minute
(n)	Refractive index
(RTD)	Resistance Temperature Detector
(RM)	Residual Moisture
(RBW)	Resolution Bandwidth
(SEM)	Scanning Electron Microscopy
(SI)	Step Index
(SD)	Standard Deviation
(SIP)	Steam in Place
(TDM)	Time division multiplexing
(TDLAS)	Tuneable Diode Laser Absorption Spectroscopy
(UV)	Ultraviolet
(WDM)	Wavelength division multiplexing

According to the following table that defines the sub-atmospheric pressure categories[1, 2], freeze drying technology operates in a medium vacuum range:

Aston University

Illustration removed for copyright restrictions

Lyophilisation is a technique used in research and commercial applications to remove water from a variety of temperature sensitive products [3] that do not have an acceptable shelf life and are not stable as aqueous solutions [4]. Typically this process is used for heat sensitive materials such as historical artefacts, pharmaceutical formulations and food produce [5]. It is also used as a method to increase formulation stability and reduce transportation and storage costs.

The three critical stages in a freeze-drying cycle are: freezing, primary drying and secondary drying. The freezing phase involves following specific cooling protocols to obtain the desired crystal morphology within the frozen matrix, which consequently influences drying times [6] and the final dry product structure. Freezing is followed by primary drying, which dries the product by subliming water vapour from the ice crystals located within the frozen structure. Secondary drying is the final stage before the vials are sealed, where residual adsorbed moisture is removed through the process of desorption.

Determining accurately the end of primary drying is critical, as the transition into secondary drying requires the use of higher temperatures and the presence of any residual ice crystals could lead to collapse of the product [7]. The desire to correctly determine the end point of primary drying is driven by the desire to reduce cost [8], due to its significant energy consumption and longer processing time than the rest of the stages, which influences productivity.

In order to ensure the product has the desired characteristics, sensing systems are incorporated into the freeze dryer to provide constant feedback during the cycle, with the goal to increase productivity, reduce cost and running times[4, 8-11]. These sensors monitor and control the critical process parameters (CPPs) that influence the product final characteristics e.g. temperature, pressure and gas composition in the chamber.

It is particularly important to control the primary drying stage due to the high risk of product failure and batch rejection as a result of a lack of product functionality or elegance. This objective is achieved using sensors that fall into two principle categories: single vial measurement and batch measurement techniques. Single vial measurement techniques involve monitoring product temperature throughout the cycle by invasively placing a probe into a sample (e.g. thermocouples, silica optical fibre Bragg gratings). Batch measurement techniques are non-invasive and measure changes in the total gas composition of the chamber. Unfortunately batch

measurement devices tend to be specialised and costly as they are required to track trace quantities of water vapour subliming within the product chamber.

Polymer optical fibre sensors (e.g. POFBGs) have been used to monitor a number of parameters in a variety of applications, including temperature, pressure, stain and humidity[12-15]. As some polymers have been reported to show an affinity for water vapour (e.g. PMMA); it was considered as a potential non-invasive system to monitor sublimation. Additionally, they could potentially provide cost-effective benefits over silica optical fibre sensors (single vial measurement) and some of the batch measurement techniques used for detecting end of primary drying time, e.g. tuneable diode laser absorption spectroscopy (TDLAS).

A literature search has not revealed that these devices have been placed inside freeze dryers and monitored for their performance and hence they were considered worthy of further investigation. As a number of parameters are known to influence the Bragg wavelength of the fibre Bragg grating (FBG), it was deemed necessary to initially characterise these sensors against CPPs in the vacuum chamber, to determine if they could have practical applications in the freeze drying industry. After characterisation, the sensors were used in 'real life' tests to determine if sublimation and end of primary drying time of pharmaceutical and biological samples (mannitol and collagen) could indeed be correctly identified.

2.1   Aims

To determine if POFBG sensors could be used for freeze drying applications, in particular to monitor CPPs in the freeze-drying environment and detect the end of sublimation during the primary drying stage.

2.2   Objectives

The objectives of the thesis were:

- Develop a housing structure that could successfully protect the POFBG sensors in the freeze drying environment
- Determine the response of POFBGs to temperatures within the freeze dryer
- Characterise the sensors at sub-atmospheric pressure conditions
- Compare the performance of the fabricated PMMA and TOPAS POFBG in the freeze drying environment. PMMA has an affinity for water vapour [12, 16, 17] and was used to determine if sublimation could be monitored during primary drying. In literature, TOPAS was determined to be insensitive to humidity at atmospheric conditions [12, 18] and was selected to serve as a control for these experiments.
- Observe the effects of backfilling the freeze drying chamber from sub-atmospheric conditions (2500µbar) to 1atm with dry nitrogen gas on POFBGs.
- Investigate the response of POFBGs in dry nitrogen gas at 1atm pressure, to the introduction of water vapour when the chamber door was opened.
- Determine if POFBGs could be used to detect sublimation under sub-atmospheric conditions (using frozen mannitol and water samples).
- Determine if POFBGs could be used to monitor sublimation and detect end of primary drying time of native collagen, which has applications for tissue engineering.

Conference paper

Donohoe SB, Peng GD, Webb DJ. Improving the response time of polymer optical fibre Bragg grating water activity sensors. In: Koike Y, Ziemann O, editors. Proceedings of the 24th International Conference on Plastic Optical Fibres, POF2015; Nuremberg, Germany: Technische Hochschule Nürnberg Georg Simon Ohm; 2015. p. 364-70

Patent application

A patent application for the work described in this thesis is currently in progress

2.3   Outline of chapters

The following sections outline the work and research conducted in this project and presented in each chapter.

Chapter 3-   Lyophilisation

This chapter discusses the freeze drying process including freezing, primary and secondary drying. The chapter also provides an overview on the industry, the typical equipment and excipients that form part of the constituents used in formulations in the pharmaceutical industry. This chapter also discusses the commercially available sensors that are currently used to detect the end of primary drying time, either by monitoring product temperature during the cycle or changes in the gas composition within the chamber.

Chapter 4 –   Optical fibre sensor

This chapter provides an overview of the fabrication of optical fibres and fibre Bragg gratings, including important principles of operation. This section will also discuss the materials used to form polymer optical fibres (POF), with a specific interest in PMMA and TOPAS, which were used in this project. This chapter also discusses advantages and disadvantages of using POF technology for this application.

Chapter 5 –   Methods and materials

This chapter lists the methods used to fabricate the POFBGs, including describing the phase mask technique, pigtailing method and interrogation system to monitor the Bragg wavelength. The customised test rig which allowed characterisation of the sensors in the environmental chambers (including freeze dryer), is presented. As the freeze dryer was designed for dying pharmaceutical samples and not as a piece of test equipment to characterise sensors, a new protocol was devised to achieve his objective by modifications to the existing chamber such as feedthroughs, in order to accommodate the different types of sensors.

Chapter 6 -   Wavelength response of POFBGs to Temperature in a Freeze Dryer

This chapter reports on the results obtained from the POFBGs response to temperature cycles in dry sub-atmospheric pressure conditions.

Step index SM PMMA and MM TOPAS fibres were surrounded by a protective housing and placed onto the temperature regulated shelf which allowed the sensitivity of the sensor to be determined. Further experiments were carried out to

study the effects of radiative heat in a freeze dryer, which is known to influence the drying rates of pharmaceutical samples.

Chapter 7- Wavelength response of POFBGs to Pressure alterations in a Freeze Dryer

This chapter reports on the characterisation of POFBGs to dry sub-atmospheric pressures in a freeze dryer. The vacuum chamber provided conditions where the Bragg wavelength shift of PMMA and TOPAS POFBGs to pressure changes could be monitored in dry conditions (-40^oC dew point), particularly as PMMA is known to have an affinity for water vapour. The chapter finishes with studying the long term effects of placing a PMMA and TOPAS POFBG in a freeze dryer for 40 days.

Chapter 8 - Wavelength response of POFBGs to Water Vapour in a Freeze Dryer

These experiments formed part of the characterisation work, to determine if these sensors could have practical applications in the freeze drying industry.
This chapter described the investigation of the response of TOPAS and PMMA POFBGs to the sublimation of water vapour from samples that were attached at controlled times to the access port of the freeze dryer. The next study involved exposing the POFBGs to a step change in pressure from sub-atmospheric pressure to 1atm within an inert gas, before opening the chamber door. This was investigated as it is a necessary stage in freeze drying prior to collecting the dried pharmaceutical samples. The project also investigated the effects of reducing POF diameter on the response time of the POFBG to changes in temperature and humidity.

Chapter 9- Detecting water vapour sublimation from mannitol and collagen samples using POFBGs

This chapter will discuss the use of step index TOPAS and PMMA POFBGs to monitor the freeze drying cycles of mannitol and collagen samples. The goal is to investigate "in real life conditions" the use of POFBG sensors as a novel alternative approach to established technologies for detecting sublimation in freeze drying applications.

Chapter 10- Future research areas

This section will discuss the areas that have been identified to require further investigation based on the work described in the thesis.

Chapter 11- Conclusion

This section provides a list of the conclusions made that have resulted from this project.

3 Lyophilisation

3.1 Chapter overview

This chapter discusses the freeze drying process including freezing, primary and secondary drying, equipment and formulation excipient requirements as well as an overview of the industry. Research is carried out into the "end of primary drying time", which is a critical transition stage marked by the removal of bulk ice from the formulation and is often followed by secondary drying. Determining this time accurately is critical, as starting the next stage either too early or late might cause product damage, batch rejection or costs associated with reduced productivity. Several sensors are analysed in this chapter which are used to determine the end of primary drying time. In chapter 4, a new sensor will be examined for its potential use as a new end of primary drying detection sensor, which was later characterised in this project.

3.2 Freeze-Drying Industry

Freeze drying (also known as Lyophilisation), is a dehydration process widely used in the pharmaceutical, diagnostic and food industries [5, 19, 20] to remove water from formulations, biologicals, food produce [21] and chemicals[20]. This process is carried out if liable materials such as proteins for therapeutics[22], are unstable in aqueous solutions and require their shelf life to be extended[23]. Lyophilisation would produce dry stable solids for distribution and storage[24] and reduce their weight to minimise transportation costs.

Established food produce markets which use this technique are coffee[25, 26] and milk[27, 28], meat[29] and emerging trends in fruits and vegetables[30].

Some biologicals and microorganisms[20] can be lyophilised, in some cases with a survival rate of more than 80% [30] including bacteria, yeast, viruses, actinomycetes and filamentous fungi.

Freeze drying can be used in other applications[30], including material sciences (e.g. ceramic powder), health-care cosmetics and sample preparation for electron microscope observation. The procedure is also used for the preservation of skin, bone, cornea, tissue engineering (e.g. scaffolds)[25, 31-33], and research into freeze drying human cells[30] such as: red blood cells[34], platelets and cord blood cells for potential use in clinical medicine.

According to Hua and Liu [30] the largest investment in lyophilisation was made in the field of biological pharmaceuticals, driven by therapeutic market areas such as

oncology, vaccines and antirheumatics[35]. In 2003, 46% of all US Food and Drug Administration(FDA) biopharmaceuticals market approvals were lyophilised biologicals, such as vaccines, peptides and proteins[19]. By 2010, more than 40% of marketed protein drugs[35], were predominantly lyophilised to powders for reconstitution to preserve potency and shelf life. Varshney and Singh (2015) report that around half of all commercial biologics are freeze dried, with Remicade leading sales at $8.2 billion USD in 2012.

Freeze-drying is carried out in a variety of circumstances outlined in the following points. Lyophilisation is used as an alternative to other drying processes, to reduce the risk of damage to heat sensitive materials and achieve specific product requirements:

- *Formulation stability needs to be enhanced[11] (e.g. removal of water to hinder hydrolysis reactions[37] and enzymatic degeneration [19]).*
- *If the item is susceptible to degradation, damage or denaturing when dried at high temperatures[3, 19, 37, 38]. It therefore needs to be dried at lower temperatures, to retain biological activity and structural stability[30]. Examples of heat sensitive medicines include[30]: liposomes[20], protein[37] drugs, vaccines, antibiotics etc.*
- *Freeze drying of food can provide advantages[30] such as: colour, smell and taste[26] preservation, avoids surface hardening and loss of nutritional ingredients*
- *Increase the concentration of solutions[21]*

Transportation and storage requirements of the finished product:

- *Transportation and storage costs associated with the weight, size and refrigeration requirements of the pre-desiccated product need to be reduced [11].*
- *The freeze dried product could allow long term storage, either at room temperature or in a refrigerator [30].*

To reduce the risk of early product degradation:

- *The shelf-life [4, 37] of the product needs to be increased, growth of organisms hindered and maintaining long term aesthetic appearance[23]. The final low moisture content of the freeze-dried product deters spoilage in the product for a specified period of time.*
- *Preservation of a variety of items (e.g. conservation of archaeological findings, biologically active molecules, temperature sensitive pharmaceuticals, foods [39, 40], animals etc.). [5]*

Despite offering numerous advantages, freeze drying is a financially expensive[10, 38, 41] and time consuming[30] process.

The system has known high operational costs [11, 41] due to:

- *Specialised equipment as well as storage facility increases capital cost*
- *Energy consumption and losses during operation and maintenance [11]*
- *Long freeze drying, handling and processing times which can be in the range of days or weeks. Most cycles consist of a freezing stage (hours), primary drying (days) and secondary drying (hours) [11].*

Improvements to the system and sensors which can increase production capacity, reduce cost, batch rejection and duration are sought after by manufacturers. This is important in pharmaceutical operational plants, where the value of one batch can be over $600,000[42] and some products can be worth millions of dollars[43]. Research into devices that can improve process efficiency has been the motivation behind the work in this project.

3.3   Freeze drying Process

Figure 1 illustrates a standard freeze drying cycle which can be broken down into the following principle stages [6, 19]:

- *Freezing stage*
- *Primary drying*
- *Secondary drying*

If required, a pre-treatment phase of the pharmaceutical product or food produce is carried out prior to the freezing stage (section 3.3.4). This may involve increasing product concentration or adding compounds to increase stability of the formulation during freeze drying. After lyophilisation, the dried products are stored according to specified storage requirements, to ensure product quality is maintained for an acceptable shelf life. The products are then reconstituted according to standardised protocols when needed.

Aston University

Illustration removed for copyright restrictions

Figure 1 Illustration of a freeze drying cycle, including temperature profile (top graph) and water content (bottom graph) from [6]. "Tcs=maximum temperature of complete solidification, Tim=minimum temperature of incipient melting, T'im=absolute limit for fast process, Td= maximum allowed temperature for the dry product, RMF=final requested residual moisture" [6].

Liquid or slurry products are placed into the freeze-dryer, frozen (section 3.3.4) below their maximum temperature of complete solidification (Tcs) and then dried under vacuum conditions, to promote the endothermic phase transition known as sublimation [3]. Sublimation occurs when the desired material (aqueous or solvent solutions), undergoes a phase transition directly from the solid state to the gaseous/vapour state (Figure 2), without initially passing through the intermediate liquid phase [3]. This stage is known as primary drying[19] and is discussed in 3.3.5. The final stage, known as secondary drying (section 3.3.6), involves the elevation of the product temperature to remove residual unfrozen water and obtain the final desired moisture content prior to sealing the container [11].

Several parameters need to be monitored to optimise the process and obtain an acceptable cake quality (morphology and appearance), as well as reduce the drying time and operational costs. Factors include the [44]:

- *Freezing rate*
- *Ice crystal morphology*
- *Drying rate*

3.3.1 Phase Diagram of Water

Figure 2 illustrates the vapour-pressure phase diagram of water, as a function of pressure and temperature and their influence on the boiling point and melting point transition curves I and III respectfully [3, 5, 40].

During freeze drying, the product is initially frozen (A to B), thereafter the chamber pressure is reduced (B to C) with a vacuum pump (Figure 3). The decrease in pressure causes a drop in the boiling point of water (curve I). The specific point of interest in the freeze drying industry is the triple point of water, where all three phases coexist (solid, liquid and gaseous water) [5, 20, 30]. Drying through sublimation is achieved below the triple point which is at 610Pascal/6.10mbar [3, 20] and 273.16 Kelvin [3, 30]. In this region (C to D) water is found to pass directly from solid ice to water vapour without initially passing through the liquid phase[3]. This would avoid unwanted melting, foaming and softening of the product[20], which could potentially compromise functionality or aesthetic appearance.

To maintain low pressure conditions, the sublimed vapour is removed from the product chamber with a condenser. This maintains a constant flux of water vapour from the sample to the condenser and allows the product to be dried [3].

Aston University

Illustration removed for copyright restrictions

Figure 2 Phase diagram of water, showing the three phases at different temperatures and pressures. The boiling point of water at 1bar (atmospheric pressure) is 100 ^{o}C [5].

3.3.2   Freeze Dryer Design and the Control System

Lyophilisation machines as depicted in Figure 3 consist of a product drying chamber connected to a unit containing refrigeration coils or plates that trap the sublimed water vapour as condensed ice. In many cases a duct or spool piece connects these two chambers. A schematic diagram of the freeze dryer unit used in this report is available in Appendix A on page 279, consisting of the following key components[5, 19, 30]:

- *Product Chamber containing the shelves upon which vials and trays are placed*

- *Proportional-Integral-Derivative (PID) Control System regulating the shelf temperature consisting of: inbuilt temperature sensor, an electric heating element and digital solenoid valves. The element heats the shelf and solenoid valves digitally control the flow of cooling fluid (items 8 and 16 of Appendix A).*

- *Programmable logic controller (PLC) or control unit used to maintain safe operation and monitor the function of the devices e.g. functioning condenser coils to trap sublimed water and protect the vacuum pump*

- *A PID system for regulating chamber pressure through the use of a vacuum pump and inlet to air or nitrogen gas*
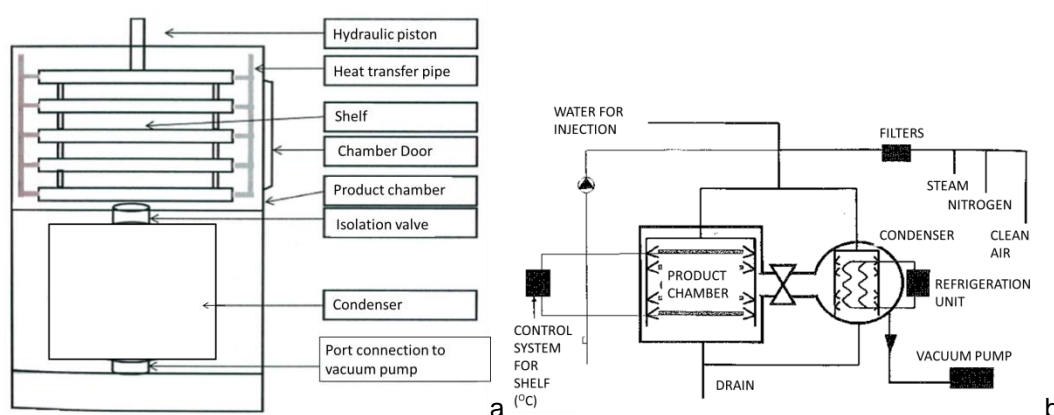
Figure 3 Typical freeze dryer set up (a) laboratory scale [45] (b) industrial scale[6]

An ideal freeze dryer would ensure that the vials within each batch experience repeatable conditions (thermal treatment, resistances etc.) during the process. This would allow consistency within the batch with respect to freezing and drying rates, as well as final product quality (morphology and appearance). It is important to control these factors, as they can influence active pharmaceutical ingredient (API) functionality, reconstitution times of the cakes and product stability. In practice it is not possible to achieve ideal conditions, particularly as there are spatial variations across the chamber and shelf. These variations include convection, conduction and radiative heat transfer differences depending on e.g. the location of the vial [46]. To

improve efficiencies and output quality, several online sensors are used to monitor and control the process to optimise the system.

The digital control of the temperature and pressure is achieved by turning on and off the process variables i.e. the relay suppling power to the heating element or solenoid valves controlling the flow of the cooling fluid see Figure 4 below. An increase in the temperature setpoint results in an increase in the on time of the relay supplying power to the heating element, once the set point has been achieved then the relay turns off and the temperature decreases. Once the lower setpoint is reached then the heating element is turned on again and the cycle repeats. This hysteresis while providing stability does mean that the temperature or pressure oscillates around a mid-point and is visible in all of the measurements in this thesis.

Aston University

Illustration removed for copyright restrictions

Figure 4 Example of digital control (On – Off operation) where solid line is a process variable (e.g. temperature or pressure) and dashed line is the control variable (e.g. power to heater or power turning solenoid valves on and off)[47].

The PID control system changes the on and off time of the process variables in proportion to the error signal i.e. the difference between the desired setpoint and the feedback from the sensors. Appropriate settings of the proportional, integral and derivative settings (Figure 5) can increase the speed in which the desired temperature or pressure is achieved or reduce the difference between the setpoint and the values achieved. Incorrect settings of these values can result in instability in the form of overshoot, increased or continuous oscillation about the desired temperature or pressure.
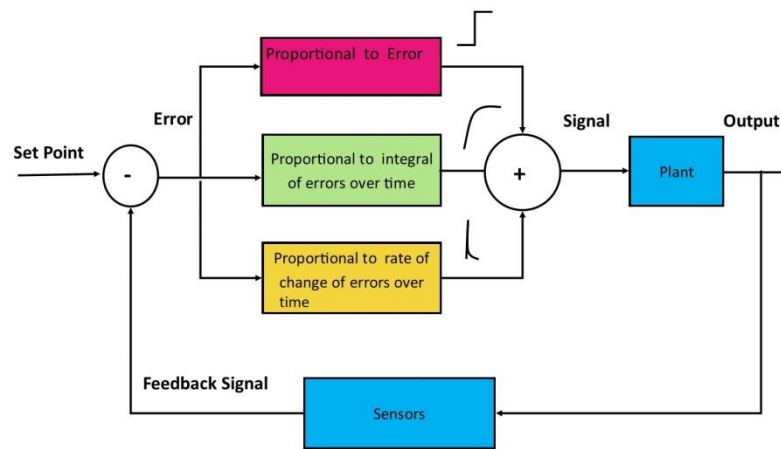
Figure 5 PID control system, adapted from [47]

3.3.3 Formulation Preparation

The pharmaceutical industry carries out this stage prior to dispensing the dosed formulation into vials and placing them onto the shelf for freeze drying.

When needed, excipients are added to the formulation containing the active pharmaceutical ingredient (API) to provide specific characteristics to either the final product or during the freeze drying cycle. They are used to produce a simple, economical, stable and elegant product.

The International Pharmaceutical Excipients Council [48] defines excipients as inactive substances[24], added with the API or prodrug [30, 49] to the solvent (water or in some cases organic solvents), to form part of the manufacturing process or the finished pharmaceutical product dosage.[50]

There are many reasons for including excipients in a formulation[48], including transporting the API to a target location in the body, avoid early drug release which could damage tissues and aid drug product identification. Some improve product taste and appearance, reduce drug disintegration time for fast absorption into the blood stream and protect the product to ensure maximum effectiveness when needed[48].

Excipients that may be used in the lyophilisation of small molecules [50] are:

- **Bulking agents** *[37], including sugars (e.g. mannitol)[24, 51], amino acids and polymers. They form the bulk supporting structure of the product [30, 51] that the drug alone could not provide. They allow proper pore formation for promoting vapour flow during drying and reduce the risk of localised higher moisture content in the final product, as that could lead to API degradation and a reduced shelf life.*

- **Buffering agents** *[50] such as pH adjusting agents[37] (e.g. Hydrochloric acid) to avoid drug degradation during processing, long term storage and reconstitution before administration to the patient [30].*

- **Solubilising agents** *[24, 50] such as complexing agents, surfactants and co-solvents(e.g. ethanol, tert-butyl alcohol[30]). Surfactants aid reconstitution[24] if the drug shows poor wetting behaviour. Co-solvents such as organic solvents (e.g. acetone) can be used to increase sublimation rate, improve stability and decrease reconstitution time.[30]*

- **Miscellaneous excipients** *[50] including tonicifying agents, antimicrobial agents and collapse temperature modifiers. Tonicity modifiers are included when the formulation containing the drug at its recommended dosage needs to be adjusted to make it isotonic with human plasma to avoid tissue damage. Collapse temperature modifiers[23, 24] shift the overall*

> *formulation collapse temperature higher, to reduce primary drying time and*
> *not compromise product quality.*

It is also possible to incorporate cryoprotectants and/or lyoprotectants to the formulation to protect the embedded API or cells [20] during the freezing and the drying stages respectively[24, 49]. These protectants can also serve as bulking agents.

3.3.4   Freezing Phase

The first stage in the lyophilisation process, involves the cooling of pre-treated liquid samples or formulations below their triple point (*Figure 2*), until they are completely frozen [11, 19, 37, 52].

Prior to freezing, the cooling solution passes a critical point and becomes known as a "supercooled" liquid, where it retains its liquid state when cooled below its equilibrium freezing point [11, 33]. In the case of *Figure 6*, pure water cooled at atmospheric pressure does not spontaneously freeze at 0^0C, but is supercooled (line A) until it reaches Point B [11, 25, 33].
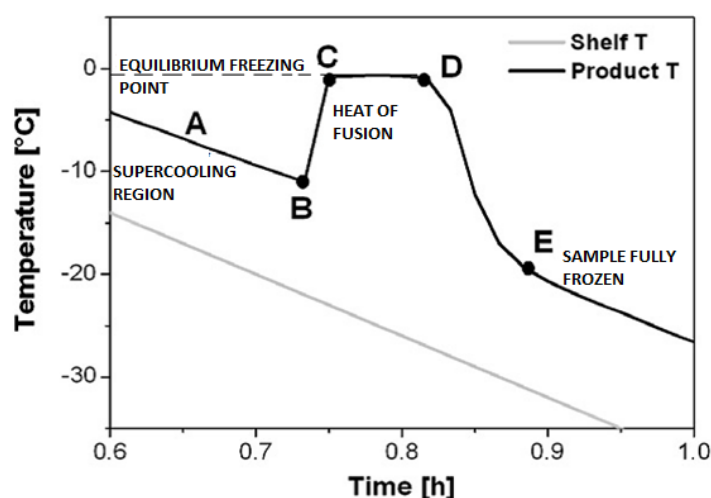
Figure 6 Freezing profile, measured using thermocouples of pure water, on a shelf having a set ramp temperature of -1^{0}C/min. Figure was modified from Kasper and Friess [11].

The degree of supercooling is defined as the difference between the temperature where equilibrium ice formation occurs and the actual temperature of ice crystal initiation/nucleation [11]. It is dependent on process conditions, the solution properties [53, 54] and often occurs in the range of 10 to 15^{0}C or greater below the equilibrium freezing point [5, 11, 23] as seen in *Figure 144* and *Figure 146* (Appendix C).

Supercooling is a non-equilibrium and meta-stable state, which can occur globally or locally in a given solution. Global supercooling is used to describe similar

supercooling conditions within the entire volume of the liquid [11, 55]. Local supercooling occurs when a portion of the total volume is supercooled [11]. Ice nucleation sites produced during supercooling are usually ice-like clusters formed through the adsorption of layers of water on foreign impurities. These "foreign impurities" can include particulate contaminants in the solution, the surface of the container or sites on large molecules or proteins [11, 23]. Another source of "foreign impurities" is the introduction of sensors into the solution, the surface roughness and material properties of the sensor coating e.g epoxy coated thermistor (*Figure 7*) and glass covered thermistor (*Figure 146*) and was observed to influence the nucleation initiation time. Once the nuclei reach a critical mass, rapid crystallisation of the system occurs, represented by point B [11, 25]. At this stage only a fraction of the water freezes and the exothermic reaction leads to an increase in product temperature until the equilibrium freezing point is reached (point C) [11]. The freezing point of a solution is defined as the maximum temperature observed during the solidification of a liquid which has been supercooled (point C) [56]. The latent heat produced (C to D) results in a phase transition and further crystal growth causes the solution to freeze. Once the latent heat is removed (point D) and the sample is fully frozen the temperature drops (point E) [11].

The amount of liquid supercooling obtained prior to ice nucleation, influences the rate of the post-nucleation ice crystal growth and is known as the freezing rate [11]. These patterns are also observed when a thermistor was placed into a saline solution to monitor the freezing stage (*Figure 7*). The standard operating procedure to record the data is available in Appendix B and other freezing profiles showing these trends are available in Appendix C (*Figure 143, Figure 144, Figure 145 and Figure 146).*
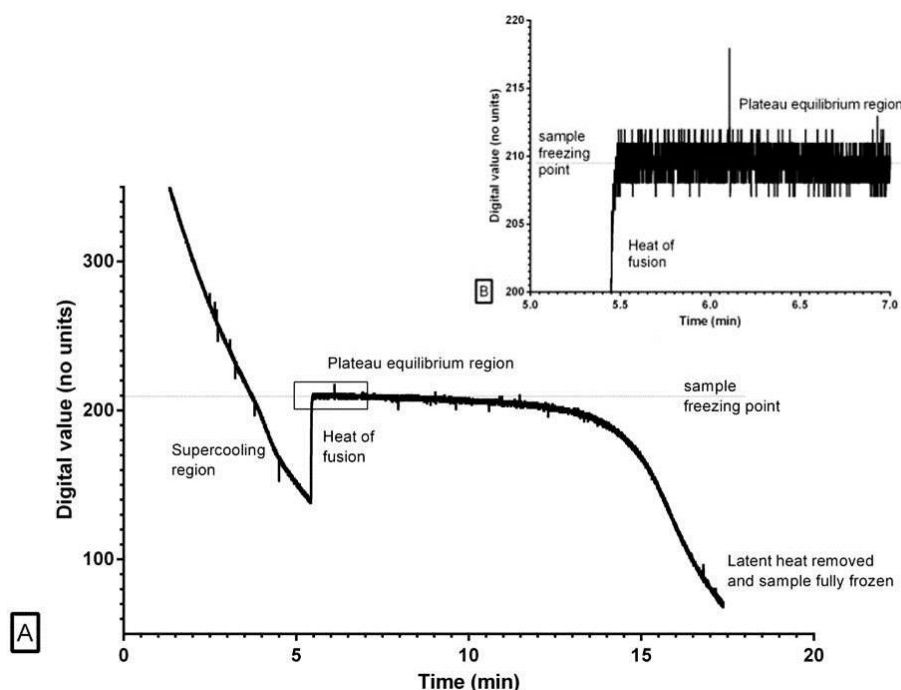
Figure 7 [A]Freezing characteristics of a 0.9% w/v NaCl (300mosm) sample, using a 100kohm epoxy thermistor sensor and 10bit ADC on an Arduino Platinum microcontroller, at 5 degᵒC/min cooling rate. Representative trace showing freezing point depression characteristics.[B] Magnified section of the plateau equilibrium region.

Figure 143 in Appendix C shows the behaviour of saturated saline solutions when frozen on the shelf of a freezer (method discussed in Appendix B). The trendlines show variability in the nucleation initiation times, likely due to differences in the level of "foreign impurities" in the solutions (as discussed above). At these high concentrations, an additional factor that needs to be accounted for is the spontaneous crystallisation of excess solute from the freezing solutions.

Freezing is a major dehydration step in lyophilisation [11, 23] as it separates the solvent from the concentrated solutes [11]. The solvent separates by forming pure solid ice crystals amongst a matrix of glassy and/or crystalline solute structures [11, 23] with characteristics shown in *Table 3-A*.

Crystalline structure	Amorphous structures
Presence of ice crystals	*Structure behaves like a frozen liquid*
Definite grain boundaries	*No crystalline boundary*
On the constitutional diagram a homogeneous eutectic mixture solidifies directly from a liquid to solid at the eutectic point (Teu) without the formation of a mixture of phases.	*The product begins to behave like an elastic rubber at the glass transition temperature Tg'. Further heating causes the material to flow, this is known as the collapse temperature Tc.*

Pharmaceutical industry uses crystalline matrices for:	Pharmaceutical industry uses amorphous matrices for:
• Faster freeze drying process as grain boundaries ease the transport of water vapour	• Embedding sensitive biomolecules • Stabilising active substances
Gradual separation of the mixture can be achieved through slow freezing, until the final drop solidifies at Teu.	

Table 3-A Properties of Crystalline and Amorphous structures, adapted from Martin Christ (2010)

Figure 8 illustrates the phase diagrams of crystalline and amorphous solutions using black and grey lines respectively. The diagram indicates that decreasing the temperature of the solutions below the critical eutectic (Teu) or glass transition (Tg') temperatures, results in crystallisation or vitrification respectively[23, 25]. These critical formulation temperatures tend to be determined through methods like Freeze-Dry Microscopy, Differential Scanning Calorimetry (DSC)[57], differential thermal analysis (DTA) with resistance or impedance measurement[35, 58] to design the freeze drying cycle.

Aston University

Illustration removed for copyright restrictions

Figure 8 Water (w) and Solute (s) system phase diagram [11] where: melting temperatures are Tm (w) and Tm (s); the eutectic temperature is (Teu) and the glass transition temperatures Tg (w) and Tg (s). Tg' is the glass transition temperature of the maximum freeze-concentrated solution [11, 23].

The ice crystals within the frozen structure are then removed by sublimation during primary drying, leaving behind a dried cake structure. Complete solidification is critical with no liquid solution at the end of the freezing stage as this would hinder sublimation, compromise the end product quality and/or appearance as well as potentially lead to batch rejection.

The freeze-dried product characteristics are dependent on the physical state and the morphology of the cake structure [5, 11, 19, 37], which in turn are determined by the kinetics of nucleation and ice crystal growth [11, 19, 44].

The following variables are found to influence ice crystal growth, size and distribution patterns [23, 59]:

- *Cooling rate or the rate at which a solution is cooled [11, 19]*
- *Nucleation Temperature*
- *Degree of Supercooling*
- *Freezing Rates*
- *Vial Size, shape and surface*
- *Filling Height*

The crystal morphology produces a scaffolding structure, which influences sublimation and desorption rates and consequently primary and secondary drying times [5, 6, 11, 20, 37, 53, 55, 59]. The process also influences the final product pore size [5, 6, 20, 39] and consequently the reconstitution time. Freezing rate determines the form, size and status of the ice crystals that can affect factors such as cell wall integrity[20, 60] and cell dehydration[61]. Freezing can lead to cell damage by factors such as solute induced damage, osmotic damage as well as structural damage [20, 60-63] as shown in Table 3-B. The process can cause changes[60] in: concentration of the unfrozen solution, pH changes [20] from crystallisation of buffer components[62], ionic strength, oxidation-reduction potential, surface and interfacial tension, viscosity[62], water activity [61] and biological activity of proteins[62].

In order to reduce salt induced damage cryoprotectants (e.g. sugars) are included in the aqueous phase; please refer to section 3.3.3 on page 34.

Aston University

Illustration removed for copyright restrictions

Table 3-B   Physical Changes and Associated Cryoinjury of red blood cells (RBC) in Response to Cooling Rate [63]

A high cooling rate, high freezing rate and low set temperature is generally implemented to achieve small ice crystals[6, 20, 44, 55]. Small crystals can result in longer primary drying times and small pore size within the final cake [5, 6], whilst increasing the internal surface area, maximising the desorption rate during secondary drying. This may lead to a decrease in the overall process time [6] which could increase productivity. Generally, quick freezing might be implemented to produce better quality [25] frozen fruits and vegetables [60, 61]. The process minimises structural and osmotic damage, having small round ice crystals increase simultaneously inside and outside of the cells[60]. Hui [60] reported that volume expansion, thermal expansion (contraction and expansion), as well as internal stresses can be present during fast freezing which causes cracking of whole fruits when exposed to extremely low temperatures.

Large inter-connected crystals reduce product resistance to sublimation, decrease the overall primary drying time[6] which can increase productivity. Slow cooling rate and freezing rate with temperature cycling (annealing) are implemented to create large ice crystals[19, 53]. Annealing is a thermal treatment process[19], where the samples are held above the glass transition temperature (Tg') for a given time interval[11, 52, 53]. This procedure improves inter-vial heterogeneity[23], allows crystalline compounds to completely crystallize and improve drying rates [11, 19, 53].

Annealing or temperature fluctuations can occur to lyophilised formulations whilst in storage, leading to recrystallisation and altering the product characteristics[60]. Although drying rates could be increased, large ice crystal growth can damage cell membrane structures and organelles, releasing enzymatic systems which lead to "off" flavours, colours and changes in texture. This can be prevented with addition of chemicals or heat treatments to denature the enzymes[60].

Slow freezing of animal tissue leads to ice crystals forming slowly outside the cells due to an initial difference in freezing point depression[25, 60] (*Figure 9*). The variance in salt concentration or osmolality(mosm) across the cell membrane, as the cell has a higher salt concentration than the external environment, leads to different freezing point depressions. Slow freezing eventually increases extracellular solute concentration, creating an osmotic pressure and water migration out of the cell to balance the chemical potential. This is followed by cell shrinkage and membrane damage[25, 61, 63], where irreversible damage can be caused upon thawing[60] as water does not return back to the cell due to cell wall damage [25] causing drip loss.

Aston University

Illustration removed for copyright restrictions

Figure 9 Cooling curves showing the difference between the freezing point of pure water (solvent) and aqueous solution, where adding solute to solvent changes the solution's freezing point, known as the "Freezing point depression" [64].

3.3.5 Primary Drying

The objective of this stage is the removal of bulk ice, without compromising the product quality. It begins once the product mass has been fully frozen and the chamber pressure has been reduced below 6.10mbar and below the vapour pressure of ice of the product. To reduce heat transfer inconsistencies between the vials, the optimum programmed chamber pressure tends to be in the region of 100-200mTorr[19, 24]. These conditions promote the migration of sublimed water vapour from the product chamber to the condenser chamber.

To improve efficiency, the shelf temperature needs to be raised as high as possible to reduce drying time, but kept below the critical temperature to avoid product damage. Literature has shown that a 13% reduction in primary drying time can be achieved by elevating the product temperature by 1°C[53, 57, 65].

It is considered to be one of the most challenging stages, particularly due to the high risk of failure and batch rejection due to lack of product elegance or functionality [4, 8, 19]. The probability of product collapse or melt-back, increases significantly if the process enters the final phase (secondary drying) prior to the removal of all the bulk ice. In this unrecoverable situation, increasing the formulation temperature above the critical point (Te, Tc or Tg', described in section 3.3.4) would cause the remaining ice to melt back into a liquid state and compromise product elegance. It could also cause the cake structure to collapse due to a lack of sufficient mechanical strength to support the structure [19].

Primary drying also has further implications as it is the most time consuming and energy demanding part in the process [11]. Ratti [10] reports that sublimation requires 45% of the total energy of the process, significantly greater than the other energy consuming operations: freezing, vacuum and condensing. As a result of these factors, primary drying becomes the most costly stage in the process[8]. Through further optimisation, drying time could be reduced, influencing the financial aspect of the procedure [4, 9] and increasing production capacity per year.

Figure 10 illustrates a schematic diagram with a list of factors which influence the sublimation rate: product temperature, heat transfer losses through different layers, resistances to vapour flow like the dried cake layer and stopper.

Figure 10 schematic diagram of a product during primary drying [35]

There are several factors which can restrict the sublimation rate, these have been summarised below and discussed in greater detail in section 3.3.5.3 on page 46. Design specifications of the freeze dryer can affect drying rate: [8, 19, 53, 66]

- *Location of the product in the freeze dryer. Front row vials have shown atypical drying characteristics due to higher radiative heat transfer through the door [9]. Atypical drying rates can also occur if the machine was designed with an acrylic transparent door or a metal door.*
- *Vacuum set point conditions; as a pressure below 6.10mbar needs to be achieved for sublimation to occur.*
- *Atypical heat transfer from the shelf to the product through conduction [19] and convection currents from the water vapour*
- *Condenser temperature, capacity and location [19]*

Drying rates depend on the specification of the cycle and requirements of the product [8, 19, 53, 66]:

- *Set point temperature of the shelf (including thermal variation across the shelf), influences sublimation rate by[19]:*
  - *Controlling product temperature through heat transfer*
  - *Providing energy for sublimation*
- *The morphology of the ice crystals that were produced during the freezing stage (i.e. larger crystals reduce product resistance and hence reduce primary drying time)*

- *Fill volume [19]. It is common to avoid depths in excess of 2cm, as this would increase product resistance to vapour flow and have it become a limiting factor of drying rate[53, 65]*
- *Formulation characteristics [19]:*
  - *Properties, chemical composition, concentration[7] and purity (which can affect the resistance characteristics)*
  - *Heat transfer coefficient*

Other factors which can affect drying rates are [8, 19, 53, 66]:

- *Probes placed into the product (e.g. thermocouple)[67]*
- *Stopper characteristics*
- *Vial or syringe characteristics [19]*
  - *Geometry and contact area on the shelf*
  - *Glass heat transfer coefficient*

3.3.5.1 Heat and Mass Transfer

During primary drying the relationship between heat and mass transfer can be modelled by Equation 1[19], where the rate of heat flow into the product dQ/dt (cal/s or J/s) can provide energy for two processes. The first part ΔH_S dm/dt is the heat flow used to promote the endothermic phase transition stage of sublimation, where dm/dt is the mass flow rate and ΔH_S is the heat of sublimation of ice (J/kg). The second term m_S c_v dT/dt is the rate of heat used to change the product temperature dT/dt (K/s), with a sample mass of m_S (kg) and a specific heat capacity c_v (J/K*kg).

$$dQ/dt = (dm/dt) \cdot \Delta H_S + m_s \cdot c_v (dT/dt)$$

Equation 1

The second term is mainly applicable during the early and end stages of primary drying. During most of primary drying the specific heat capacity c_v is considered negligible compared to the heat of sublimation; therefore, during steady state of primary drying the heat transfer equation can be simplified to Equation 2[7, 19, 43, 57].

$$dQ/dt = (dm/dt) \cdot \Delta H_S$$

Equation 2

Equation 2 implies that the heat transfer is used to promote the phase transition of ice to water vapour through the process of sublimation, with the assumption that the product temperature remains constant [19, 68]. When the bulk ice in the product has

been removed the product temperature begins to rise, signalling the end of primary drying and the beginning of secondary drying (Figure 13(b) on page 51).

3.3.5.2 Heat transfer Mechanisms

Figure 10 illustrates three basic heat or energy transfer pathways including: conduction, convection and radiation [46, 69, 70].

Conduction occurs when molecules in direct contact with each other collide and transfer thermal energy from molecules with higher kinetic energy to those with lower kinetic energy. The heat transferred is dependent on the temperature gradient, material properties, heat-transfer cross-sectional area and thickness of the barrier[70]. Figure 10 shows conduction occurring at the interface between the vial and the shelf. Generally well-plates or injection moulded vials for freeze drying (Figure 10) are partially in contact with the shelf [69], limiting the cross sectional area available for conduction.

Convection occurs when currents are formed in a fluid (gas or liquid) due to heated particles which expand and become less dense, leading to mass movement away from the heating source, transferring the thermal energy to cooler denser regions. Convection imparts energy between a solid and the fluid flowing across it[70], such as the gap between the base of the vial and shelf in Figure 10. In this region, potentially trapped molecules could transfer heat received from the shelf to the vial though a combination of conduction and convection. The vial geometry, such as the size of the gap between the base of the vial and the shelf can influence convection currents.

Convection is dependent on the chamber pressure, increasing the pressure allows more energy to be transported by more molecules per unit area to the target vial.

The final heat transfer mechanism is known as thermal radiation, it transfers energy in the form of electromagnetic waves, even in vacuum, from matter that has a temperature above absolute zero. Radiation heat transfer (typically by infrared) occurs in the freeze dryer between two surfaces such as the walls, vial, shelf, through the transparent door etc. Using the Stefan-Boltzmann law, the net radiative heat transferred from one radiating surface to another is described in Equation 3[71, 72].

$$\frac{dQ_r}{dt} = A_v \bar{e} \sigma (T_2^4 - T_1^4)$$

Equation 3

The net transfer of radiative energy per unit time is dQ_r/dt (W=J/s), A_v is the area of the emitting body (e.g. vial in m^2) and $(T_2^4 - T_1^4)$ is the difference of the absolute temperature(K) to the fourth power.

The Stefan-Boltzmann constant is expressed as σ (5.67×10^{-8} $W \cdot m^{-2} \cdot K^{-4}$)[71, 72] and e is the emissivity of the body (scale of 0 to 1) which describes the effectiveness of the body at radiating energy, with 1 representing an ideal black body which effectively absorbs radiative energy.

3.3.5.3 Product Resistance

The product's resistance to water vapour is an important parameter which influences the rate of sublimation during primary drying. Mass transfer can be expressed as a function of the following resistances to water vapour flow rate [19]:

- *Morphology of the pathways in the dried layer (e.g. diameter of the dried pores and interconnected pathways created by sublimation)*
- *Geometry of the opening between the stopper and vial*
- *Chamber to condenser pathway*

Figure 11 illustrates the different resistances to vapour flow during primary drying with the dry layer above the sublimation front creating the greatest resistance to mass transfer. This layer varies with time as the sublimation front proceeds from the top surface down to the bottom of the sample [19].Generally this creates the greatest resistance, however exceptions include very low concentrations or the start of primary drying when no dry layer is present.

Aston University

Illustration removed for copyright restrictions

Figure 11 Representation of the different resistances to vapour flow and mass transfer during primary drying [19]

Equation 4[19, 20, 57, 73] identifies the inversely proportional relationship between the resistance and sublimation rate, as well as proportional relationship with the pressure gradient between the sublimation front and the chamber pressure.

$$\frac{dm}{dt} \propto \frac{(P_o - P_c)}{(R_s + R_p)}$$

Where:

$\frac{dm}{dt}$ = rate of sublimation $(\text{gcm}^{-2}\text{hr}^{-1})$

P_0 = vapour pressure of ice at the product temperature interface (mmHg)

P_c = chamber pressure (mmHg)

R_p = product resistance $(\text{cm}^2\text{mmHg hr g}^{-1})$

R_s = stopper resistance $(\text{cm}^2\text{mmHg hr g}^{-1})$

Equation 4

The product resistance Rp limits sublimation as the vapour front needs to pass through a network of pores within a dried cake matrix[46], where the thickness of the dried layer changes over time (Figure 11). The pores were created after layers of ice crystals from the freezing stage sublime, leaving behind void spaces as the sublimation front moved through the product, changing Rp with time.

The stopper resistance Rs tends to be negligible when compared to Rp[46], as most products tend to be loaded semi stoppered in the vial neck with a large open area for vapour flow. Once freeze drying is complete the stoppers are pressed to seal the vials under vacuum or a nitrogen environment ready for storage.

The design of the freeze dryer can also create resistance to vapour flow between the product chamber and condenser. An example would be if the vapour flow had to pass through a duct, the dimensions of the channel would need to be sufficient not to restrict the high velocity vapour flow during the process, which can occur during aggressive cycles. In these cases loss of control of the chamber pressure and an increase in product temperature could be expected thus affecting the morphology and stability of the product. Another consideration is the condenser's ability to convert the water vapour to ice and to trap it on the plates or coils. The ability of the condenser to behave as a trap can be restricted if the ice thickness becomes too large or the condenser temperatures becomes too high.

The two key parameters that are controlled during the primary drying phase are the shelf temperature and the chamber pressure. To maximise the sublimation rate, according to *Equation 4* a combination of lowest possible chamber pressure and the highest allowable product temperature should be used [19]. To increase the batch output and decrease process time, the shelf temperature is increased to supply

energy for sublimation [11], but kept below the collapse temperature. The most efficient method is achieved by having a high but within tolerance shelf temperature and reducing the chamber pressure, to decrease the product temperature below its critical temperature (Figure 12). It is important to avoid going <50mTorr[57] as this begins to limit heat transfer to the product and restrict sublimation.

Figure 12 shows the relationship between temperature and pressure on the sublimation rate. The graph shows the following trends [19, 21]:

- *Increase in sublimation rate when increasing the chamber pressure but keeping the shelf at a constant temperature (points B, A, C)*
- *Increase in sublimation rate with an increase in shelf temperature at a constant chamber pressure (points B, E)*
- *When maintaining a constant shelf temperature but increasing the pressure, there is an increase in the product temperature (B vs C). This would need to be accounted for to avoid exceeding a critical product temperature such as the collapse temperature.*

Aston University

Illustration removed for copyright restrictions

Figure 12 Schematic diagram to illustrate the relationship between shelf temperature, product temperature and chamber pressure on the sublimation rate[19, 54] of a formulation in[54]

3.3.6 Secondary Drying

Secondary drying is the final stage carried out in most processes prior to sealing the freeze-dried material. Secondary drying is carried out to further reduce the moisture content of the cake to a final content between 3% to less than 1% by weight [6, 19, 37, 74, 75]. The process is beneficial as it increases product shelf life for long-term storage or increases formulation stability.

The residual water content, in some cases between 15-20% unfrozen water [11, 19] at the end of primary drying, is reduced in secondary drying through the process known as desorption [6, 59]. The low pressure is maintained and the shelf temperature is usually increased in order to gradually heat the product and promote desorption [11]. The gradual heating reduces the risk of collapsing materials, which could otherwise occur if fast heating is implemented [19].

Another concern is prematurely starting secondary drying, when there is still ice present in the product [6]. In this situation should the temperature increase past the melting point of ice, melt-back could occur. This would likely compromise product appearance and potentially increase drying time [11].

3.4   End of primary drying measurement technologies

A critical stage in the freeze drying process is the transition between the primary drying and secondary drying stage as inaccurate timing can lead to increased costs, profit loss and product damage. To minimise the risk, it is becoming common practice to monitor Critical Process Parameters (CPP) [7, 37] throughout the cycle rather than just measuring them at the end of the process [76]. Examples of CPPs include moisture and temperature as they influence Critical Quality Attributes (CQA) [37] of the batch products.

The aims of in-line process monitoring, include long-term optimisation by [76]:

- *Reducing production time and costs*
- *Improve product quality and reduce/minimise batch rejections*
- *Increase process automation*
- *Increase efficiency and reduce wastage (e.g. energy, over-processing and use of materials)*

Table 3-C lists some of the different technologies used to monitor drying and compares their performance against desired characteristics such as steam sterilisation compatibility and batch measurement properties *[7, 37]*.

Aston University

Illustration removed for copyright restrictions

Table 3-C Comparison of monitoring technologies [7]

These devices are specially designed, to different degrees, to resist to the extreme conditions experienced within the freeze dryer. This may include resistance to a wide range of temperatures in some cases between -50°C and +40°C, low temperatures, vacuum conditions and sterility [7]. These requirements render many commercially available devices incompatible for use in freeze-drying [7].

The technologies used in freeze drying fall into two main categories: single vial measurement and batch measurement techniques. *Figure 13* (b) shows both types used during the same drying cycle, thermocouples are "single vial probes" inserted into bulk ice, whilst Pirani comparative pressure measurement was the non-invasive

"batch measurement technique". The endpoint of primary drying and drop in sublimation is determined from a distinguishable sharp decrease in the signal as observed in *Figure 13*(a) and red circles in (b). At this stage the chamber vapour composition changes from predominantly water vapour to nitrogen [8, 53, 77] which can be detected with sensitive technologies. Invasive temperature probes, on the other hand, track temperature during the cycle and termination of sublimation cooling. A rise in product temperature towards the shelf temperature indicates end of drying (red circle in *Figure 13*(b)).

Aston University

Illustration removed for copyright restrictions

Figure 13 (a) Profile showing the Pirani pressure during primary drying, and the characteristic trends for the detection of the end of primary drying time [8]. (b) 500ml distilled H_2O placed in a steel tray at a fill depth 0.88cm; red circles indicate the end of primary drying for thermocouples and Pirani gauge. Thermocouples were centrally positioned within the steel tray and located at the bottom of the sample.

These techniques will be discussed in greater detail in the following sections including main advantages and disadvantages of the systems. The sensors used in this project will also be analysed: comparative pressure measurement (3.4.2.2), Dew Point (3.4.2.1), Thermocouple (3.4.1.3), windmill sensors (3.4.2.3). Chapter 4 will introduce a new device that will be characterised for its use in a freeze dryer: Polymer Optical Fibre Bragg Grating (POFBG) Sensors.

3.4.1 Single vial measurement techniques

3.4.1.1 Product Probes

Sensors that fall in this category include thermocouples (section 3.4.1.3), resistance thermal detectors (RTDs) (section 3.4.1.4) and wireless sensing probes. These methods involve placing a probe inside a single vial to track the temperature profile of the sample during the freeze drying cycle.

There are several types of invasive wireless sensors [37] that monitor and transmit temperature data to an interrogation unit [57]. Wireless sensors offer up advantages over cables as they do not require a specialised vacuum tight port into the chamber to ensure that it remains leak proof. One type of sensor discussed in literature operates passively without a battery, using a quartz-based resonance circuit that oscillates at a characteristic temperature dependent frequency and provides the user with real-time data[78]. Schneid described a wireless monitoring device that operates actively with a battery but can have a large thermal mass which measures the average temperature across the sample fill depth [57]. This has similar problems to temperature probes with large packaging (e.g. RTD), as focal point measurement to determine when the sublimation front has reached the base of the vial is challenging to detect.

Another issue is the size of the packaged sensor compared to the sample fill depth, as seen in *Figure 14*(b), as the sensor might extend above the solution and measure an average temperature of the product and gas headspace.

One of the most commonly used "gold standard" sensor is the thermocouple particularly as it is inexpensive [8, 79] and compared to other devices does not require specialist training to use in commercial environments. The Seebeck effect (3.4.1.3) allows the thermocouples to be self-powered and not to require external excitation current from a power source like other temperature sensors (RTDs and thermistors) which may introduce heating effects in to the product. The sheaths offer protection to the internal circuits compared to bare fibre sensor arrangements, some provide corrosion resistance and are suitable for sterilisation, allowing their use in industrial applications. *Figure 14* shows the placement of the thermocouple within vials.

These different types of temperature measurement devices allow several critical stages to be monitored during the process, such as the formation of a stable frozen formulation matrix during the freezing stage. It is also critical to monitor the temperature during primary drying and transition to secondary drying, in order to ensure that the product temperature remains below the collapse and/or eutectic melt

temperatures [19]. The temperature profiles are also used to estimate the end of sublimation. The presence of ice in the product during primary drying causes sublimation induced cooling (from the latent heat of vaporisation of ice) which allows the product temperature to be maintained below that of the shelf temperature. The product temperature begins to rise once the ice has been removed from the product (*Figure 13*(b)). The characteristic trend which indicates the end point of primary drying is the point at which the product temperature approaches the shelf temperature set point [8, 19].

Unfortunately single vial measurement sensors are not considered representative of the entire batch [38, 80], as the probes facilitate product ice nucleation at higher temperatures [67] and lead to less super-cooling as well as larger ice crystals[38]. This difference in temperature could be in the region of ~1.4°C in laboratory conditions but as high as~10°C in manufacturing scale freeze dryers[81] which may be particulate free environments (class 100). This lowers product resistance, increases sublimation rate and reduces primary drying time[8, 53, 67, 80]. The probes need to be placed centrally at the bottom of vials to reduce radiative edge vial effects[9]. To ensure maximum sterility, manufacturers often place thermocouples in front row vials[9, 38], however operators are required to load the probes as they are incompatible with automatic loading systems[67] and the handling process may compromise product sterility[67].

Due to atypical radiation heat transfer effects, front row vials tend to finish primary drying sooner than interior vials[9, 46, 81].

In these circumstances an additional "soak time" is added to determine the endpoint time, to allow sufficient time for the removal of all ice from the rest of the batch. This safety margin is often in the region of 10-30%[8, 19, 53].

Figure 14 Image of (a) thermocouple placement within a vial and (b) comparison of probe sizes placed into the sample vial[82]

A different type of probe that has been used either adjacent to vials or within the solution, was connected to a Near Infra-Red (NIR) spectrum analyser [81-83]. This system takes advantage of molecules that can be excited by IR radiation at specific

frequencies, as is the case with water, by inducing higher energy molecular vibrations. By monitoring the absorption patterns it is possible to track the reduction in water content and estimate an end of primary drying time. These NIR spectra are however highly dependent on the content of the formulation, requiring calibration and correlation between the spectra and water content[57]. It is currently a system limited to the laboratory, as the placement in a modified array would interfere with large scale production protocols and implementation into sterile Good Manufacturing Practices(GMP) is not available[57].

3.4.1.2 Weighing systems

Section 3.4.1.1 describes single vial measurement techniques that are invasive and consequently influence freezing and drying rates of the samples. Depending on the requirements, weighing systems in research or pilot scale[5] applications can intermittently measure the loss of weight from a sample during lyophilisation. Balances such as the Christ microbalance (CWS-40) [7, 84] can be placed in the freeze dryer and measure the weight of a single commercial vial (2R-20R) [57]. This microbalance lifts the vial at periodic intervals during primary drying every 10sec[57] or 5min[7], using a specially designed lifting arm to track changes in mass. This system can be used to find the end of sublimation however is not reliable during secondary drying, cannot be autoclaved[5, 84] and may create atypical heat transfer effects.

3.4.1.3 Thermocouple

Temperature provides a measurable physical indication related to the average kinetic energy of the particles within a material.
In laboratory and industrial scale freeze driers, it is important to control and monitor both the temperature of different components within the machine (e.g. shelf, condenser etc.) as well as product temperature [19, 67].
Thermocouples are commercially used temperature sensors, formed through the connection of two dissimilar metal alloys to create a point junction[79, 85]. The area around the junction produces a voltage difference (emf) which is non-linearly dependent on the absolute temperature (known as the Seebeck effect).[86] Specialised circuits are required for reliable measurements as the signal level picked up is in the millivolt (mV) range [79], making the device susceptible to electromagnetic interference (i.e. it possesses a low signal to noise ratio).

The circuit would consist of a thermocouple connected to the meter via a reference junction (usually referenced at 0^0C) [79, 85]. The cold junction is required to avoid inaccurate measurements obtained through the production of an undesired second thermocouple junction [86]. This undesired junction is formed due to the connection of another dissimilar metal to those used in the thermocouple.

Specific material combinations have been produced (K, J, N, R, S, B, T, E types) for their reproducible voltage output and corresponding tabulated temperature. [79, 85] Each type is selected depending on key factors, including [87]: operational temperature range, corrosion resistance (e.g. chemical or moisture), accuracy, cost-effectiveness and installation requirements. Some have limitations on their accuracy and the error varies depending on the type used, e.g. standard T type thermocouples can show an error of $\pm 1^0$C [86], but some can be made suitable for steam sterilisation and corrosion resistance for industrial applications [8].

Material combination type 'K' chromel-alumel thermocouples, used in this project, are generally used due to their relatively linear temperature-emf properties across the temperature range +700 to +1200°C [79]. However their full measurement range spans across -200 to +1300°C, allowing their use in a wide range of process systems [79, 85] not possible with many other temperature probes. Shtargot and Mirza [88] documented the output voltage against temperature for a type-K thermocouple where the curve is reasonably linear within the range -50°C to +350°C, suitable for use in a freeze dryer.

3.4.1.4 Resistive Temperature Measurement Devices

Data acquisition systems use these sensors to measure changes in a material's electrical resistance as a function of temperature. The change in electrical resistance is measured and converted into a corresponding temperature value using tabulated coefficients [79, 85]. The conventional method of measuring resistance is to use a Wheatstone bridge [79] as shown in *Figure 15*.

Care needs to be taken when selecting an appropriate excitation voltage to use in the Wheatstone bridge configuration. A high voltage is desirable to increase the measurement sensitivity however lower voltages are recommended to minimise or avoid self-heating errors. Self-heating occurs as high currents pass through the circuit and artificially increase the transducer temperature due to power dissipation. The increase in temperature changes the observed resistance.

There are two types of devices which are commercially used:

- *Resistive Temperature Detectors (RTDs)*
  Metallic devices (typically platinum based) which produce a measurable change in resistance as a function of temperature.
- *Thermistors*
  Devices that measure the resistance change of a ceramic semiconductor which varies nonlinearly with respect to temperature. Examples of use include osmometer applications[56, 64]

Figure 15 Set up for the Löser Micro-Osmometer Type 6. The thermistor is placed into the eppendorf containing the solution. The solution is cooled using Peltier-elements and complete solidification is initiated by placing an ice crystal into the solution at a pre-defined temperature. A Wheatstone bridge is used to measure voltage and determine the osmolality [64].

3.4.1.5 Optical Fibre Sensors

Kasper and Wiggenhorn[89] discuss the use of Glass Optical Fibre Bragg Gratings in a freeze dryer to invasively measure the temperature of the sample during freeze drying and in a separate configuration incorporated in to the vial for non-invasive measurements. The operating principle of these sensors will be discussed in greater detail in chapter 4.

In this study [90] the optical fibres were placed through the stoppers into the vials containing the samples, to track temperature as an alternative method to thermocouples and RTDs. The Optical Fibres were placed in different configurations directly in contact with the product or within helical structures to protect the fibre. The sensors were used to track the freezing events of a number of excipients, including freezing point depression, supercooling, as well as temperature behaviour during primary drying. Friess and Resch[91] published a patent on this work in 2014. This thesis will document the work carried out on a new optical fibre sensor to track different parameters, including humidity in a freeze dryer, without requiring the

sensor to be submerged in the solutions or incorporated in the vials. Polymer optical fibres have the potential to be a cost effective alternative to silica optical fibres[92, 93]. Certain polymers like PMMA also have an affinity for water vapour[93], which could have applications in freeze drying.

The literature search has revealed that polymer optical fibre Bragg grating (POFBG) sensors have not previously been used to detect end of primary drying, this became one of a number of focus areas of the thesis.

3.4.2 Batch measurement techniques

These devices have the advantage of being non-invasive, allowing batch monitoring of the sublimation rate[8] and other desirable parameters (*Table 3-D*) of the sample, without the need to interrupt the process[53]. These technologies obtain measurements without the need to insert probes into samples to monitor temperature, which would influence product freezing and drying behaviour[84]. They do not require atypical vials to be removed at set time intervals during the cycle by "sample thief" method[53, 94], for gravimetric analysis or residual moisture analysis e.g. using Karl Fisher[74, 95].

The equipment tends to be costly and highly specialised in order to detect trace quantities of water vapour during primary drying. They may require alterations to the freeze dryer to support the sensing unit e.g. TDLAS [57], and may be limited to specific locations on the unit due to the size or design of the component. Some can be susceptible to damage if not handled with care [8], require specially trained maintenance teams e.g. frost point/chilled mirror hygrometer [96] and dew point sensors as they can be susceptible to contamination.

Device	Advantages	Disadvantages
Pirani/ capacitance manometer (section 3.4.2.2)	• Suitable for clean in place (CIP) • Inexpensive components when compared to TDLAS • Measures changes in gas composition (i.e. water vapour)	• Accuracy of device • Difficulty to monitor vapour flow rate during drying
Manometric temperature measurement (MTM) (section 3.4.1.1)	Measurement of: • The vapour pressure of ice • Temperature at the moving sublimation front • Product resistance • Mass flow rate	• Capital cost is high • Fast acting chamber isolation valves (CIV) required, leading to wear, cost, limit lifespan and dryer size • Multiple readings required
TDLAS (section 3.4.2.4)	• Can be steam sterilised • Measurement of: • The vapour velocity • Vapour concentration • Mass flow rate	• High capital cost • Cannot measure the temperature at the sublimation front • Custom duct needs to be fitted into the freeze dryer

		• Costly to maintain and train personnel
Dew Point/Chilled mirror/moisture sensors (section 3.4.2.1)	• Compatible with clean in place (CIP) and automatic loading • Dew point or humidity measurement	• Steam sterilisation not possible • Handled with care by trained personnel • Long term calibration drift and aging effects
Windmill (section 3.4.2.3)	• Visual inspection of vapour flow • Very low cost when compared to other batch measurement devices • Flow rate for the entire batch	• Low moment of inertia and friction between bearings required • System to protect blades against backfill velocities • Susceptible to gathering particulates, would require a sterilisation procedure
Cold Plasma (section 3.4.2.6)	• Sensitivity to changes in gas composition • Can be steam sterilised • Inexpensive components when compared to TDLAS	• Ionisation could degrade some products e.g. human growth hormone • External Calibration and signal integration required • Limited to certain locations in the freeze dryer, particularly during scaling up
Mass Spectrometer e.g. LYOPLUS (GEA)[97-99], HOF Mass Analyser[100]	• Monitor gas and moisture content[35] • Accuracy • Detecting contaminants: 　• Silicone Oil Detection in the freeze dryer[28] 　• Chamber Leak Tests	• High capital cost • Costly to maintain and train personnel

Table 3-D Batch measurement devices for monitoring primary drying

3.4.2.1 Dew Point and Capacitive Humidity Sensors

Dew point sensors or electronic moisture sensors are devices used to detect the relative humidity and frost point of the vapour within the chamber [8, 53, 77]. The frost point is where for a given temperature, the ice equilibrium vapour pressure is equal to or saturated with the measured partial pressure of water of the surrounding air [8, 77]. This unique characteristic is used to monitor the change in vapour composition throughout the process [8, 53, 77]. A sharp decrease in the moisture content towards 0% [80, 84, 101] and decrease in dew point indicates end of primary drying (Figure 13(a)).

Typical sensors used in the detection of humidity and end of primary drying are based on the use of an aluminium oxide moisture sensor to measure change in capacitance. Some capacitive sensors consist of a water permeable gold electrode, an aluminium electrode and sandwiched between them a thin porous aluminium oxide film [96] which changes capacitance depending on the relative humidity of the gas in the chamber. The change in capacitance (and voltage output) is related to the adsorption of water for a given partial pressure [8]. This device is often mounted in the product chamber of the freeze-dryer [77].

Another device is based on a 'chilled' mirror dew/frost point sensors as shown in Figure 16 [85, 96]. This device consists of a temperature controlled surface which is cooled until the surrounding cooling gas[102] reaches the dew/frost point where water begins to condense out onto the surface. A photo resistor/detector is used to pick up the optical signal that is transmitted across a mirror. The mirror could be the gold or cold side of a Peltier device [96, 103]), with a sensing element that records the temperature [96].

Aston University

Illustration removed for copyright restrictions

Figure 16 Schematic of a frost point sensor, consisting of a hygrometer as well as a fibre optical dew point detector, adapted from Chen [96]

These batch measurement non-invasive sensors have advantages for industrial applications as they can be cleaned in place (CIP) and are compatible with

automatic loading [8]. However these sensors cannot be steam sterilised and often need to be handled with care[8], they can suffer long term calibration drift [96] and aging effects.

3.4.2.2   Comparative Pressure Measurement

Comparative pressure measurement is a technique which generally measures a differential between the conductivity pressure (Pirani) gauge and the capacitance manometer[37]. The capacitance pressure gauge is used to measure the absolute pressure of the chamber vessel during the lyophilisation cycle [8]. The Pirani gauge is calibrated against a nitrogen atmosphere, and used to measure the thermal conductivity of the gas within the chamber [8, 53].

The presence of water vapour during primary drying increases the chamber's vapour pressure and affects the thermal conductivity of the gas by about 1.5 times that of air [53]. During this interval the Pirani gauge is shown to have a 60% higher gauge pressure than the capacitance manometer [8].

When the sublimation rate begins to decrease, the gas composition changes from predominantly water vapour to nitrogen (Onset in *Figure 13*(a)) and the pressure reading from the Pirani sharply decreases [19].

The capacitance manometer illustrated in *Figure 17* is an electro-mechanical type gauge. Changes between the inlet pressure and the high vacuum reference cavity results in the displacement of a thin diaphragm between them[79, 104].

Consequently, the distance between the diaphragm and the electrode assembly in the reference vacuum cavity varies and a change in the capacitance is observed[104-106]. This is translated to an electrical signal proportional to the pressure change. These devices are generally accurate to 0.25% to 0.5% of the actual reading[105].

The Pirani is a type of thermal gauge (Figure 18) consisting of four coiled tungsten or platinum wires (Figure 18a) connected in parallel in a typical bridge circuit (Figure 18b). Often two identical tubes are used along with one evacuated to low pressure and the final tube containing the gas at an unknown pressure [79]. A current is passed through the tungsten element and reaches a specific temperature subject to the thermal conductivity of the gas. The resistance of the element changes with respect to the temperature, causing an imbalance in the bridge which can then be measured. These devices are used for a pressure range 10^{-5} to 1mbar [79] and tend to be accurate to 2% of the actual reading[105].

Aston University

Illustration removed for copyright restrictions

Figure 18 Pirani gauge set-up (a) and (b) Wheatstone bridge circuit [79]

Another thermal gauge used to measure pressure in freeze dryers is a thermocouple vacuum gauge[106]. In this configuration an encapsulated thermocouple is placed adjacent to a constantly heated element[107] or hot wire[106], whilst avoiding electrical contact between the two components. The chamber pressure can be obtained by measuring the rate of heat loss from the heated filament to its surrounding environment[106]. At high pressures, more gas molecules are present around the heating filament which allows energy to be carried away and cool the wire[107]. Conversely, fewer molecules are present at lower pressures, reducing the cooling effect and increasing the temperature of the filament[107]. This temperature is detected by the thermocouple and the voltage is converted to pressure units[107]. Like the Pirani gauge, this sensor is dependent on the gas composition[107] and the heat transfer characteristics of the gas (pressure and gas species).

The comparative pressure measurement technique offers up several advantages by comparison to other devices available on the market. It is a non-invasive, batch measurement process with inexpensive components when compared to other techniques for measuring the end of primary drying time such as TDLAS[7, 8]. For industrial purposes it is possible to clean in place (CIP) without major disassembly and reassembly.

Unfortunately the accuracy of the gauge is not as high as other methods and it is challenging to monitor the vapour flow rate during drying. Steam sterilisation of the device for use in manufacturing has been tested in the literature [7, 8].

3.4.2.3   Windmill or Anemometer Sensor

The "windmill sensor" or anemometer is a device which uses propeller type blades to provide either visual or electronic feedback on the vapour flow rate. This technique is non-invasive and allows tracking of the batch vapour flow behaviour from the product chamber to the condenser chamber rather than an individual vial. Mechanical (kinetic) energy is transferred from the flow of water vapour to the sensor, causing the turbine fan blades (rotor) to move. The vapour flow rate is driven by the pressure difference between both chambers, produced during the drying stages of the lyophilisation process. The blade speed is proportional to the rate of dying and mass transfer rate [108]. Towards the end of primary drying as the rate of sublimation and vapour flow decrease, the speed of the fan blades will consequently decrease.

The patent [108] of the commercially available VIRTIS® Advantage Series freeze-dryer model from S.P. Industries Inc., mentions that an additional "manual drying rate windmill" sensor could be incorporated into the machine. The configuration involves placing the windmill between the drying and the condensation chamber track the vapour flow. This would allow the user to visually and qualitatively determine the flow rate through the clear acrylic door as shown in *Figure 19*.

Aston University

Illustration removed for copyright restrictions

Figure 19 Position of the windmill as part of the freeze dryer (a) image of the entire freeze dryer with the fan placed within the channel coupling the product chamber to the compressor chamber [108] (b) components within the freeze dryer [108]

The patent describes the components, their function and the control system of the freeze dryer, however it mentions using the windmill as a visual aid for determining end of sublimation and does not provide data collected from an inbuilt windmill.

A different arrangement was proposed by Couriel[109], where the tray containing the formulations would be covered to direct the vapour flow through 4 specially constructed holes, each in line with a windmill that was rested on supports[110]. This system provided visual information to the user who saw the blades stop gyrating when vapour flow from the product finished, marking the end of primary drying. Unfortunately it was pointed out that such an arrangement could limit the vapour flow and influence product temperature[109].

Other resources [35, 75, 109, 111] also mention the possibility of using this type of sensor in the freeze dryer, but to this author's knowledge no data of blade speed has been recorded from a device in the freeze dryer and published. This will be one of the objectives of the thesis.

These sensors provide advantages such as low cost and visual cues of the end of primary drying, not available with other devices, however some design modifications might be required. They would need to be designed with a low mass and low friction bearings to allow movement in response to the vapour flow, particularly at the end of primary drying when trace ice is subliming. They could be susceptible to gathering of particulates due to their moving parts and provide challenges for aseptic conditions, however depending on the material properties could allow steam sterilisation.

3.4.2.4   Tuneable diode laser absorption spectroscopy (TDLAS)

Tuneable Diode Laser Absorption Spectroscopy (TDLAS) shown in Figure 20 measures in real time the water vapour passing through a duct, by calculating the vapour concentration (molecules/cm^3)[112] and mass flow rate (grams/second)[112].

Two lasers are positioned in the duct connecting the product and condenser chambers[8], one beam is in the direction of the flow and the other against the flow of the stream[8]. The angle between the laser beam and vapour flow [8, 94] allows the calculation of the velocity (m/s) by observing a Doppler shift in the water vapour absorption spectrum of the targeted gas. The velocity and concentration of the water vapour are used to determine the real time sublimation rate of the product during primary drying [8].

Prior to sublimation, the beam's wavelength is tuned to an absorption line of the target gas within the infrared region[112]. The device then measures the quantity of

absorbed radiation by the water vapour to determine the average concentration integrated over the beam's path length [8, 112].

Literature has typically shown this equipment implemented in laboratory and pilot scale freeze dryers[112] and described potential implementation in production scale dryers[43].

The endpoint of primary drying is determined from the water vapour profiles as a characteristic sharp decrease in water vapour concentration (*Figure 13*(a)). Patel[8] found this is comparable to readings obtained from mass spectrometry, comparative pressure measurement and cold plasma.

Aston University

Illustration removed for copyright restrictions

Figure 20 TDLAS configuration attached to the freeze dryer [57, 112]

This technology has several advantages, including being non-invasive and monitoring batch flow rather than individual vial characteristics like a thermocouple [8]. It is a robust device which can be steam sterilised and Cleaned in Place (CIP) [8], advantageous for industrial settings.

TDLAS is significantly more expensive (~$100K USD) than the thermocouple which may have commercial implications [8] due to high capital and maintenance costs as well as specialised training required for operation. The system needs to be attached in a specific configuration[101] in a custom-made freeze dryer diagnostic spool or duct between the product and condenser chambers[113] not required by many other sensors. The dryer configuration can also influence the installation process and if there are flow disturbances it can affect the output results.

TDLAS can monitor mass, concentration and velocity flow rates however it cannot be used to measure the temperature of the sublimation front like MTM.

It is worth noting that this technique does offer advantages for measuring a wide velocity range such as ~1.5 - 300 meters/second[113, 114] and low mass flow region of ~0.001 - 2.5 grams/second[69, 114], not possible with many other sensors.

3.4.2.5 Pressure Rise Test (PRT)

The pressure rise test(PRT)[37, 109] records the rise in chamber pressure induced by sublimation, when isolating the product and condenser chambers for a brief time interval (typically 5 to 30s) [8, 43, 109] to cause an interruption in the flow rate between the two chambers [67]. Historically, PRT data has been used in commercial scale freeze dryers to estimate end of primary drying time[43].

Mathematical models can also process the PRT data to estimate the sublimation flux, the product temperature and vapour pressure of ice at the sublimation interface[109] as well as mass transfer resistance of the dried product [8]. Additional information on the temperature of the moving sublimation front during drying, can be estimated from the monitored rise in chamber pressure to the saturation vapour pressure, through water vapour temperature diagrams[28]. Several algorithms [109] have been proposed, including Manometric Temperature Measurement (MTM) [22, 38], Barometric Temperature Measurement [28, 42, 115], Pressure Rise Analysis[116], Dynamic Pressure Rise [27], and the Dynamic Parameter Estimation[38].

At the end of primary drying, there is minimal pressure rise as most of the ice has been removed from the cake structure [67]. At this stage (Figure 13(a)) the calculated vapour pressure of ice approaches the chamber pressure [8, 67].

This process had advantages characteristic of batch measurement non-invasive techniques discussed in section 3.4.1.3 on page 54 and with MTM allows estimation of the temperature of the sublimation interface[28], not possible with thermocouples or RTDs. MTM allows the estimation of parameters such as the vial heat transfer coefficient Kv and heat transfer dQ/dt into the vial[43, 57], not possible with many other measurement methods. By estimating these parameters it is possible to optimise sublimation rate without risking collapse or eutectic melt of the cake.

There are also some disadvantages to the system. Fast acting Chamber Isolation Valves (CIV) for MTM are required which limit the dryer size and is a challenge for commercial scale [43]. The forces involved would also lead to accelerated wear and tear and limit the lifetime of the device. This process is also costly as multiple readings are required and potentially time consuming algorithms. Oetjen and Haseley [28] claimed that if T_{ice} (therefore saturation vapour pressure) goes above the critical temperature during this process, there is a risk of meltback or collapse of the product.

3.4.2.6   Cold Plasma Ionisation Device

Gas Plasma Spectroscopy is used to measure the water vapour concentration during the course of the cycle [7]. A commercial device based on this principle is called the Lyotrack [8] introduced by Adixen [5, 57, 117, 118] in 2007 before the company was acquired by Pfeiffer Vacuum in 2010. It was based on optical emission spectroscopy and primarily consists of a plasma generator and an optical spectrometer to analyse the spectrum of light emitted by the rarefied gas plasma to determine the chemistry of the gases. The plasma sensor is used to measure the ratio of water vapour to nitrogen under vacuum conditions.
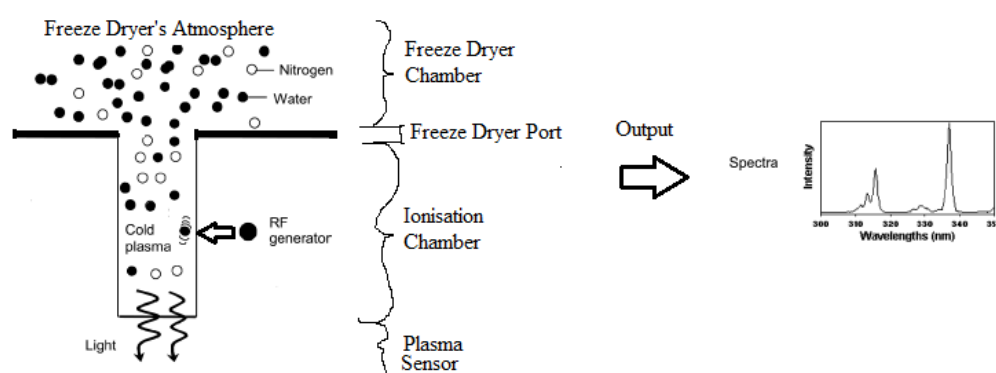
Figure 21 Principle of the cold plasma ionisation device, adapted from Mayeresse et al. [7]

The device consists of a quartz tube which is in contact with the atmosphere inside the lyophilisation chamber. When the pressure is below 3 mbar, a Radio Frequency (RF) source creates the cold plasma within the quartz tube.

The excited atoms or molecules produced when the plasma is formed can then be analysed by the characteristic wavelength each species emits during de-excitation (in order for the atom to return to its initial stable energy level). The point where water vapour begins to decrease indicates the end of primary drying, it was also reported to observe changes in the gas composition during secondary drying[7]. The technology has advantages for use in the manufacturing industry as it has good reproducibility and sensitivity in the product chamber and duct [7, 8], is compatible with steam sterilisation[7] and clean-in-place (CIP). However due to the ionisation involved, radicals can be generated which can cause degradation of the product which limits the use during production runs. This could be problematic for protein products, as the sensor has been shown to likely influence the degradation properties of human growth hormone (hGH) [8]. Positioning of the sensor in the lyophilisation chamber is challenging, particularly when scaling-up from pilot studies[7], as well as calibration cannot be carried out onsite [7].

3.5   Summary

Freeze drying is an expensive process carried out when formulations are unstable in aqueous form and require drying at low temperatures to increase shelf life of the product. The longest phase during freeze drying is the primary drying stage and efforts have been made to optimise this process to reduce cost and increase productivity. To achieve this target, sensors are used within the chambers to monitor changes in gas composition in order to determine the end of sublimation, hence end of primary drying time. Literature has revealed that these sensors fall into two main categories: single vial and batch measurement techniques. Single vial measurement methods involve placing temperature probes into a sample (e.g. thermocouple, glass optical fibre Bragg gratings etc.). This allows the user to track product temperature and determine the end of primary drying time. There are disadvantages to using these devices as the samples containing probes are typically not representative of the entire batch. This is due to probes affecting the ice crystal morphology during the freezing stage, therefore reducing primary drying time of the samples in those vials.

Batch measurement techniques are non-invasive and measure changes in the gas composition of the chamber. These devices tend to be specialised and costly as they are required to track trace quantities of water vapour subliming within the product chamber.

The literature search has revealed that polymer optical fibre sensors (e.g. POFBGs), were not previously reported to have been placed within freeze dryers. Some polymers like PMMA were reported to show an affinity for water vapour and this was felt to be potentially useful for non-invasive detection of sublimation. Additionally, they could potentially provide cost-effective benefits over silica optical fibre sensors (single vial measurement) and some of the batch measurement techniques used for detecting end of primary drying time.

The next chapter documents the theory of operation of optical fibre Bragg grating sensors and discusses polymer optical fibres. The following chapters will discuss the fabrication process and the protocols required to insert the sensors into the chamber. Finally the sensors will be characterised against CPPs in the freeze dryer before being used for a real life test by monitoring the freeze drying of mannitol and native collagen.

4   Optical Fibre Sensor

4.1   Chapter Overview

The previous chapter detailed the current state of technology used by the freeze drying industry and in particular the sensors available to detect the end of primary drying time. That part of the process has the longest duration and therefore the greatest associated operational cost. The literature search in the prior chapter revealed that polymer optical fibres (POF) have not currently been tested in this environment and identified opportunities for application in this area. This is in light of the fact that some polymers like PMMA display a significant affinity for water, which should be useful for tracking sublimation in a freeze dryer. The following chapter provides an overview of the fabrication of optical fibres and fibre Bragg gratings, including important principles of operation. The chapter will conclude by discussing the two types of POF materials used in this research project i.e. PMMA and TOPAS, as well as exploring the advantages and disadvantages of POF.

4.2   Optical Fibres

The refractive index (n) of an optical medium is a dimensionless number defined by the ratio of the velocity of a light wave in vacuum (*c*) to the velocity of a light wave in the medium (*v*) being examined[119], seen in Equation 5.

$$n = \frac{c}{v}$$

Equation 5

Optical fibres are thin cylindrical wave guides that through the process of total internal reflection transmit light through the fibre. They are manufactured from transparent dielectric materials with the core and cladding forming the critical components of that structure. It is then usually surrounded by a buffer (jacket) to provide strength and protection for the critical parts[119].

In a process known as Total Internal Reflection, light waves are carried by the core located at the centre of the fibre, whilst the cladding surrounds and confines the light in the core by having a lower refractive index than that of the core[120] $n_{core} > n_{cladding}$ as seen in Figure 22.
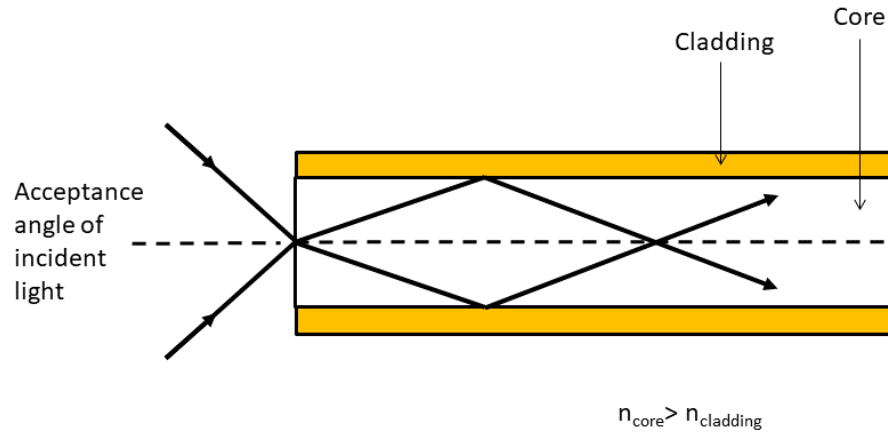
Figure 22 Optical wave guide

During total internal reflection, light propagates through the core when it strikes the core-cladding boundary at an angle (θ) greater than the critical angle (θ_c) with respect to the normal of the interface $\theta_c = \arcsin(n_{cladding}/n_{core})$.

The choice of refractive indices for the core and cladding also define the numerical aperture (NA) and is calculated as follows $NA = (n^2_{core} + n^2_{cladding})^{1/2}$. This number defines the range of incident angles of light waves which can be accepted and propagate through the optical fibre[119, 121], outside of this range light would escape through the core-cladding boundary.

4.2.1   Optical fibre categories

There are several types of optical fibres developed for a variety of different applications and the common ones are illustrated in Figure 23, including how light propagates within them. Depending on their refractive index profiles and dimensions of the cable[119, 122], optical fibres can be categorised as step-index or graded-index, in addition depending on the number of propagating modes as single-mode or multimode fibre. The modes that propagate through the optical fibre are variations in the intensity of light or optical energy, across the length of the fibre and its cross section[122].

Single mode fibres guide a single spatial mode through the waveguide and multimode fibres, which have a larger core than single mode fibres can propagate several modes through the waveguide[119, 121].

Step index fibres possess a uniform refractive index profile in the core with a characteristic sharp decrease in refractive index at the core-cladding interface[119].

4.2.2 Modal dispersion

Depending on the angles of the internally reflected light rays and the number of modes, it has been documented that different modes propagate at different velocities in the medium and begin to spread out the signal over long distances in a phenomena known as modal dispersion[119, 122]. This distortion mechanism occurs in multimode fibres and was a limiting factor in their use in the telecommunications industry. To reduce these effects a graded index fibre with a varying refractive index profile along the cross section of the core was developed[122]. In this situation as the refractive index varies along the path the light takes, a sinusoidal or to be more exact helical propagation of the light is observed[122].
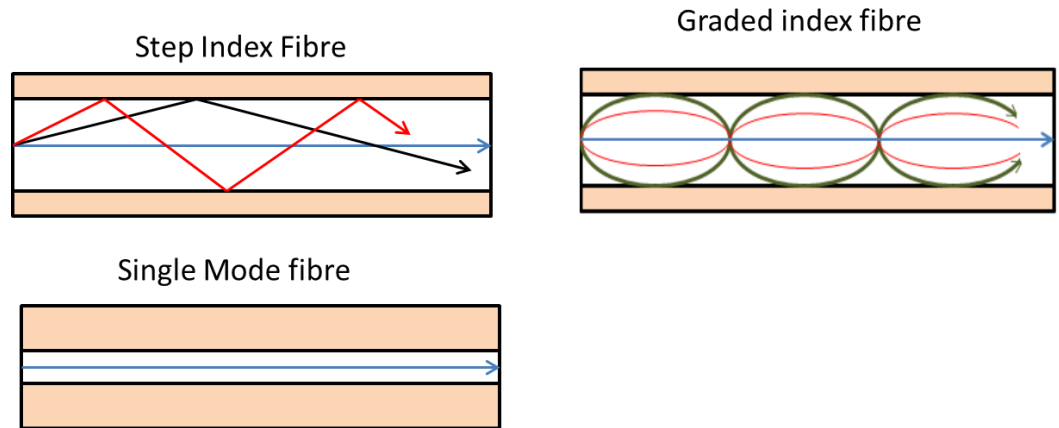
Figure 23 Optical fibres

4.2.3 Microstructured optical fibre

Microstructure polymer optical fibres (mPOF) are designed based on concepts derived from microstructured silica optical fibres and photonic crystal fibres (PCF) technology[123]. These fibres are manufactured by implementing a specific pattern of holes along the cross section of the chosen material, which run along the length of the optical fibre[123]. A schematic representation of the cross section of a typical solid core mPOF is illustrated in Figure 24, where the core is enclosed by a series of tubes containing a gas (e.g. air) in the outer region of the fibre. The presence of the holes (air), lowers the average refractive index profile of the cladding compared to the solid polymer core[124], allowing wave guiding through total internal reflection. It is the arrangement and design of these structures that allows tailoring of these fibres to different applications, including potential in the fields of engineering, sensing and medicine [123, 124].
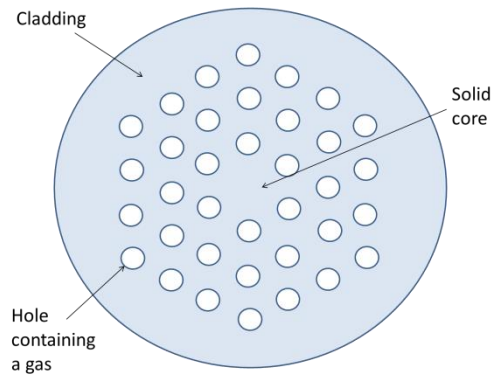
Figure 24 Solid core mPOF

There are two principle mechanisms which govern wave-guiding in microstructured fibres, these are total internal reflection (section 4.2) and/or the photonic band-gap effect[124].

In silica PCF technology, the photonic band-gap (PBG) effect can allow guiding of light in a hollow (air) core due to the highly periodic structure of air holes in the fibre cladding[125]. In this arrangement, the PBG effect may confine specific wavelengths within the core, as it does not allow them to propagate into the cladding[124, 125]. These types of fibres have the advantage of not requiring a difference in the refractive index profile between the core and the cladding as in the case of index guiding fibres[125], which may require different materials, doping or copolymers to achieve total internal reflection. Some current applications for this technology are listed as follows[126]:

- Power delivery
- Pulse shaping and compression
- Sensors
- Nonlinear optics (gas-filled core)

4.3   Gratings in optical fibres

Fibre Bragg Gratings (FBGs) are one of the most common types of commercially available optical sensors. They are used as wavelength specific filters for a transmitted signal or as a wavelength specific reflector, depending on the requirements of the system.

FBGs are typically created using an ultraviolet (UV) source to inscribe modulations in the refractive index into the core, which can be periodic or aperiodic depending on the requirements of the system. This exposure increases the refractive index of the core and produces a grating whose properties are dependent on the exposure pattern[127]. As light propagates through the optical fibre, see Figure 25, it

encounters changes in the refractive index this leads to a small quantity being reflected at each boundary. The reflected spectrum (Bragg response) in Equation 6 has a centre wavelength known as the Bragg wavelength (λ_b), where Λ is spatial period of the grating and n is the effective refractive index of the guided mode.

$$\lambda_b = 2n_{eff}\Lambda$$

Equation 6

External factors (temperature, pressure, strain[128, 129]) can lead to changes in the refractive index and the geometry of the fibre resulting in a shift in the Bragg wavelength. The reflected spectrum can then be examined using an interrogator.
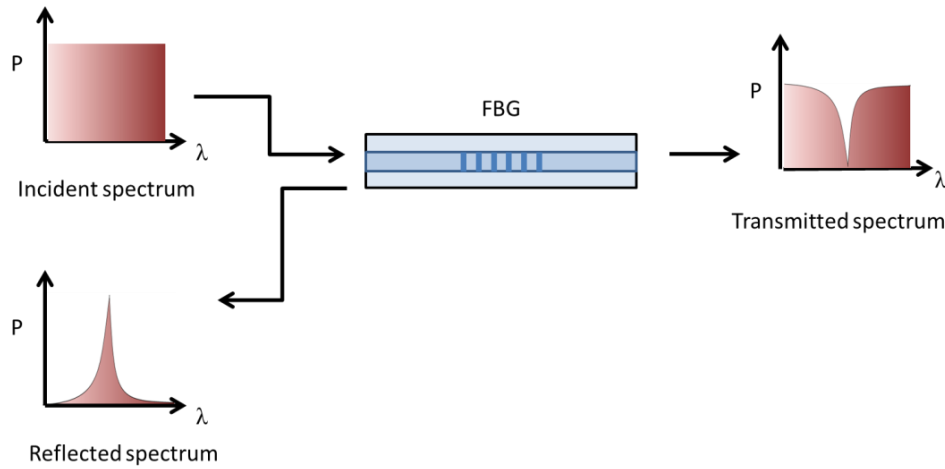
Figure 25 illustration of the operating principle of a Fibre Bragg Grating (FBG) in an optical waveguide

In this project the interrogation system will monitor the shift in the Bragg wavelength of the reflected spectrum, as it shifts depending on changes in parameters such as temperature, pressure and in the case of some polymer optical fibres (POFs) like PMMA, humidity [12]. The individual effects of temperature, pressure and humidity on the Bragg wavelength of the polymer optical fibre Bragg gratings (POFBGs) used in this project (PMMA and TOPAS based); will be covered in chapters 6, 7 and 8 respectively.

FBGs have advantages as sensors in that they can be multiplexed to form large linear sensing arrays[130, 131] and are immune to electromagnetic interference. The most common multiplexing techniques used to interrogate the FBGs are time division multiplexing (TDM)[130, 131] and wavelength division multiplexing (WDM)[119, 130].

Provided each grating has a different Bragg wavelength, multiple gratings can be inscribed onto a single optical fibre and interrogated simultaneously using a WDM system[128, 130]. To detect the Bragg wavelengths in this system, the combination of a tuneable swept-wavelength light-source and photodiode detectors or a

broadband light-source and a spectrometer are used to interrogate the FBG array[130].

The other system used is TDM, which uses a pulsed broadband light-source and identifies the gratings in the array by measuring the time taken for their reflected signal to arrive at the detector[130]. The time that the signal is received depends on the location of the grating along the fibre.

4.3.1 Applications of FBG

FBGs were initially found in applications for optical communications devices[121] but have in recent years been used as sensing elements. Early sensors were designed as packaged gratings or embedded sensors, to operate as single-point sensing elements that detect changes in parameters in the local region of the grating e.g. temperature, pressure and strain[132, 133]. The market is now focusing on greater functionality and value for money by demanding greater mechanical strength and multiple sensing points.

In order for industry to adopt this technology, it is essential that there is a significant cost reduction in the associated interrogating systems, standardisation of the sensors, multiple gratings and the development of niche specific packaging for these devices. FBG based sensors have been developed and installed in a wide variety of sensing applications (Table 4-A), such as structural health monitoring of civil engineering structures (tunnels, bridges, dams etc)[128].

New trends are emerging that involve developing niche sensors for biological, chemical and medical applications using specially developed coatings, reagents and different polymer composites[92].

Civil Engineering	Oil and Gas Industry	Other fields	Marine industry	Aerospace
Bridges[134], buildings, dams, roads, flyovers, water treatment plans, turbines, rail monitoring, tunnels, land-slides[135]	Oil and gas production and transportation, oil rigs, oil wells.	Sport equipment and textile monitoring[15], electric power systems, non-destructive testing, structural health monitoring (SHM)[136]	Offshore platforms, harbour structures, SHM of Liquefied Natural Gas (LNG) pressure compartments, ship hulls and sails[137]	Vibration monitoring and SHM, airplane wings, space stations, aircraft runway

Table 4-A applications of FBG sensors[92, 128, 129, 138-140]

4.3.2 Fabrication of Fibre Bragg Gratings (FBGs) in Optical fibres

There are several techniques involving a UV beam from a laser source, which can obtain the desired periodic modulation in refractive index in the core of the optical fibre. These techniques are generally classified into two categories: internally written or externally written gratings.

Internally written gratings

Internally written gratings are created when a laser is launched into the optical fibre, in the case of Hill et al [141, 142] an argon ion laser operating at 488nm or 514.5nm was launched into germanium doped silica optical fibre and created a periodic modulation in the refractive index of the core.

The disadvantage of using this method is that the Bragg wavelength produced is limited to the inscription wavelength, for silica around 488nm or 514.5nm and POF around 325nm. Another factor that limits the application of this technique for FBG inscription in POF is the absorbance of the polymer in the 325nm region, which limits the propagation of light to a few centimetres[143] and the size of the final sensor.

Externally written gratings

Externally written gratings tend to use optical interference techniques to create the desired change in refractive index in the core of the optical fibre.

1. *Amplitude splitting Interferometry*

A two beam interference technique can be used to produce a FBG; this involves splitting the UV inscription beam with a beam splitter into two beams of equal intensity, which are then recombined using mirrors to create an interference pattern in the core of the optical fibre[144]. The advantages include a range of output Bragg wavelengths by controlling the angle between the recombining beams[143]; however the optical components are vulnerable to mechanical vibrations which can deform the interference pattern[143].

2. *Wavefront splitting interferometry*

This technique exposes the optical fibre to an interference pattern which creates a grating in the core of the optical fibre. There are two configurations which are used to fabricate Bragg gratings including the prism interferometer[145] and the Lloyd's mirror interferometer[129, 146]. These instruments operate on the principle that a collimated UV beam has been directed to a reflective surface (mirror or prism edge), in order to cause half of the beam to be reflected and to cross over the other half of the incident beam, which has the optical fibre in its path. The process of overlapping part of the beam from the UV source on to the rest of the transmitted beam produces an interference fringe pattern in that region, which can be focused into the core of the optical fibre using a cylindrical lens. The advantages of using this technique include the reduced optical path and optical components, which allows better quality of the grating to be achieved as the system is less influenced by environmental factors. The disadvantages of this system include a limit on the size of the grating to half the width of the incident UV beam, along with the tuning range of the Bragg wavelength being limited by the arrangement of the interferometer.

3. *Point-by-point*

This technique fabricates individual grating planes using a pulsed laser system to create point changes in the refractive index of the optical fibre[147-149]. The optical fibre is then translated along the fibre axis by the distance of the desired period of the final grating, before carrying out another pulse to locally change the refractive index[129]. This technology allows the fabrication of a large range of grating periods;

however this system requires long duration times as each plane needs to be individually fabricated.

4. Phase Mask Technique

This is a commercially used method to fabricate Bragg gratings[127, 150] in optical fibres[151]. This process involves a phase mask which diffracts the incident beam into several orders which then combine to produce an interference pattern in the optical fibre[119].

Generally the phase mask is a fused silica plate, which has a periodic surface relief pattern[15, 119, 143] and can be produced using either electron beam lithography or holography[129]. This pattern has an etching depth D and a period Λ[15, 119].

As the phase mask is placed in close contact to the optical fibre, it increases the stability and reproducibility of the system in order to produce the required periodic variations in the refractive index and consequently Bragg gratings[129]. As the period of the phase mask determines the Bragg wavelength, several expensive phase masks are required in order to produce a range of operational wavelengths.

4.3.3 **Photosensitivity in Polymer Optical Fibres**

Studies have been conducted into mechanisms responsible for the formation of periodic structures or changes in optical properties of polymers due to irradiation. There are several mechanisms known to have altered birefringence and/or refractive index (e.g. to form Bragg gratings) in polymers, they are discussed in Table 4-B. Polymerisation could be one of the mechanisms triggered in these situations, which is a process that involves the linking of monomer molecules to form long chains called macromolecules[152].

Mechanism	Photo-polymerisation [153, 154]	Photo-isomerisation [153]	Photo-cross-linking [153]	Photo-degradation (photolysis) [153]
Method	Free radicals produced under irradiation (UV laser) may react with existing monomers in the polymer, increasing the refractive index[154].	Isomerisation process triggered by irradiation, could change refractive index e.g. irradiation of trans-4-stilbenemethanol with 325nm initiates isomerization and lowers the refractive index[153]	Irradiation causes polymer chain-cross linking and increases material density (densification), this changes the refractive index.[154, 155]	Change of the polymer structure due to irradiation. The polymer could be doped or un-doped.
Process to induce change	The free radicals react with the residual monomers in the polymer. This process causes polymerization; however there may be long term stability issues and in-homogeneity in the resulting polymer.	Speciality fibres doped with specific isomer (cost). Changes in isomer states e.g. trans-cis isomers (isomerisation), may lead to different physical and/or chemical properties	Functional side chain, which can be activated if needed (e.g. by oxidising PMMA). These can then be irradiated to induce cross linking. If used the oxidation process may reduce long term stability. [153]	• Oxidation process (in oxygen rich environment) • Chain-scission

Table 4-B Mechanisms that alter birefringence and/or refractive index in polymers[15, 156]

4.4   Polymer optical fibre

Polymer optical fibres are typically used for applications such as short range data communication (e.g. homes, cars) and for illumination, as they are mechanically more robust and a more cost-effective solution in these cases than glass optical fibres (e.g. easier handling and installation)[121, 157].

Commercial polymer optical fibres are typically manufactured on mass from poly (methyl-methacrylate)[121]. For specialised applications, other materials can be used depending on the desired POF characteristics, examples include polystyrene (PS)[158], polycarbonate (PC)[158] and TOPAS. Figure 26 shows the chemical structures of these materials[158-161].

PC is suitable for use in high ambient temperatures applications (e.g. vehicles), however it is worth noting that the polymer possess higher optical attenuation than PMMA[158, 160]. TOPAS has no monomers, is humidity insensitive and has excellent biocompatibility making it suitable for bio-sensing applications [18, 162].

Aston University

Illustration removed for copyright restrictions

Figure 26 Chemical structures of materials used in POF where (A) PMMA, (B) TOPAS, (C)polystyrene and (D) polycarbonate[152, 158, 159]

Depending on the requirements of the POF, the refractive index could be modified with the addition of a co-monomer to the base monomer (co-polymerisation) [163] or the addition of a compound (dopant)[119, 163] that is appropriately dispersed in the material without forming a bond to it. Dopants should not be susceptible to out-diffusion over time as this would change the optical properties[163], additionally they

can change the glass transition temperature[163, 164], therefore affecting the service temperature of the polymer.

4.4.1 Poly (methyl methacrylate) (PMMA)

Polymers from the methacrylate family, possess properties that allow their use in a variety of different applications, in particular for PMMA these include[152]:

- Good weathering properties
- High transparency
- Good optical properties
- Rigidity and toughness
- Have poor insulating properties
- Have poor resistance to organic solvents

These properties allow PMMA to be used in display signs[152], as a building material and as a data communications medium[121, 159].

The material has a typical T_g of 105°C[165], a refractive index of 1.49[158], a melting temperature range between 120-160°C[152] and a drawing temperature in the region of 190-280°C[158, 159], making the material an attractive choice in POF fabrication. Additionally PMMA has a lower density (1.16-1.20 g/cm^3) [152, 166] than silica (2.2 g/cm^3)[166], resulting in lighter optical fibres.

PMMA POFBGs have been used in sensing applications to monitor temperature, strain, pressure and humidity[12-15]. As a result of the polymers affinity for water (1.6% to 2% in weight[14]), which results in swelling of the fibre[16, 17], it will be used in this project to monitor sublimation of water vapour within the freeze dryer.

4.4.2 TOPAS cyclic olefin copolymers (COC)

TOPAS COC is an amorphous, transparent copolymer and can be customised by varying the chemical structure of the copolymer[161]. Copolymers are produced through the process of co-polymerisation of two different monomer species in order to form a polymer chain[152].

TOPAS COC is used in industrial applications for the packaging of diagnostic disposables, pharmaceuticals and medical devices, as well as production of transparent moulds and optical components(e.g. lenses, sensors)[161].

Some of the advantages of using TOPAS COC include [18, 161]:

- Low water absorption of <0.01% (24hr immersion at 23°C)
- High transparency
- Good electrical insulating properties

- Transmission of light in the visible spectrum and having a refractive index (1.53), making the polymer suitable for optical applications
- High strength, rigidity and hardness
- Low density
- Biocompatibility, for medical applications
- Good chemical resistance properties to acids, alkalis and solvents such as methanol

4.4.3 Hysteresis

Hysteresis is a history dependent phenomenon observed in materials which have a characteristic delay or lag which occurs during cyclic loading, i.e. applying and removing the force acting on the material. Hysteresis has been observed in viscoelastic polymers like PMMA. This was observed in PMMA POFBG sensors [167, 168], where techniques such as annealing have been implemented to reduce the effects of hysteresis in POFBG sensors[143, 169, 170].
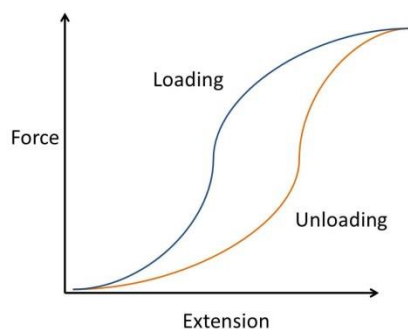
Figure 27 schematic representation of hysteresis

4.4.4 Attenuation in optical fibres

The current market applications for plastic optical fibres require materials that minimise the optical attenuation and this section discusses optical losses in POF, the mechanisms that contribute to that attenuation, as well as techniques implemented to reduce them.

The wavelength dependent losses are considerably higher for POF than conventional silica optical fibres (SOF). Telecommunication systems operate in the spectral regions where the lowest attenuation is observed, for silica they are in the 1300nm or 1500nm spectral regions, while POFs typically operate in the visible

spectral region (generally 550 – 650nm)[121, 143, 158, 159]. Outside of these regions, particularly for POF, losses rise significantly to a point where operation may no longer be practical.

POF are used for data transportation in some military applications and niche areas of the telecommunications, automotive, and aerospace industries[92, 159, 160, 171] where they have replaced SOF because they are more economical, easier to handle and flexible.

The attenuation of an optical fibre is defined as the loss in the intensity of the optical power as light waves propagate through that media. The attenuation coefficient β (dB/km)[158, 172] in Equation 7, is the ratio between the input optical power (P_{in}) and the optical power output (P_{out}) after the light propagated a distance ("l" in km) along the fibre.

$$\beta = \frac{10}{l} log_{10} \left(\frac{P_{in}}{P_{out}} \right)$$

Equation 7

The main factors which lead to attenuation losses are absorption and scattering of light which are affected by the material properties, fibre structure and the propagating wavelength. The losses can be separated into two categories, known as intrinsic and extrinsic losses[121, 160, 171], which are summarised in Table 4-C below.

Intrinsic losses		Extrinsic losses	
Absorption	**Scattering**	**Absorption**	**Scattering**
Carbon-hydrogen bond vibration	Random density fluctuations	Contamination by organic compounds	Fluctuations in core diameter
Electronic transition	Variation in composition or refractive index	Absorbed water	Micro-fractures or cracks, dust and voids or bubbles in the fibre
	Changes in molecular orientation		Core-cladding boundary imperfections

Table 4-C sources of attenuation in polymer optical fibres[160]

<u>Intrinsic losses</u>

Intrinsic losses are the most significant source of loss in a POF[160, 171], they occur due to material absorption and Rayleigh scattering which are both dependent on the structure of the material.

- Absorption in optical fibres occurs due to the electronic transitions and vibrations of molecular groups within the material[121]. Electronic transitions result from exciting electrons with photons that allow their transition from a lower energy state to a higher energy level. Absorption overtones also result in optical losses in POF materials (PMMA, PC and PS) due to absorption of carbon-hydrogen (C-H) bonds [143, 159, 171] for vibration or rotation. Literature has shown that these losses could be reduced if the hydrogen atoms were replaced with heavier atoms like: chlorine, fluorine[159] and deuterium[160].
- Rayleigh scattering[121, 159] in optical fibres is the result of random density fluctuations as well as variation in composition and molecular orientation.

<u>Extrinsic losses</u>

Extrinsic losses are associated with imperfections in the POF, likely created during the fabrication stage or during fibre handling e.g. poor winding practices which damage the POF. These imperfections could be introduced due to the mechanical conditions of the manufacturing plant environment as well as temperature of the fibre drawing process[160]. They can include contaminants in the core as well as physical imperfections such as micro voids, cracks and core-cladding boundary imperfections[121, 160]. These act as scattering centres and depending on their size, would determine the scattering mechanism[171].

<u>Scattering</u>

Light scattering in optical fibres can be classified into two categories: microscopic and macroscopic scattering[160, 172].

Microscopic scattering is mainly caused by variations in composition, molecular orientation and density of the polymer material, which can cause two types of scattering. These are Rayleigh scattering and Mie scattering.

- Rayleigh scattering occurs when the light hits particles or defects that are less than a tenth of the wavelength of light[160, 171, 172].
- Mie scattering refers to scattering by particles equivalent or greater than one-tenth of the wavelength[160, 172].

Macroscopic scattering, also known as bulk scattering is the result of imperfections such as micro-bends, micro-cracks and micro-voids within the fibre[160, 171]. They can be introduced into the fibre during the drawing process[160], along with other imperfections from dust contamination, core-cladding boundary imperfections, core diameter fluctuations and orientation birefringence. Micro-voids, micro-cracks and dust within the fibre are capable of acting as scattering centres, where the scattering mechanism is dependent on the physical size of the imperfection.

4.4.5 Advantages and disadvantages of POF

Table 4-D compares the advantages and disadvantages of using POF for transmission of data and sensing applications:

POF vs silica optical fibre		POF vs copper cables	
Advantages	Disadvantages	Advantages[160]	Disadvantages
High ductility, low Young's modulus[160] for strain sensing applications	Significantly higher attenuation, limiting operating distance	Resistance to harsh environments (moisture, acid, base, oils, and some organic solvents)	Longer installation times. Precision equipment and training required
Resistance to impact and vibrations.[160]	Elevated temperatures and humidity can artificially age polymers[173]	Insensitive to electromagnetic interference	
Biocompatible e.g. for in-vivo applications[173]	Lower temperature operating range (<70°C vs <480°C) [174]	Portable, small size and light weight (important factor for applications in the automotive industry)	
Low production and component[157] costs.	Hysteresis occurs at high strain due to POFs viscoelastic nature	Material cost	
High fracture toughness [173, 175]			

Table 4-D advantages and disadvantages of POF

4.5   Summary

This chapter provided an overview of the important principles of operation of optical fibres and fibre Bragg gratings, as well as the methods used to fabricate them with a specific emphasis on polymer optical fibres that will be used in this project. The two types of POF materials used in this research project were also discussed (PMMA and TOPAS), as well as exploring the advantages and disadvantages of POF. The next chapter will discuss the fabrication process of the sensors that will be used in this project, as well as the customised environmental chamber rigs required to place and characterise the polymer optical fibres in the freeze dryer. As FBGs are influenced by several environmental factors, the POFBGs were initially characterised against the CPPs within the freeze dryer (temperature, pressure, humidity), before testing their ability to monitor freeze drying cycles and sublimation.

5 Methods and Materials

5.1 Chapter Overview

One of the main objectives of this thesis is to determine if Polymer Optical Fibre Bragg Grating (POFBG) technology could be used to detect sublimation and the end of primary drying time for pharmaceutical applications. This would involve inserting devices into the freeze drier and characterising the sensors to Critical Process Parameters (CPPs), before using the POFBGs to monitor the freeze drying process of pharmaceutical and biological samples.

This chapter lists the methods used to fabricate the POFBGs and assemble the sensors in the environmental chambers (including freeze dryer). The next chapters (6 to 8) will discuss the experiments designed to characterise the sensors to temperature, pressure and humidity, using the protocols outlined in this chapter. This chapter will initially describe the standard phase mask technique that was used to inscribe Fibre Bragg Gratings (FBGs) operating in reflection in the 1550nm region into step index Polymer Optical Fibres (POFs). The next section discusses the pigtailing technique and interrogation system, which allows the characterisation of the optical response of the FBG. The chapter will finish by describing the customised rigs developed following standard safety protocols, in order to incorporate these sensors into the freeze dryer and climatic chamber. To this author's knowledge, POFBGs were not previously reported to have been placed within freeze dryers, which are designed for dying samples and not as machines to characterise sensors. Therefore a new protocol was devised with modifications to the existing chamber such as feedthroughs, in order to accommodate the different types of sensors.

5.2 Polymer Optical Fibre Sensors manufacturing process

5.2.1 Polymer Optical Fibre Preparation

5.2.1.1 Polymer Optical Fibres

The effects of critical process parameters on polymer fibre Bragg gratings in climate chambers were investigated using POF manufactured according to Table 5-A, in which FBGs were later inscribed at Aston University. The inscription time refers to the time when the grating reached saturation and stopped growing; the UV beam

was subsequently switched off to avoid overexposure. In the freeze drying project, the humidity sensitive PMMA fibres were compared against humidity insensitive fibres formed from TOPAS[12, 18] and Zeonex materials, in order to determine if sublimation could be tracked by PMMA fibres during a cycle with pharmaceutical samples.

POF	PMMA	TOPAS
Material	Substantially PMMA Core: PMMA, EMA and BzMA Cladding: PMMA and EMA	Core: high Tg TOPAS (134ºC) Cladding: Zeonex 480R
Fibre Name	F15E and F1F*	-
Structure	Step index fibre	Step index fibre
Annealed	No (unless specifically noted*)	No
Type	Single mode (SM) fibre	Multimode (MM) fibre
Dimension specifications	Outer Diameter: ≈120 µm Core diameter: ≈7 µm	Outer Diameter: ≈170µm Core Diameter: ≈20µm
Inscription time (He-Cd laser)	Doped (photosensitive) fibre 7-15minutes	Un-doped fibre 90 to 150 minutes
Water absorption	1.6% to 2% in weight[14] 2% at 23°C[12]	TOPAS: 0.01% at 23°C[176] Zeonex 480R: <0.01%[177]
POF manufacturer	Prof. Gang-Ding Peng, University of New South Wales (UNSW), Sydney, Australia	Technological University of Denmark (TDU)

*Table 5-A Properties of Polymer Optical Fibres used in the experiments. F15E and F1F are PMMA based POFs obtained from different sections of the same spool. Only *F1F fibres were annealed prior to FBG inscription in an oven at 80ºC for 7hrs[178]*

5.2.1.2 Light Microscopy

The fibre diameters were measured using a Carl Zeiss microscope (Axioskop2 *mot plus*) with a camera system (AxioCam HRC) and imaging software (Axiovision version 4.8). Polyamide tapes were used to secure the POF to a glass microscope slide (VWR, UK) as shown in Figure 28. Samples were viewed at magnifications of x10 eyepiece and x10 or x20 objective lens. Images were taken in the vicinity of the inscribed Fibre Bragg Grating.
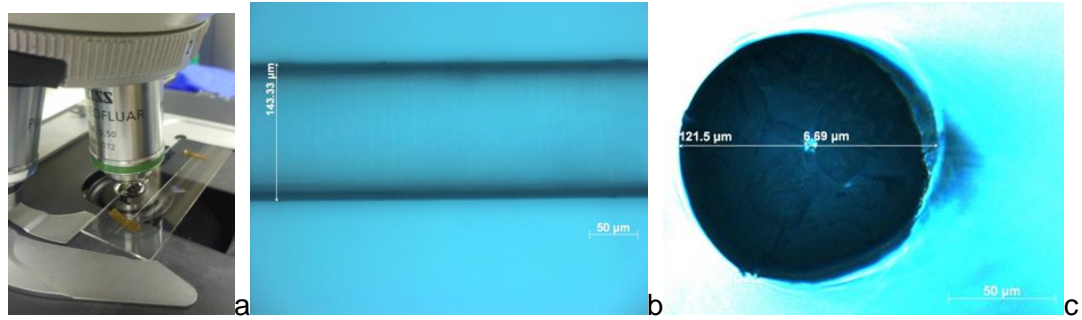
Figure 28 (a)POF secured to slide (b)TOPAS/Zeonex fibre x20objective lens, scale 50μm
(c)PMMA fibre x40objective lens, scale 50μm

5.2.1.3 Cleaving Optical Fibres

Due to the availability of a portable, commercially manufactured light-source and
I-MON interrogator operating in the 1550nm region (section 5.5); gratings were
inscribed that reflect wavelengths in this range to permit inspection of POFBGs in
the freeze dryer and environmental chamber.

Literature has shown a large number of Bragg gratings fabricated into PMMA optical
fibres to reflect wavelengths in the 1500nm range[154, 178-181]. Unfortunately, high
attenuation (section 4.4.4) is present within this region[159, 171, 182], for PMMA
between ~50dB/m at 1530nm to ~100dB/m at 1590nm[178, 183] and TOPAS having
70dB/m at 1550nm[143, 184]. As a result, short lengths of fibre <10cm were used in
this project to reduce losses and ensure reflected gratings could be measured using
the interrogation units.

The gratings were positioned ~2cm away from the butt coupled end which was
connected through a silica pigtail to the interrogation unit. Generally small lengths of
POF would limit the applications of sensors that operate in the 1550nm region;
however a splicing technique (section 5.3) was used to allow the sensor to be
extended into the environmental chambers and remain connected to the
interrogation unit. Silica fibre pigtails/cables were used as silica has significantly
smaller attenuation in this wavelength region than POF, within the range of 0.17-
0.18dB/km at 1550nm[185]. The shorter length of POF proved beneficial, as the
freeze dryer's shelf size had a limited product capacity, where too long fibres could
restrict the quantity of samples which could be freeze dried in a given timeframe,
reducing commercial productivity.

To ensure effective butt-coupling when producing gratings and UV gluing, it is vital
to have the end faces of the <10cm long polymer optical fibres cleaved as efficiently
as possible to reduce losses. The optical fibre ends were cleaved on a hotplate at
80°C using a 80°C hot blade[186, 187] (Gillette super thin platinum). Care had to be

taken to ensure a good cut was achieved, as the following can affect the quality of the coupling joint: razor blade sharpness and thickness, incorrect temperature, cleaving angle, debris or particulate accumulation on the tip of the POF and vibrations. In the worst case, losses and surface roughness would not allow coupling between the cores in order to carry out inscription or UV gluing.

5.2.2 Fibre Bragg Grating Inscription procedure

Once the optical fibres had been cleaved, the FBG fabrication procedure known as the phase mask technique (Figure 29) was used to inscribe Bragg gratings into all POFs[15, 129, 179]. This process was chosen as the optical setup needs to be kept incredibly stable during inscription. As long inscription times can be expected with POF[143, 178], this set-up provided stability and was not influenced by mechanical vibrations, which could affect the grating structure. Using a phase mask, diffracted beams have a small optical path to travel before recombining to produce a desired interference pattern in the fibre thereby reducing the influence of mechanical vibrations.

The inscription times required vary depending on the properties of the POF material and whether the core was previously doped. For an un-doped PMMA POF, the technique has a minimum inscription time of 40-60 minutes[143, 168, 178], whilst for doped PMMA fibres the inscription time can reduce to the order of 7-12 minutes. Maintaining the stability of these fibres is considerably more demanding than during the fabrication of FBGs in germanium doped silica optical fibres, which require short inscription times in the region of 20 to 180 seconds[143, 188, 189].
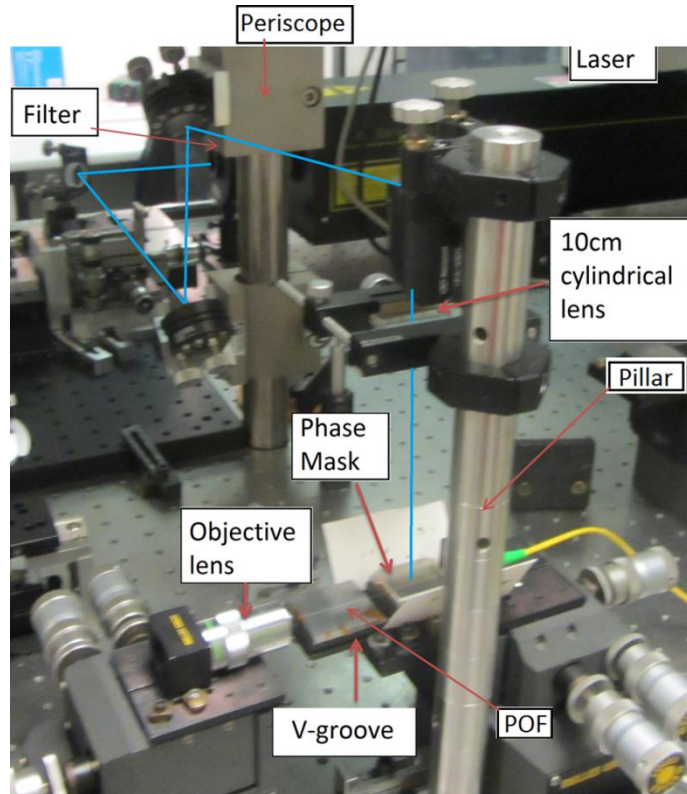
Figure 29 Polymer Optical Fibre Bragg Grating inscription set-up fixed to the optical table

The vertical beam inscription set-up in Figure 29 was used to fabricate the FBGs, the image illustrates the UV beam (blue line) being directed to the Polymer Optical Fibre (POF) on the v-grooves.

The cleaved POF was secured to the v-groove plates with polyamide tapes and mounted to a Melles Griot XYZ translation stage[143, 178] to keep it immobile, stabile and allow alignment with the core for inscription by[178, 179]:

- Preventing sagging caused by heat from the UV laser beam and long term suspension of the POF in mid-air held between clamps (this technique is used in silica optical fibre and the POF inscription system in 5.2.3).
- Reducing displacement of the POF from air currents, fibre curling or vibrations

In order to track the fabrication of the POFBGs, a silica optical fibre (SOF) pigtail (FC/APC) with polymer index matching gel (RI = 1.4917) applied to the ferrule, was butt coupled to one end of the cleaved POF. Figure 30 and Figure 31 show the coupling of the silica pigtail to the POF, which is overhanging the v-groove by 1mm. The index matching gel was used to reduce transmission losses caused by Fresnel reflections that occur at the interface between the silica connector and polymer optical fibre[179, 180].

The alignment of the silica pigtail (FC/APC) was adjusted using the XYZ translation stage, a 635nm visible red laser diode fibre optic fault locator (Oz Optics FODL-23S-635-1) and a x20 microscope objective lens (Photon Control). These components were used to monitor the propagation of red light through the optical fibre and determine when light was observed to be guiding through the core (Figure 31(b)). The screen in Figure 30, facilitated monitoring of the light projected from the POF, to allow the user to determine when optimum core guidance was achieved, as seen by Figure 31(b). At this stage, the red laser was removed from the assembly and the silica pigtail was coupled to the broadband light source and Optical Spectrum Analyser (OSA) as shown in Figure 30. The phase mask (period of 1034.20nm or 1061.18nm from Ibsen Photonics) could then be placed on top of the optical fibre[143] as shown in Figure 31(a), followed by opening the UV beam shutter to begin FBG inscription.
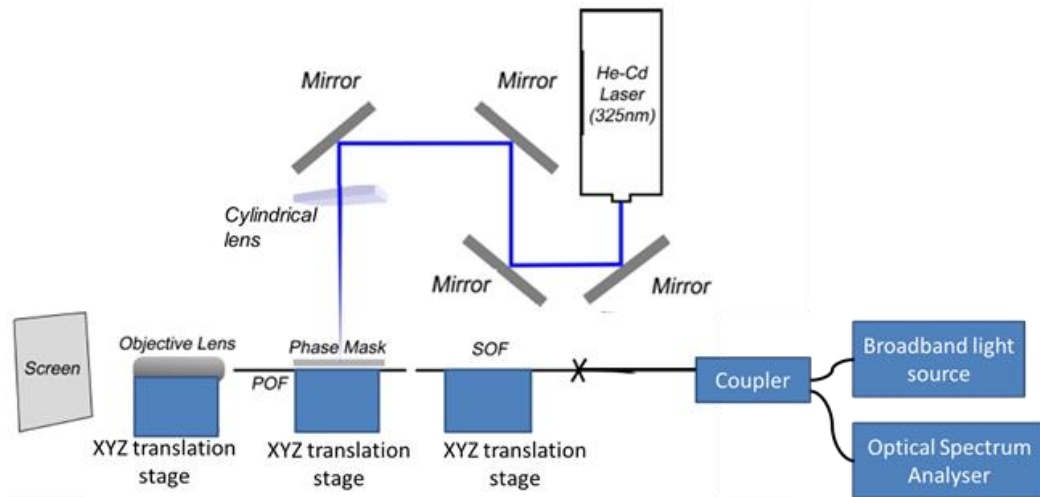
Figure 30 FBG inscription arrangement on the optical table

The phase mask with a pitch of 1034.20nm was used to inscribe a grating into TOPAS core fibre to reflect wavelengths in the 1560nm range. For PMMA, the phase mask with a period of 1034.20nm inscribed gratings that reflect wavelengths in the 1530nm range and phase mask with a pitch of 1061.18nm produces a grating which filters wavelengths in the 1570nm range. These combinations were chosen in order to obtain gratings that will reflect wavelengths within the operating range of the broadband light source, which can then be detected by the interrogator (OSA or the IBSEN I-MON 400E and 512 USB).

(a)

(b)
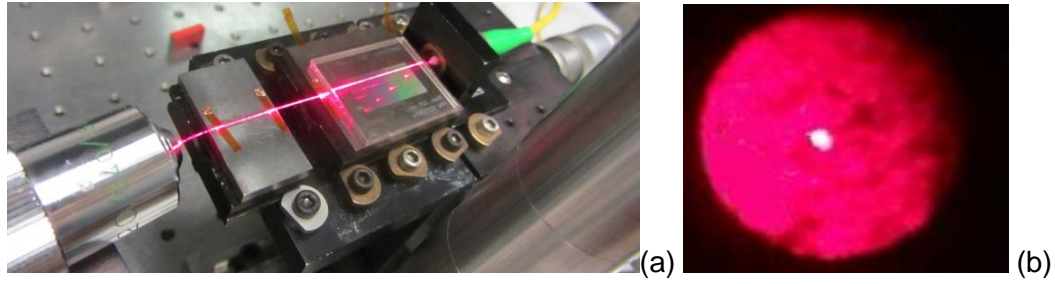
Figure 31 (a) POF taped to v-grooves and butt-coupled to a SM silica optical fibre. (b) Picture of the projected end-face of the SM step index POF onto a white screen placed behind the objective lens, showing the cladding and a bright core in the centre of the optical fibre.

To track the reflected Bragg grating response (Figure 32), the POF was butt coupled to a silica fibre connected through a 2x2 1550nm Corning single mode (SM) 50:50 silica coupler (9/125µm) to a broadband light source (BBS) and an optical spectrum analyser (OSA):

- Thorlabs ASE-FL7002-C4 5mW, erbium white broadband light source operating in the spectral range of 1.53-1.61µm
- Hewlett Packard HP 70951B optical spectrum analyser (OSA)
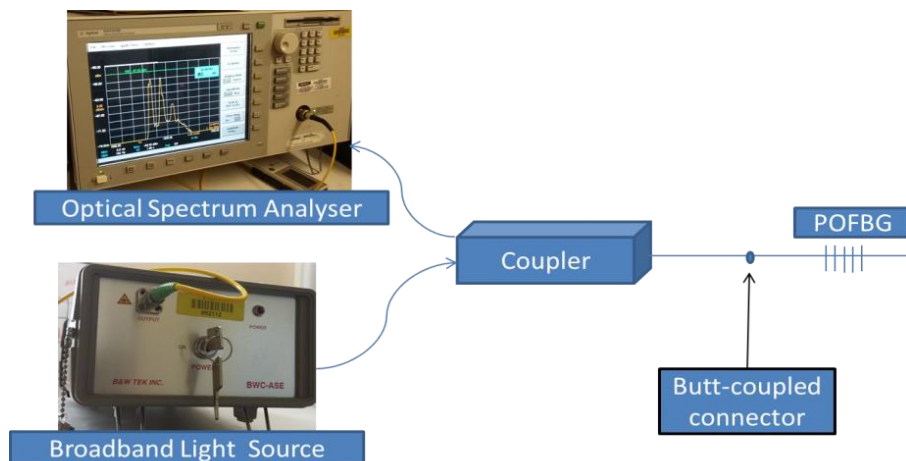
Figure 32 Schematic of the POFBG interrogation system

The shutter of a CW 325nm[178, 180] helium cadmium (HeCd) laser (from Kimmon Koha Co, Ltd, IK3301R-G) with an optical power output of 30mW was opened at this stage. Mirrors on periscope and pillar components (max height of beam ≈40cm) directed the UV beam (Figure 29), until it was perpendicular to the optical bench and aimed vertically down onto the POF taped onto the v-groove plate[143].
The UV beam passes through a 10cm focal length plano-convex cylindrical lens[179] and the phase mask, where the diffracted orders project an interference pattern into the core of the fibre resulting in periodic changes in the refractive index[153]. The alignment of the beam with the core was monitored through reflection back scattering[143, 180] as seen in Figure 33. For this system a 1.8mm

long grating was inscribed due to the width of this UV beam. During the fabrication process when a decrease in the growth of the reflected Bragg grating was observed on the OSA, the process was stopped to prevent UV over-exposure which can lead to a broadening/increase in the bandwidth of the Bragg grating.

Figure 33 Reflection fringe scattering from the POF fibre

Typical inscription times for these fibres are listed in Table 5-A, with doped SM SI PMMA POF taking 7-15min to inscribe, whilst un-doped MM SI TOPAS took 90-150min in order to approach maximum grating reflectivity.

Once the grating had been inscribed (e.g. Figure 34), the POFs were each glued to silica pigtails (section 5.2.2) and placed into a housing (section 5.3). The Bragg gratings in reflection were captured using a PC with the LABVIEW OSA capture.vi software (National Instruments vs7.1 2004), which interfaced with the OSA.
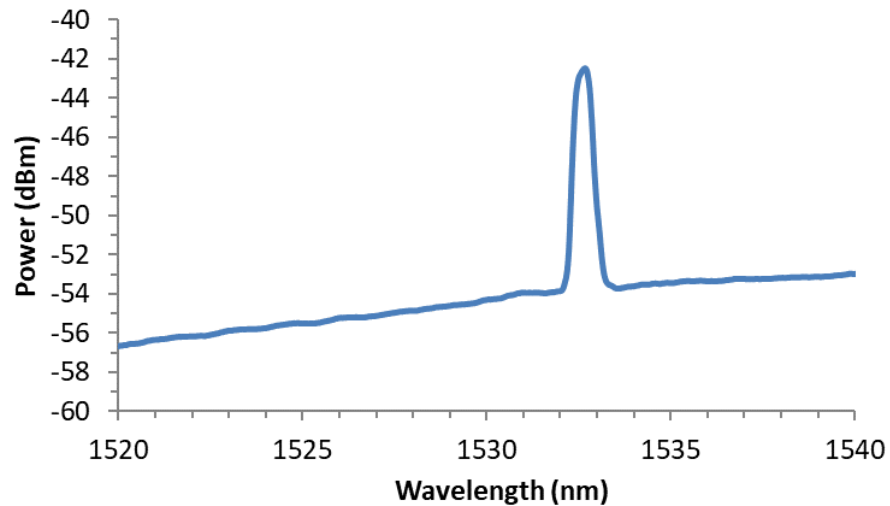
Figure 34 Reflection spectrum of an annealed single-mode F1F PMMA, POFBG produced using a phase mask period: 1034.20nm, peak signal: 1532.6nm, FWHM: 0.5nm, 11dB above the noise floor, outer diameter: 117μm

The FBGs were analysed using the centroid calculation in Equation 8 [143], where the Bragg wavelength λ_b was obtained from data points of the reflected spectrum that were within 3dB of the peak value[143]. In the centroid calculation, λ_i is the

wavelength (nm) of the data point and P_i the optical power (dBm)[143]. At this stage the POFBGs were placed into the environmental chamber and freeze dryer to carry out a series of experiments.

$$\lambda_b = \frac{\sum \lambda_i P_i}{\sum P_i}$$

Equation 8

5.2.3 Second Fibre Bragg Grating Inscription procedure

As part of a collaboration between UNSW (Australia) and Aston University (UK), a secondment took place whereby:

1. Training would take place on the high pressure instrumentation system owned by UNSW, to allow characterisation work of sensors under high pressure complementing vacuum experiments in Aston University

2. FBG sensors would be produced using the UNSW inscription setup and brought back to Aston University to be tested in the Freeze Dryer. Training and assistance was provided by Mr Kishore Bhowmik of UNSW.

Figure 35 illustrates the inscription setup used in UNSW to produce 10mm long POFBGs, using a phase mask (pitch=1030nm) and an almost identical standard operating procedure (SOP)[190] to that described in sections 5.2.1 and 5.2.2. The following differences were identified between the two set-ups: the POF was suspended in mid-air (Figure 36) whist section 5.2.2 discussed the grating being fixed to a v-groove (Figure 31). Other differences included: paraffin-oil was used instead of index matching gel, inscription timeframe was between 4-10min and length of the grating produced(10mm against 1.8mm).
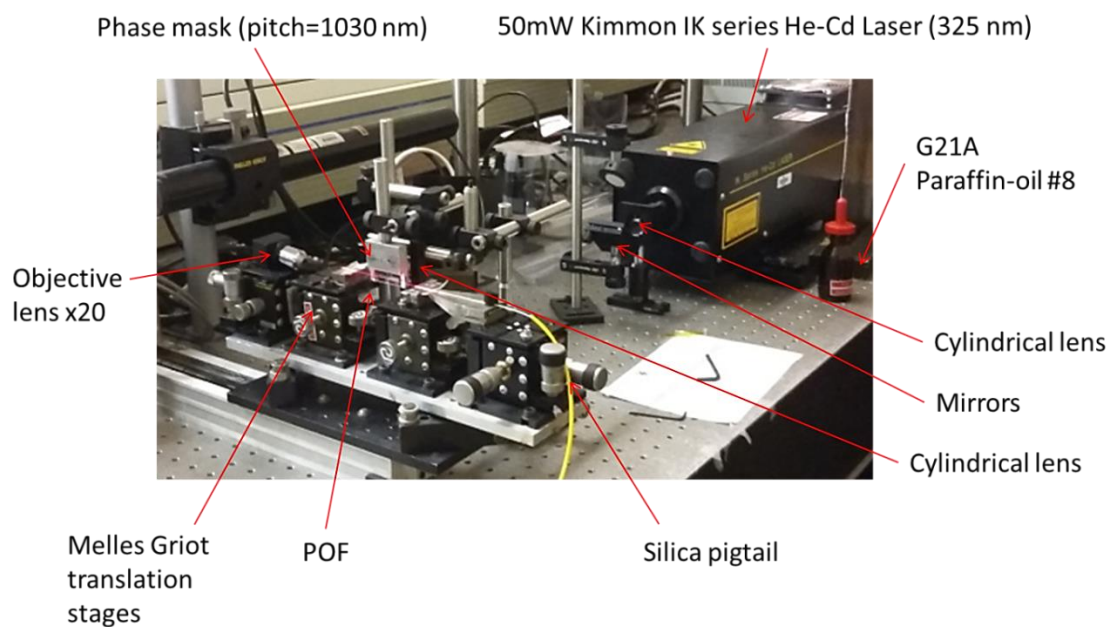
Figure 35 Equipment used in UNSW for FBG inscription into POF, silica pigtail was connected to an Agilent 86140B OSA and BWC-ASE (B&W TEK Inc.) 1550nm broadband light-source to monitor grating growth
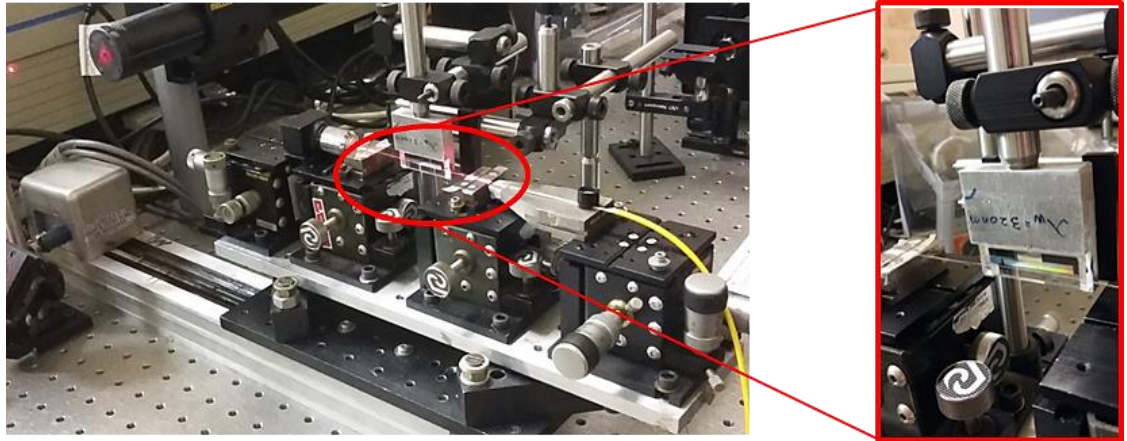
Figure 36 POF suspended in mid-air with the phase mask almost touching the fibre. To couple the cores, the silica pigtail was connected to a helium-neon laser (Melles Griot 632.8nm, 05-LHR-991)

Gratings were inscribed into the POF that reflected wavelengths in the 1530nm region, which could be detected by the OSA (Figure 37 and Figure 38), using a resolution bandwidth (RBW) of 0.2nm and sensitivity input: -80dBm. The Bragg wavelengths were calculated using the centroid Equation 8.

The resolution bandwidth determines the smallest frequency component in the spectrum that can be resolved and distinguished as a distinct component. Using a higher RBW may reveal only one broad spectrum signal about a specific peak frequency, whilst lower RBW allows more frequency components or features to be clearly distinguished potentially revealing multiple and split peaks or sidebands within the measured frequency range. Reducing the RBW also leads to longer acquisition times and sweep times; this could become problematic if a fast sampling rate is required for the experiment or peak tracking.
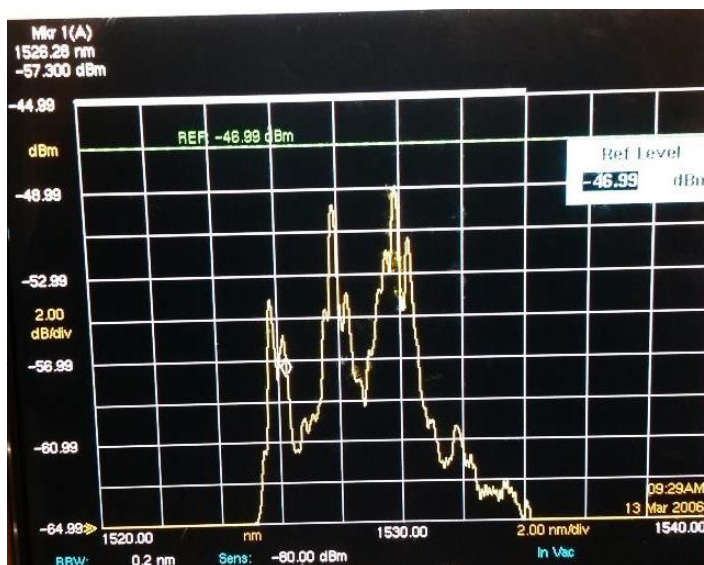
Figure 37 Reflected wavelengths in 1530nm region
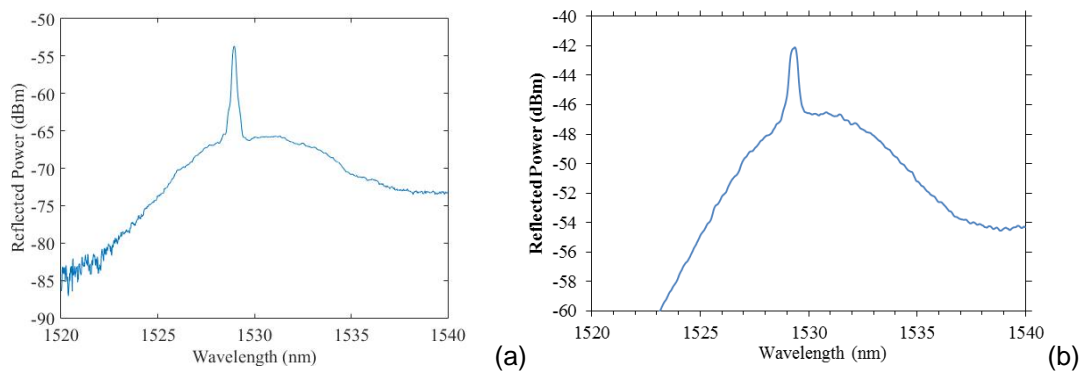
Figure 38 FBG in two F15E PMMA fibres, ≈120µm diameter, (a) 12dBm above the noise floor, 1528.84nm (b) 4dBm above the noise floor, 1529.31nm, Full width at half maximum (FWHM) 0.6nm

The gratings were brought over to Aston University to be glued and placed into the environmental chambers; however regrettably after transportation they were found to no longer be visible using the inspection system in order to be coupled to silica pigtails. This could have resulted from weakening of the grating that it could no longer be monitored using the OSA or internal damage to the fibre or glued joint.

5.2.4   Polymer Optical Fibre Bragg Grating pigtailing

This section describes the splicing technique required in order to couple the POFBG to the interrogation units and broadband light-source. This technique was used to make an efficient link to the fibres, particularly as POF splicing techniques are currently not commercially established like their silica counterparts, especially for single or few mode fibres. It is due to the lack of these commercial components, that it is currently necessary to connect the POF to a silica pigtail in order to interrogate the POFBG. Early work used the butt coupling technique[180] described in section 5.2.2 to monitor changes in Bragg wavelength; however this limited sensing applications to the optical table. This technology was superseded by the development of permanent optical transparent adhesive connections[15, 143, 153, 181] between POF and silica optical fibre. This allowed the POFBG to be removed from the optical bench and placed into a range of environmental conditions to test their capabilities e.g. structural health monitoring or textile tapestries assessment[15, 191].

These connections tend to be weaker at the joint than the rest of the fibre which can cause handling issues and are also not demountable, leading to the production of a demountable connector between silica and POFBG by Abang and Webb in 2012[192]. In this case a microstructured POF (mPOF) with a 50micron-core was

used, which provided a large tolerance to core misalignment[181, 192], however this technique would be significantly more difficult to use with SM fibres having a core size of ≈7µm like those used in this project. The size of the completed device could become problematic for embedding the sensor into certain structures, particularly the large size of the FC/PC ferrule connector body and short POF length. In these situations a UV splicing technique could be considered more beneficial.

In order to take the newly produced POFBGs with a POF length: <10cm (due to attenuation losses described in 5.2.1.3), away from the optical bench in order to interrogate them in the two climatic chambers, each POF was spliced to a silica pigtail. Coupling between the POFBG and silica single mode step index fibre was achieved using a LOCTITE® AA 3936 UV curable optical adhesive in Table 5-B, chosen for its:

- Viscosity which allows it to form a stable joint once cured, as well as stability during long curing times (30+min)
- Service temperature range suitable for operating in the chambers.

Table 5-B LOCTITE® AA 3936 UV curable optical adhesive properties[193, 194]

As with butt-coupling in the inscription stage (section 5.2.2), the end faces of the POF and silica pigtail need to be suitably cleaved to form a stable joint that allows the grating to be tracked using the OSA and commercial interrogation monitors.

To produce the joint, the jacket/buffer from a section of the SM silica pigtail needed to be stripped using a wire stripper (Abisolier-Technik) and the fibre cleaned using methanol (ACROS Organics). At this point a Ox-FAC-06 cleaver (Oxford Fibre Optics Tools) was used to cleave the silica pigtail end at 6° to reduce Fresnel and back reflections, before being placed in the v-groove attached to a precision translation stage (Figure 39).

The 80°C hot cleave method[186, 187] from section 5.2.1.3 was used to cleave both ends of the POF, before it was secured with polyimide tape to the v-grooves attached to a translation stage.

Figure 39 shows the alignment of the POF and silica pigtail cores using the same technique as in section 5.2.2, however a drop of LOCTITE® AA 3936 was applied to the POF-silica joint rather than index matching gel.
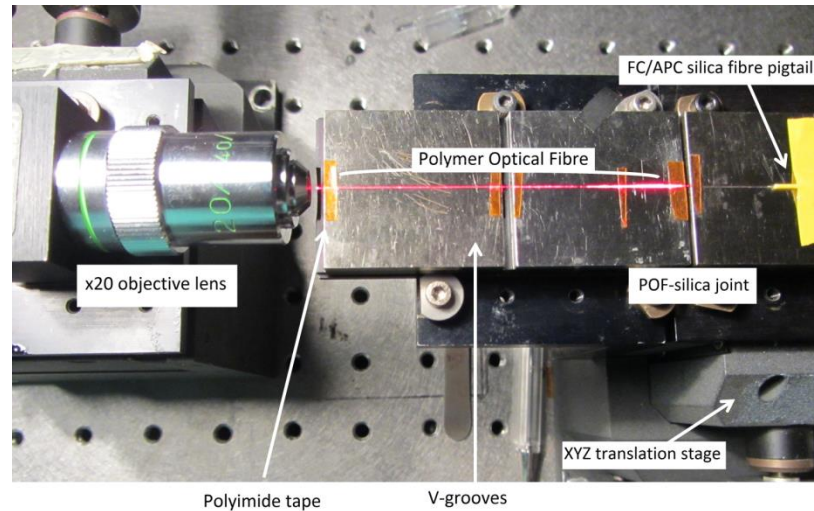
Figure 39 Aligned optical fibre assembly prior to curing.

The translation stage was used to make minor adjustments to the alignment, to maximise the Bragg grating reflection (described in section5.2.2) observed with the interrogation system (Figure 32). The adhesive was then cured as shown in Figure 40, using the EFOS NOVACURE UV/Visible spot cure system, model NOVACURE N2001-A1.
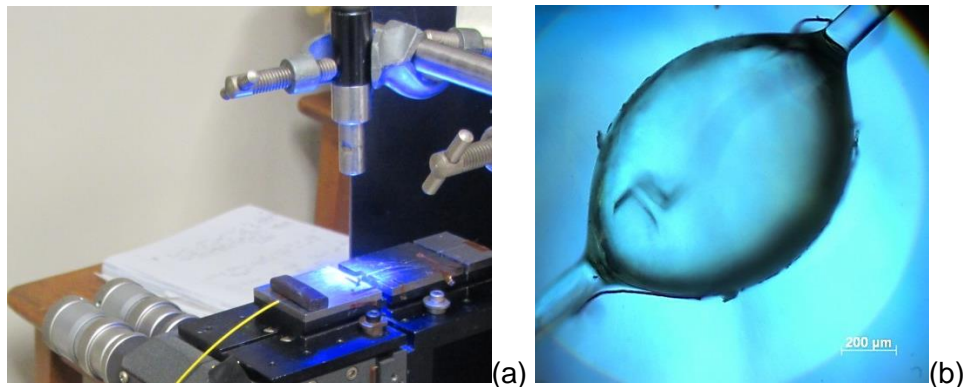
Figure 40 Pictures of (a) UV adhesive curing step to form (b) a stable joint between the POF and silica fibre end faces (using a x10 microscope objective lens), scale 200µm

Table 5-C illustrates the optimised procedure obtained from curing multiple POFBGs to silica pigtails. The table lists the number of times that a small quantity of glue was added at the silica-polymer optical fibre interface and the curing time to ensure that a suitable joint was made, to allow tracking of the gratings for extended durations in the chambers. A small quantity of glue should be carefully applied to this interface as its weight has the potential to misalign the cores and not allow the FBG to be tracked. It should be noted that it is important to avoid touching the v-grooves (generally a 2-3mm gap between the v-grooves in Figure 40) with the UV glue, as the POF would be glued to this surface during curing and damaged once an attempt is made to remove it.

	Curing Time (min)	
Adhesive application stage	PMMA POF	TOPAS POF
1	20	27
2	15	26
3	-	27
Total curing time	35	80

Table 5-C UV glue curing times for different POFs

Once the glue had been cured, the polyamide tapes were carefully removed to reveal the POF connected to the silica pigtail as shown in Figure 41. These fibres could then be placed into a housing structure to protect the joint and the POF once they are placed in the chambers. The reflected spectra of the Bragg wavelengths were captured using the OSA and national instruments software as described in section 5.3.
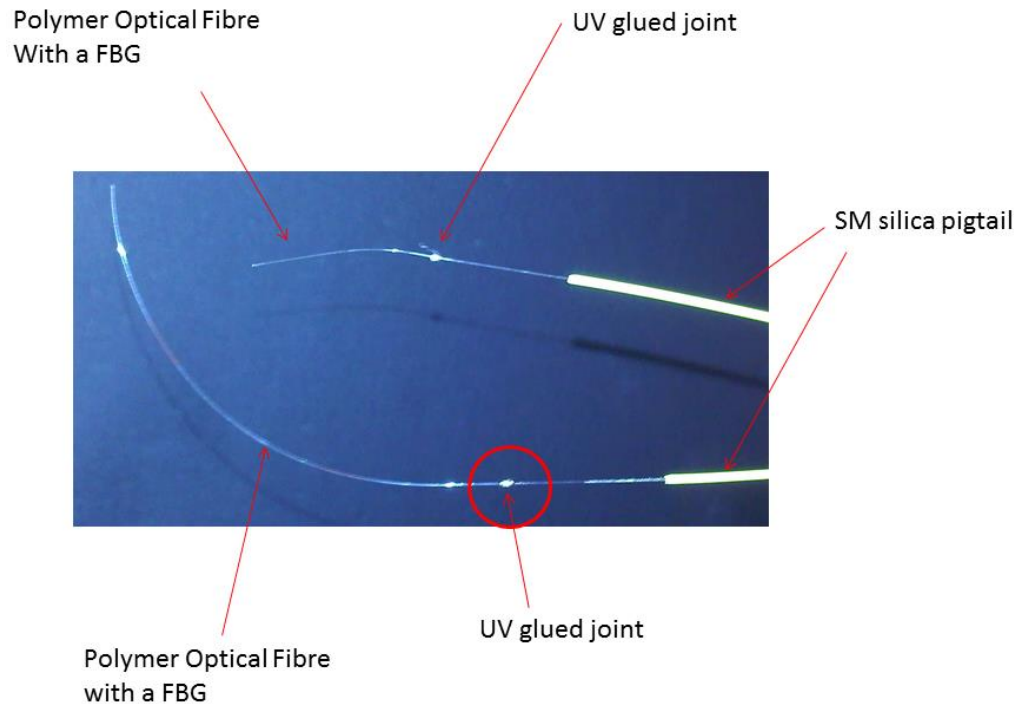
Figure 41 SM POFBGs UV glued to SM silica fibre pigtails

5.3   Polymer Optical Fibre Bragg Grating sensors for the Freeze Dryer

The previous sections described the preparation of the POFs (5.2.1.3) before inscribing the FBGs according to the procedures listed in section 5.2.2. The POFBGs were then glued to silica pigtails (5.2.4), before being placed in to a custom built housing (Figure 42). Figure 43 shows the schematic diagram of the sensor consisting of the housing and POFBGs, that was developed to protect the

POFBGs and glue joint against the rapid wind velocities experienced within the freeze dryer (described in 5.7.1).
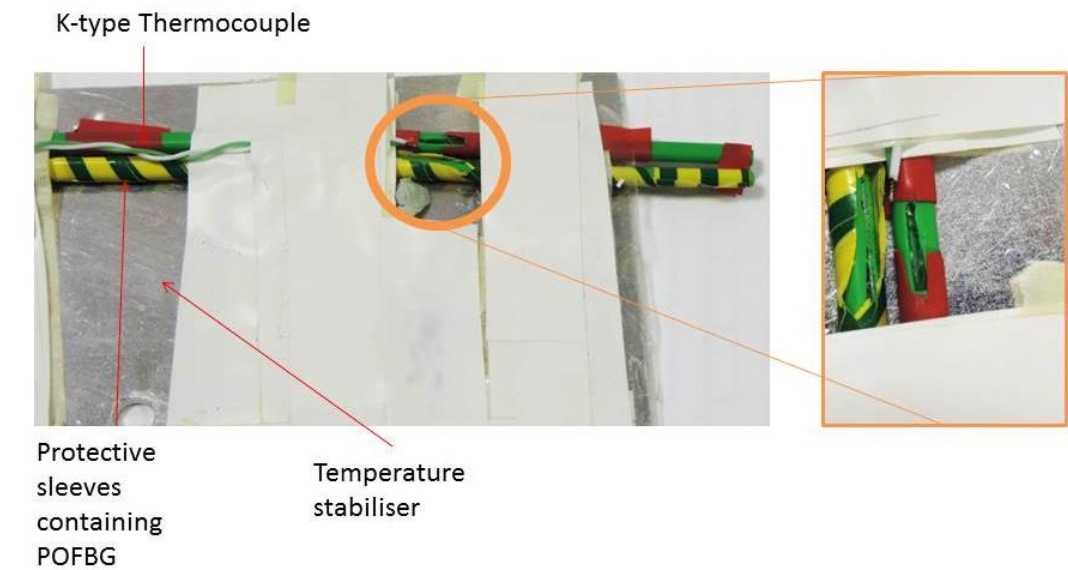
Figure 42 Housing structure to protect PMMA and TOPAS POFBGs
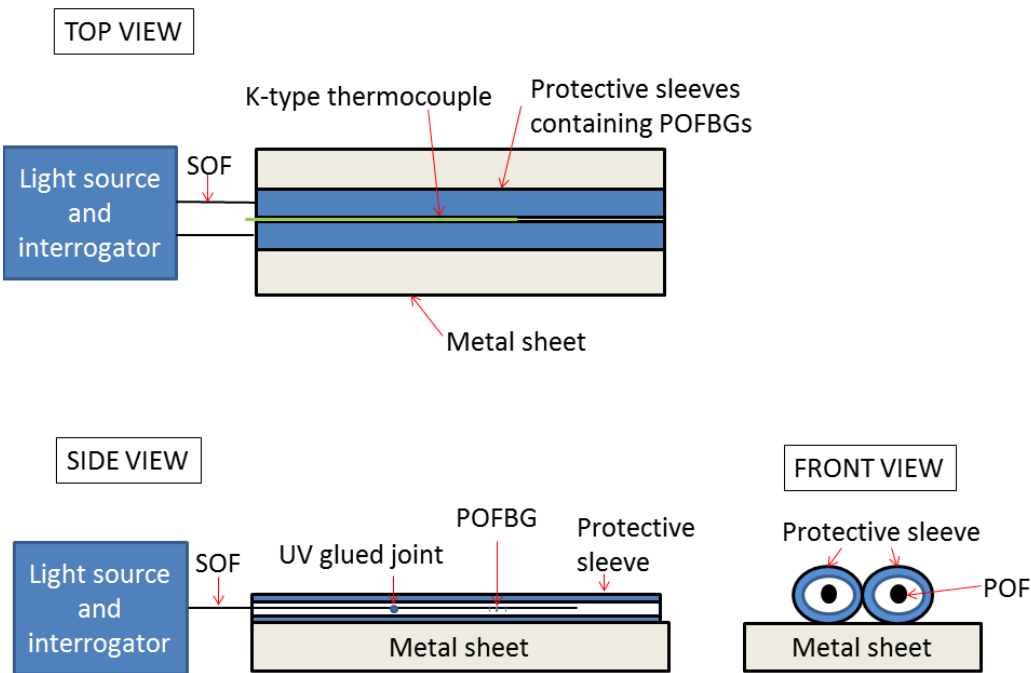
Figure 43 Schematic diagrams of the assembled housing containing the POFBGs

The following gratings (*Figure 44, Figure 45, Figure 46*) were captured at a Resolution Bandwidth (RBW) of 0.5nm using National Instruments software interfaced with the OSA; the peaks were calculated using the centroid calculation in Equation 8. The Bragg grating length was 1.8mm, which was determined by the diameter of the beam, inscription times are listed in Table 5-A.
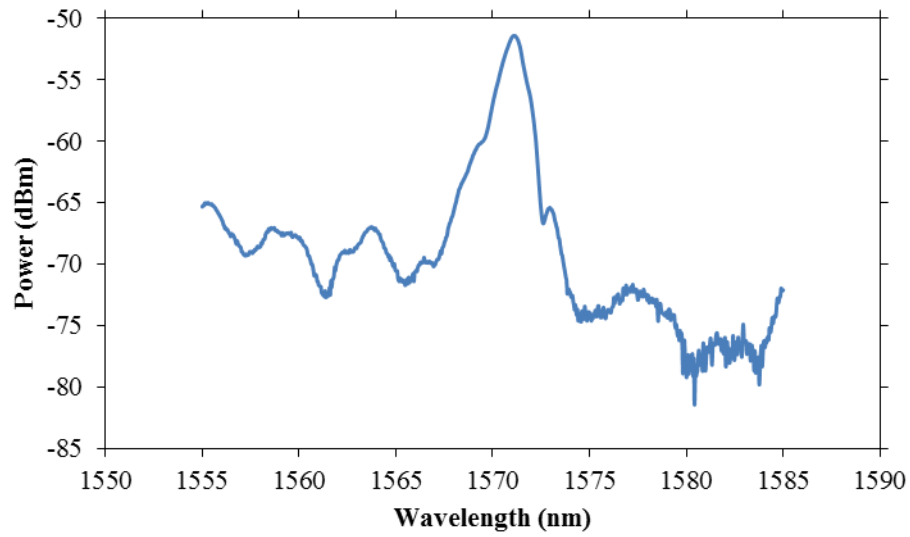
Figure 44 POF1. Reflection spectrum of a single-mode F15E PMMA POFBG produced in the 1570nm region, outer diameter 96μm (after etching with acetone for 2.5min from 120μm), phase mask period: 1061.18nm, peak signal 1571.03nm, Full width at half maximum (FWHM) 1.3nm, 20dB above the noise floor
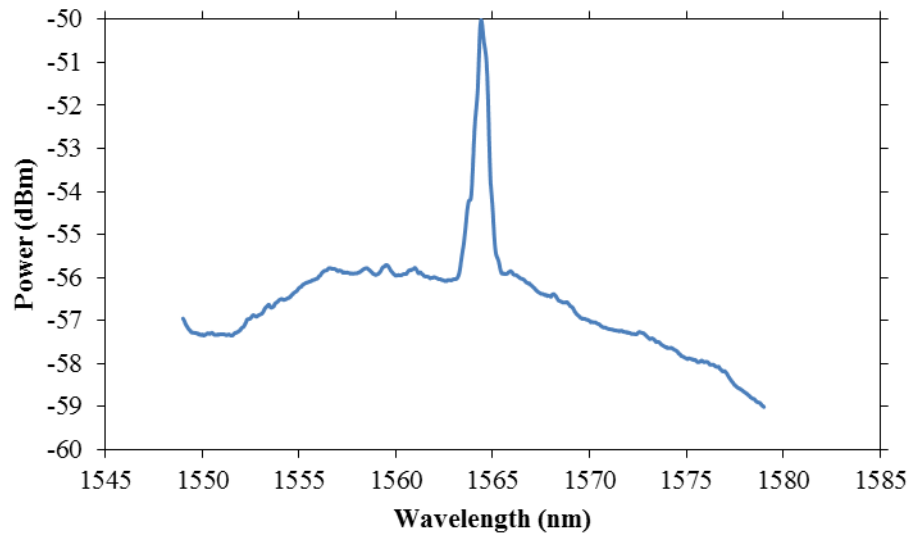
Figure 45 POF 2. Reflection spectrum of a multimode-mode TOPAS POFBG using a phase mask period: 1034.20nm, peak signal: 1564.4nm, FWHM: 0.9nm, 6dB above the noise floor, inscription time: 90min
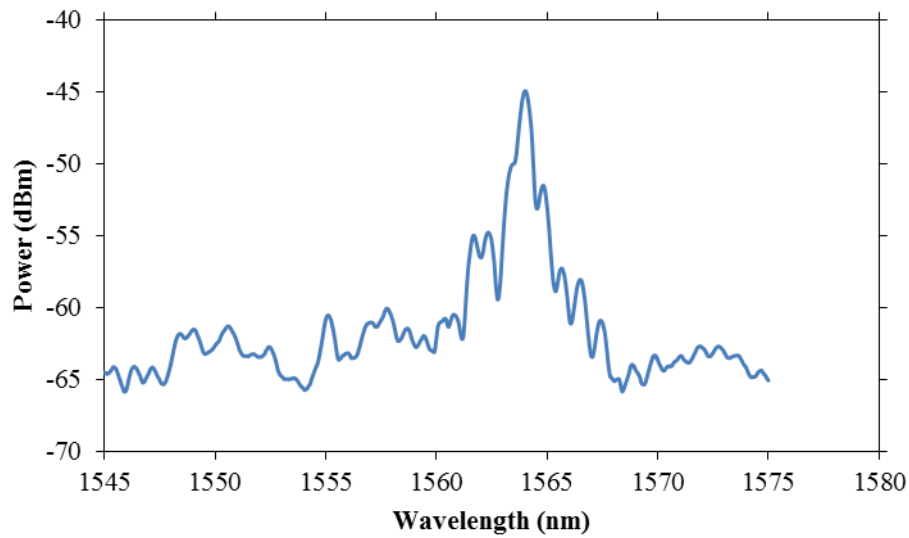
Figure 46 POF3. Reflection spectrum of a multimode-mode TOPAS POFBG produced using a phase mask period: 1034.20nm, peak signal: 1564nm, FWHM: 0.6nm, 18dB above the noise floor, 143µm outer diameter, inscription time: 120min

The gratings in Figure 48 and Figure 49 were inscribed in a PMMA polymer optical fibre (1cm separation distance), to reflect wavelengths in the 1570nm and 1530nm regions. These POFBGs were UV glued to a silica pigtail before being placed in the protective housing. Figure 47 shows the arrangement of the sensors in the freeze dryer.
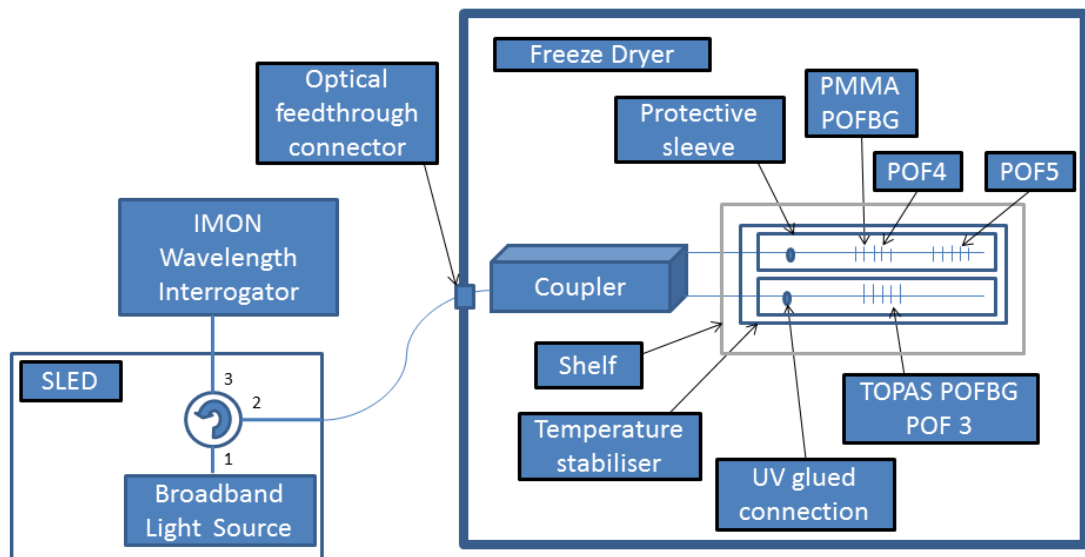
Figure 47 Arrangement of optical fibre sensors in the freeze dryer
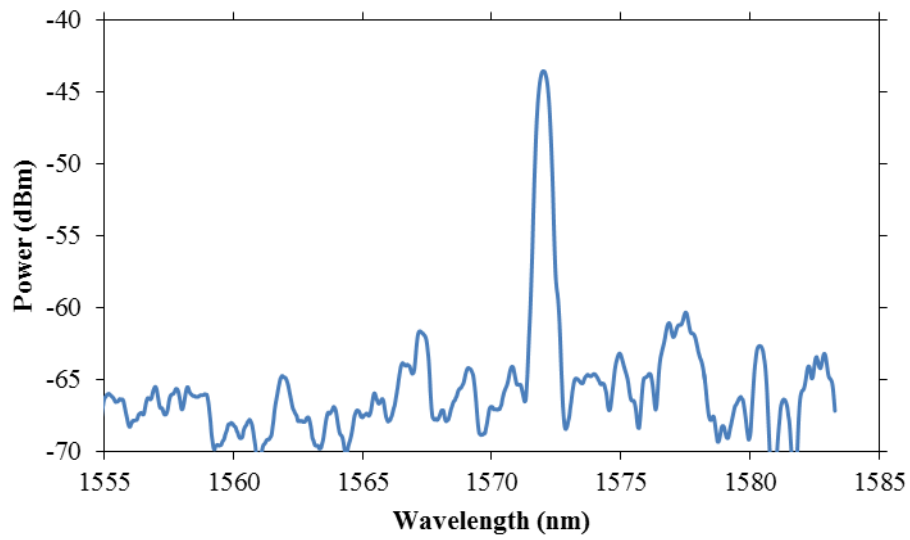
Figure 48 POF 4. Reflection spectrum of an annealed single-mode F1F PMMA, POFBG produced using a phase mask period: 1061.18nm, peak signal: 1572nm, FWHM: 0.5nm, 20dB above the noise floor, outer diameter: 114µm, RBW: 0.5nm, Bragg grating length 1.8mm
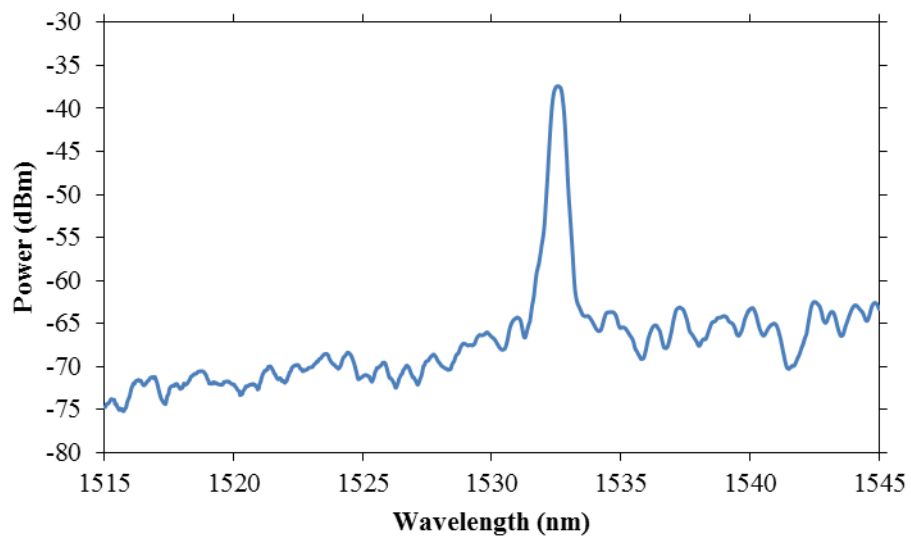
Figure 49 POF5. Reflection spectrum of an annealed single-mode F1F PMMA, POFBG produced using a phase mask period: 1034.20nm, peak signal: 1532.6nm, FWHM: 0.5nm, 26dB above the noise floor, outer diameter: 114µm, RBW: 0.5nm, Bragg grating length 1.8mm.

5.4   Climatic chamber

After having reviewed the POFBG manufacturing process, which includes cleaving (5.2.1), the inscription (5.2.2) and splicing techniques(5.2.4), the next few sections will examine the chambers and sensors that were used in the POFBG characterisation experiments.

A PMMA based POFBG (section 5.4.1) was placed into an environmental chamber (SANYO Gallenkamp plc). The project involved reducing the diameter of the fibre (section 5.4.2) in order to study the effects of relative humidity (%RH) and temperature on the response time[15, 195] of the POFBG.

The dimensions of the interior of the chamber were 90x90x75 cm and the control system allowed the user control of a range of %RH depending on the input temperature (Table 5-D). The chamber had fluctuations with time in the range of [196] 3%RH to 5%RH (at max and min %RH respectively) and 0.3°C for temperature with time, with a distribution gradient of 1°C.

Aston University

Illustration removed for copyright restrictions

Table 5-D SANYO climatic chamber specifications[196]

5.4.1   Polymer Optical Fibre

A doped single-mode PMMA POFBG was produced using the cleaving method (5.2.1.3), inscription (5.2.2) time of 7min, coupled to silica pigtail (5.2.4) and had a Bragg grating length of 1.8mm. The grating in *Figure 50* was captured at a RBW of 0.5nm using the OSA and National instruments interface software, and peaks calculated using the centroid calculation in Equation 8. This sensor would be inspected for the Bragg wavelength response to temperature, humidity and fibre diameter when placed in the environmental chamber.
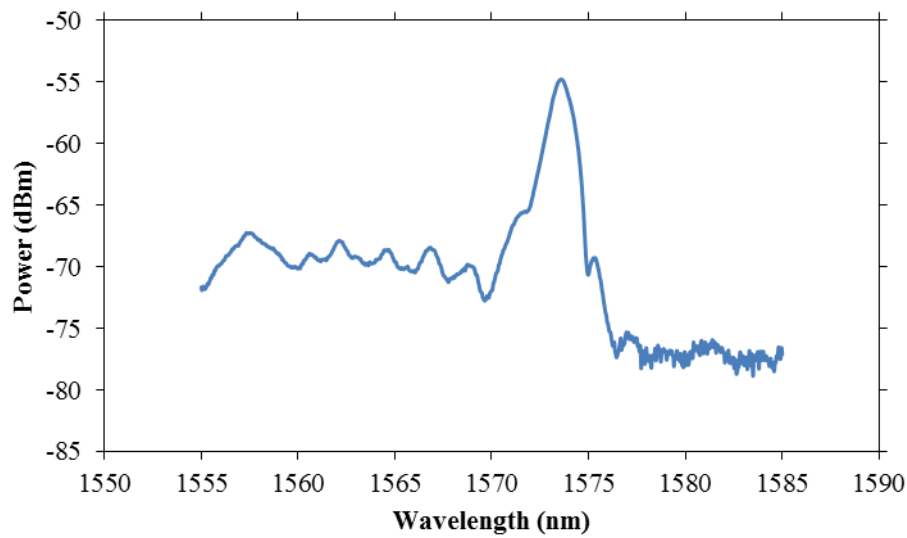
Figure 50 POF6. Reflection spectrum of a single-mode F15E PMMA POFBG produced in the 1570nm region, outer diameter 120µm, phase mask period was 1061.18nm, peak signal 1573.6nm, Full width at half maximum (FWHM) 1.2nm, 20dB above the noise floor

5.4.2 Polymer Optical Fibre Etching

Acetone (ACROS Organics) was used in these experiments to test the effect of POF diameter on the POFBG response time, as it is a chemical solvent known to dissolve PMMA[195]. Acetone was used to etch the fibre for a known timeframe and then the POFBG was tested in the environmental chamber described in section 5.4. The 120µm POFBG described in section 5.4.1 was etched within acetone for 1min and subsequently for 30seconds. In between each session the outer diameter was measured using the Carl Zeiss microscope (Axioskop2 mot plus) described in section 5.2.1.2 and the sensor was placed into the environmental chamber, to collect data using the Thorlabs ASE730 broadband light source and Ibsen I-MON 400E (section 5.5).

5.5   Interrogation Units

The interrogation units used for the environmental chamber studies offer real-time monitoring and data acquisition of the FBG spectra. A high-resolution spectrometer spatially separates the input wavelength spectrum using internal transmission gratings[197]. The FBG spectra obtained in reflection are focused onto a diode array where the interrogator processes the signal and performs a wavelength peak fit to allow the FBG wavelength to be determined[197]. The technology allows multiple FBG sensors, to be processed in parallel (Wavelength division multiplexing (WDM) system), Table 5-E illustrates the specifications of both interrogators[198-200].

Specification	I-MON 400E-USB	I-MON 512 USB
Maximum number of FBG sensors (units)	<50	<70
Wavelength Range (nm)	1520-1585nm	1275-1345nm/1510-1595nm
Minimum FBG spacing	1200pm	1000 / 1200pm
Measurement frequency	200Hz	3000Hz
Wavelength fit resolution	< 0.5pm	< 0.5pm
Wavelength accuracy	5pm(typ)	5pm(typ)
Ibsen Software loaded on PC to interface with I-MON	I-MON Series E-USB	I-MON USB Evaluation software v1.1

Table 5-E I-MON interrogation monitor specifications from Ibsen Photonics [198-200]

5.6   Characterisation of POFBGs

The POFBGs were placed in the climatic chamber and exposed to step changes in critical process parameters (CPPs), such as temperature, pressure, and humidity. The effect these step changes have on the wavelength of the POFBGs was logged at 1 sample every 15sec (unless otherwise stated) by interrogation units outlined in section 5.5. The data were then gathered from all the sensors and analysed in Excel 2010.

For the environmental chamber study, the response time was estimated as outlined by Zhang and Webb[195]. It was defined as the time required for the relative wavelength change (Δλ/Δλmax), to reach 10% or 90% (0.1 or 0.9 respectively) of the output step height (Figure 51).
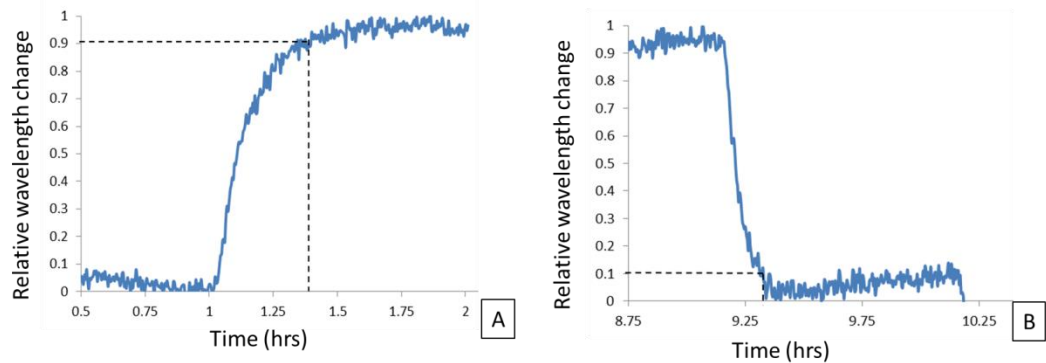
Figure 51 relative wavelength change response to a step change in a CPP

The same technique was utilised to examine data obtained from the freeze drying experiments, analysing relative wavelength change in response to step changes in CPPs provided information on the sensitivity of the fibres.

The end of primary drying time was taken as the point at which "offset" occurs during the end of the primary drying stage[8], as seen in Figure 13(a) when analysing the typical output signals. This time was taken using the same procedure as described for Figure 51, to maintain consistency with literature and allow data to be comparable. For thermocouples the end of primary drying is defined as the time the product temperature approaches the shelf temperature[8], an example is shown in Figure 13(b). For Pirani gauges used in freeze drying applications, the end of primary drying time is when the gas composition changes from predominantly water to nitrogen[8] and resembles the profile of Figure 13(b).

5.7   Freeze Dryer

A Virtis Advantage 2.0 data centre benchtop scale freeze dryer model No Advantage: EL-85 (SP scientific) was used in this project; it allows the control of sub atmospheric pressure and low temperatures required for freeze drying of pharmaceutical formulations and biological samples. The Virtis Lyophilisation Mentor/Wizard Synoptic Software (Version 5.6 Multiple Wizards 2004) was used to record the pressure, shelf and condenser temperatures during the cycles. The system regulated the pressure using feedback from a thermocouple vacuum gauge (Varian Type 0531) and solenoid valves connected to a nitrogen gas cylinder and vacuum pump. The condenser was kept at -80°C during cycles and had a maximum capacity of 3.5L. The shelf dimensions are 273mm x 355mm x 19mm (shelf area 969.15cm^2) and the temperature was regulated (≈+/-2°C) using feedback from an internal thermocouple (resolution 0.1°C), a heating element and solenoids controlling refrigerant fluid into the shelf.

Figure 52 illustrates the freeze dryer configuration used, where the following sensors were attached to existing access ports leading into to the vacuum chamber: SF52 dew point transmitter (Michell Instruments) and a Thermovac TM101 Piezo/Pirani combined pressure sensing device (Oerlikon Leybold). These devices track the conditions experienced within the chamber independently of the freeze dryer gauges and controller.

As literature does not report that POFBGs have been previously placed into freeze dryers, new protocols were devised, with modifications to the existing chamber e.g. feedthroughs, in order to pass the optical fibres through the chamber wall.

A custom made feedthrough for the optical sensor was designed and attached to the existing access port of the freeze dryer; this will be discussed in section 5.7.1.
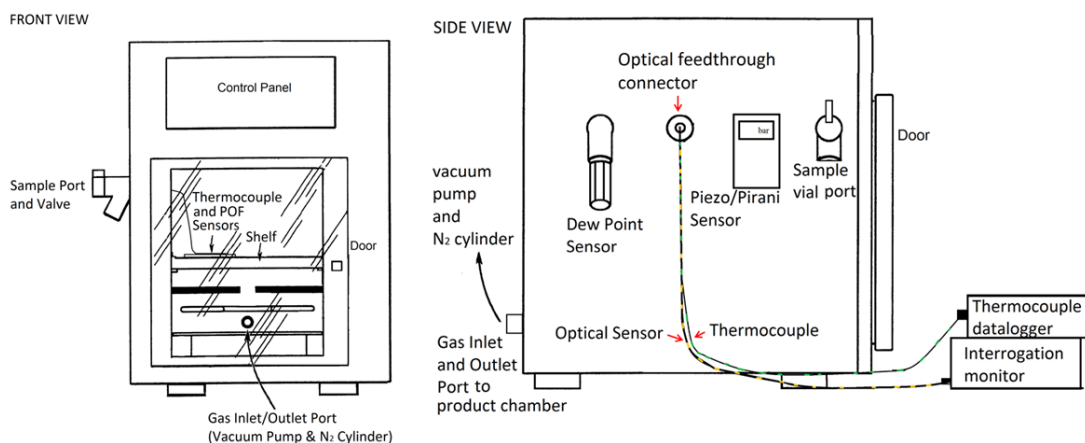
Figure 52 schematic diagram of the freeze dryer configuration

To ensure dry conditions are maintained during the process:

- The condenser is maintained at low temperatures below -70ºC to trap water vapour in the chamber by condensing it and maintaining it as bulk ice on the coils during the experiment.
- The freeze dryer's PID controller maintains the pressure about a user-specified value below the triple point of water, using solenoid valves connected to the gas inlet and outlet port of the freeze dryer (Figure 52) attached to:
  - a N2 cylinder (Zero grade, Nitrogen N4.8, No impurities reduced and analysed from Boconline) and a desiccant (Drierite 26800 Drying column, 200 L/hr, 90 psi from Cole-Parmer)
  - vacuum pump (Oerlikon leybold vacuum TRIVAC D4B)
- A dew point sensor (SF52, Michell Instruments) has been attached to a port in order to monitor the environmental conditions during the cycle

5.7.1 POFBG sensor implementation into the Freeze Dryer

The POFBGs were placed in a customised housing structure (Figure 42) onto the shelf along with K-type thermocouples (5.7.3) to track local temperature changes as heat transfer and radiative effects are known to be an influential factor in a freeze dryer [46].

The cables were fed through a custom made compression fitting attached to the wall of the chamber in order to ensure a suitable vacuum seal is produced, shown in Figure 53. The optical and thermocouple feedthrough was built by passing the cables through a 15mm diameter rubber bung into the existing port on the product chamber. An interference fit was formed between the two materials and remaining leaks were sealed with blu-tack and silicone sealant. The external FC/APC cable connector in Figure 53(a) is then coupled to the DL-BP1 SLED broadband light source (Denselight semiconductors) with an integrated optical circulator (Denselight semiconductors) and I-MON 512 USB interrogator monitor (Ibsen).

The I-MON 512 USB evaluation software v1.1 was used to analyse the FBG spectrum and calculate the Bragg wavelength using peak tracking algorithms. Three repeats were carried out on each POF and the data were analysed using Microsoft Excel 2010.
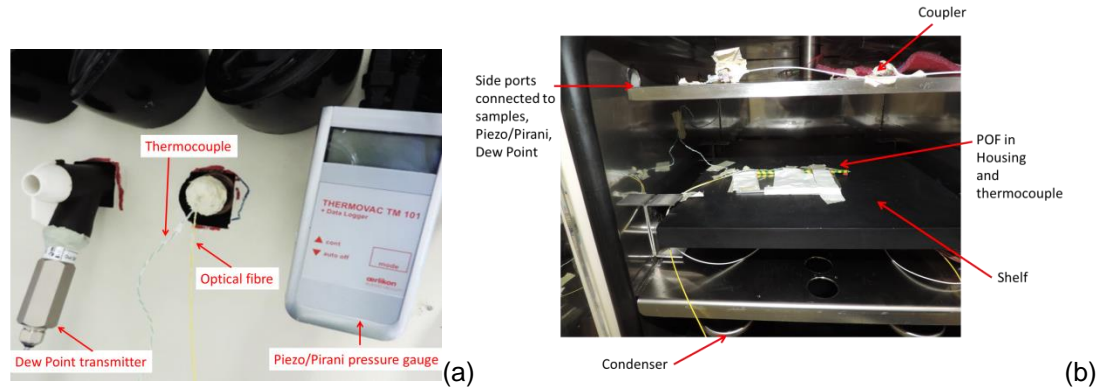
Figure 53 (a) Sensors attached to separate ports leading into the vacuum chamber; (b) POFBGs inside vacuum chamber

The POFBGs were placed in a custom built housing (described later) to protect the POF against extreme air velocities experienced within the freeze dryer, whilst allowing them to track trace water vapour flow from sublimation. The device was placed on the shelf within the freeze dryer and connected to a 2x2 1550nm Corning single mode (SM) 50:50 silica coupler (9/125µm), shown in Figure 53(b) and Figure 54. The coupler was coupled to the SM silica fibre which passes through the custom-made feedthrough to the interrogation unit outside the freeze dryer.

The response of both humidity sensitive PMMA POFBG as well as humidity insensitive TOPAS POFBG was monitored during the same cycle. They monitored critical process conditions and the TOPAS POFBG acted as an additional control to the dew point and Pirani sensors, when monitoring sublimed water vapour.
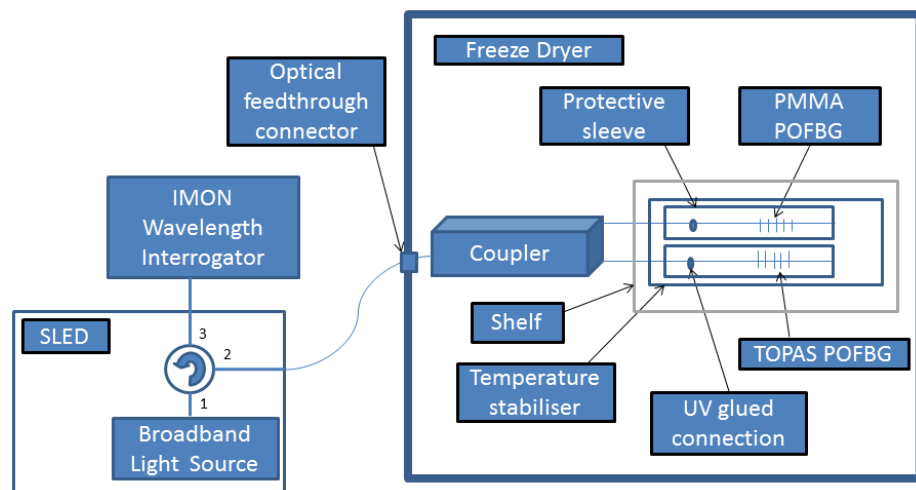
Figure 54 schematic diagram of the POF configuration

5.7.2   Development of the POFBG sensor housing structure

This section will describe the tests carried out in order to demonstrate that POFBGs can operate in a freeze dryer and the final housing structure that was placed around the sensors to shield them against rapid air movement. The following tests were carried out to obtain information on wind velocities in the chamber and the influence of different POFBG configurations:

1. A Testo 410-1 Compact Vane Anemometer (measurement range:0.4 to 20m/s[201]) was inserted into the Virtis benchtop freeze dryer, to measure the gas velocity range during a freeze drying cycle (Figure 55(a))
2. The UV glued joint between the silica and POF was shielded with a metal or ceramic sleeve (Figure 57(a)) before being placed inside the freeze dryer
3. POFBG were placed into a 15mm diameter hose located within the freeze dryer (Figure 57(b))
4. POFBGs were taped to a metal sheet (Figure 57(c)) and placed onto the shelf
5. Protective housing structure for TOPAS and PMMA POFBGs (Figure 55(b)) was placed into the freeze dryer

The anemometer made it possible to monitor the wind velocities in a freeze dryer particularly since literature has reported a large range of velocities can be experienced in different types of freeze dyers. Velocities have been reported in the range of >20m/s [112, 113] for laboratory scale freeze dryers and some reported ≈120 m/s[112] (hurricane force according to the Beaufort scale). Unfortunately the Testo 410-1 anemometer suffered catastrophic failure during the initial drop in pressure from 1atm to 2500µbar, a necessary stage in order to begin the experiments. This confirmed that velocities >20m/s are achieved in this freeze dryer as reported in the literature. At these rates, protection for the vulnerable optical fibre is required to ensure the joint/connector would not get damaged during the experiments. If the fibre and joint were not sufficiently protected, there is a significant risk that the POF could break away during the cycle and if suctioned, could damage the vacuum pump and/or contaminate the pharmaceutical samples.
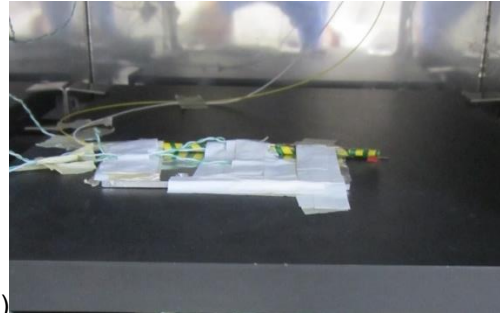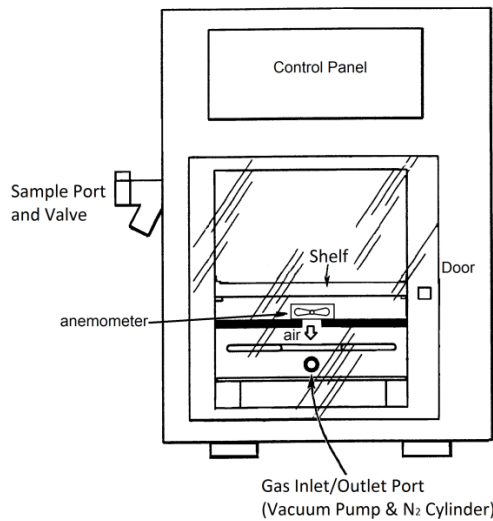
Figure 55 (a) Anemometer in the freeze dryer (b) final housing structure placed onto the shelf

Another anemometer (LAC-EA3000), that had a higher resistance to high flow rates than the Testo 410-1 was placed into the chamber, to observe the behaviour during primary drying of distilled water. This sensor survived the initial pressure drop from 1atm to 2500µbar; however without sufficient baffling to direct the vapour flow from the product chamber through the anemometer to the condenser, it was unable to monitor sublimation. This experiment showed the challenging conditions that the sensors within the chamber would need to endure in order to monitor low sublimation rates during freeze drying.

Providing sufficient baffling was achieved and large samples of water used (minimum 250ml), the anemometer was able to track the vapour flow in the chamber during primary drying. Figure 56 shows the anemometer monitoring water vapour flow during primary drying, which was compared against other established (end of primary drying) technologies. The procedure to develop the data logger in order to monitor the movement of the anemometer is available in Appendix D. The graph shows the thermocouples monitoring sublimation cooling during primary drying, before detecting a characteristic increase in temperature towards the shelf temperature, which marks the end of sublimation. The Pirani gauge monitored a characteristic increase in the pressure during sublimation of water vapour and a decrease when the gas composition in the chamber returned to a dry nitrogen atmosphere. At the same time the anemometer monitored an increase in speed during sublimation, before gradually reducing as the sublimation rate reduced over time. Visual observations were also used to confirm that the blades of the anemometer moved when ice was present and being sublimed in the chamber and stopped when no ice was present at the end of primary drying. These patterns were

observed on multiple occasions and a representation of the results is available in Appendix E (Graphs 1 to 4).

To this author's knowledge no publications have previously reported data obtained from an anemometer, profiling rate of sublimation within the freeze dryer. Previous publications (section 3.4.2.3) reported placing anemometers within freeze dryers; however they were only visually inspected to determine when the blades stopped moving as this indicated the end of sublimation.
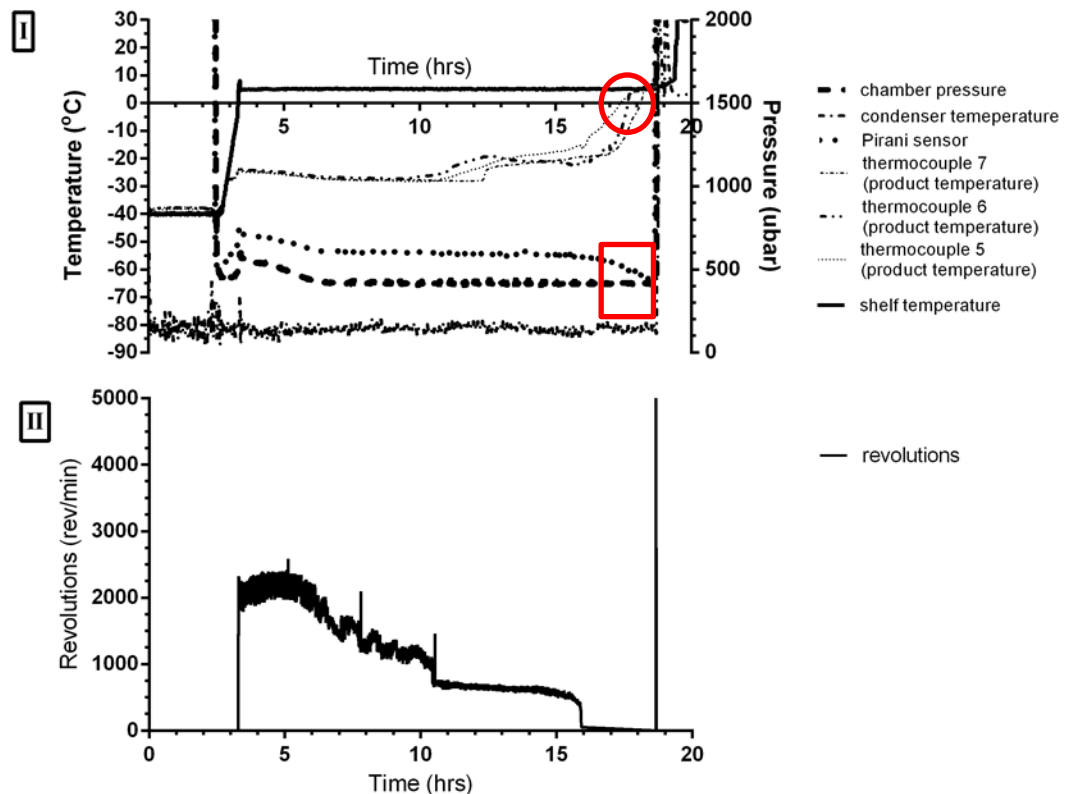
Figure 56 Primary drying of a 500ml sample of distilled water in a metal tray that was frozen for 6hrs at -40ºC.(I) thermocouples (red circle) and Pirani gauge (red box) detecting end of primary drying, (II) anemometer monitoring revolutions during primary drying (shelf temperature set point 5ºC)

These experiments provided useful information about the environment that the POFBGs would be exposed to and required to operate in. Anemometers have moving components that could pose a contamination risk to pharmaceuticals within the chamber, so they were therefore not pursued any further in this project.
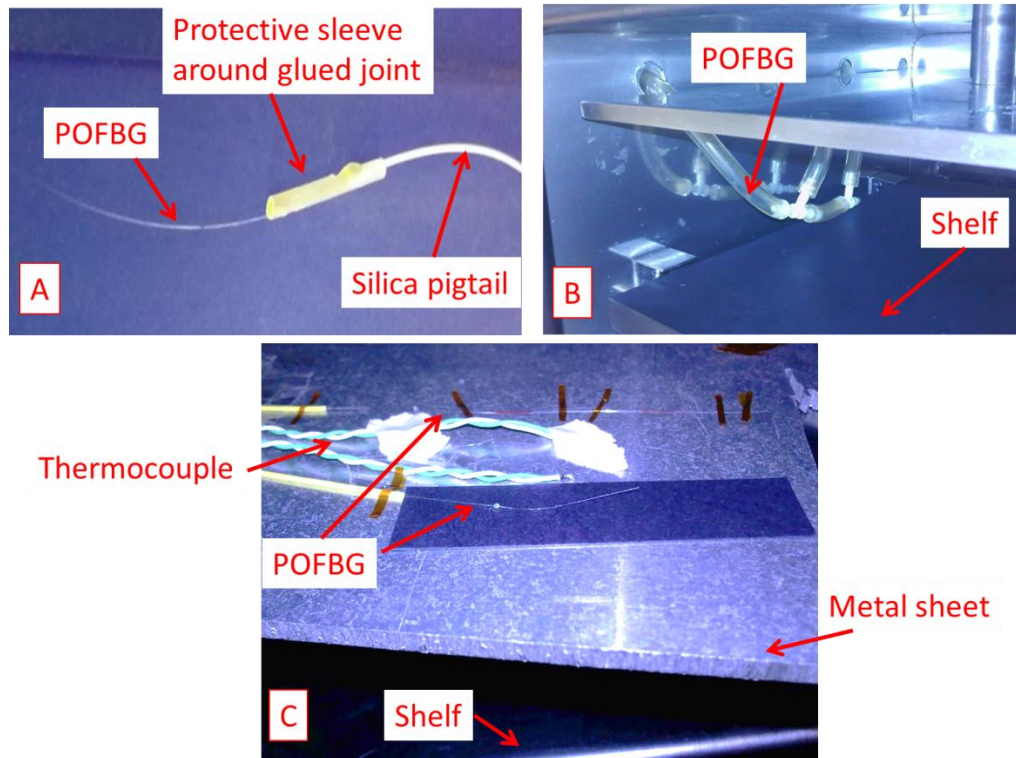
Figure 57 Experiments carried out where POFBGs were placed into the freeze dryer in (a) protective sleeve, (b) tube, (c) taped to metal sheet on shelf

To protect the spliced UV glue joint, a 15mm long metal or ceramic sleeve was placed over the joint which couples the silica to the POFBG[143], UV glue was then applied to the edges of the sleeve-POF interface and cured for 30min as seen in Figure 57(a). This system was not found to be successful when placed into the freeze dryer, often fibres were found to have weakened at the edge of the new UV cured interface against the sleeve, which lead to fracture. A similar problem was experienced when taping or fixing the POFBGs to the metal sheet that was placed onto the self, seen in Figure 57(c). Often this procedure would introduce internal stresses into the fibre and joint which could lead to damage, reduce accuracy and increase noise.

Figure 57(b) shows an experimental rig where a POFBG was placed into a tube, used as a shield for the fibre and to direct vapour flow. This experiment showed a drift in wavelength over time, as the walls connected to the rig were gradually cooling over time due to conduction from the metal wall connected to the -80ºC condenser coils. This temperature gradient causes a gradual change in temperature, which reduced the accuracy of the readings. On occasions the likelihood of detecting vapour flow was reduced due to air movement which caused the POF to vibrate.

Apart from providing protection to the fibres against high velocity flow rates, it was important to create a housing structure which allowed vapour to pass over the fibre for detecting low sublimation rates. Literature has shown sublimation rates to be in the range of <4m/s[112, 113], and mass flow rates using a: TDLAS <0.24 g/s[112], freeze drying microbalance <348.1mg/hr[202] and using MTM technology <1.51g/hr/vial[203].

Figure 55(b) shows the protective housing chosen for use in the experiments in this project. The POFBGs were placed into sleeves to provide protection and structural support to the POF, joint and portion of the silica pigtail which was spliced to the POF. The sleeve is attached to a temperature stabiliser (3mm thick aluminium sheet) as the shelf was subjected to large oscillations in temperature (+/-2°C) which can mask other effects. The housing avoids introducing internal stresses into the fibre that would otherwise have been there if it were taped to the shelf or plate. The sleeve has a gap for vapour to flow across the sensors during sublimation, whilst protecting the fibres during the vacuum pull or release phases.

5.7.3   Thermocouples

Grounded K type thermocouples (RS Components, UK, stock number: 621-2158) were used to monitor the temperature in the region of the POF sensors, the equipment (e.g. shelf temperature and POF housing), water bath and product temperature. They were chosen for their suitable temperature range -50^{0}C to +260^{0}C, for operating on a shelf or within the products placed into a freeze dryer. The 8 Channel Thermocouple Temperature Recorder OctTemp by MadgeTech (MadgeTech Data Recorder Software Version 2.02.5) was used to log the temperature, having a resolution of 0.05 °C and an accuracy of ±0.5°C. Thermocouples were carefully positioned centrally within the vials and at the base of the product to ensure detection of the sublimation front when it reaches the bottom of the container. The thermocouples provide information on the temperature profile of the product in order to give an estimate of the end of primary drying time, which can then be compared against other sensors such as Pirani and POFBGs.

The 4 Channel TM-947SD Datalogger (Digital instruments) recorded the POF temperature and the room temperature, with a resolution of 0.1°C and accuracy of ±(0.4%+0.5°C).

5.7.4 Comparative pressure measurement

A comparative pressure measurement process was applied to a Pirani Gauge and the freeze dryer's internal thermocouple vacuum gauge. A THERMOVAC TM101 digital piezo/Pirani combination gauge for Pressure Measurements (Oerlikon Leybold Vacuum) was attached to a port on the product chamber using a KFCF16-075-1ss compression fitting (Oerlikon Leybold Vacuum) as shown in Figure 53. The combination gauge (Table 5-F) measures pressures using a piezo-resistive pressure sensor which is independent of gas composition at >15mbar and switches to a Pirani for pressures below this value[204]. The Pirani detects changes in the gas composition, which will be used as a measurement tool to compare against when determining the end of primary drying time.

The standard thermocouple gauge (Varian Type 0531 To Vacuum Gauge) having a 15% accuracy, was installed by SP Scientific into the commercial Virtis freeze dryer. In order to measure chamber pressure and minimise the risk of detecting changes in gas composition during sublimation, the thermocouple gauge had been fitted in the vicinity of the condenser coils to avoid being in-line with the water vapour flow. The Virtis Lyophilisation Mentor/Wizard Synoptic Software (Version 5.6 Multiple Wizards 2004) was used to record the data sent by the freeze dryer to the PC and the Oerlikon Leybold Vacuum VacuGraphTM 8.2.4 was used to record the pressure data from the THERMOVAC TM 101 gauge.

The only sampling rate available on the Virtis freeze dryer software was 2min, this sampling rate tends to be sufficient for monitoring industrial cycles as:

- They are long cycles, which tend to run over many hours or even days
- Changes in controlled parameters tend to occur at slow rates (e.g. shelf temperature could take minutes to hours to reach desired temperature setting). The slower rates can be carried out to avoid excessive wear on internal components.
- Reduce cost and storage requirements, as high acquisition devices are not generally required

A sampling rate of 10sec was chosen for the TM101 gauge software, as this rate allowed detection of rapid events in the experiments such as pressure rise during the introduction of water vapour when opening a valve on the sample port.

Illustration removed for copyright restrictions

Table 5-F Properties of TM101 device[204]

5.7.5 Dew Point Sensor

The SF52 dew point transmitter (Michell Instruments) has a dew-point measurement range of -40 to +60°C (-40 to +140°F), output of 0-5Vdc and an accuracy of ±2°C (±3.6°F) dew point or 0.4 to 3 g/m^3 (absolute humidity).

LabVIEW^{TM} 2012 and NI USB-6009 DAQ from National Instruments recorded the raw data from the sensor into a text (.lvm) file which could then be analysed in Excel 2010 at the end of the cycle. The schematic diagram used to program the DAQ is summarised in Figure 58.
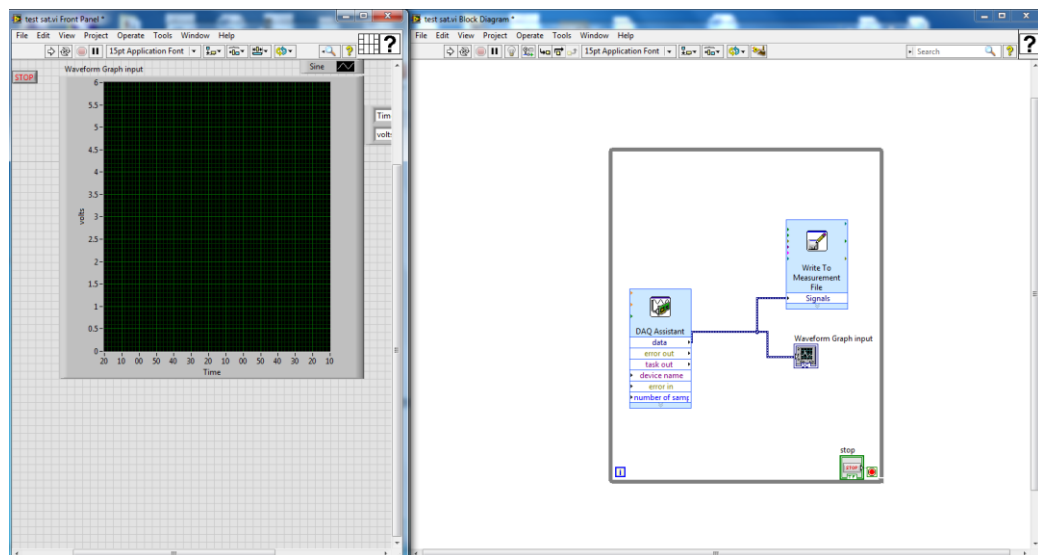
Figure 58 National Instruments software LabVIEW was used to communicate to the DAQ, (1 sample every 10sec).

5.7.6   Samples

Samples were used to simulate different sublimation conditions to be tracked with the different types of sensors including the POFBG, to provide an indication of its viability as an end of primary drying detection sensor.

Fixed 5ml volumes of solutions of distilled water or mannitol (10% weight/volume%) were used in these experiments, poured into vials and placed directly in the freeze dryer. Some samples were frozen overnight in vials in a -80°C or -20°C freezer to be introduced through the access port of the chamber (Figure 52). The freeze drying vials used had dimensions 68,0x 42.5x 1,50mm (Schott AG).

D-mannitol was obtained from Fagron UK (Ph. Eur., Product number (no.) 102220). A Sartorius BP221S mass balance was used to measure the mass of mannitol and OHAUS TS400D mass balance to measure changes in the weight of the vial over time whilst conducting sublimation experiments.

Samples of native collagen (sourced in-house from rat tails) were prepared and kindly provided by Mr Haris Choudhery. The 2.5 mg/ml native collagen samples were prepared using 0.2M acetic acid (Fisher Chemicals) and distilled water to form a 2ml volume that was stored in 35mm wells (2mm fill depth). The samples were placed overnight in an incubator in 37°C at 5% CO^2 to gelatinize. The samples were then frozen overnight in a -80°C freezer, ready to be placed into the freeze dryer the following day for drying.

5.7.7   Scanning Electron Microscope

Micrographs of the freeze dried native collagen scaffolds were acquired with the assistance of Professor Kameel Sawalha, using a Cambridge Stereoscan '90' Scanning Electron Microscope at an accelerating voltage of 25 kV and Orion 6.60.5 software.

5.8   Summary

This chapter lists the materials and methods used to fabricate the POFBGs, connect them to silica pigtails and the protocols and feedthroughs developed to pass the sensors into the freeze dryer.

The chapter also discusses the methods used to minimise leaks into the chamber, to complete the assembly of the freeze drying unit and the protocols required to maintain dry conditions during characterisation of the POFBGs.

The methods discussed in this chapter will be referred to throughout the thesis as they were critical to the characterisation process of the POFBGs with respect to temperature (chapter 6), pressure (chapter 7) and water vapour (chapter 8). These chapters will characterise the POFBGs against standard sensors used in freeze drying applications including thermocouples, dew point sensor and the Pirani gauge. Chapter 9 will then carry out a trial to test the ability of POFBGs to monitor sublimation during freeze drying of mannitol and collagen. This chapter will also compare the POFBG sensor results against standard end of primary drying technologies used in the pharmaceutical industry.

6.1   Overview

Literature suggests that POFBGs have not been tested previously in a freeze dryer, once characterised against CPPs, they were used to determine if POFBGs could be used to monitor sublimation in chapter 8. The aim of this work was to determine if this technology could be used to monitor and detect the end of primary drying time, for applications in the pharmaceutical and food industries. Primary drying was determined to be the longest and most costly stage in the freeze drying cycle and investment is carried out into technologies that can increase productivity, reduce cost and running times[4, 8-11].

This chapter reports on the results obtained from POFBGs placed in a freeze dryer and characterised to determine their response to temperature cycles programed into the PLC of the climatic chamber.

The freeze dryer environment allows the possibility to test POFBGs under vacuum conditions and simultaneously dry conditions of -40°C dew point, as humidity is known to influence the Bragg wavelength of POFBGs made from PMMA. Step index SM PMMA and MM TOPAS fibres were placed into a protective housing and placed onto the temperature regulated shelf which allowed the sensitivity of the sensor to be determined. Further experiments were carried out to study the effects of radiative heat in a freeze dryer which is known to influence the drying rates of pharmaceutical samples. The following chapters will discuss the effects of pressure on the POFBGs along with sublimed water vapour introduced through a side valve into the chamber and samples of mannitol and native collagen freeze dried on the shelf.

6.2   Background

The effects of temperatures (≈20°C and above) on FBG gratings inscribed in PMMA and TOPAS step index (SI) POF have been documented in the literature[12, 153, 205]. Studies suggest the behaviour is dependent on the type of fibre (e.g. structure, composition etc.) and that the Bragg wavelength usually has a negative correlation with respect to temperature, due to the dominance of the negative thermo-optic coefficient of polymers[12]. Equation 9 [12, 195] describes the relationship between the Bragg wavelength shift ($\Delta\lambda_{Bragg}$) and change in temperature (ΔT) for a constant relative humidity, where α is the thermal expansion coefficient and ξ is the thermo-

optic coefficient. It is important to note that α and ξ may not lead to a simple linear equation because they could be functions of humidity and temperature.

$$\Delta\lambda_{Bragg} = \lambda_{Bragg}(\alpha + \xi)\Delta T$$

Initial studies reported PMMA POFBG sensitivities as -360pm/°C[12, 15] with regions of non-linearity across the measurement range and -149pm/°C for a working range of 20-65°C[12, 206]. It is important to note that these studies were often conducted under conditions were the humidity in the environment was not controlled and could have influenced the Bragg wavelength shift.

Some projects investigated the sensitivity of POFBG fabricated in mPOF, and reported a range between -71.8pm/°C and -97pm/°C[12, 15, 143, 178], with the wavelength shift being partially linear across the operating temperature range of ≈20°C to 92°C[15, 143, 178]. This work additionally determined that hysteresis can be observed when carrying out temperature cycles, with fibre shrinkage occurring above a threshold value[12, 143]. The threshold value is influenced by the fibre drawing parameters and the level of exposure to UV[143]. Literature reported hysteresis above 55°C for un-annealed PMMA SM POF and 75°C for PMMA SM POF annealed at 80°C for 2days[169] and shrinkage was observed after 60°C in PMMA mPOF[143].

Harbach measured the temperature sensitivity of step index PMMA fibres, which had gratings inscribed to reflect wavelengths in the 1550nm region. Harbach reported a sensitivity of -10±0.5pm/°C when the devices were placed in a chamber flushed with nitrogen gas to achieve 1.4±1%RH [153]. Harbach also submerged these types of fibres in water and reported a different temperature sensitivity of -36±2 pm/°C[153]. Harbach suggested the difference was the result of an increase in the thermal expansion coefficient and changes in polarizability[153].

Under constant relative humidity (RH) conditions, authors have reported different temperature sensitivities depending on the type of fibre, such as Zhang et al reported about -55pm/°C for a SI PMMA based POFBG reflecting in the 1540nm region for a set humidity of 50%RH[207]. Zhang et al, reported sensitivities ranging from -37 to -52pm/°C for unstrained PMMA based POFBGs in the 1570nm region when kept at a constant %RH level in an environmental chamber (tested 40 to 85%RH), with -43pm/°C at 55%RH[208].

Gratings have also been inscribed in TOPAS mPOF[209], which is a cyclic olefin copolymer[210] and known to be humidity insensitive[18]. Studies have shown for a grating at 1568nm the temperature sensitivity of -37pm/°C was observed[18, 210],

another a SI TOPAS fibre with a ZEONEX cladding[162] had a sensitivity of
$\approx$ -17pm/^{o}C for a grating in the 850nm region[211].

6.3   Aim

This section will study the effect of temperature on POFBGs inscribed in step index
SM PMMA and MM TOPAS fibres in vacuum and dry conditions. To this author's
knowledge, no prior research has been carried out into the capabilities of these
devices to function under sub-atmospheric pressure or within a freeze dryer, which
is a chamber used for the drying process of heat-sensitive samples under vacuum
conditions. The sensitivities of these sensors will be determined in order to
characterise their behaviour within this environment, before testing their viability for
tracking the freeze drying process of mannitol and collagen.

The objectives for this chapter are:

- Determine the sensitivity of the manufactured POFBGs to temperature
  within a freeze dryer, particularly spanning across the negative
  temperature region (below 0°C), which to this author's knowledge has not
  been reported in literature.
- Study the effects of temperature on POFBGs in a freeze dryer under
  constant vacuum pressure at recorded dew point values of -40°C.
  According to the literature search, pressure ranges around the 200µbar
  region and dry environments of -40°C dew point have not been
  previously reported in literature.

6.4   Method

Figure 60(a) illustrates the schematic diagram of the assembled freeze dryer,
sensors and interrogation units used in this chapter. The freeze dryer set-up and
protocol described in section 5.7 (page 109) and 5.7.1 (page 110) were used in this
chapter to study under vacuum conditions, the effects of temperature on the
sensitivity and response of POFBGs (section 5.3, page100). The sensitivities of the
POFBGs were calculated using linear regression and least squares for the curve
fitting error.

The methods discussed in section 5.7 were used to ensure dry conditions during the
course of the experiments. The POF sensors were left for a minimum of 24hrs to dry
under vacuum conditions in the freeze drying chamber and to minimise the effects of
degassing[212, 213], prior to starting the experiments. It concurrently allows drying

of the Perspex door which is facing the vacuum chamber along with adsorbed water on the walls of the chamber as they are other significant sources of moisture in the system.

The POFBGs were connected to a 2x2 1550nm Corning single mode (SM) 50:50 silica coupler (9/125μm), in order to allow both gratings to be tracked during the course of the experiment. An arm of the coupler was connected to a FC/APC silica optical cable that had been fed through the chamber wall using a custom built feedthrough seen in Figure 60(a), to minimise leaks into the chamber. The optical cable was connected to the DL-BP1 SLED broadband light source and I-MON 512 USB interrogator monitor. The I-MON 512 USB evaluation software v1.1 was used to analyse the FBG spectrum and calculate the Bragg wavelength using peak tracking algorithms. Figure 60(c) shows the recorded Bragg wavelengths at a sampling rate of 15sec, from TOPAS and PMMA POFBGs within the chamber during the cycle. The Bragg wavelength response of PMMA and TOPAS POFBG with respect to pressure, dew point and temperature changes are shown in Figure 61 and Figure 152 (Appendix F).

The POFBGs were placed in a protective housing structure (Figure 42) on the temperature regulated shelf in the freeze dryer as described in section 5.7.1 (page 110) and seen in Figure 59. This sensor design is necessary in order to protect the fragile optical fibres from extreme wind speeds which are experienced within the freeze drying chamber, whilst still allowing it to monitor trace water vapour during sublimation experiments. The shelf provides a degree of control over the temperature experienced by the POFBG sensors through heat transfer from the shelf (mainly by conduction and radiation). Independent sensors to the freeze drying unit, shown in Figure 60(a) were connected to the system according to section 5.7 (page 109), to monitor dew point (SF52) and pressure (TM101) in the chamber and temperature (Figure 61). The temperature in the region of the POFs was measured using a K-type thermocouple, which was passed through the chamber wall into the vacuum chamber, using a customised feedthrough connector seen in Figure 60(a). The TM-947SD data-logger was used to collect the temperature readings and the output was plotted in Figure 60(b) and Figure 61(c).

As heat transfer issues through radiative effects are a known influential factor in atypical freeze drying of pharmaceutical formulations[9, 57], 2 K-type thermocouples and an ISO-Tech ILM-01 light meter were placed next to the chamber to monitor air temperature and light levels. This allows the observation of changes in the room temperature which could influence the performance of the machine as well as

observe if the sensor's temperature remains steady on the shelf or if it can be influenced by external factors.

As this freeze dryer is conventionally programmed to carry out "industrial type" recipes for the freeze drying of biological applications, a non-standard program was uploaded into the on-board PLC to allow step changes in temperature for sensor characterisation purposes.

The program was written to carry out a temperature cycle, initially decreasing the shelf temperature from 20°C to -20°C in steps of 5°C and then increasing it from -20°C back to 20°C in steps of 5°C. The chamber was programmed to carry out the step change and maintain the set conditions for 60min before carrying out the next step change, illustrated in in Figure 60(b) and Figure 61(c). These values were selected to begin the step changes at room temperature and to aim towards the temperature range that could be expected during primary drying, generally at <0°C shelf temperature but the cycle is chosen depending on the Tg' of the pharmaceutical samples. The step changes in temperature were selected as the maximum that could be carried out by this system without triggering a "fail-safe mode" and due to limitations of the "automatic" VirTis software program. This software is necessary to interface with the freeze dryer and allows cycles to be automatically carried out over many hours/days without user input; however it possesses limitations such as a maximum number of stored commands (e.g. temperature) per uploaded cycle.

The pressure was set to 200µbar, since this is within the typical operating pressure range of 100-200mTorr[19, 24], that would be used in a standard freeze drying cycle of biological samples. This pressure was monitored by the VirTis thermocouple vacuum gauge and the independent Pirani gauge that was attached to the chamber seen in Figure 61(a), which showed good agreement in pressure in Figure 60(b). Figure 60(b) and Figure 61(b) show that dry conditions were maintained within the chamber, seen by the dew point sensor reading an average of -40°C dew point. Figure 61(c) shows that the thermocouple in the vicinity of the POFBGs is reading a higher temperature than the shelf inlet temperature; this is likely due to heat transfer issues from the shelf to the sensor via conduction and radiation. In freeze drying of pharmaceutical samples it has been documented that there are several barriers to heat transfer which could account for a temperature profile observed from the shelf to the sample[19, 46]. The temperature profile is additionally dependent on[19] the chamber pressure, container (e.g. vial), dryer design and sublimation rate of the sample. There are several barriers to heat transfer[19, 46], including a temperature difference from the interior of the shelf (set point) and the surface of the shelf, the

aluminium sheet not being in perfect contact with the shelf, and incomplete contact of the vial[19, 46] or in this case the POFBGs.
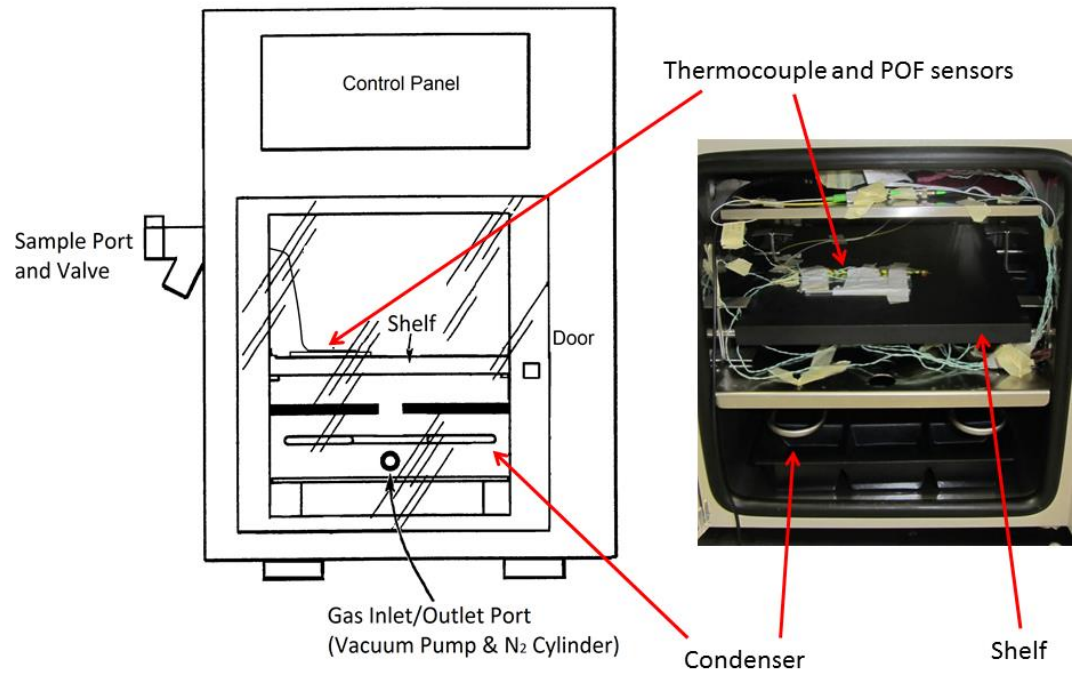
Figure 59 POFBG sensors placed onto the shelf of the freeze dryer
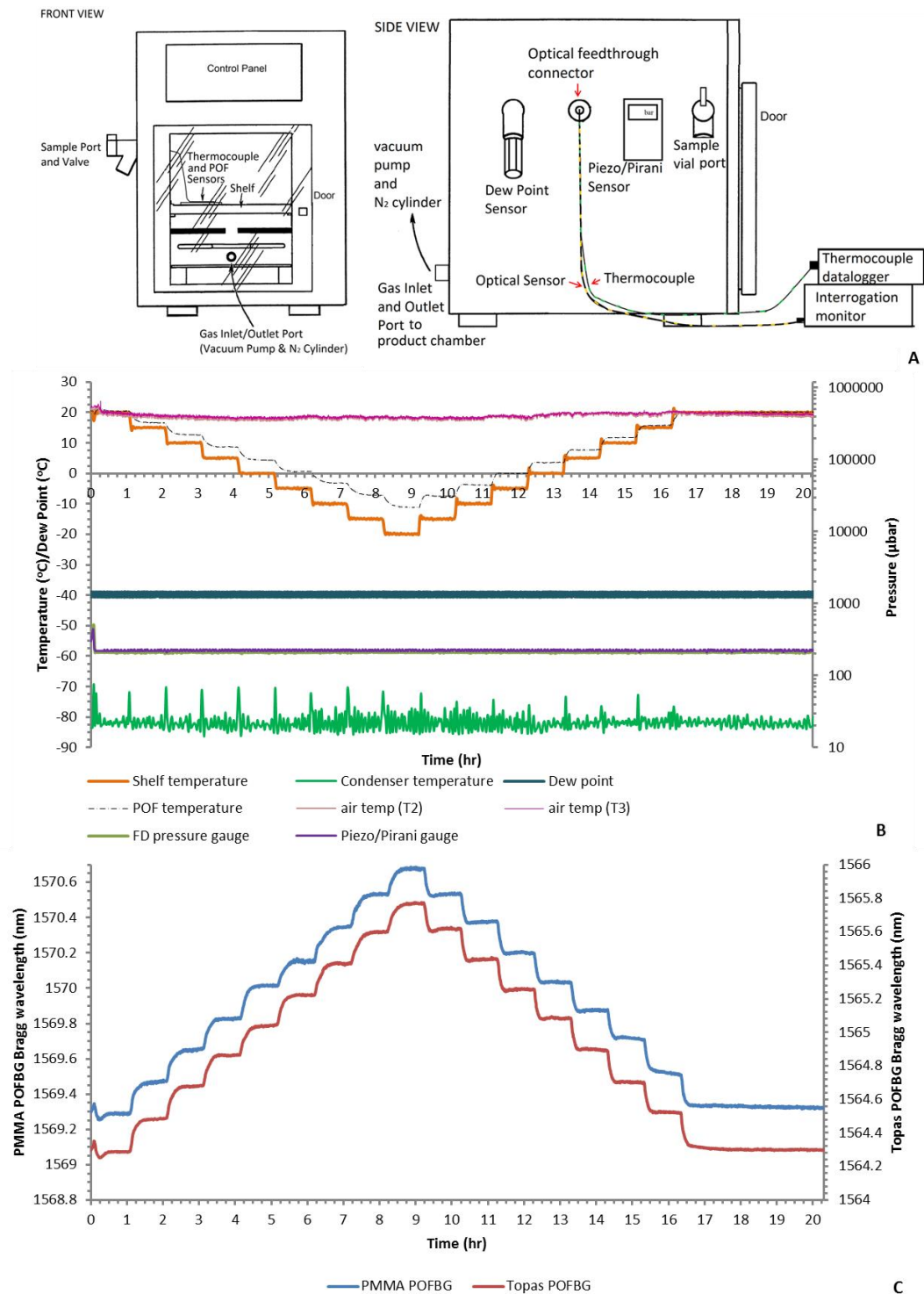
Figure 60 Experimental protocol for characterising PMMA and TOPAS based POFBG. (A) Schematic representation of the purpose built freeze drying experimental unit (B) Cycle uploaded to the freeze dyer controller, showing step changes in temperature at a constant pressure and constant dew point. (C) Wavelength output of the POFBG sensors.
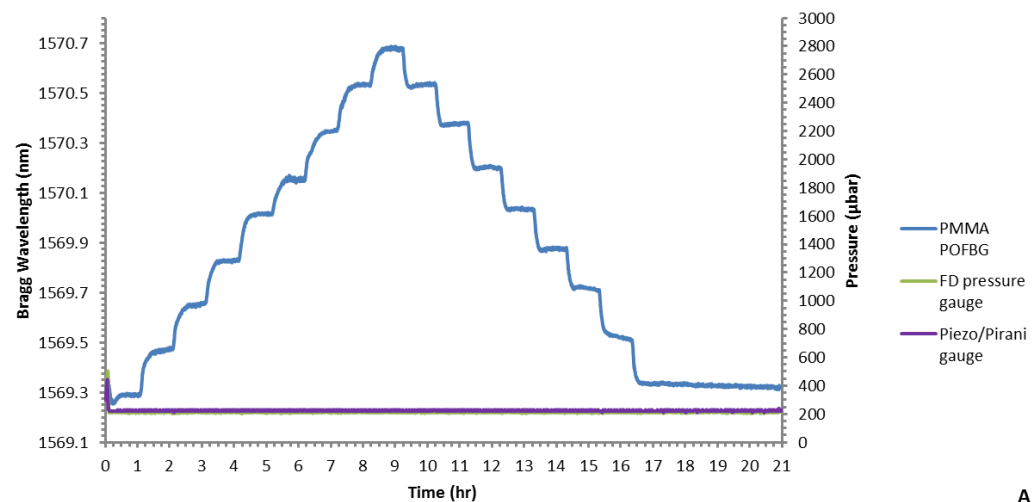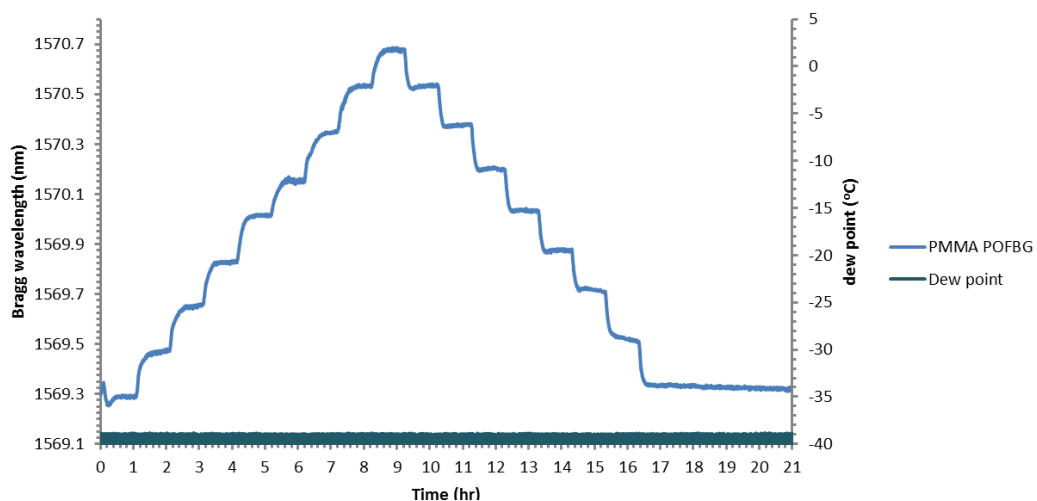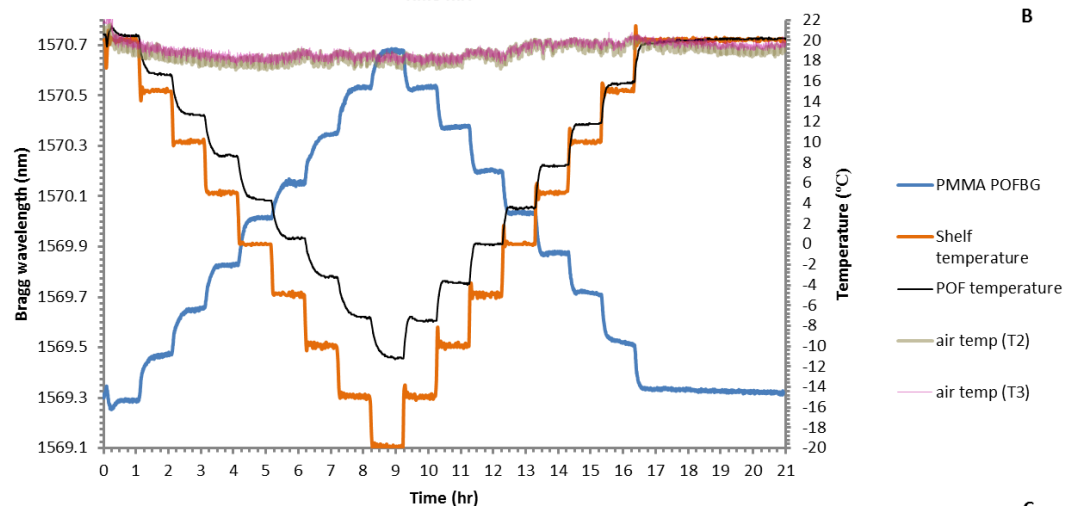
Figure 61 POFBG wavelength against (A) pressure in the chamber, (B) dew point in the chamber, (C) temperature of the shelf, thermocouple temperature in the region next to the POF sensors ("POF temperature") and air temperature outside the freeze dryer (T2 and T3)

6.5 Results and Discussion

6.5.1 PMMA and TOPAS POFBG

Figure 62 shows the wavelength shift for POF1 and POF2 (section 5.3, page 100) in response to the input step changes in temperature. In this experiment, these types of fibres show a reversible 1.38nm shift in the PMMA Bragg wavelength and a 1.47nm shift in the TOPAS POFBG when the shelf temperature is cycled between 20°C and -20°C. The graph also reveals that both POFBG sensors experience a red shift in response to a decrease in temperature from 20°C to -20°C. The red shift in the Bragg wavelength as the temperature decreases is in good agreement with literature, due to the dominance of the negative thermo-optic coefficient of polymers[12]. It is important to note that the observations reported in literature are at atmospheric pressure in humid environments, rather than a vacuum chamber containing a dry nitrogen atmosphere at sub-atmospheric pressures (200µbar), as investigated in this project.

Sensitivities of -34.0±0.4pm/°C and -33.0±0.3pm/°C were observed for PMMA POFBG, for increasing and decreasing step changes in temperature respectively, and -36.0±0.3pm/°C and -37.0±0.2pm/°C for TOPAS POFBG. The values are within the range of those reported in literature[18, 207, 208, 210]; however it must be noted that these experiments were carried out under humid conditions, higher temperatures and at atmospheric pressure.

Harbach tested the sensitivity of SI PMMA POFBGs operating in the 1550nm region and found -10.0±0.5pm/°C in ≈1.4±1%RH[153]. The difference in performance could be due to differences between the two types of fibres, particularly drawing tension, thermal history, composition (e.g. dopants) and chain orientation (e.g. annealing process) which could influence the thermal expansion coefficient. It is also likely that as humidity was still present in the chamber ≈1.4±1%RH, it could have affected the wavelength shift as both the refractive index and the grating pitch are influenced by temperature and water content of the PMMA fibre[14]. Research has shown that water acts as a mild plasticiser for PMMA for bulk materials up to about 1% [214]and at higher content haziness, clustering or aggregation of water molecules[16, 214] occurs.
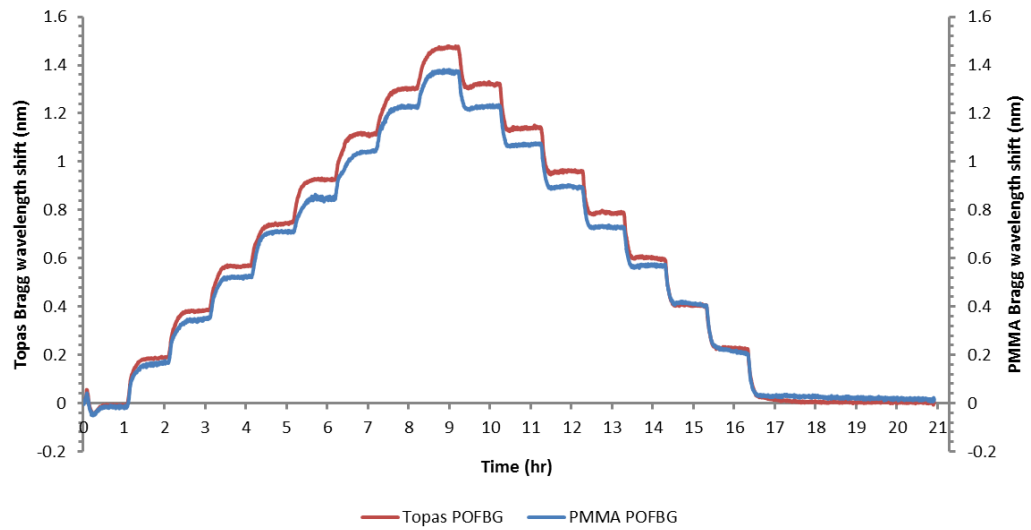
Figure 62 Bragg wavelength shift of PMMA and TOPAS based POFBG (POF1 and POF2), shelf temperature varied between 20ºC to -20ºC in increments of 5ºC

Figure 63 shows differences in the observed Bragg wavelength between the increase and decrease stages of the experiment. This could have resulted from differences in the observed temperature in the region of the POFBG that was detected by the thermocouple, between the rising and falling step changes in temperature as seen in Figure 64. The difference in temperature could have resulted from differences in heat transfer to the sensor, most likely due to radiative effects from the wall of the chamber or through the Perspex door[9] as seen in Figure 70 and Figure 71. The pressure and dew point sensors were showing no change in performance during this range (Figure 61 (a and b)).
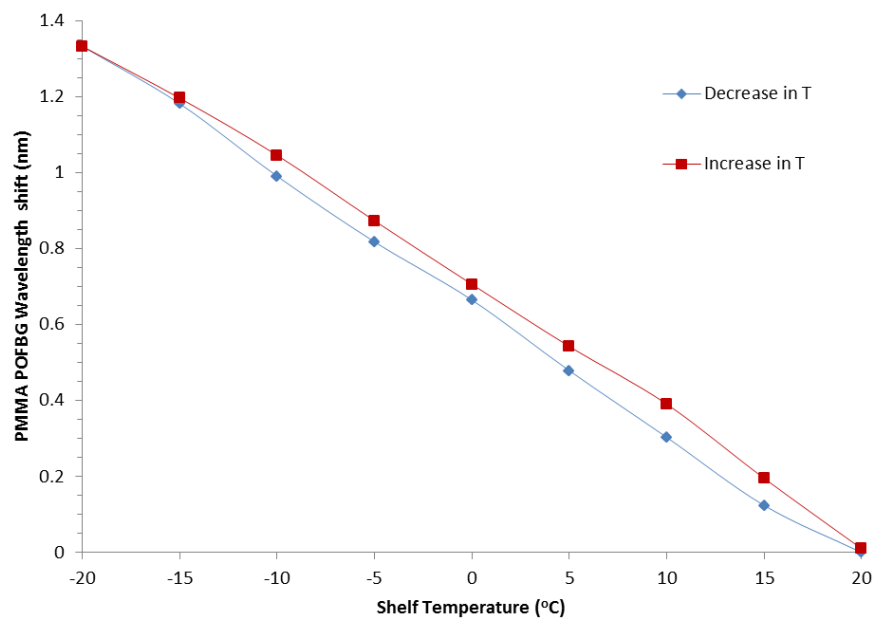
Figure 63 Bragg wavelength shift of PMMA POFBG (POF1) for increase and decrease in temperature cycles, where the temperature is measured at the inlet of the shelf
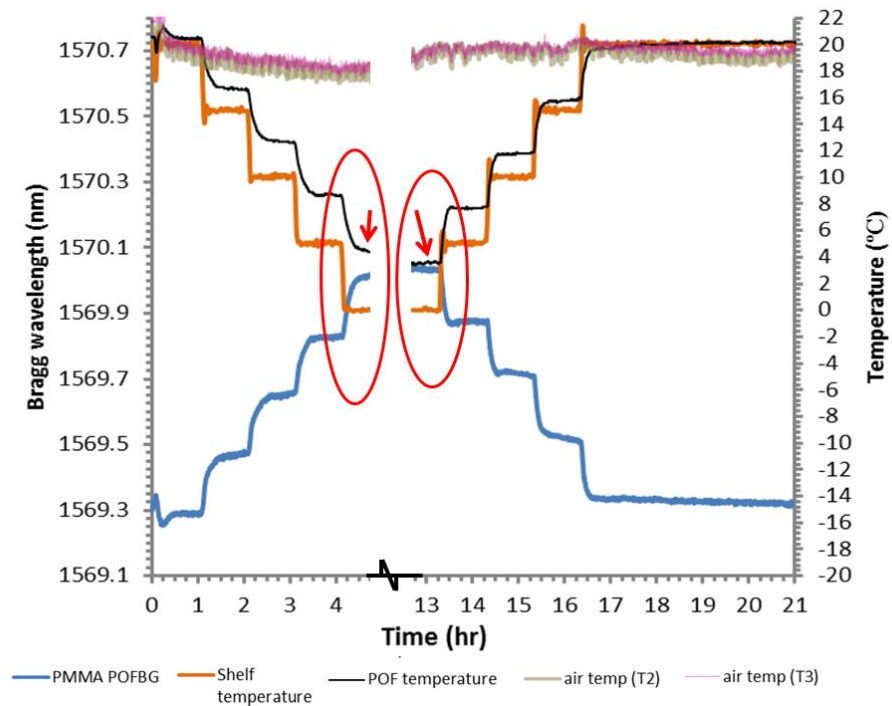
Figure 64 Bragg wavelength shift of PMMA based POFBG (POF1), temperature profile of the freeze dryer inlet shelf temperature, thermocouple reading the POF temperature and outside air temperature of the room where the freeze dryer was stored. Red circles illustrate differences in temperature detected by the thermocouple in the vicinity of the POFBG

Figure 64 shows a delay in the response of the thermocouple to the step change in temperature from the shelf; this is likely to be the result of barriers to heat transfer (shelf design, aluminium sheet, protective sleeves). It is also possible that there is a delay in the heat transfer between the cooling and heating stage, as the cooling fluid needs to be separated using solenoid valves into either the shelf or condenser (which must remain around -80°C), whilst there is an independent heating element in the shelf.

Figure 65(a) shows PMMA POFBG data from 4 repeats which had the same program uploaded to the PLC to carry out step changes in temperature from 20°C to -20°C, at 200µbar and recorded -40°C dew point. The chart shows the POFBGs have the same sensitivity; however "trial 3" has a noticeable blue shift offset from the other 3 repeats. It was found that the pressure and dew point remained constant during all 4 cycles. The temperature of the thermocouple in the vicinity of the PMMA POFBG was showing a significantly higher temperature during cycle "trial 3", seen in Figure 65(b), up to 2°C higher per step change than the other cycles. Due to the dominance of the negative thermo-optic coefficient of polymers[12] this could explain the blue shift in wavelength observed across "trial 3", which experienced a higher temperature than the other three cycles. It was also noted that the room

temperature at the beginning of the "trial 3" experiment was higher than the other experiments (≈3°C); this could have contributed to the increase in heat transfer.
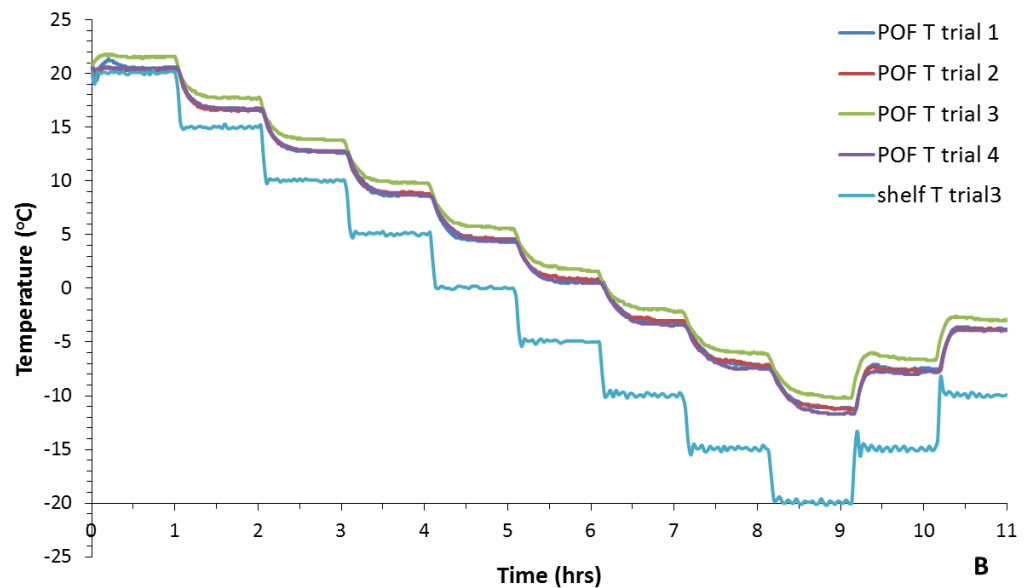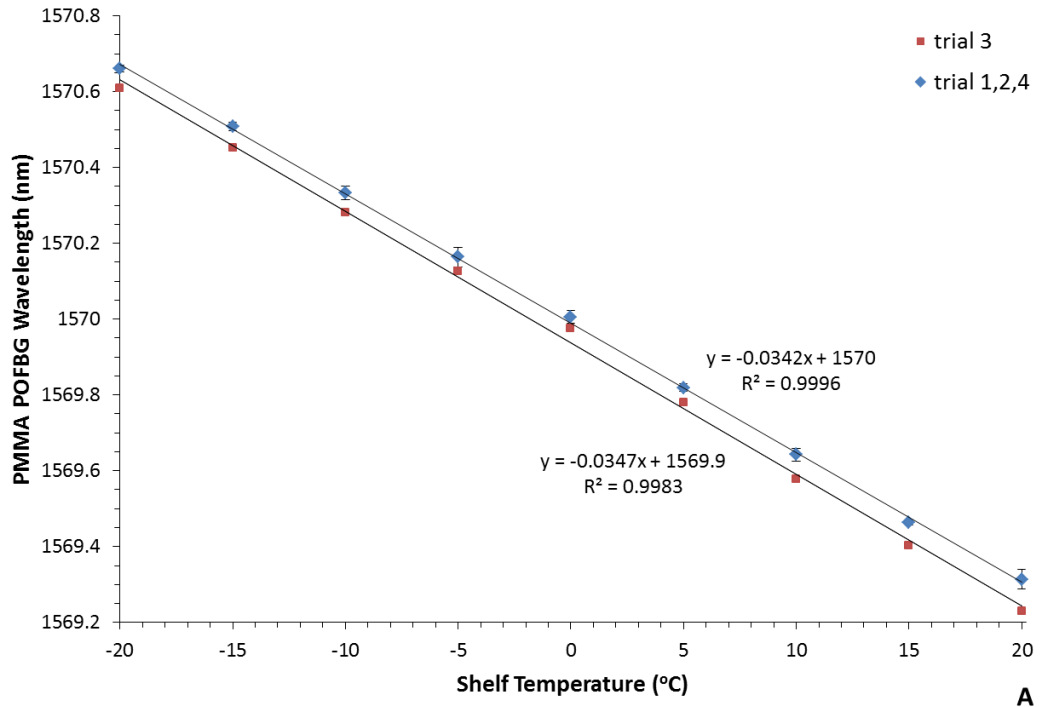
Figure 65 (A) Bragg wavelength shift of PMMA based POFBG (POF1) for step changes in temperature from 20°C to -20°C, n=4, (B) POF temperature profile, n=4 and shelf temperature profile for trial 3

The data from Figure 65 were compared against TOPAS POFBG (POF2) that was present in each cycle in the same location next to the PMMA POFBG (POF1); the data were plotted in Figure 66. Figure 66 also illustrates a blue shift in the Bragg

grating of the "trial 3" cycle, for the same conditions experienced by the PMMA POFBG in Figure 65. It is very likely that both POFBGs were reacting to the different temperature profile experienced in "trial 3" and observed in Figure 65(b).
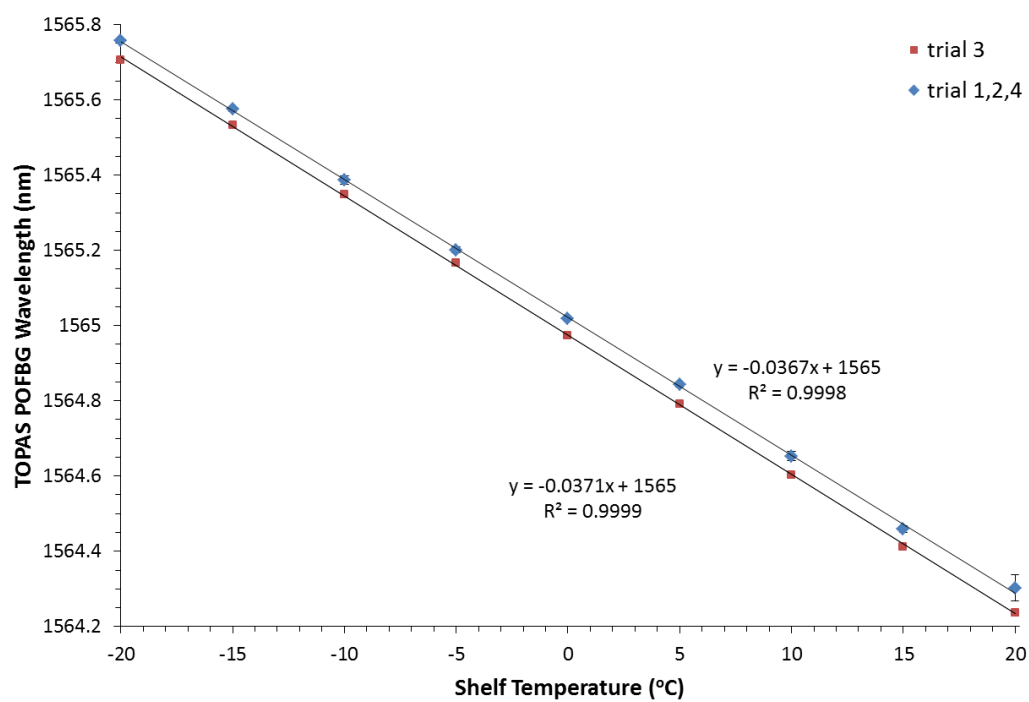
Figure 66 Bragg wavelength shift of TOPAS based POFBG (POF2) for step changes in temperature from 20ºC to -20ºC, n=4

6.5.2   Annealed PMMA POFBG

The same temperature cycle as described in section 6.4, was tested on additional POFs, to observe their response to temperature. Figure 67 shows the data plotted from a TOPAS POFBG (POF3) and PMMA based POFBG (POF4), the PMMA fibre was annealed at 80°C for 7hrs before inscription was carried out. PMMA based POFBG (POF5) was inscribed on the same fibre as POF4, they are separated by 1cm, Figure 153 (Appendix F) shows the response of the grating to step changes in temperature.

As with the previous experiments a red shift with decrease in temperature is observed; there is good reproducibility in the data with a small difference in the sensitivity between the decrease and increase temperature stages, likely due to equipment measurement error. Table 6-A shows that TOPAS POFBG (POF 3) and TOPAS POFBG (POF 2) have a small difference in their sensitivity (of 1pm/°C). Since both fibres were produced using the same protocol and batch of fibre, the differences are potentially due to equipment measurement error. Figure 155 shows the results from TOPAS POFBG (POF 2) and is available in Appendix F.

A difference is observed between the sensitivities of PMMA based POFBG (POF4) and PMMA POFBG (POF1), with POF1 showing higher sensitivity to temperature than POF4. This is possibly due to different fibre composition, internal stresses due to temperature cycling and annealing process on POF4 which is known to cause fibre shrinkage and relaxation of the axial orientated chain molecules[12, 15, 209, 215, 216]. The drawing tension and thermal history during the processing of the fibre, results in axial orientation of the polymer chains and residual strain in the fibre[15, 209]. Annealing can be carried out to relax the chains along the axis and to reduce hysteresis[170] for sensing applications.
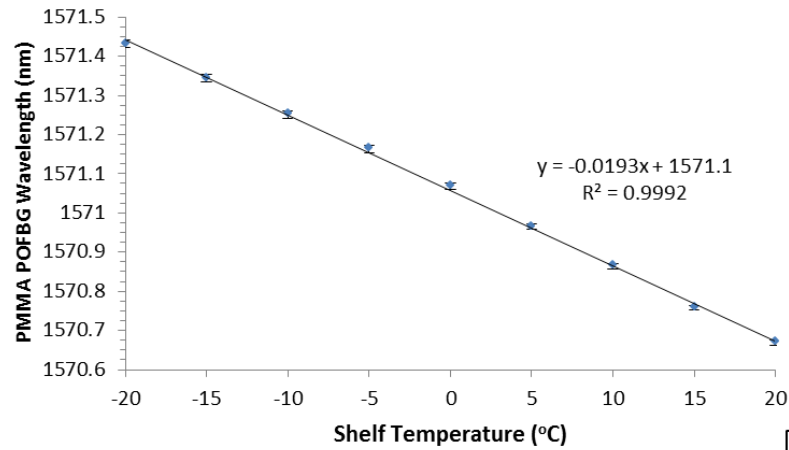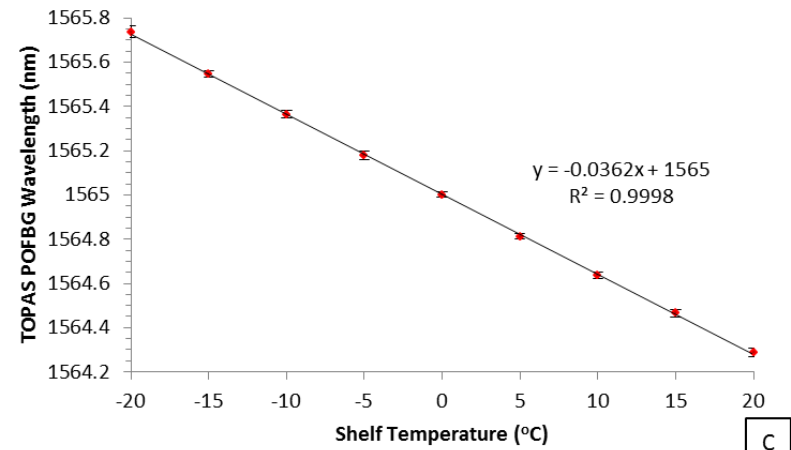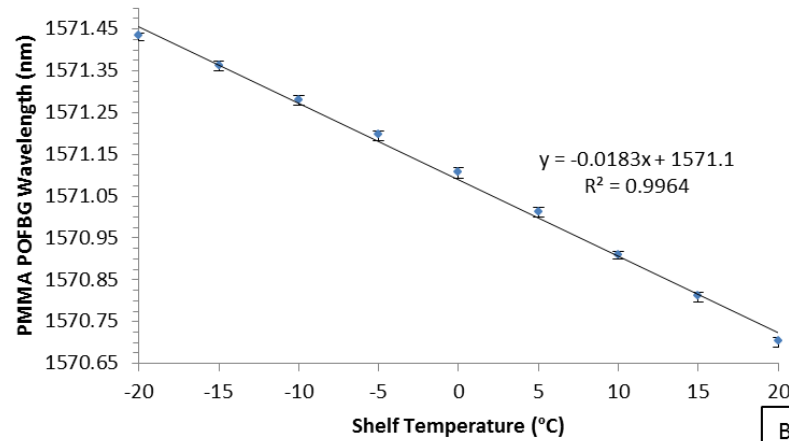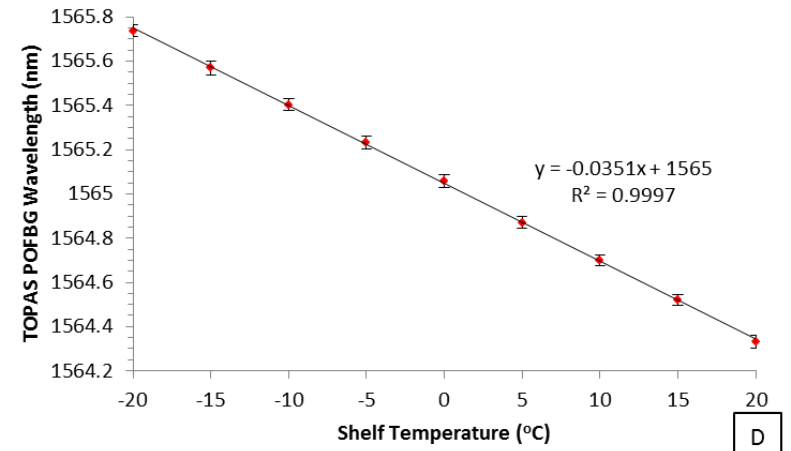
Figure 67 Bragg wavelength shift with respect to temperature in a freeze dryer (n=3), where: (A) the step changes in shelf temperature decreased from 20ºC to -20ºC for PMMA POFBG (POF4), (B) the step changes in shelf temperature increased from -20ºC to 20ºC for PMMA POFBG (POF4), (C) the step changes in shelf temperature decreased from 20ºC to -20ºC for TOPAS POFBG (POF3), (D) the step changes in shelf temperature increased from -20ºC to 20ºC for TOPAS POFBG (POF3)

Some cycles show POFBGs experienced a degree of hysteresis as seen in Figure 68, where a 43pm shift was seen for PMMA POFBG (POF4) and 52pm shift for TOPAS POFBG (POF3). This pattern was observed by other POFBGs, including PMMA POFBG (POF5) shown in Figure 154(Appendix F). The pressure and dew point had not changed during the decreasing and increasing step changes in temperature and remained stable at 200µbar and an average of -40°C dew point.

The hysteresis could be due to internally built up stresses from the cycling of temperature between 20°C and -20°C. Another influential factor is the change in temperature due to radiative effects, as seen previously with POF1 in Figure 64. POFBGs that experienced a hysteresis had a different temperature in the vicinity of the grating at the start and end of the experiment (for the same 20°C inlet shelf temperature), as the temperature drifted over the course of the cycle (e.g. Figure 69). The Bragg wavelength recovered if the temperature in the vicinity of the POFBG returned to the same temperature that was recorded at the start of the experiment; however it would not if the temperature difference remained large. These trends are seen in Figure 69, where the thermocouples in the vicinity of the FBG registered differences in the temperature between the rising and falling step changes in temperature (arrows). This is likely to have resulted from radiative effects e.g. from changes in the ambient room temperature, which contributed to the shift in the Bragg wavelength.

PMMA POFBG

A

TOPAS POFBG

B
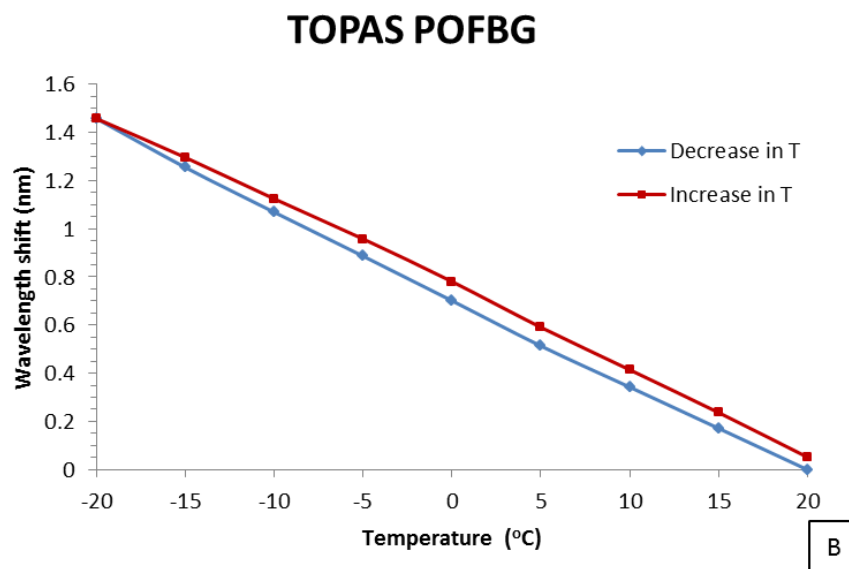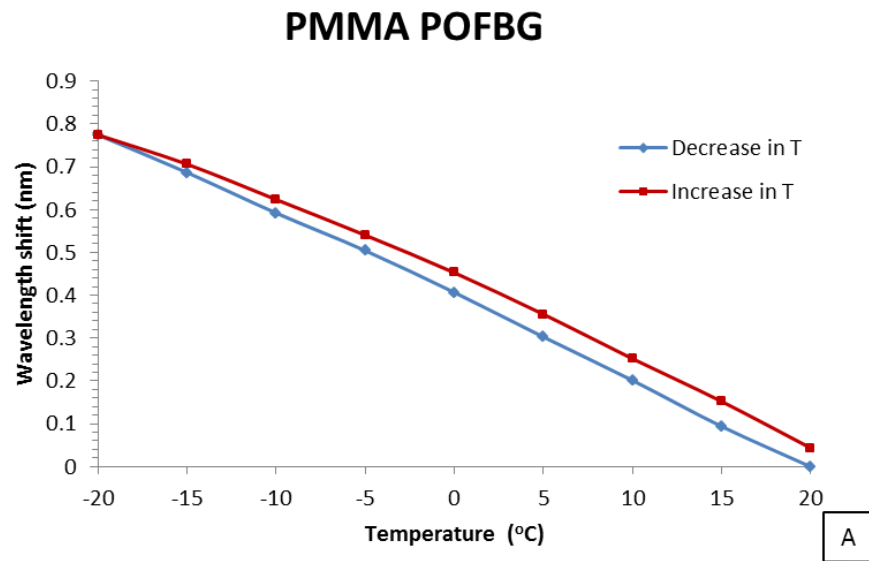
Figure 68 Bragg wavelength shift with respect to temperature in a freeze dryer (a) PMMA POFBG (POF4), (b) TOPAS POFBG (POF3)
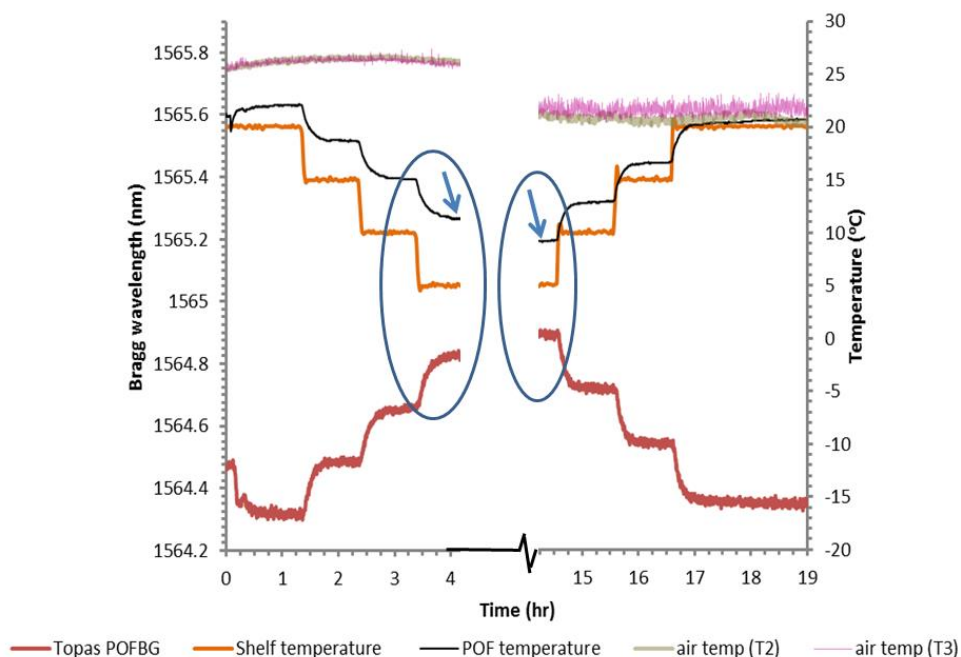
Figure 69 Bragg wavelength shift of TOPAS POFBG (POF3), and temperature profile of the freeze dryer inlet shelf temperature, thermocouple reading the POF temperature and outside air temperature of the room where the freeze dryer was stored. Blue circles illustrate differences in temperature detected by the thermocouple in the vicinity of the POFBG.

Figure 70 and Figure 71 show some of the potential sources of radiative effects which can influence samples within a freeze dryer or vacuum chamber. The shelf temperature was initially cycled between 20°C and -20°C and from 17hrs onwards held at a set point of 20°C at 200µbar and -40°C dew point. POF 3 and POF 4, with FBG profiles described in section 5.3 were used in this experiment. It is possible to see in Figure 70 and Figure 71 that the TM-947SD temperature Data logger recorded cyclic patterns in the surrounding air temperature depending on the time of day. In this case, amplitude oscillations of about 10°C peak to trough (±5°C) can be seen in the ambient air temperature around the freeze dryer, with peaks and troughs observed during daytime and night time respectively. Both the POF and the thermocouple are also showing similar oscillating patterns across the boxed regions in Figure 70 and Figure 71 despite the shelf temperature being set at 20°C. This oscillating pattern was observed by the thermocouple (≈±1°C), PMMA POFBG (±17pm) as well as TOPAS POFBG (±30pm) in Figure 72(b) during the same experiment. Table 6-A lists the sensitivities of the POFs, where TOPAS POFBG has a temperature sensitivity of -35.0±0.4pm/°C and PMMA POFBG of -18.0±0.3pm/°C, explaining the observed Bragg wavelength oscillations being due to oscillations in temperature. Radiative heat transfer, is a known factor in influencing freeze drying of pharmaceutical

vials, and has been documented in literature as causing edge or front row vials to finish sublimation prior to the rest of the batch[9, 46].
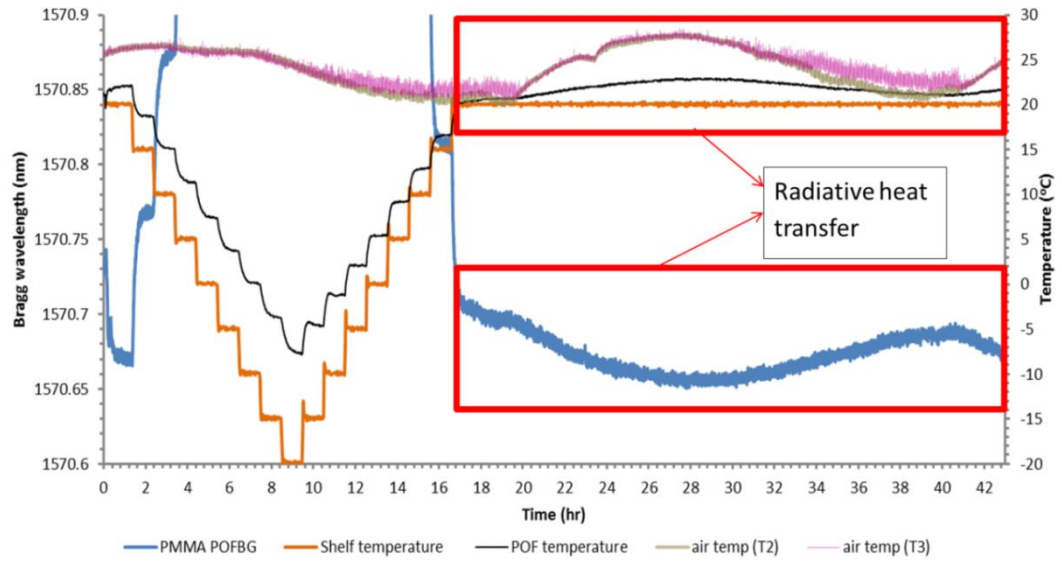
Figure 70 temperature cycle carried out on PMMA POFBG (POF4) and left at 20C shelf temperature set point after 17hrs. During the whole process the pressure was set at 200μbar and kept at -40ºC dew point.
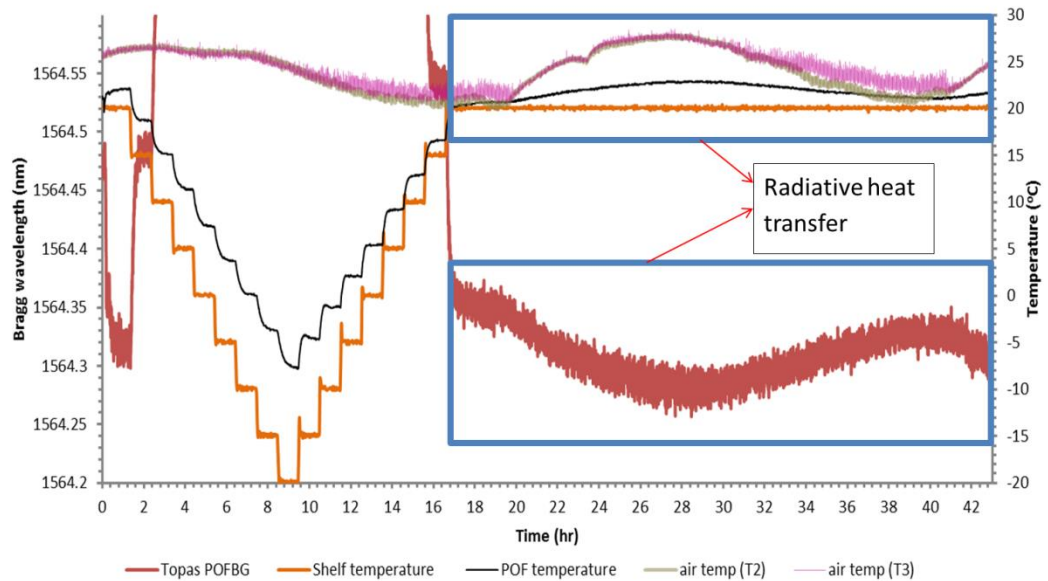
Figure 71 temperature cycle carried out on TOPAS POFBG (POF3) and left at 20C shelf temperature set point after 17hrs. During the whole process the pressure was set at 200μbar and kept at -40ºC dew point.

Figure 73 shows the data obtained from the OctTemp (MadgeTech) temperature data logger that was placed in the freeze dryer in Figure 72(b), with a temperature cycle (20ºC to -20ºC), 200μbar and -40ºC dew point spanning across several days. The thermocouples were placed on the shelf and on the POFBG sensor, seen in Figure 72(a), to obtain the temperature profile in the freeze dryer across the days.
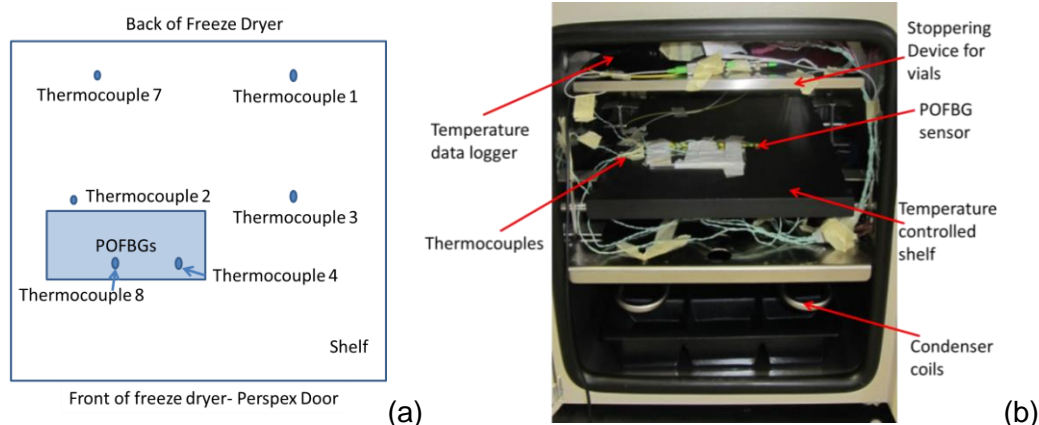
Figure 72 (a) Thermocouple positions on the shelf and on the POFBG sensor (b) freeze drying unit showing the location of the sensors and one of the temperature data loggers
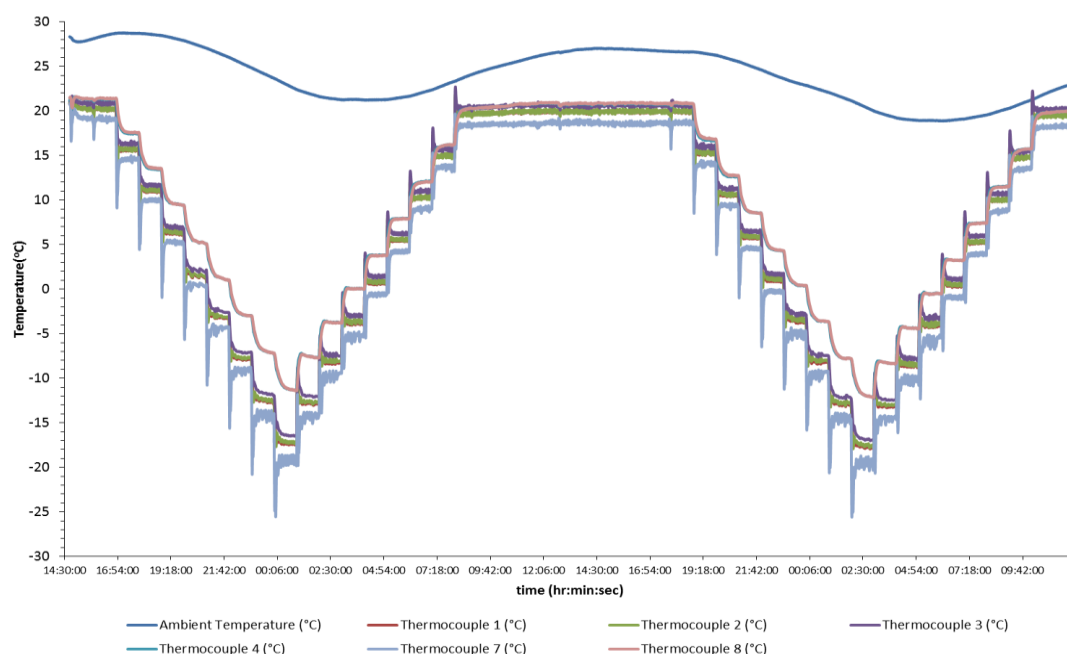
Figure 73 temperature profile within the freeze dryer logged with the OctTemp (MadgeTech) over 2 days. Thermocouples 1,2,3,7 are positioned on the shelf and thermocouples 4,8 are positioned on the POFBG sensor. The Ambient temperature logged is in vacuum in a space above the "stoppering device for vials" away from the shelf.

Figure 73 shows limitations in the design of the control system and design of the freeze dryer which can contribute to changes in the heat transfer to the POFBG sensor and the detection of other variables in the system. The control system creates overshoots at the beginning of the step changes in temperature in Figure 73, which is picked up by the thermocouples 1,2,3,7, attached to the surface of the shelf. The thermocouples reveal the presence of a temperature profile across the surface of the shelf with some thermocouples reading surface temperatures higher than the inlet temperature set by the uploaded program and a delay in

reaching an equilibrium temperature. There are also large oscillations in temperature at the surface of the shelf depending on the location of the thermocouple, with the largest at the inlet cooling fluid area in the back of the shelf, where thermocouple 7 is oscillating up to ±1°C. The graph reveals a predictable profile likely due to the liquid cooling system present in the shelf which is controlled by the opening and closing of a digital solenoid valve.

The data logger also picked up higher average temperatures from thermocouples 4 and 8 positioned on the POFBG sensor than the shelf temperature, likely from barriers to heat transfer, confirming the observations from the TM-947SD temperature data-logger (Figure 70 and Figure 71). The ambient temperature of the space above the "stoppering device for vials" marked in Figure 72(b) was also shown to have rhythmic oscillations in temperature depending on the time of day, like those detected by the TM-947SD temperature data-logger.

These experiments have shown the influence of radiative heat and barriers to heat transfer on the temperature of the POFs and the thermocouples, some sources of radiative heat that contribute to these changes include:

- Heat from the room, which is shown to oscillate depending on the time of day or night. This occurs as there is no air conditioning available in the room to control the temperature, particularly as the freeze dryers generate significant heat due to refrigeration system (compressor) and vacuum pump.

- Heat generation from freeze dryer through the internal walls by conduction and radiative heat transfer (compressor, radiator, vacuum pump etc.). At higher room temperatures than manufacturer's recommendations (15 to 25°C[217]) could cause the freeze dryer to overheat if sufficient cooling from the external air temperature cannot be achieved. This could lead to an increase in machine temperature and could cause radiative heat into the vacuum chamber and via the conduction of heat into the chamber wall. If the temperature of the room goes above a critical limit outside of the recommended operating temperature range, the cooling system cannot keep the freeze dryer cool, ultimately resulting in damage to the electronics and freeze dryer malfunction[218].

- Other heat generating equipment (e.g. motors) in the room

- Perspex door allows the user to observe their samples during the course of the cycle, however it also allows transmission of light through the door,

which can lead to different radiative effects particularly on the front row samples[9]. This effect was also observed by pointing a torch against the door at the POF and thermocouple. The temperature was found to increase by 0.3°C when the beam of light was aimed at the sensors for 1min whilst they were in vacuum and a drop in temperature observed when the torch was removed.

- There are large south facing windows next to the machine, which allowed solar gain to occur and significantly oscillate the lux and temperature inside the room. An ISO-Tech ILM-01 light meter was used to measure the lux values across the day and the range varied from 0.18 lux (darkness at night) to 1667 lux (sunny bright day in summer), with overcast days capable of having up to ≈640-950 lux in the room.

- Shelf is a controlled source of radiative heat

6.5.3 POFBG comparison

Table 6-A shows the results from the POFBGs that were exposed to the temperature cycles between 20°C and -20°C, at 200µbar and remained under dry conditions at -40°C dew point, as humidity is known to influence Bragg wavelength.

	PMMA POFBG (POF1)	TOPAS POFBG (POF2)	TOPAS POFBG (POF3)	PMMA POFBG (POF4)	PMMA POFBG (POF5)
Increase in temperature	-34±0.4 pm/°C	-36±0.3 pm/°C	-35±0.4 pm/°C	-18±0.3 pm/°C	-17±0.3 pm/°C
Decrease in temperature	-34±0.3 pm/°C	-37±0.2 pm/°C	-36±0.3 pm/°C	-19±0.2 pm/°C	-18±0.2 pm/°C
Average max wavelength shift (mean ±SD, n=3)	1.350nm (±0.019)	1.460nm (±0.036)	1.450nm (±0.012)	0.760nm (±0.011)	0.700nm (±0.013)

Table 6-A POFBG sensitivities and wavelength shift (n=3)

TOPAS POFBGs (POF2 and POF3) in Table 6-A have reproducible sensitivities in response to the step changes in temperature (n=3) and have a small offset between the two POFBGs. The differences could be due to variation within the

same batch of TOPAS core and ZEONEX cladding fibres, differences in inscription time or due to equipment measurement error.

There is an observable difference between POF 1 that was inscribed in un-annealed PMMA POF and POF4 and POF 5, which were two gratings separated by 1cm that were inscribed in a PMMA POF annealed at 80°C for 7hrs.

The fibre drawing process causes axial orientation of the polymer chain molecules which during the cooling stage can introduce internal stresses into the fibre[12, 209]. Annealing is a thermal cycle used to relax the axial orientation of the fibres which causes fibre shrinkage [12, 15, 209, 215, 216] and changes in the polymers properties. It is possible that the annealing process has changed the thermo-optic coefficient[12], potentially reducing its influence on the Bragg wavelength shift and reducing temperature sensitivity. The annealing process may also have affected the thermo-expansion coefficient, this would require further investigation in future projects.

6.6   Future Work

Studies could involve investigating the behaviour of the thermo-optic coefficient and the thermal expansion coefficient of the optical fibre, particularly the effect of different POF annealing procedures on the FBG behaviour within dry sub-atmospheric conditions.

Future investigations would involve etching the fibre to observe whether the response time of the sensor could be improved and determining the temperature sensitivity of the fibres at different chamber pressures.

Studies would involve the characterisation of other types of optical fibres such as polycarbonate (PC), polystyrene (PS), mPOF to temperature within the vacuum chamber and to determine whether they could be used in freeze drying applications.

Radiative effects and heat transfer from the shelf are influential factors in freeze drying and could influence the ability of the grating to monitor water vapour in the chamber to allow detection of the end of primary drying time. Future work would investigate different temperature compensation techniques e.g. using multiple FBGs on the same fibre, to compensate for the effects of temperature and output Bragg wavelength shift as a result humidity.

Investment in the machine such as a new PLC (including PID controller option) and changes to some of the design, would produce a climatic chamber that allows more flexibility and customised cycles to be written for characterisation of

sensors e.g. to study the POFBG behaviour at lower temperatures. The PLC could improve control over the CPP and by connecting all the different sensors to the same PLC unit, allow simultaneous logging of the data and provide timing data according to its internal clock. This would allow the user to investigate the response time of the sensors to the stimuli or CPP. The sensors would also provide real time feedback to the controller, in order to continuously assess the freeze drying cycle and determine when to automatically complete a stage e.g. determine the end of primary drying time.

6.7   Conclusion

This chapter studied the effects of temperature on step index SM PMMA and MM TOPAS POFBGs, under dry, sub-atmospheric conditions in a freeze dryer. The POFBGs were inserted into a housing structure that successfully protected the POF and its associated glue joint against the chamber high wind velocities, allowing monitoring of temperature inside the freeze dryer. The sensors revealed that red shifts in the Bragg wavelengths occurred as the temperature decreased from an inlet shelf temperature of 20°C to -20°C. Literature reports that an increase in the Bragg wavelength occurs when the temperature decreases, due to the dominance of the negative thermo-optic coefficient of polymers[12]. The sensitivities documented in this project are within the range of those reported in literature[18, 207, 208, 210]; however it must be noted that they were exposed to different environmental conditions. Those studies reported POFBGs sensitivities obtained using climatic chambers maintained at atmospheric pressure, higher temperatures and a humid environment. Future work would involve expanding the range of temperatures that the POFBGs are exposed to, in dry atmospheric and sub-atmospheric conditions in order to determine in greater detail the effect that dry conditions have on temperature sensitivities.

Two FBGs were inscribed into a PMMA POF that had been annealed at 80°C for 7hrs and were exposed to step changes in temperature at 200μbar. The sensitivities were compared and showed good reproducibility for n=3. The same trend was observed in two un-annealed TOPAS POFBGs, producing temperature sensitivities of -36±0.3pm/°C and -37±0.2pm/°C. The small difference in the sensitivities could have resulted from batch variations in the fibres or equipment measurement error.

A reduction in the sensitivity to temperature was observed when the PMMA POF had received an earlier annealing treatment. Research suggests that the

annealing process relaxes the molecular chains in the axial orientation; it is hypothesised that this process changes the thermo-optic coefficient and the thermal expansion coefficient of the fibre and this would need to be tested and confirmed in future experiments.

During some of the cycles in the dry vacuum chamber (at 200µbar), a small hysteresis in the Bragg wavelength occurred when the temperature drifted over several hours in the region of the POFBGs. The Bragg wavelength recovered if the temperature drift returned to values in the vicinity of the original temperature; however this did not occur if the temperature difference remained significant. The drift in temperature was likely caused by external heat transfer to the POFBGs, as experiments and literature showed radiative effects from the external environment affected the temperature within the vacuum chamber.

The optical fibres were used with thermocouples to study the temperature distribution in the freeze dryer, particularly as it is an influential factor in the freeze drying of pharmaceutical samples. It was found that the freeze dryer has design and control system limitations which results in differences in the temperature distribution across the surface of the shelf and a temperature profile across the separation distance between the POFBG sensors and the shelf, due to heat transfer barriers. Tests also confirmed that the room temperature also play's an influential role on the temperature observed by all sensors (including the POFBG) in the vacuum chamber due to radiative effects; the room had a large amount of glazing making it particularly vulnerable to the influence of solar gain.

7 Wavelength response of POFBGs to Pressure alterations in a Freeze Dryer

7.1 Overview

This chapter reports on the effects of low pressure cycles in a freeze dryer on POFBGs. This work uses POFBGs that were manufactured according to section 5.2 and in chapter 6 characterised for their performance to temperature in a freeze dryer. These experiments have not been attempted previously in a freeze dryer and provide information on the behaviour of these devices under these conditions, which can be used when assessing the response of the POFBGs to sublimation.

This environment allows the possibility to test POFBGs under vacuum and dry conditions in which the dew point sensor reads -40°C dew point. This equipment allows the study of these sensors under dry conditions, as humidity is known to influence the Bragg wavelength shift of POFBGs inscribed into materials made from PMMA. Step index SM PMMA and MM TOPAS fibres in a protective housing, were placed onto the temperature regulated shelf prior to reducing the chamber pressure, to test the performance of the sensor. The chapter finishes with studying the long term effects of placing a PMMA and TOPAS POFBG in to a freeze dryer for 40 days.

The following chapters will discuss the effects of sublimation of water vapour and freeze drying of samples of mannitol and native collagen on POFBGs.

7.2 Background

The effects of pressure on silica optical fibres inscribed with FBGs have been studied in the literature[132, 219-221] as they provide additional advantages such as size, weight and resistance to electro-magnetic interference compared to traditional sensors[132, 133]. Despite these advantages, silica optical fibres have been found to possess limitations such as low sensitivity to pressure due to inherent material properties. Some studies report sensitivities of: -3.88pm/MPa[222] and -3.04×10^{-3}nm/MPa[220] when placed in pressurised vessels operating up to 10MPa and 70MPa respectively. Due to their demand for use in medical applications or extreme environmental conditions[132, 133] (e.g.

oil and gas industry[223]), research has been carried out into different techniques to improve their properties[133, 219, 221].

An alternative approach looks at the application of POF for their potential use as hydrostatic pressure sensors. Johnson and Webb[222] observed the behaviour of POF placed in a pressurised air cylinder or pipe configuration, which allowed the gauge pressure of the chamber to be manually varied between 2MPa and 10MPa (20 to 100 Bar) using a valve[222]. This arrangement reported sensitivities ranging between 0.07nm/MPa and 0.13nm/MPa[222] for PMMA multimode microstructured POF (MMmPOF) with an outer diameter of 150μm and a 50μm solid core region. Another study used compressed air from a cylinder to increase the pressure of a chamber that contained the SI PMMA POFBGs from 0kPa to 1000kPa gauge pressure and found a sensitivity of 0.20pm/kPa [13] for an un-etched fibre and a sensitivity of 0.75pm/kPa for a fibre that was etched to a diameter of 55μm [224].

Literature suggests that a change in pressure can lead to two possible effects on the POFBG wavelength[143, 222]. An increase in pressure on the material was proposed to cause fibre compression, a decrease in the period of the grating planes within the core, followed by a negative Bragg wavelength shift. The other possibility is the increase in chamber pressure increases the refractive index of the fibre leading to a positive Bragg wavelength shift.

Equation 10 [143] describes the ideal relationship between pressure (P) and change in grating wavelength (λ_B) inscribed in silica optical fibre, an isotropic solid, where n is the refractive index, v is the Poisson's ratio, E is the Young's modulus and p_{11} and p_{12} are the strain-optic tensor components. The first term $(1-2v)$ describes the effect of change in pressure on the FBG period from fibre compression, whilst the second term $-\frac{n^2}{2}(1-2v)(p_{11}+2p_{12})$ describes the change in refractive index due to the strain-optic effect[143].

$$\frac{1}{\lambda}\frac{d\lambda_B}{dP} = -\frac{1}{E}\left[(1-2v) - \frac{n^2}{2}(1-2v)(p_{11}+2p_{12})\right]$$

Equation 10

As a result of the drawing process, the polymer molecular chains align differently along the fibre axis, leading to the fibre possessing transverse isotropic properties[143]. The sensitivity can be expressed in Equation 11 [143], where E is the elastic modulus parallel (E_P) and perpendicular (E_T) to the fibre axis, the components of the strain-optic tensor are P_{11}, P_{12} and P_{13} and the Poisson's ratios are v_P and v_T.

$$\frac{1}{\lambda}\frac{d\lambda}{dP} = -\left(\frac{1}{E_T}(1-2v_T) - \frac{n^2}{2}\left(\left(\frac{1}{E_p} - \frac{v_p}{E_p} - \frac{v_T}{E_T}\right)(p_{11} + p_{12}) + \frac{p_{13}}{E_T}(1-2v_T)\right)\right)$$

Equation 11

Publications have examined the use of POFBGs in chambers that provide above atmospheric pressure conditions, however to this author's knowledge, no journal papers currently examine their application in vacuum environments suitable for freeze drying applications. The following work will focus on this task using step index single-mode and multimode POFBGs.

7.3   Aim

The aim of this work was to study the effect of sub-atmospheric pressure on POFBGs inscribed in step index SM PMMA and MM TOPAS fibres, whilst keeping a constant inlet shelf temperature and dry conditions. This would allow the POFBGs to be characterised and determine their sensitivities to pressure. This information would then be used in subsequent chapters to determine whether POFBGs could monitor sublimation of water vapour and freeze drying of mannitol and collagen.

The objectives for this chapter are:

- Determine the sensitivity of the manufactured POFBGs to sub-atmospheric pressures within a freeze dryer at a set shelf temperature and a recorded dew point value of -40°C. There have currently not been reports of POFBGs being exposed to pressures in the region of 200μbar and in dry nitrogen environments of -40°C dew point.
- Investigate the long term effects of exposing POFBGs to vacuum.

7.4   Method

The freeze dryer set-up and protocol described in section 5.7 and 5.7.1 were used in this chapter to study under vacuum conditions, the effects of chamber pressure on the sensitivity of POFBGs (section 5.3). Several sensors were attached to the freeze drying unit (Figure 75(a)) according to section 5.7, to monitor dew point (SF52), pressure (TM101) and temperature (Figure 76). A customised feedthrough connector seen in Figure 75(a) was used to pass the K-type thermocouple into the vacuum chamber, in order to record the temperature in the region of the POFs. The TM-947SD data-logger was used to collect the temperature readings and the output was plotted in Figure 75(b) and Figure 76(c).

The TOPAS and PMMA POFBGs were connected to a 2x2 1550nm Corning single mode (SM) 50:50 silica coupler (9/125μm). The coupler was connected to a FC/APC silica optical cable that had been fed through the vacuum chamber wall using a custom built feedthrough (Figure 75(a)). The optical cable was connected to the DL-BP1 SLED broadband light source and I-MON 512 USB interrogator monitor. The I-MON 512 USB evaluation software v1.1 was used to analyse the FBG spectrum and calculate the Bragg wavelength using peak tracking algorithms. Figure 75(c) shows the measured Bragg wavelengths from TOPAS and PMMA POFBGs at a sampling rate of 1 sample every 15sec. The sensitivities of the POFBGs were calculated using linear regression and least squares for the curve fitting error. Figure 74(a) shows that the POFBGs were placed in a protective housing structure (Figure 42) on the temperature regulated shelf as described in section 5.7.1.

The methods discussed in section 5.7 were used to ensure dry conditions during the course of the experiments. The POF sensors, Perspex door and chamber wall were left to dry in sub-atmospheric conditions for a minimum of 24hrs prior to starting the experiments. This procedure was also carried out to minimise the effects of outgassing[212, 213, 225, 226] during the experiment.

As this freeze dryer was programmed by VirTis to carry out standard freeze drying recipes for biological or pharmaceutical applications, a non-standard program was uploaded into the on-board PLC to allow step changes in pressure for sensor characterisation purposes. The inlet shelf temperature was set to 20°C (room temperature) and the dew point sensor recorded a reading of -40°C dew point during the cycle.

The cycle parameters are available in Table 0-A in Appendix G, the program was written to carry out step changes in pressure between 2500μbar to 200μbar and to maintain the set pressure for 90min (Figure 75(b) and Figure 76(a)). These values were selected to obtain information on the behaviour of the POFBG sensor, over the maximum achievable pressure range of the machine. The controller was set up by VirTis to have a maximum programmable pressure of 2500μbar, in order to remain sufficiently below the triple point of water for sublimation and to reduce the risk of damage to the samples (e.g. melt) and the vacuum pump. The lowest value that could be achieved was 200μbar, due to leaks into the system from the custom feedthrough connector for the optical fibre. The pressure was monitored by the chamber's VirTis thermocouple vacuum gauge and the independent Pirani gauge that was attached to the chamber seen in Figure 75(a). Figure 75(b) and Figure 76(b) show that dry conditions were

maintained within the chamber, as seen by the dew point sensor reading an average of -40°C dew point.

Initial tests showed that within the pressure range (200 to 2500µbar) there were regions that were found to be very unstable and where extreme ringing occurred about the pressure set point value. An example of a region of instability is shown in Figure 74(b) is between 650µbar and 850µbar, which could influence the Bragg wavelength and was therefore avoided during the characterisation experiments. Upon investigation, these oscillations were found to be due to limitations with the control system and the digital solenoid valve, which allowed significantly more gas into the chamber than the set point value. These tests were carried out at the start of the project without the use of a nitrogen cylinder, to determine the pressure set points that could be used in the program (Table 0-A in Appendix G) and provide preliminary data on the behaviour of the Bragg wavelengths. Figure 74(b) was one of the experiments that revealed potential regions of non-linear sensitivity of the Bragg wavelength to pressure. In these preliminary experiments, air entered the chamber through the port (Figure 75(a)) when the digital solenoid valve was activated and because PMMA has an affinity for water vapour, it was not clear if water vapour could be influencing the Bragg wavelength. As a result, the port was connected to a dry nitrogen gas cylinder and a desiccant (Figure 75(a)) to reduce the leakage of air into the chamber to as low as practically possible for the equipment, in order to characterise the sensors to dry sub-atmospheric pressures.
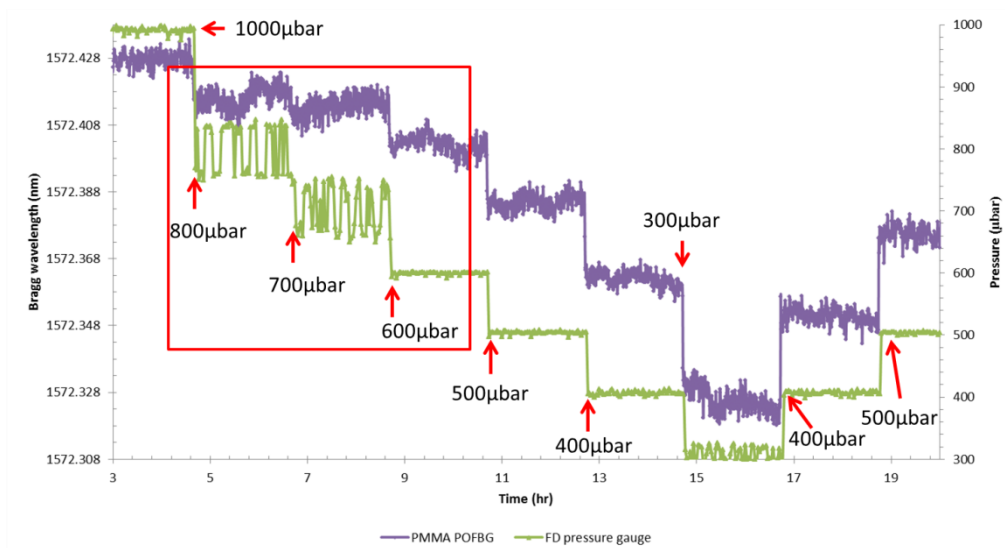
Figure 74 (a) POFBG sensors placed onto the shelf of the freeze dryer; (b)PMMA POFBG sensor (POF1) response to step changes in pressure (marked with red arrows), inlet shelf temperature was maintained at 20ºC and dew point at -40ºC. Red box shows a region of instability at pressure set points 700µbar and 800µbar.
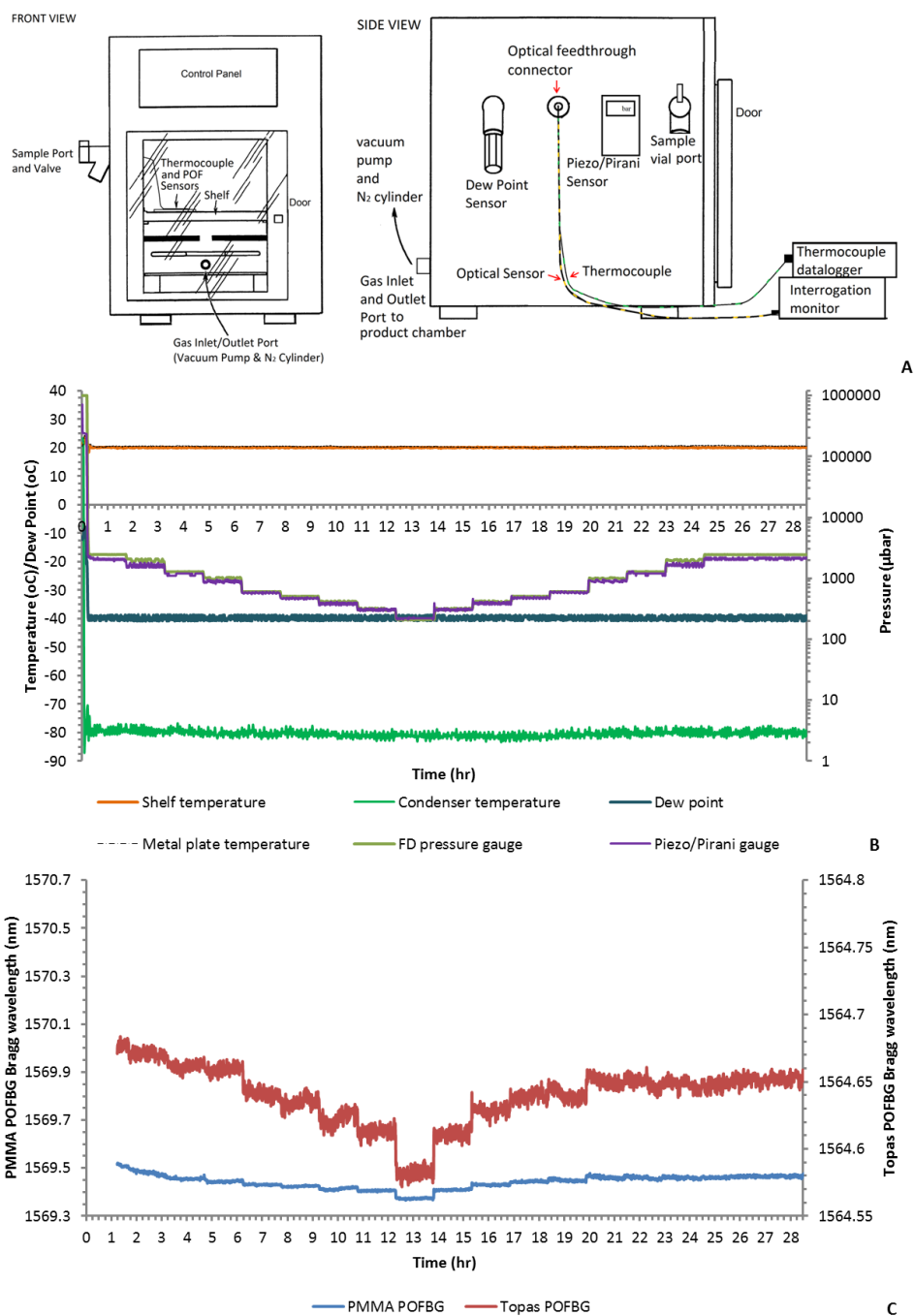
Figure 75 Experimental protocol for characterising PMMA and TOPAS based POFBG. (A) Schematic representation of the purpose built freeze drying experimental unit (B) Cycle uploaded to the freeze dyer controller, showing step changes in pressure at a constant shelf inlet temperature and constant dew point. (C) Wavelength output of the POFBG sensors when cycled between a pressure range of 2500 μbar and 200 μbar.
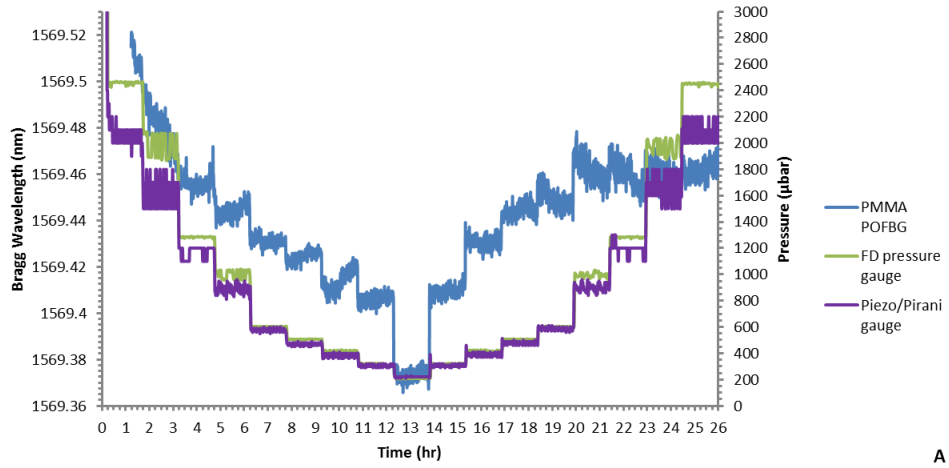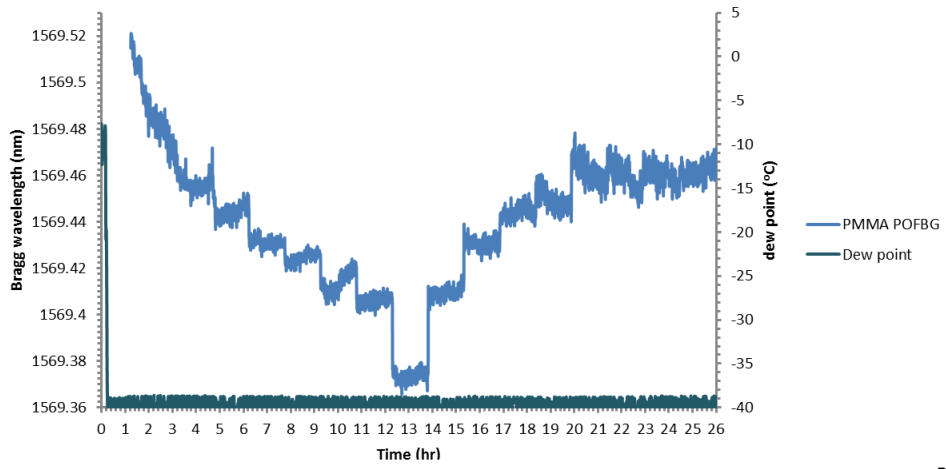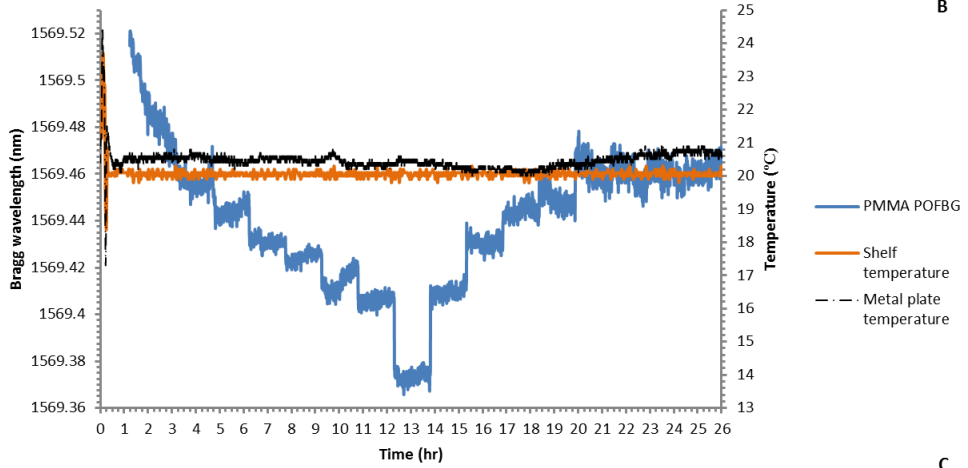
Figure 76 PMMA POFBG (POF1), where Bragg wavelength is plotted against (a) pressure in the chamber, (b) dew point in the chamber, (c) temperature of the shelf, thermocouple temperature in the region next to the POF sensors

7.5   Results and Discussion

7.5.1   PMMA and TOPAS POFBG

Figure 76 and Figure 78 show the response of both PMMA and TOPAS POFBGs in the sensor housing to step changes in the chamber pressure.

The graphs show that at the start of the experiment the dew point sensor detected -10°C dew point in the chamber at atmospheric conditions. When the program cycle was activated to test the performance of the POFBGs at sub-atmospheric pressures, the chamber pressure reduced to 2500µbar and the dew point to -40°C. At this stage the program began to step change the pressure between the range 2500µbar and 200µbar, whilst maintaining an inlet shelf temperature of 20°C and an average dew point of -40°C.

Figure 78(a) shows the response of POFBG wavelength to changes in chamber pressure under constant dew point. The graph shows the freeze dryer controller is creating oscillations in the pressure about the set point value (as seen in Figure 74(b)), which appears to worsen in amplitude at higher set point pressures and occasionally overshoots the target. There is an apparent offset in the higher pressure region between the Pirani and VirTis thermocouple gauge readings. These sensors are based on differing technologies, the Pirani gauge being more accurate at 10% of the measured value than the chamber gauge at 15% (thermocouple gauge); hence the offset becomes more pronounced at higher values. VirTis have optimised the system, through component selection or settings of the controller to accurately operate in the standard freeze drying region of 100-200mTorr[24]. These limitations in the freeze dryer inbuilt system would need to be considered as they are potentially additional sources of noise in the POFBG data, particularly as the rapid input of gas could lead to vibrations. Despite the limitations, a correlation between the pressure and Bragg wavelength is visible and appears to be non-linear, this will be discussed later in the chapter. These trends were also observed with other POFBGs, including TOPAS POFBGs (Figure 157 and Figure 158 in Appendix G) and PMMA POFBGs (Figure 156 and Figure 159 in Appendix G).

As heat transfer issues from radiative effects are a known influential factor in atypical freeze drying of pharmaceutical formulations [9, 57], a K-type thermocouple was placed next to the POFBGs to track the temperature during the pressure cycle. The thermocouple reveals that the temperature was initially consistent but drifts in temperature occurred (within 0.7°C) that could influence the Bragg wavelength as seen in Figure 77. Despite the temperature drift due to

radiative effects, a correlation between the Bragg wavelength and rapid step changes in pressure is still visible.
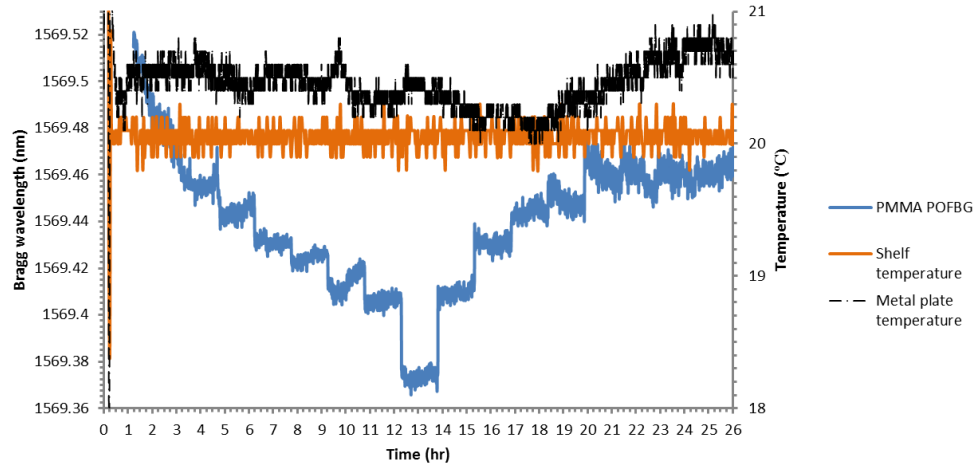
Figure 77 PMMA POFBG (POF1), where Bragg wavelength is plotted against the temperature of the shelf and data from the thermocouple data logger, to record the temperature in the vicinity of the POF sensors. The step changes in pressure were carried out from 2500µbar to 200µbar before returning back to 2500µbar at -40ºC dew point.
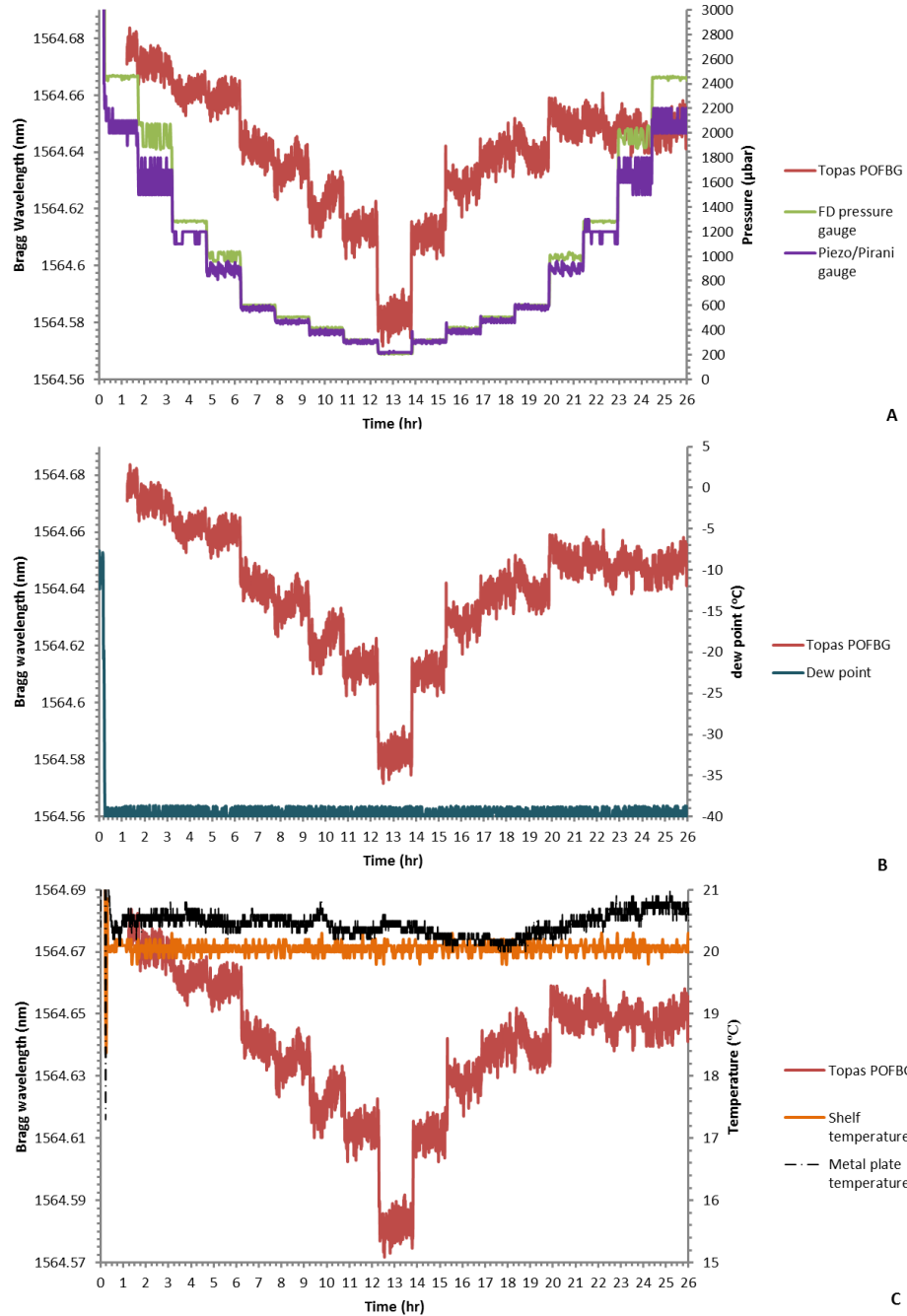
Figure 78 TOPAS POFBG (POF2), where Bragg wavelength is plotted against (a) pressure in the chamber, (b) dew point in the chamber, (c) temperature of the shelf and thermocouple temperature in the region next to the POF sensor.

Figure 79 shows the wavelength shifts for PMMA POFBG (POF1) and TOPAS POFBG (POF2) during the course of the pressure cycle.

The data reveals a wavelength shift of -0.152nm for PMMA POFBG (POF1) and -0.107nm for TOPAS POFBG (POF2) when the pressure decreased from 2500µbar to 200µbar. During this time a drift in temperature of 0.6°C was detected by the thermocouple but the dew point remained at -40°C. The

sensitivities of these two POFs were determined in the previous chapter as -34±0.4pm/°C for PMMA POFBG (POF1) and -36±0.3pm/°C for TOPAS POFBG (POF2). It can be deduced that the Bragg wavelength shifts in this experiment, are not primarily due to temperature fluctuations but likely the result of the POFBGs detecting changes in chamber pressure. The same pattern is observed when increasing the pressure from 200µbar to 2500µbar, with a shift of 0.098nm observed for PMMA POFBG and 0.078nm for TOPAS POFBG where a maximum drift in temperature of 1°C was observed in the area.
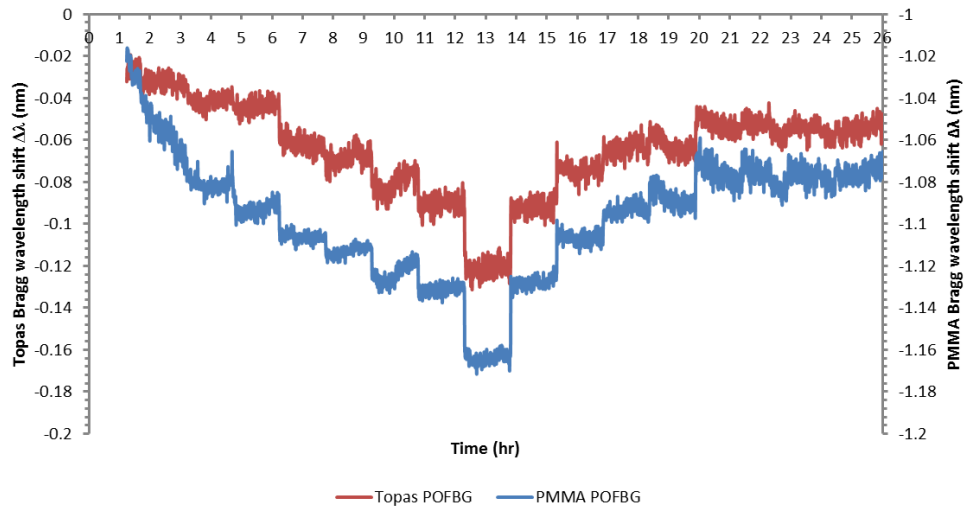
Figure 79 Bragg wavelength shift of PMMA and TOPAS based POFBG (POF1 and POF2)

The experiment was repeated and the results are shown in Figure 80, where a drift in Bragg wavelength is observed due to an increase in temperature at 12hrs from radiative effects. This behaviour was also experienced in other experiments; however there is still a correlation between the Bragg wavelength and the applied step changes in pressure.
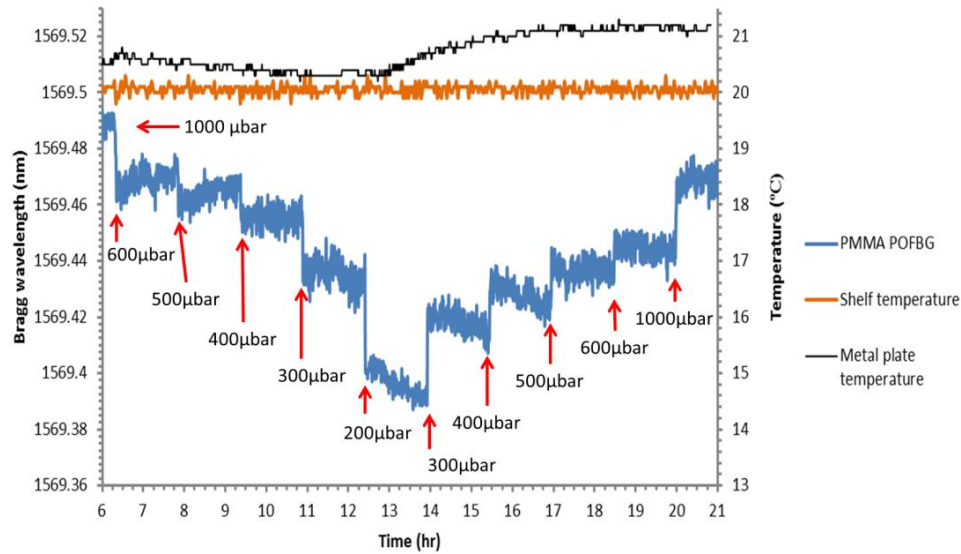
Figure 80 PMMA POFBG (POF1), where Bragg wavelength is plotted against the temperature of the shelf and data from the thermocouple data logger, which recorded the temperature in the vicinity of the POF sensors. Each step change in pressure is marked with a red arrow across the range 1000μbar to 200μbar and the pressure was kept at that set point for 90min, -40°C dew point was observed during the course of the experiment.

The data in Figure 81 illustrate the Bragg wavelength shift with respect to chamber pressure (n=3), where it can be seen that both PMMA and TOPAS POFBG are showing non-linear tendencies. This pattern was also observed in the data obtained from the other POFBGs (Figure 160 and Figure 161), which have been placed in Appendix G. In this situation, to obtain a representation of the trends between the Bragg wavelength and pressure for n=3, a piecewise linear approximation was created and the fit optimised with linear regression for the individual pieces. The calculated sensitivities and wavelength shifts for the tested POFBGs have been summarised in Table 7-A.

The graphs show large standard deviations amongst the samples (n=3) for most pressures; this is likely the result of the previously reported radiative heat effects which can vary between experiments and cause a drift in the results. The variance in the data sets could also be the result of the large oscillations in pressure due to the limitations in the control system and digital solenoid valves. Future work would need to research into different techniques to obtain temperature compensation for the fibres, which would allow the influence of pressure changes on Bragg wavelength to be obtained, whilst minimising the influence of radiative heat. By investing in the control system and in components for the freeze drying chamber, it could also be possible to improve and ideally reduce the amplitude of the oscillations and expand the pressure range of

operation. This would allow more readings to be obtained throughout the sub-atmospheric pressure range, which is currently not achievable with this machine as the regions between the chosen settings in the program are regions of high pressure instability (e.g. between 650µbar and 850µbar in Figure 74(b)). This process would likely allow the non-linear sensitivity relationship between pressure and the Bragg wavelength to be calculated, rather than a piecewise linear approximation.

	Pressure region	PMMA POFBG (POF 1)	TOPAS POFBG (POF 2)	TOPAS POFBG (POF 3)	PMMA POFBG (POF 4)	PMMA POFBG (POF 5)
Drop in pressure	2500 to 1000μbar	6×10^{-5} nm/μbar ($\pm 2 \times 10^{-5}$)	2×10^{-5} nm/μbar ($\pm 5 \times 10^{-6}$)	1×10^{-5} nm/μbar ($\pm 0.1 \times 10^{-5}$)	6×10^{-6} nm/μbar ($\pm 2 \times 10^{-6}$)	6×10^{-6} nm/μbar ($\pm 0.8 \times 10^{-6}$)
	600 to 200μbar	2×10^{-4} nm/μbar ($\pm 0.3 \times 10^{-4}$)	1×10^{-4} nm/μbar ($\pm 0.2 \times 10^{-4}$)	1×10^{-4} nm/μbar ($\pm 0.1 \times 10^{-4}$)	6×10^{-5} nm/μbar ($\pm 0.8 \times 10^{-5}$)	6×10^{-5} nm/μbar ($\pm 0.6 \times 10^{-5}$)
Rise in pressure	1000 to 2500μbar	9×10^{-6} nm/μbar ($\pm 7 \times 10^{-6}$)	4×10^{-6} nm/μbar ($\pm 5 \times 10^{-6}$)	1×10^{-5} nm/μbar ($\pm 0.6 \times 10^{-5}$)	6×10^{-6} nm/μbar ($\pm 2 \times 10^{-6}$)	5×10^{-6} nm/μbar ($\pm 1 \times 10^{-6}$)
	200 to 600μbar	2×10^{-4} nm/μbar ($\pm 0.2 \times 10^{-4}$)	2×10^{-4} nm/μbar ($\pm 0.3 \times 10^{-4}$)	2×10^{-4} nm/μbar ($\pm 0.2 \times 10^{-4}$)	7×10^{-5} nm/μbar ($\pm 0.9 \times 10^{-5}$)	7×10^{-5} nm/μbar ($\pm 0.7 \times 10^{-5}$)
Average max wavelength shift (mean ±SD, n=3)	Drop in pressure	-0.182nm ±0.05	-0.113nm ±0.007	-0.095nm ±0.010	-0.038nm ±0.006	-0.041nm ±0.004
	Pressure rise	0.109nm ±0.009	0.084nm ±0.006	0.095nm ±0.009	0.044nm ±0.005	0.046nm ±0.004

Table 7-A POFBG sensitivities and wavelength shift (n=3), each cycle lasting about 30hrs
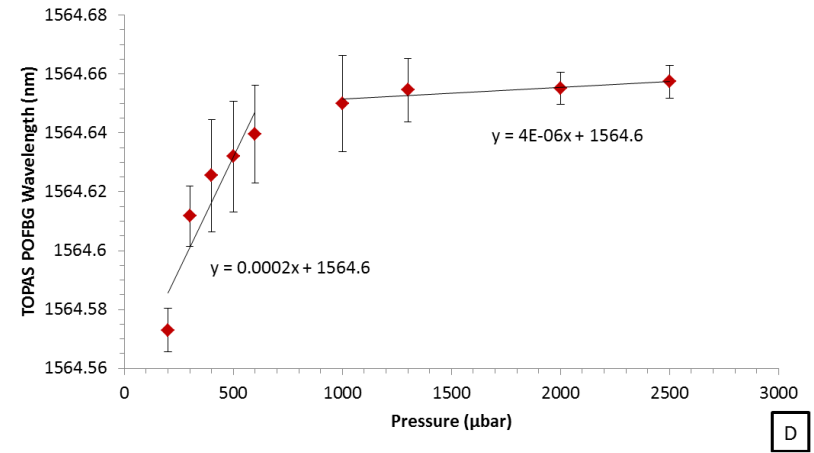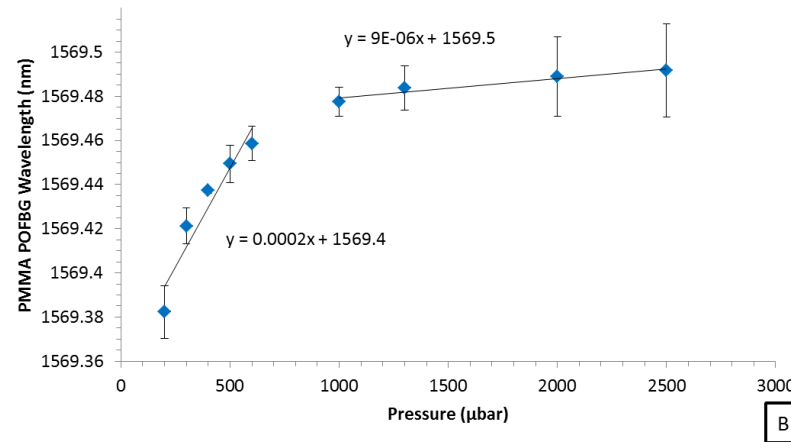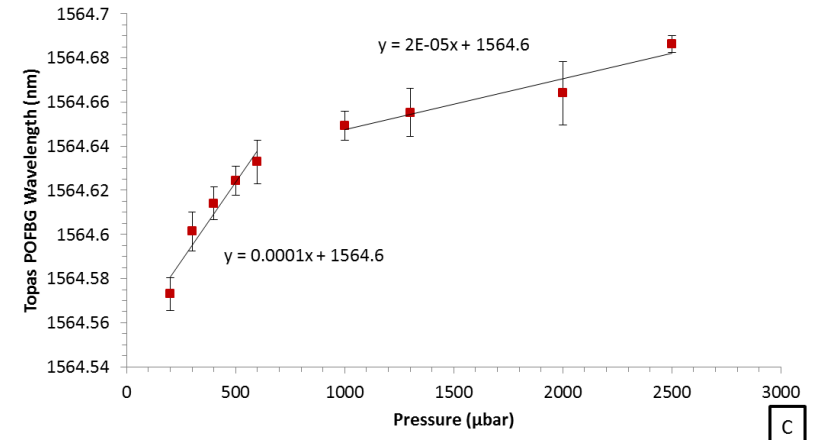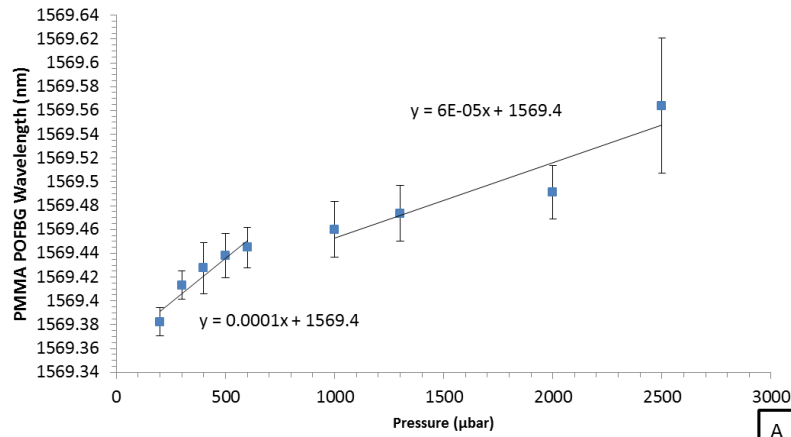
Figure 81 Bragg wavelength shift with respect to chamber pressure (n=3), where (A) the pressure was reduced from 2500µbar to 200µbar for PMMA POFBG (POF1), (b) the chamber pressure was increased from 200µbar to 2500µbar for PMMA POFBG (POF1), (c) the pressure was reduced from 2500µbar to 200µbar for TOPAS POFBG (POF2), (d) the chamber pressure was increased from 200µbar to 2500µbar for TOPAS POFBG (POF2)

Table 7-A illustrates that the pressure sensitivities of both TOPAS POFBGs (POF 2 and 3) are in good agreement with each other for the same pressure range, either 1000µbar to 2500µbar or 200µbar to 600µbar. This pattern was observed in both increase and decrease step changes in pressure. The same trend was observed for POF 4 and 5, which were two FBGs that were inscribed into PMMA POF after the fibre was annealed at 80°C for 7hrs. It is likely that any differences in the POFBG sensitivities between the rise and drop in pressure stages could have been due to the influence of the oscillations in pressure and drifts in temperature from radiative heat, as each experiment lasted over 30 hours. The last chapter reported that the temperature in the vacuum chamber could vary depending on the time of day and the storage room conditions (e.g. solar gain effects).

The data was analysed and it was found that dry conditions of -40°C dew point were maintained throughout the cycles. There were shifts in temperature observed in some experiments, however only up to a maximum of 1°C across the entire pressure cycle. The previous chapter determined the temperature sensitivities of POF1 to be -34±0.4pm/°C, POF2 and POF3 are -36±0.3pm/°C, POF4 and POF5 are -18±0.3pm/°C. It is possible that the observed blue shifts in the region of 100pm (POF1, POF2 and POF3) and 40pm (POF4 and POF5), were partially due to temperature effects but also caused by pressure influencing the strain-optic tensor coefficients and properties of the fibre.

There is an observable difference in the sensitivities and wavelength shift of POF1 against POF4 and 5. POF1 shows higher sensitivity and a higher wavelength shift than POF4 and POF5, which could be due to differences in the materials, etching the fibre with acetone (POF1) or the annealing process (POF4 and POF5). Annealing is a thermal cycle used to relax the axial orientation of the chain molecules in the fibres and ideally reduce internal stresses in the fibre created during the drawing process. This treatment has been shown to cause fibre shrinkage [12, 15, 209, 215, 216] and changes in the polymer properties. It is possible that the annealing process has changed the strain-optic tensor components[143], potentially reducing its influence on the Bragg wavelength shift and reducing pressure sensitivity. The annealing process and the mechanism which influences the fibres at low pressures would require further investigations in future projects.

The data also reveals that all the POFBGs have a higher sensitivity (n=3) to pressure in the 200µbar to 600µbar range than at the higher pressure range of

1000μbar to 2500μbar, which was not found to have been the result of changes to dew point nor temperature in the region of the POFs.

The pressure sensitivity range for POF1 across the full measured pressure range was found to be between 9×10^{-6} nm/μbar ($\pm 7 \times 10^{-6}$) and 2×10^{-4} nm/μbar ($\pm 0.2 \times 10^{-4}$), corresponding to values in the region of 90nm/MPa to 2000nm/MPa. The pressure sensitivity range for POF2 and POF3 across 200μbar to 2500μbar was found to be between 4×10^{-6} nm/μbar ($\pm 5 \times 10^{-6}$) and 2×10^{-4} nm/μbar ($\pm 0.3 \times 10^{-4}$), corresponding to values in the region of 40nm/MPa to 2000nm/MPa. The pressure sensitivity range for POF4 and POF5 across 200μbar to 2500μbar was found to be between 5×10^{-6} nm/μbar ($\pm 1 \times 10^{-6}$) and 7×10^{-5} nm/μbar ($\pm 0.7 \times 10^{-5}$), corresponding to values in the region of 50nm/MPa to 700nm/MPa. These values were compared against literature, in which PMMA POFBGs were placed in high pressure chambers, controlled using compressed air. For a PMMA MMmPOF, sensitivities ranging between 0.07nm/MPa and 0.13nm/MPa[222] were found between the gauge pressure of 2MPa and 10MPa (20 to 100 Bar)[222]. For a PMMA SI POF, a sensitivity of 0.20pm/kPa[13] was obtained between the gauge pressure of 0kPa and 1000kPa. The pressure sensitivities obtained in this project, for humidity sensitive PMMA POFBG are several degrees of magnitude higher than those reported in literature. The difference is likely to be the combination of the following: these POF for use in sensing applications are manufactured in small bespoke batches with significant variability and performance differences between them and water may have been present in the compressed air which is known to influence the Bragg wavelength. Research indicates that water acts as a mild plasticiser for PMMA for bulk materials up to about 1% [214], causes swelling with approximately 50% of sorbed water residing in microvoids[16, 17]. Shen et al. reported that dry samples of bulk PMMA have smaller average craze lengths, higher average tensile strength and higher craze initiation stress than in samples with higher water content[16].

It is possible that the properties of the PMMA POFs were influenced by water; the drying process may cause fibre shrinkage, changes to the surface water content and changes in the properties like tensile strength, which likely influenced the strain-optic tensor components. It is also possible that there are other currently unknown mechanisms that are responsible for the significantly higher PMMA pressure sensitivities at sub-atmospheric pressure and would require further investigation.

To this author's knowledge no pressure sensing experiments have thus far been published on humidity insensitive TOPAS POFBG to compare against. Future work could involve placing these fibres in a dry high pressure vessel to observe if the non-linearity Bragg wavelength behaviour to pressure can also be observed for this type of polymer.

7.5.2   Long term exposure of POFBGs to vacuum

POF 1 and POF 2 were placed inside the freeze dryer and kept for 40 days at 200µbar, 20°C inlet shelf temperature and -40°C dew point. During this timeframe the vacuum was not released as this would return the pressure to ambient conditions and introduce humidity. This stress test was carried out to observe any potential long term implications of vacuum conditions on these fibres beyond the duration of a standard freeze drying cycle, while desorbing them and the chamber. At the end of this experiment the sensor was exposed to changes in temperature and sublimation and found to still be responsive to the stimuli. Figure 82 shows the Bragg wavelength response of PMMA SI POFBG before and after it was placed inside the vacuum chamber (measured using a Hewlett Packard optical spectrum analyser at RBW of 0.5nm). The peak of the Bragg wavelength was found to have blue shifted from 1571.03nm to 1570.79nm, the full width half maximum (FWHM) was 1.3nm and became 1.2nm and the signal increased from 20dB to 24dB above the noise floor.

The graph also shows that the fibre appears to have few mode characteristics, this would need to be factored and sensors optimised in future projects, as some conditions may lead to the dominance of certain modes which could cause peak tracking issues for the interrogator units.

The shifts in the peak may have occurred due to changes in material properties of the polymer in dry conditions. Studies have reported that bulk PMMA (in the presence water) tend to have different material properties to dry samples of bulk PMMA, as water behaves like a mild plasticiser [16, 214]. The studies report that dry samples had smaller average craze lengths, higher average tensile strength and higher craze initiation stress than in samples with higher water content[16]. The fibre originally contained water in the sample because it was exposed to ambient air conditions, but when exposed to vacuum over long periods of time drying of the fibre could have occurred and may have caused fibre shrinkage.

These hypotheses would need to be verified in future projects in this area, along with testing the properties of different types of PMMA POF.
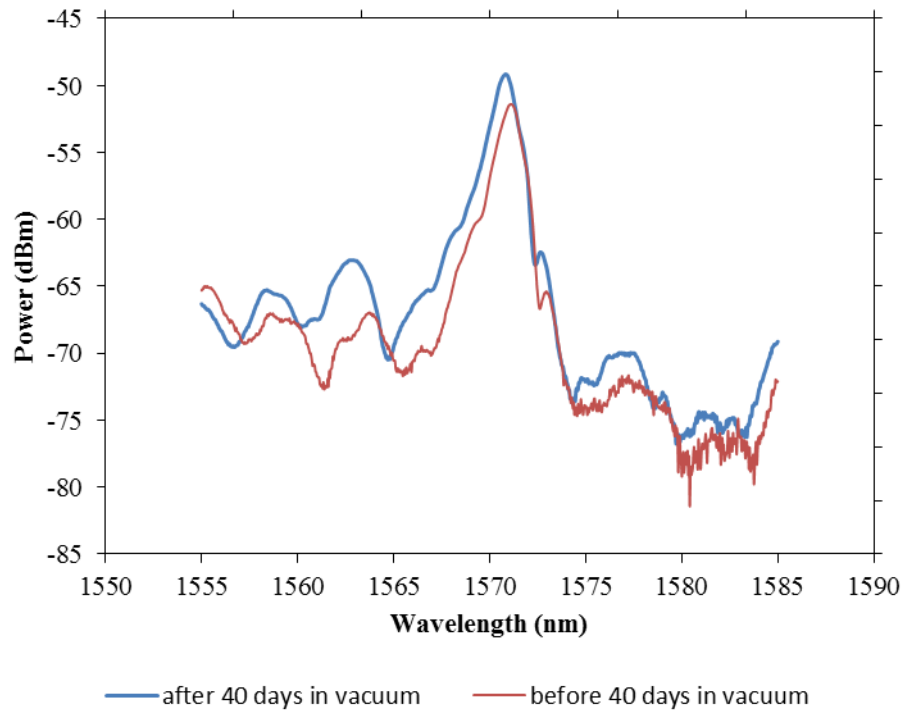
Figure 82 long term exposure of PMMA POFBG (POF 1) to vacuum in a freeze dryer, RBW 0.5nm

Figure 83 shows the response of TOPAS POFBG to 40 days in dry and vacuum conditions. As with the PMMA POFBG a blue shift is experienced in the grating peak, from a peak signal of 1564.4nm to 1563.9nm, FWHM from 0.9nm to 0.8nm and the grating intensity remained 6dB above the noise floor. The graph also reveals that the noise floor rose by about 2dB after the experiment was carried out.

These changes could have resulted from changes in the properties of the UV glued joint, particularly if there were any microbubbles in the joint that may have caused cracks to release the gas and increased attenuation (section 4.4.4). TOPAS advanced polymers [227] mention in their brochure that TOPAS COC is hydrophobic in nature and exhibits negligible swelling when immersed in water, where water absorption of the polymer was 0.01% after it was immersed for 24hrs at 23°C. The document mentions that changes in the %RH in the environment have essentially no effect on material properties and that a small uptake in water occurs as traces of moisture on the surface of the material, during a change in temperature in a warm, humid atmosphere[227].

The data may have resulted from the removal of the trace water on the surface of the polymer, which then influenced the Bragg grating. This would need to be

investigated in future projects, along with different types of optical fibres and the effects of annealing on these fibres.
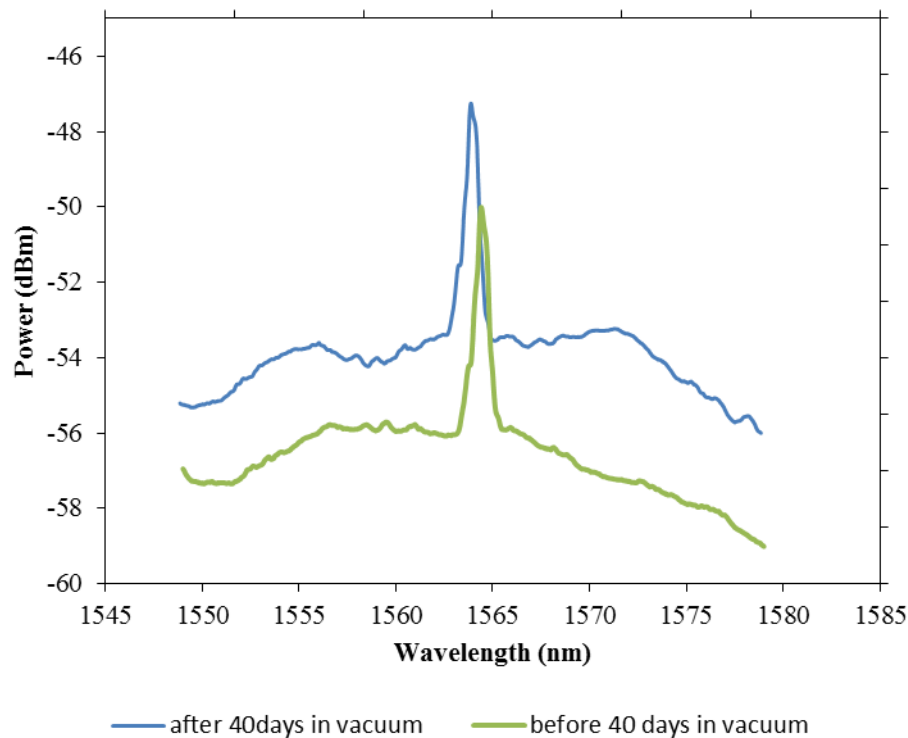
Figure 83 long term exposure of TOPAS POFBG (POF 2) to vacuum in a freeze dryer, RBW 0.5nm

The optical fibres were measured again several days and again weeks later and found that the peaks had recovered, potentially implying that the shift is temporary and as a result of the effects of being exposed to a vacuum chamber. This behaviour would also need to be investigated further in future work.

7.6   Future Work

Studies would investigate the effects of different annealing procedures on POF and exposing the POFBG sensors to sub-atmospheric pressure. This would allow the sensitivity profiles to be determined and to tailor the fabrication procedure, with the intention of producing sensors with the desired features for freeze drying applications.

Future investigations would study the effects of other POF such as polycarbonate (PC), polystyrene (PS), mPOF in vacuum conditions, to observe if the non-linear sensitivity observed is specific to certain types of polymers or optical fibre structures.

This is the first study that tested the behaviour of TOPAS POFBG with a ZEONEX cladding in a vacuum chamber. Future studies would require this type

of fibre to be subjected to high pressure conditions to determine sensitivity profile and whether it is non-linear at higher pressures.

As there is a possibility that water content in the fibre is influencing the POFBGs when carrying out pressure experiments, future work could involve drying the fibres before they are placed in the high pressure vessels and backfilled with dry gas.

The mechanism that leads to the apparent high pressure sensitivity under vacuum conditions for PMMA POFBGs tested in this work is still not fully understood. Future work could investigate whether the material properties have changed e.g. due to drying of the fibre, or if the surface properties have changed significantly to be detected by the POFBG.

Further research needs to be carried out into the long term effects of PMMA and TOPAS POFBG in vacuum conditions for freeze drying applications, including improving the UV glued joints or developing demountable connectors.

Radiative effects and heat transfer from the shelf are influential factors in freeze drying and was found to influence the Bragg wavelength. Future work could investigate different temperature compensation techniques e.g. using multiple FBGs on the same fibre, to compensate for the effects of temperature and output Bragg wavelength shift as a function of pressure.

Investment in the machine such as a new PLC (including PID controller option) and changes to some of the design, could produce a climatic chamber that allows more flexibility and customised cycles to be written for characterisation of sensors e.g. to study the POFBG behaviour in a wider pressure range. The PLC could improve control over the pressure set point and hopefully reduce the amplitude of the pressure oscillations which introduce noise into the data.

7.7   Conclusion

The POFBGs were placed in a vacuum chamber, in a dry environment of -40°C dew point in order to characterise the sensors and obtain their pressure sensitivities. The humidity sensitive PMMA POFBG and humidity insensitive TOPAS POFBG were tested under these conditions (200µbar to 2500µbar) after the fibres had been dried for a minimum of 24hrs. The aims and objectives of this work were achieved and the fibres were characterised in sub-atmospheric pressure conditions. This information will be used in the next chapters to determine whether POFBGs could be used to monitor sublimation of water vapour and monitor primary drying of mannitol and collagen samples.

The data indicated that the fibres have unexpected non-linear tendencies when measuring pressures in the range of 200μbar to 2500μbar for n=3 at -40°C dew point, particularly when compared against literature for pressures greater than atmospheric conditions. The temperature in the vicinity of the POF was measured by a thermocouple, as radiative effects[19, 46] are known to influence the temperature in a vacuum. The drifts in Bragg wavelength due to changes in temperature is insufficient to account for the increased POFBG sensitivity under vacuum conditions. It is possible that this pressure range coupled with drying of the fibre has changed the strain-optic tensor components of the fibre, causing the non-linearity. This would require further investigation as the exact mechanism is still not fully understood.

There was a difference observed between the annealed and non-annealed PMMA POF, showing reduced sensitivity to pressure for the annealed fibre. This could be the result of the history of the thermal treatment of the fibre as well as the annealing phase relaxing the axial orientated molecules in the POF, influencing the optic-strain tensor coefficients of the fibre. Future work could involve testing the POFBGs at higher pressures, to observe if annealing influences pressure sensitivity in this range.

A PMMA and TOPAS POFBG were placed under vacuum conditions for 40 days and the spectra of the gratings revealed a blue shift in the Bragg wavelength. Further research into this area would need to be carried out to determine the long term viability of the POFBG sensors in vacuum conditions for freeze drying applications.

8 Wavelength response of POFBGs to Water Vapour in a Freeze Dryer

8.1 Overview

The chapter builds on the characterisation work documented in the previous two chapters, where the sensitivities of these sensors to step changes in temperature and pressure in the freeze dryer were determined. This chapter investigates the response of TOPAS and PMMA POFBGs to the sublimation of water vapour from samples attached at the access port of the freeze dryer. Step Index SM PMMA and MM TOPAS POFBGs manufactured according to section 5.2 were used in these experiments. There are currently no publications available documenting the performance of POFBGs in a freeze dryer, therefore the characterisation of these potential sensors is vital to determine if they could have practical applications in the freeze drying industry.

The information from this chapter will be used to analyse the output of mannitol and native collagen freeze drying cycles in the next chapter, to determine if the end of primary drying is correctly detected for these well-known pharmaceutical constituents.

Additionally this chapter will examine the backfill of the chamber to 1atm pressure with an inert gas, which is a necessary stage in the pharmaceutical industry prior to collecting the samples.

Finally, this chapter discusses the effects of a process to reduce the PMMA POF diameter on the response time of that POFBG to changes in relative humidity and temperature, in a climatic chamber at atmospheric pressure.

8.2 Background

The changes in the properties of PMMA due to water sorption, makes the material useful for humidity sensing applications. The material has been used to detect water in aviation fuel [228, 229] and to measure the concentrations of saline solutions[230] using POFBG technology.

The wavelength of the POFBG changes depending on the grating pitch (Λ) and effective core refractive index (n_{eff}) according to the relationship described in Equation 12. These parameters are dependent on the water content (ω) and temperature (T) of the material.

$$\lambda_{Bragg} = 2n_{eff} (T, \omega) \Lambda (T, \omega)$$

A PMMA POFBG exposed to an environment of increasing water content will experience a swelling of the material[16, 17] and an increase in the refractive index of the polymer[231], resulting in a red shift of the Bragg wavelength[12]. Turner's [17] study of PMMA sorption kinetics indicated that approximately 50% of sorbed water is taken up by the mechanism of swelling and the remainder is accommodated in microvoids[16, 17].

Published literature reveals that these POFBG sensors have been tested in environmental chambers operating at 1atm, to study the effects of humidity and temperature on the Bragg wavelength. There have been a range of sensitivities reported in the literature for these types of devices, including 38pm%RH (in the range 40%RH to 90%RH)[12] and ~33 pm/%RH(in the range 30%RH to 90%RH)[14, 195].

A literature search has not revealed publications (to-date) where POFBG technology has been used in freeze drying applications, to monitor processes under vacuum conditions and sublimation of water vapour. This chapter will investigate the performance of step index single-mode (SM) and multimode (MM) POFBGs for water vapour detection in a freeze dryer.

Harbach studied these devices at 1.5+/-1%RH in a chamber flushed with nitrogen gas at 1atm pressure[153], however this project will attempt to dry the polymer and maintain dry conditions of -40°C dew point throughout the experiments.

The following paragraphs detail the mechanical properties of bulk PMMA that change depending on the water content of material in the range from 0% to greater than 1%. The behaviour at low water content could provide an indication of the type of response that might be experienced by the PMMA sensors operating within a freeze dryer.

Research has revealed that for bulk PMMA, water acts as a mild plasticiser up to a content of ≈1% [214] and can reduce fatigue resistance[214]. At higher water content reduced transparency, changes in deformation response (e.g. elongation to failure[232]), clustering or aggregation of water molecules was observed[16, 214]. Increasing the water content in PMMA beyond 1%, increases fracture toughness and decreases crazing strength, tensile strength and creep strength[232].

Shen et al.[16] reported that dry samples of bulk PMMA observed smaller average craze lengths, higher average tensile strength and higher craze initiation stress than in samples with higher water content[16, 232].

8.3   Aim

This chapter will document the use of POFBGs inscribed in SM PMMA and MM TOPAS fibres (section 5.3) to detect sublimation under vacuum conditions. The POFBGs would also track the backfill of the chamber with dry nitrogen gas to 1atm pressure and detect water vapour entering the freeze drying chamber upon opening the chamber door. This backfill stage is typically carried out in the pharmaceutical industry prior to stoppering the vials, keeping the samples in an inert gas, under dry conditions. If this stage is included in the freeze drying process it would be carried out before the door is opened to remove the vials, as otherwise it would expose the product to humidity in the air.

These two stages are critical as literature has reported that water content can affect product quality[19, 233], particularly if primary drying is terminated early. One of the main objectives for this project is to investigate the application of POFBG technology for monitoring sublimation during primary drying and to determine if this technology could be used to detect the end of primary drying time. The primary drying stage is the longest and most costly stage in the freeze drying cycle. In order to optimise the freeze drying cycles, reduce production costs and increase productivity, different types of sensors (e.g. thermocouples, TDLAS) have been trialled and documented in literature. They are now sold as part of commercial freeze drying units and used to determine the end of primary drying time during the manufacturing process.

The pressure and temperature sensitivities of the POFBGs, determined in the previous chapters, will be used where necessary to identify temperature effects caused by heat transfer issues or changes in pressure.

The aim is to compare the different POFBGs exposed to water vapour under these different conditions and as PMMA POFBG has an affinity for water vapour it is expected to show the biggest reaction. As literature has determined that TOPAS POFBG is at least 50 times less sensitive to water than PMMA[12], it is expected to show only limited changes in Bragg wavelength. It is likely that any changes are due to radiative effects, air currents and pressure changes in the chamber.

The objectives of this chapter are:

- After drying the fibres, observe the effects of backfilling the chamber to 1atm with dry nitrogen gas on POFBGs. This procedure was implemented in section 8.5.

- Monitor POFBGs when the chamber door has been opened, as would be expected in industrial applications when collecting freeze dried samples. This test will also provide information on the behaviour of dried POFBGs (in -40°C dew point conditions), to the exposure to water vapour entering the freeze dryer, which has not be found in literature. This was investigated in section 8.5.

- Sublimation experiments involving vials containing ice or frozen mannitol solutions. These vials are attached to an access port fitted with a valve, mounted on the outside of the freeze dryer; opening the valve allows the sample in the vial to be dried under vacuum conditions. This permits sublimation of the sample without the need for it to be placed directly onto the shelf and sealed in the vacuum chamber. The advantage of this technique is it allows the vial to be removed and weighed after a given timeframe, in order to measure the quantity of water which has sublimed into the freeze dryer. This procedure was applied in section 8.6.

- Section 8.7 had the PMMA and TOPAS POFBGs initially subjected to short step changes in pressure under dry sub-atmospheric conditions, afterwards a vial containing a sample will be attached to the access port to allow sublimation while the PLC repeats the step changes in pressure. The aim is to determine if there is a difference between these two conditions, as PMMA POFBG has an affinity to water vapour which can shift the Bragg wavelength.

- A PMMA POFBG was used to investigate in section 8.8 the relationship between the POF diameter size and response time to step changes in relative humidity, at 1atm in the Sanyo climatic chamber. This research was carried out to test the potential for improving the response time of the sensors to changes in humidity. Improvements in response time could allow the sensors to be used in a wide range of other industries where changes in humidity need to be detected rapidly e.g. food and pharmaceutical industry.

The next chapter will use POFBGs to monitor the freeze drying process of native collagen and mannitol solutions in the chamber. This will be carried out to determine if POFBGs can be used to detect end of primary drying of biological samples.

8.4   Method

The protocols described in sections 5.7 and 5.7.1 were used in this chapter to investigate the effect of water vapour on PMMA and TOPAS POFBGs (section 5.3). This was carried out to determine if POFBGs could be used to detect water vapour entering the dry chamber at 1atm and for monitoring of sublimation during the primary drying stage.

Several sensors were attached to the freeze drying unit in Figure 84 according to the specifications in section 5.7, to monitor dew point (SF52), pressure (TM101) and temperature. The dew point sensor and Pirani gauge are instruments that can detect changes in the gas composition of the chamber[8, 53, 77]. The POFBGs will be baselined against these devices as they are established technologies for monitoring of sublimation in a freeze dryer[8, 53, 77].

A customised feedthrough connector (section 5.7.1), was used to pass the K-type thermocouple into the vacuum chamber as seen in Figure 84, it was connected to a TM-947SD data logger that recorded the temperature in the immediate region of the POFs.
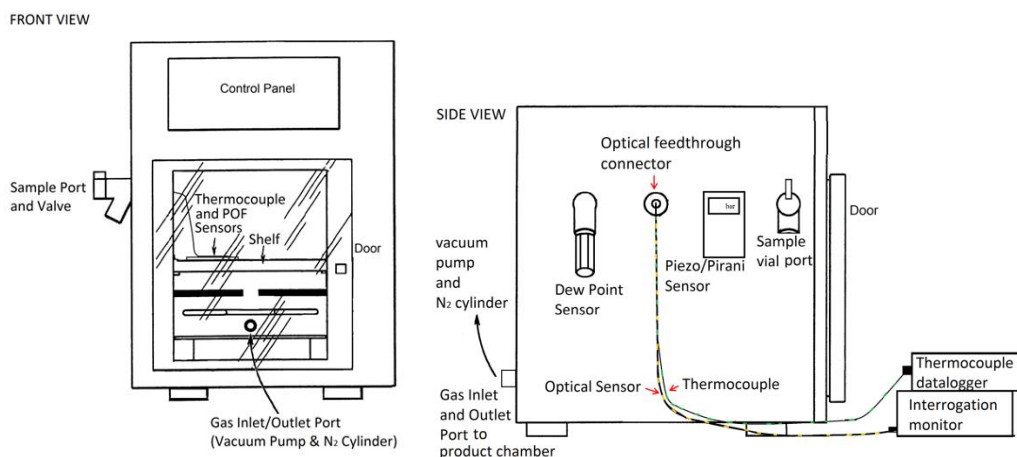
Figure 84 Assembly of the sensors in the freeze dryer to monitor water vapour inside the chamber

The TOPAS and PMMA POFBGs were placed into a protective housing structure and onto the temperature regulated shelf in the freeze dryer as seen in Figure 84 and in greater detail in Figure 85. The POFBGs were coupled to a 2x2 1550nm Corning single mode (SM) 50:50 silica coupler (9/125μm), which was connected to a FC/APC silica optical cable. Figure 85 shows that the FC/APC silica optical cable was fed through the vacuum chamber wall using a custom built feedthrough and connected to the interrogator (section 5.7.1). The I-MON 512

USB evaluation software v1.1 was used to analyse the FBG spectrum and calculate the Bragg wavelength using peak tracking algorithms at a sampling rate of 1 sample per 15sec.

The methods discussed in section 5.7 were used to ensure dry conditions in the chamber prior to the introduction of water vapour, as water content is known to influence the properties of PMMA and the Bragg wavelength of the POFBG. The POF sensors were dried for a minimum of 24hrs prior to carrying out the experiments, which also minimised the effects of outgassing [212, 213, 225, 226]. In industry, polymer pellets may be dried if degassing of unwanted materials is necessary (e.g. oxygen, water), this is carried out before extrusion as they can cause bubbles in the melt [234, 235]. The polymer may be heated at high temperatures in a vacuum dryer for several hours to promote degassing, these temperatures are kept several degrees below the Tg of the polymer[234, 235]. The glass transition temperature (Tg) depends on the grade of the polymer, with the Tg of PMMA being in the region of 105°C[165] and high-Tg TOPAS of 135°C[176, 209]. It is likely that at the lower temperatures used in the freeze dryer, the degassing phase would take longer than the protocol to dry the pellets. This procedure is necessary to avoid the high temperatures used in industry to degas polymers in high vacuum, damaging the optical fibre and FBG.

Different freeze drying cycles were used in each section to achieve the objectives described in the aim; the cycles will be described accordingly in each subsection.
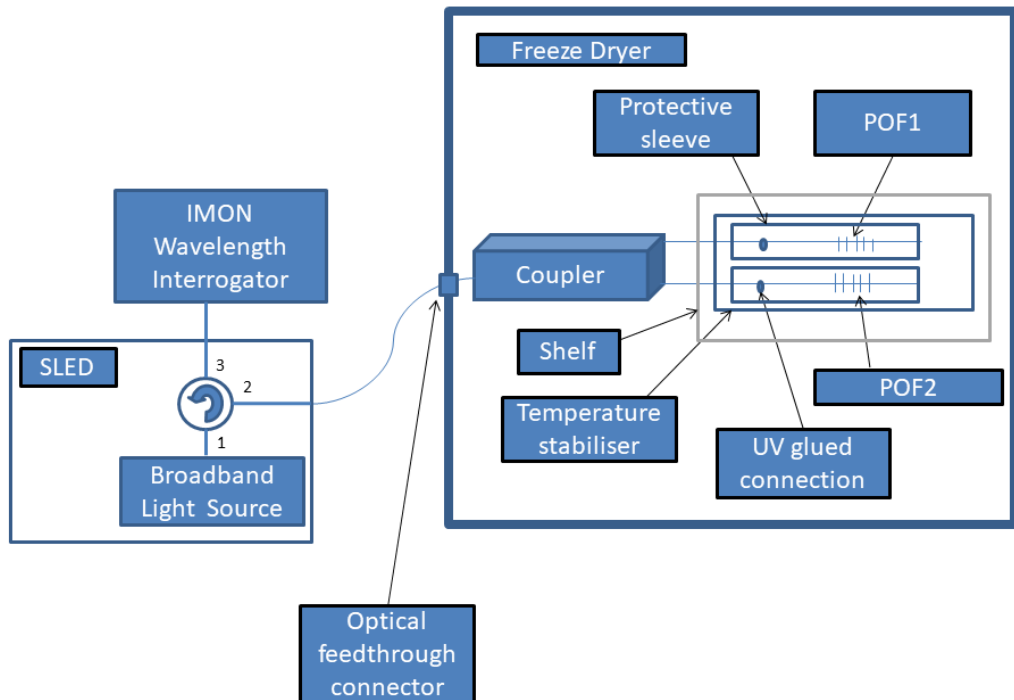
Figure 85 schematic diagram of the POFBG assembly used in this chapter. The interrogator is monitoring a PMMA POFBG (POF1) and TOPAS POFBG (POF2).

8.5 Water detection in the freeze dryer at atmospheric pressure after backfilling with nitrogen gas

Initial studies investigated the behaviour of PMMA POFBGs placed inside the freeze dryer and revealed large shifts in the Bragg wavelength (in the range of 0.8nm or greater), when the pressure was step changed between 1atm pressure and 300µbar. At this early stage, the freeze dryer was not connected to a nitrogen cylinder but directly to air (Figure 84). The pressure in the chamber was regulated with a solenoid valve connected to the vacuum pump and a gas inlet port; in this case air (containing water vapour) was introduced into the chamber when the pressure needed to be increased. It was hypothesised that a significant portion of the observed Bragg wavelength shift of the PMMA POFBGs was the result of changes in the level of water vapour in the chamber, as well as effects from changes in temperature and pressure.

Figure 86 show the results obtained from a step index single-mode PMMA POFBG, fabricated using the protocols described in section 5.2 in this thesis. A Thorlabs ASE730 broadband light source and an IBSEN I-MON 400 system were used to interrogate the POFBG. The fibre was kindly provided to Aston University by Prof. Gang-Ding Peng (UNSW, Australia) and was doped during the manufacturing stage to increase its photosensitivity to UV light [12, 236, 237]. Prior to inscription, the fibre was annealed for 24hrs at 80°C, the diameter of the fibre was measured using a Carl Zeiss microscope and determined to be 180µm with a core size of 10µm.

In Figure 86, the PMMA POFBG was exposed to pressures between 1atm pressure (1.01×10^6µbar) and 900µbar, which lead to a 1.47nm blue shift in the Bragg wavelength, likely due to a reduction in humidity or dew point, pressure and changes in temperature.

The step changes in pressure additionally indicated non-linear tendencies in the Bragg wavelength response in the sub-atmospheric pressure region, which were not observed in pressure regions higher than 1atm pressure described in the literature[13, 143, 224] (chapter 7). In Figure 86, a 0.6nm shift in the Bragg wavelength was observed from 900µbar to 300µbar, whereas a 1.47nm shift was observed from 1atm pressure (1.01×10^6µbar) to 900µbar.

The chamber was subsequently modified by connecting a nitrogen cylinder to the freeze dryer (Figure 84) and the protocol was modified as described in section 5.7, to allow nitrogen gas into the system and reduce the risk of contamination

with water vapour. This modification was necessary as water is known to influence the Bragg wavelength of PMMA POFBGs. These adaptations allowed experiments to be carried out to determine the influence of <2500µbar pressure on Bragg wavelength in a dry nitrogen atmosphere (chapter 7) and from 2500µbar to 1atm. Additionally this assembly allowed the sublimation experiments in section 8.6 and 8.7, to be conducted in a dry nitrogen environment in order to determine if the controlled introduction of water vapour through a valve influences the Bragg wavelength.
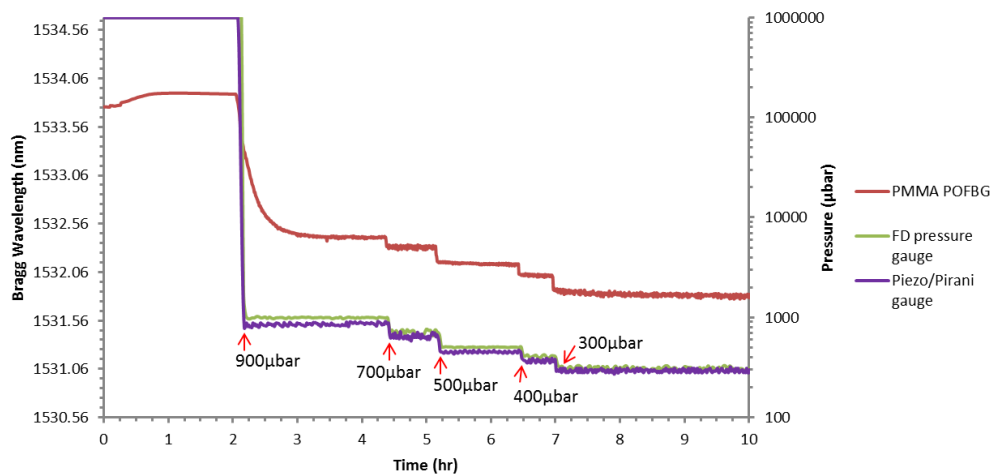
Figure 86 PMMA POFBG placed into the freeze drying unit and subjected to step changes in pressure from 1atm pressure to 300µbar

8.5.1   Method

This section investigates the behaviour of POFBGs dried in the freeze dryer for a minimum of 25hrs, prior to backfilling the chamber to 1 atmosphere (atm) pressure with dry nitrogen gas (-40°C dew point).

This procedure is carried out in the pharmaceutical industry, where the vials containing the freeze dried material are stoppered in an inert gas (e.g. dry nitrogen)[233] before being collected by the operator. This is a useful procedure to reduce the risk of contamination and minimise changes in the water content of the sample and avoid influencing product quality. This enclosed environment reduces the risk of water and oxygen from the air, coming in contact with the hygroscopic freeze dried powders[233], as this would affect their shelf life once removed from the dryer. Figure 87 illustrates this procedure being used after freeze drying of mannitol or native collagen samples, the results from these experiments will be discussed in the next chapter.

In this section only POFBGs (i.e. with no samples present in Figure 87), were dried under vacuum conditions at an inlet shelf temperature of 20°C. The sensors were subsequently subjected to 1atm dry nitrogen gas for a minimum of 30min and allowed to stabilise. At the end of this stage the chamber door was opened to observe the reaction of the POFBGs to humidity entering the dry chamber. This test may have applications in some industries (e.g. sectors of the food industry) who would freeze dry in bulk without stoppering. This device could provide useful information on the humidity entering the chamber at that stage or could be used to create a leak detection function.

It is hypothesised that PMMA POFBG having an affinity for water, will show the greatest reaction compared to TOPAS POFBG during this final phase, where water vapour is entering the chamber. It is expected that TOPAS and ZEONEX being hydrophobic in nature, would experience a limited shift in the Bragg wavelength, potentially due to air current movement or temperature variations.
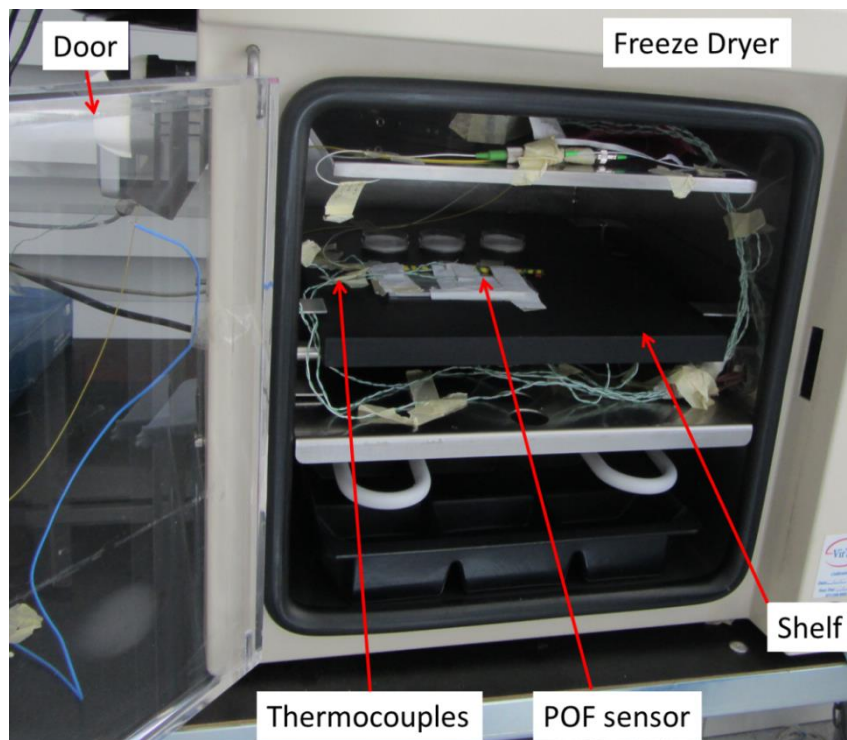
Figure 87 POFBG sensor located on the shelf in the freeze dryer, in this situation the door has been opened to remove samples on the shelf behind the POF sensor.

8.5.2   PMMA and TOPAS POFBG (POF 3, POF 4, POF 5)

Figure 88 shows the arrangement of the POFBGs in the freeze dryer, the FBGs were monitored using the peak tracking I-MON 512 USB evaluation software v1.1 throughout the programmed cycle and vacuum release phase.

In this arrangement "POF4" and "POF5" (section 5.3) were two FBGs inscribed in the same polymer optical fibre and connected to a silica pigtail using the techniques described in section 5.2. The gratings are separated by 1cm and reflect wavelengths in the 1570nm and 1530nm regions for POF4 and POF5 respectively. As the materials used for the sensors have a high attenuation in the 1500nm region[171, 182], the lengths of the POFs were kept to less than 10cm. POF4 and POF3 (Figure 88) were also positioned 2cm away from the butt coupled joint to reduce losses.
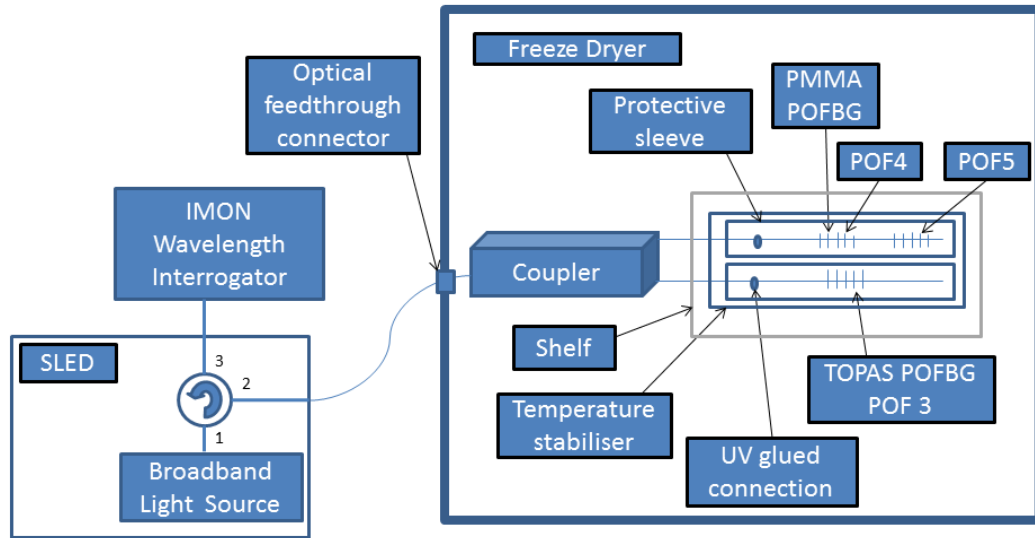
Figure 88 Arrangement of optical fibre sensors in the freeze dryer

Figure 89 and Figure 90 show the results obtained from POF3 and POF5, where the Bragg wavelength was plotted against the outputs of other sensors attached to the access ports of the freeze dryer. Graph (A) in Figure 89 and Figure 90 show the output of the pressure sensors and graph (B) illustrates the output of the dew point sensor used to provide information on the water vapour content in the chamber. Finally, graph (C) in Figure 89 and Figure 90 depicts the changes in temperature in the vicinity of the POFBGs, the air surrounding the freeze dryer and the inlet shelf temperature.

The conditions that the POFBGs in Figure 89 and Figure 90 were exposed to during this investigation are as follows:

1. POFBGs are dried for more than 25hrs under vacuum conditions at an inlet shelf temperature of 20°C and a pressure of <2500µbar. Figure 89 and Figure 90 show the response of the different sensors including POFBGs, to the low pressure conditions up to the initiation of the backfill stage at 28hrs (line a*).

2. The chamber was backfilled with dry nitrogen gas to 1atm, Figure 89 and Figure 90 show this stage commencing at time 28hrs (line a*). The test shows the response of the POFBG sensors in dry conditions (-40°C dew point) in the freeze dryer, to a pressure rise from vacuum to 1atmosphere, which was not previously reported in literature. The chamber remained sealed with dry nitrogen gas up to time 28.6hrs, marked with line b*. Figure 89(B) and Figure 90(B) show that -40°C dew point was kept during this timeframe. The equipment described in section 5.7 was used to maintain dry conditions and the water vapour content in the chamber was monitored using a SF52 dew point sensor.

3. The chamber door was opened and the POFBGs monitor the process of water vapour entering the dry chamber. In Figure 89(B) and Figure 90(B) the chamber door was opened at time 28.6hrs, marked with line b*. The dew point sensor attached to the access port confirmed that water vapour entered the chamber, where it tries to reach equilibrium with the surrounding environment.

Figure 89(A) shows the response of TOPAS POFBG (POF 3) to -40°C dew point and vacuum conditions of <2500ubar from 17hrs to 28hrs into the cycle. A drift in the wavelength of -58pm was observed during the "vacuum phase" between 17hrs and 28hrs. This wavelength shift is likely caused by a drift in temperature (Figure 89(C)) as a result of heat transfer into the chamber, from radiative heat through the door and wall[9, 46] as studied in chapter 6. The thermocouple read a drift in the temperature of 1.5°C and as the sensitivity of TOPAS to temperature is -36.0±0.3pm/°C, it can be deduced that temperature likely influenced the Bragg wavelength shift. A shift of -44pm was observed in Figure 90(C) from PMMA POFBG (POF5) during the same experiment, which has a temperature sensitivity of -18.0±0.2pm/°C.

Another parameter that could influence the Bragg wavelength shift is the diffusion of residual water out of the cylindrical polymer fibre, as this is a long term process with exponential and asymptotic trends[238].

Figure 89(A) shows at 28hrs into the cycle (marked with a*), that the vacuum was released, the chamber was backfilled with dry nitrogen gas and the pressure increased to 1atm. During this period the dew point remained stable at -40°C as seen by Figure 89(B). Figure 89(C) shows a sudden drop in the temperature next to the POFBGs by 1.5°C, due to the rapid flow of gas from the backfill process. At this time the TOPAS POFBG shifted by 202pm, which is likely the combination of temperature effects, increase in pressure, air currents and vibrations or

stresses placed on the fibre due to the vacuum release phase. The same behaviour was observed by PMMA POFBG in Figure 90 with a red shift of 91pm.
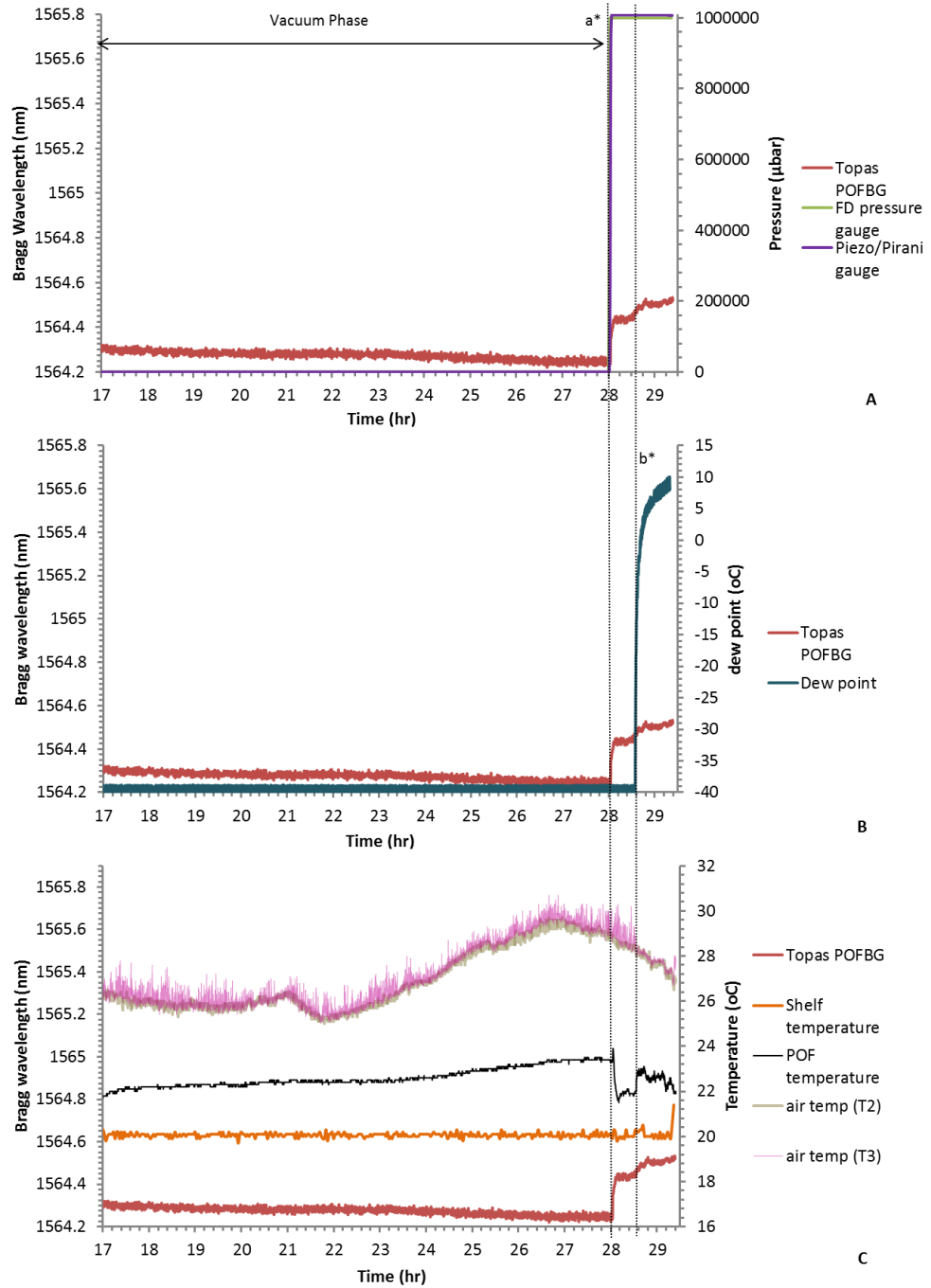
Figure 89 TOPAS POFBG (POF 3) Bragg wavelength shift with respect to (A) changes in pressure, at 28hrs (line a) the vacuum is released to 1atmosphere, (B) dew point. The dew point remains at -40ºC until time 28.6hrs (line b*) when the freeze dryer's door was opened, which allowed water vapour into the chamber, (C) temperature in the chamber. The shelf inlet temperature was set to 20ºC. A drop in POF temperature is observed at 28hrs (line a*) when the chamber was rapidly filled with nitrogen gas.*
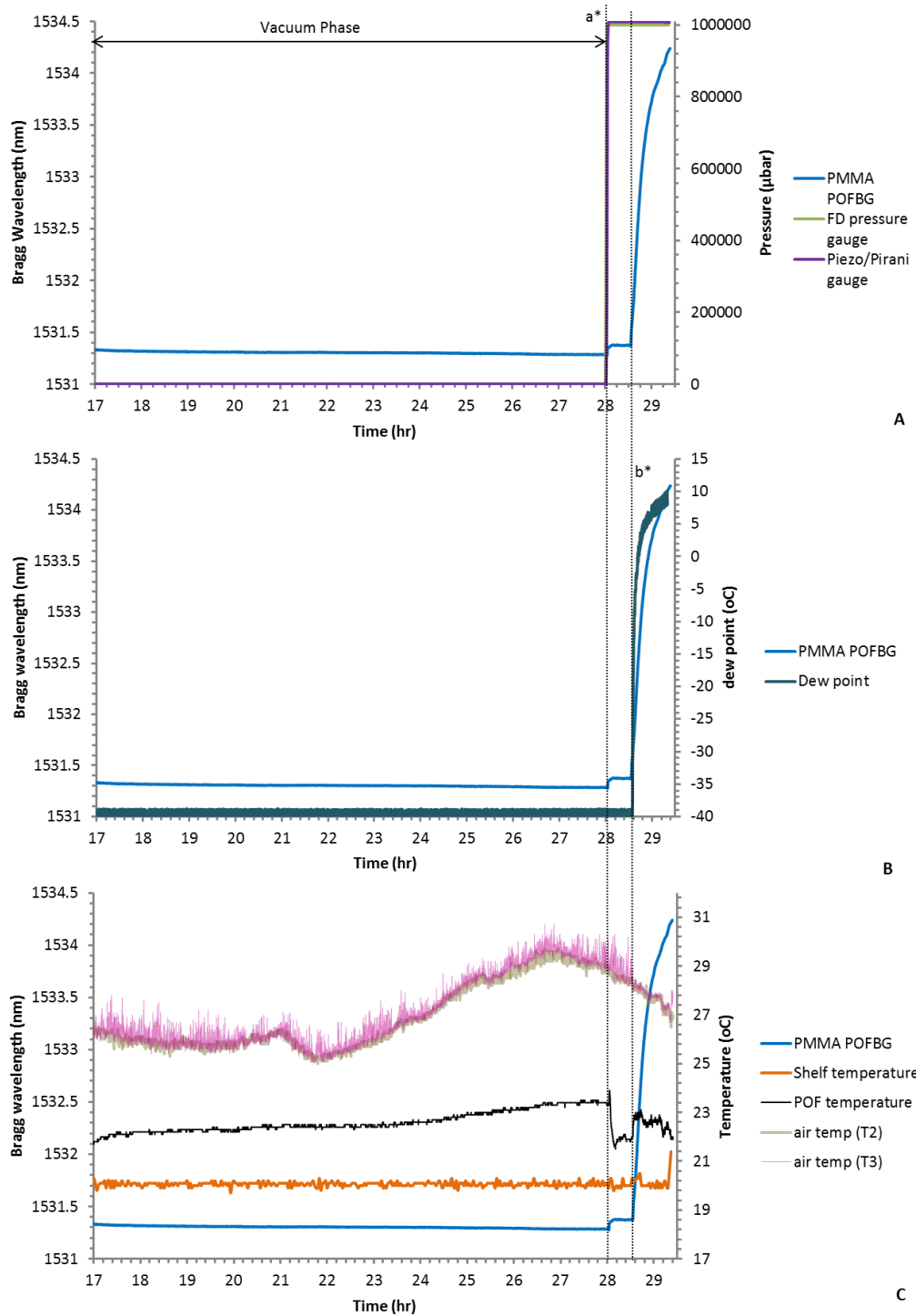
Figure 90 PMMA POFBG (POF 5) Bragg wavelength shift with respect to (A) changes in pressure, at 28hrs (line a*) the vacuum is released to 1atmosphere, (B) dew point. The dew point remains at -40ºC until time 28.6hrs (line b*) when the freeze dryer's door was opened, which allowed water vapour into the chamber, (C) temperature in the chamber. The shelf inlet temperature was set to 20ºC. A drop in POF temperature is observed at 28hrs (line a*) when the chamber was rapidly filled with nitrogen gas.

Figure 89 and Figure 90 show that the dew point in the chamber rapidly increases towards 10ºC and the pressure remained at 1atm at time 28.6hrs (line

b*). This is the result of the chamber door being opened exposing the sensors to air with a 55.8%RH, which was measured using a Testo 625 humidity sensor. A rise in the temperature around the region of the POFBGs was observed (1°C), potentially due to heat transfer from the shelf as well as the air temperature of 28°C being higher than inside the freeze dryer. An increase in the Bragg wavelength of 2.58nm and 60pm was observed for PMMA and TOPAS POFBG respectively. As the PMMA POFBG has a sensitivity of -18±0.2pm/°C, this experiment shows that water vapour has a significant impact on the Bragg wavelength of the grating well beyond expected.

PMMA is a material known to swell when exposed to water and about 50% of water in the polymer is accommodated in microvoids[16, 17]. It is possible that as the initial response is rapid after opening the door (within 30sec) and as diffusion in to the core is expected to be a long term process (Figure 91 and Figure 92), that water effects the surface of the fibre and enters microvoids, causing a shift in the Bragg wavelength.

Figure 91 (POF5), Figure 92 (POF4) and Figure 93 (POF3) are graphs of the last 2hrs of the experiment carried out in Figure 89 and Figure 90, to show in greater detail the effects of the vacuum release phase and exposure to water vapour at 1atm.

Figure 91, Figure 92 and Figure 93 show at time 1682min (box "a") that a red shift occurred for the Bragg wavelengths of PMMA and TOPAS POFBGs. This occurred as the chamber was backfilled with dry nitrogen gas from 2500µbar absolute to atmospheric pressure and was left for 30min to allow the sensors to stabilise. The door of the freeze dryer was opened (box "b") to allow water vapour from the air (55.8%RH) to enter the chamber. A rise in the dew point was noted and once conditions stabilised, a 2.58nm (Figure 91) and a 90pm (Figure 93) red shift in Bragg wavelength was detected by the PMMA and TOPAS POFBG respectively.

A short time lag in the reaction of the sensors to the changes in gas composition was observed (box "b"), as water vapour in the air required time to diffuse into the dry freeze drying chamber. During this time condensation and fog was visible to the naked eye in the chamber as gases circulated between the cold surface area (-80°C condenser coils) and warm area (above the shelf). As convection currents, condensation, and fog were observed in the chamber, it is possible that they could be putting stresses or causing minor movements of the fibre, therefore influencing the Bragg wavelength. This process could also be occurring to the hydrophobic TOPAS POFBG(POF3) in Figure 93 and Figure 89(line b*), as the

shift in wavelength cannot be explained by temperature effects alone. The data shows an increase in the temperature (1°C in Figure 93 box "b") and a positive Bragg wavelength shift of TOPAS POFBG (60pm) during this timeframe, however due to the dominance of the negative thermo-optic coefficient, it suggests another mechanism is involved. The red shift was observed on multiple occasions by several TOPAS POFBGs (examples include Figure 163 and Figure 164 in Appendix H) and would require further investigation. Future work could incorporate an independent temperature stabilisation system (e.g. using a Peltier) for the sensors, in order to avoid using the refrigeration system of the freeze dryer, which causes wide temperature variations across the chamber. Other projects could develop temperature compensation techniques on the same POF.

Figure 91 (marked "b") shows that as the gas composition changed in the surrounding area, the PMMA POFBG (POF5) red shifted ~2min before the SF52 sensor registered a change in dew point. This response was also observed in PMMA POFBG (POF4) in Figure 92. This could have resulted from a combination of factors:

- The water vapour in the air took longer to reach the dew point sensor, as the sensor was attached to an access port physically further away from the door of the freeze dryer than the POFBG.

- The PMMA POFBG is sensitive to vibrations and air currents. The fog and the convection currents from the temperature differences and water vapour gradient across the chamber could influence the Bragg wavelength.

- The PMMA POFBG could be detecting variations in gas temperature as they circulate. The thermocouples recorded wide temperature differences across the chamber from the condenser region (-80°C), shelf temperature region (22°C) and external air temperature (28°C). A temperature shift of almost 1°C was seen in Figure 93.
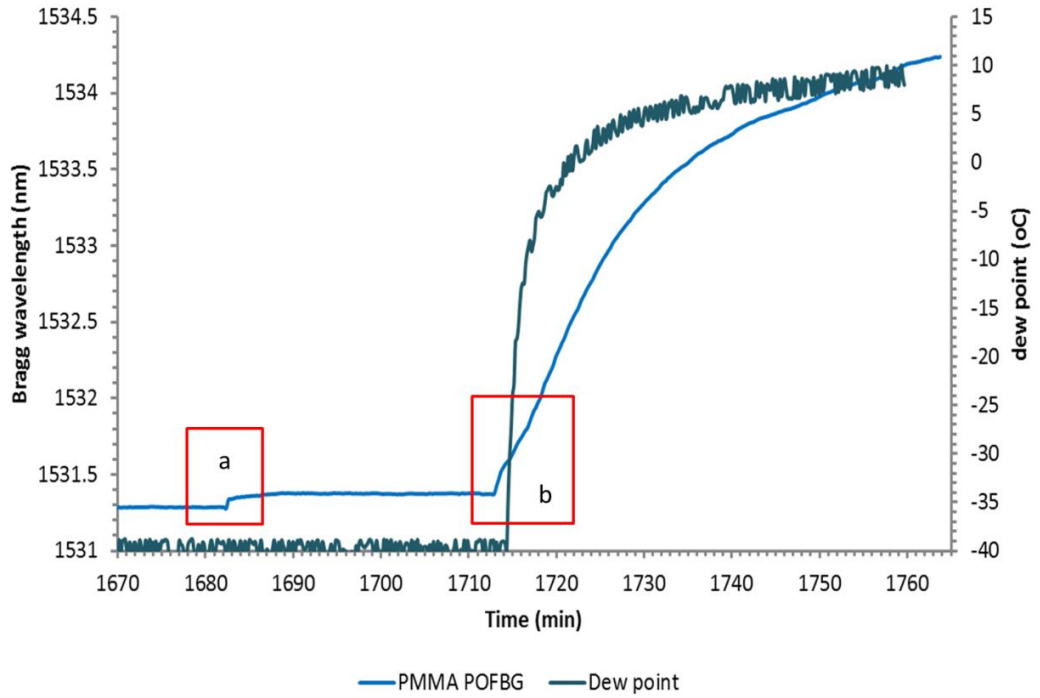
Figure 91 PMMA POFBG (POF5), (a) chamber backfilled with nitrogen gas to 1atm, (b) an increase in the humidity in the chamber, gas convection currents and 1°C shift in temperature caused a 2.58nm shift in the Bragg wavelength
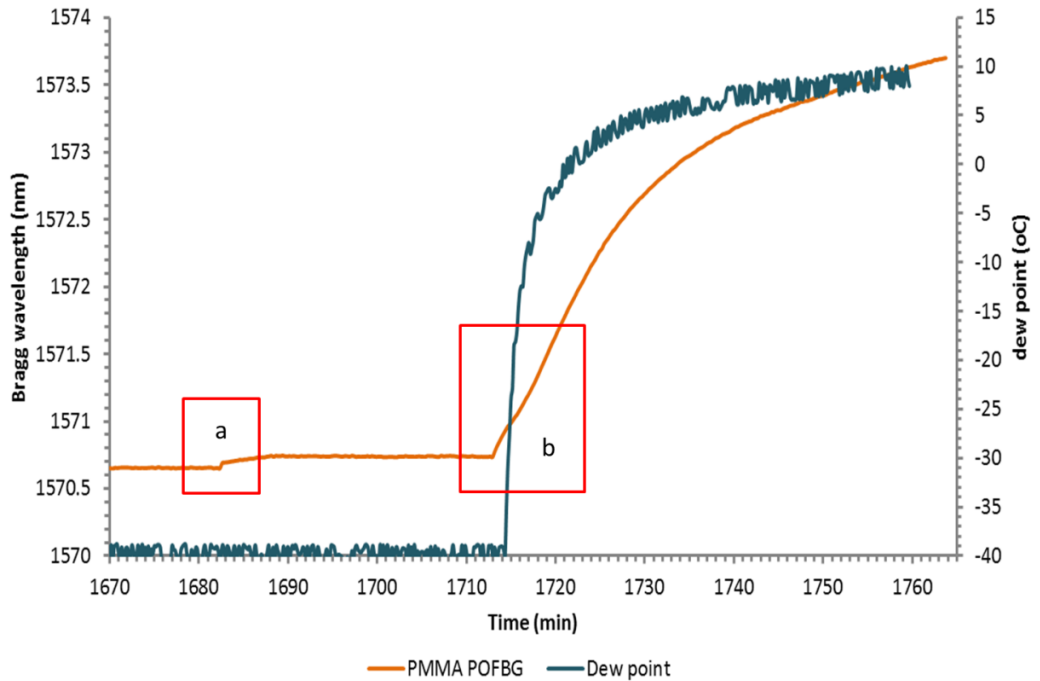
Figure 92 PMMA POFBG (POF4), (a) chamber backfilled with nitrogen gas to 1atm, (b) an increase in the humidity in the chamber, gas convection currents and 1°C shift in temperature caused a 2.67nm shift in the Bragg wavelength
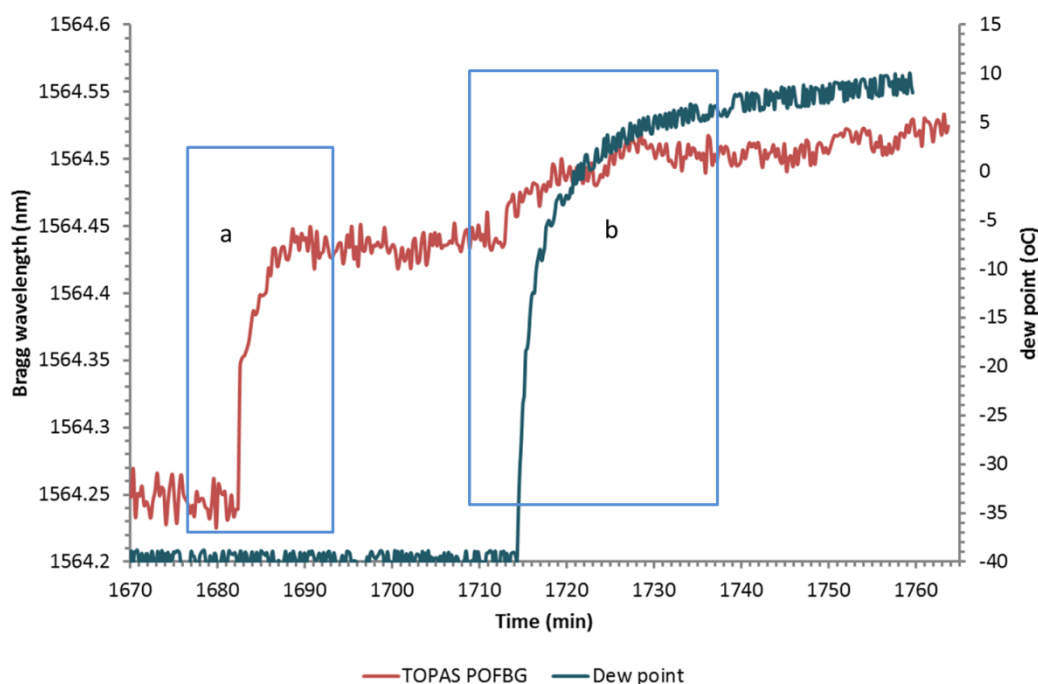
Figure 93 TOPAS POFBG (POF3), (a) chamber backfilled with nitrogen gas to 1atm, (b) a 90pm shift in wavelength as the chamber door is opened

8.5.3 PMMA and TOPAS POFBG (POF 1, POF 2)

This section uses the method described in section 8.5.1 on POF1 and POF2, to monitor the rise in pressure from vacuum to 1atm with dry nitrogen gas and then exposing the POFBGs to humidity. Figure 94 shows the shift in the Bragg wavelength of PMMA and TOPAS POFBGs (POF1 and 2), in response to the changes in pressure, temperature and humidity in the chamber. The graphs of the cycle and the data from the Pirani gauge, POFBGs, thermocouples and dew point sensor are available in Figure 162 and Figure 163 in Appendix H. As with the prior experiment, the inlet shelf temperature was set to 20°C and a K-type thermocouple was placed in the vicinity of the POFBGs to monitor the temperature in the region throughout the cycle, see Figure 84.

The fibres were dried for 27hrs in the chamber at 2500μbar absolute, -40°C dew point and 20°C inlet shelf temperature (region a) prior to the pressure rise phase. At 27hrs into the cycle (line marked "b"), the chamber was quickly backfilled with nitrogen gas to 1atm and a sharp decrease in the temperature reading (-0.7°C) was measured by the thermocouple. The drop in temperature caused a spike in the Bragg wavelength of PMMA and TOPAS POFBG, due to the dominance of the negative thermo-optic coefficient. The temperature recovered after the completion of the backfill stage and as the gas was allowed to reach equilibrium.

At this time the Bragg wavelength of the PMMA and TOPAS POFBG stabilised and were found to have shifted by 47pm and 60pm respectively, for a pressure step change from 2500μbar to 1atm (1.01bar). Chapter 7 determined that the sensitivities for the POFBGs in the 2500μbar region were 9×10^{-6}nm/μbar($\pm7\times10^{-6}$) (POF1) and 4×10^{-6}nm/μbar($\pm5\times10^{-6}$) (POF2). The results show that the obtained shift in the Bragg wavelength is significantly lower than the sensitivity to pressure in the <2500μbar region. This result supports the work carried out in chapter 7, which determined that the POFBGs displayed non-linear tendencies in the low pressure region. This non-linearity would need to be investigated in future projects, to determine the mechanism and if this trait allows the POFBGs to be used for additional pressure sensing applications.

Figure 94 shows from "b" to "c" that the Bragg wavelengths stabilised in the 1atm nitrogen gas environment, the other sensors confirmed that -40°C dew point and a temperature of 20°C was maintained during this timeframe.

At point (c) the chamber door was opened and the dew point rapidly increased to -8°C, while the thermocouple did not register a drift in temperature. As a result, a 42pm and 0.79nm red shift in the Bragg wavelength was observed for TOPAS and PMMA POFBG respectively. A red shift in the Bragg wavelength of PMMA POFBGs at 1atm pressure as a result of an increase in the chamber humidity, supports the trends observed in literature[12].

Fog and gas movement was visibly observed in the chamber as in the previous experiment, which could potentially cause movement or introduce stresses in the fibres. Further studies would need to be carried out to determine the exact mechanism which is influencing the TOPAS POFBG. The graphs of the data showing the outputs from the different sensors in the chamber are available in Figure 162 and Figure 163 in Appendix H.
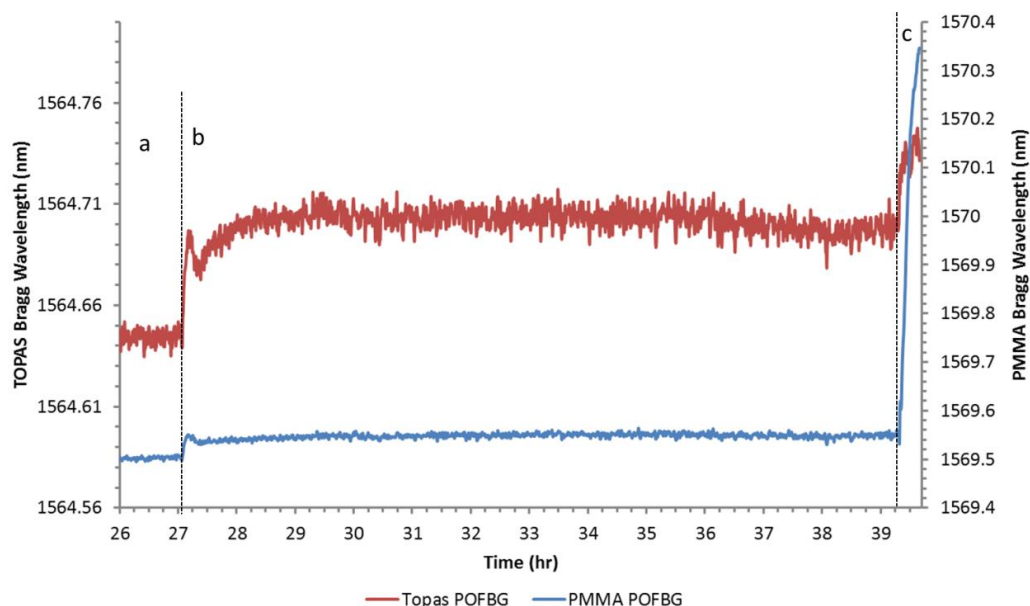
Figure 94 PMMA POFBG (POF 1) and TOPAS POFBG (POF 2) Bragg wavelength shift at 20°C inlet shelf temperature (a) pressure set to 2500μbar (b) the pressure increased to 1atmosphere and backfilled with dry nitrogen gas. A -0.7°C drop in temperature is observed and detected by the POFBGs, (c) at 39.25hrs the chamber door was opened, allowing water vapour into the freeze dryer

Figure 95 is another experiment carried out on POF1 showing the same trends as documented in the previous graphs. In this experiment an additional test was carried out after the backfill stage, to observe if changing the humidity in the chamber influences the Bragg wavelength. To monitor the humidity in the chamber a Testo 625 humidity sensor was placed next to the POFBGs after the door was opened. The refrigeration system of the freeze dryer was kept running to keep the shelf temperature at 20°C, as well as the condenser running to act as a water trap in the unit. To increase the humidity in the chamber, the door was opened (b* and d* in Figure 95) and the Bragg wavelength increased as previously reported. At time 29hrs (b*), the introduction of 24.3%RH air caused an increase in the dew point to -5°C, a red shift of 35pm and 0.82nm for TOPAS and PMMA POFBG respectively. As previously documented, the shift is larger for PMMA POFBG than for TOPAS POFBG, likely due to the polymer's affinity for water. The graph for TOPAS POFBG (POF 2) is available in Appendix H, Figure 164.

At time 29.8hrs (c* in Figure 95) the chamber was sealed and the -80°C condenser caused the humidity to reduce to 17%RH, dew point in region of -15°C and the Bragg wavelength of PMMA POFBG shifted by -350pm.

This investigation shows that this PMMA POFBG is capable of tracking humidity at 1atm pressure after exposure to vacuum conditions and that humidity has a significant effect on the Bragg wavelength. As TOPAS was determined to be at least 50 times less sensitive to water than PMMA[12], future work would investigate the mechanism influencing the TOPAS FBG, as these experiments indicate that humidity or another parameter is having some influence.
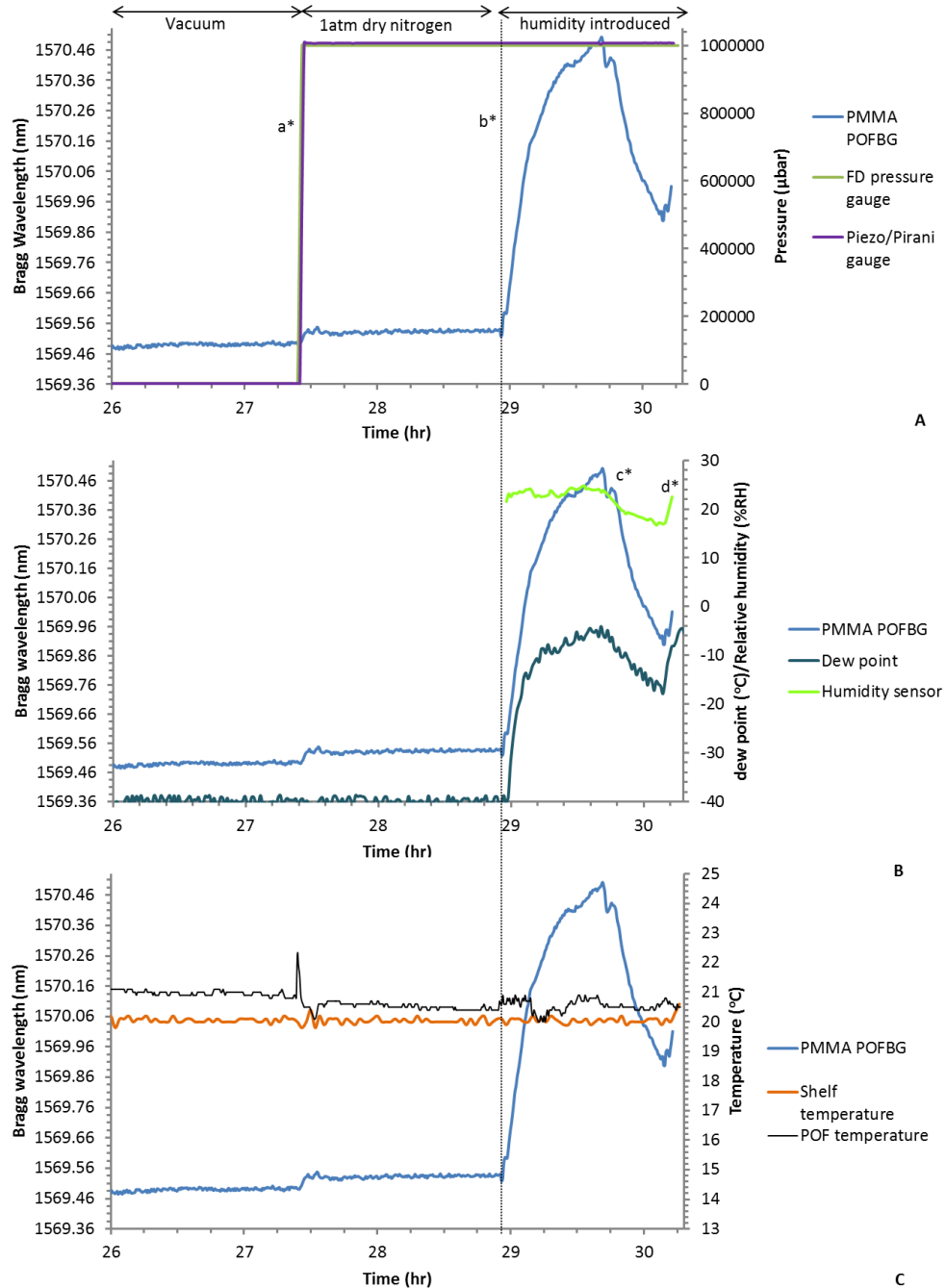
Figure 95 PMMA POFBG (POF 1) Bragg wavelength shift with respect to (A) Pressure, at 27.4hrs (a*) the vacuum was released to 1atm and backfilled with dry nitrogen gas, (B) dew point. The dew point remained at -40ºC until (b*) when the freeze dryer door was opened and water vapour entered the chamber, at 29.6hrs the door was closed (c*) and opened at (d*).

(C) Temperature in the chamber. The shelf inlet temperature was set to 20°C and a drift in the thermocouple temperature was observed.

8.6 POFBGs used to detect sublimation in a freeze dryer

8.6.1 Method

The commercial Virtis freeze dryer was designed by the manufacturer to increase production output by allowing samples to be freeze dried on the shelf, as well as in vials attached to the access ports (Figure 96) on the outside of the chamber. In this chapter, the access ports will allow the vials (and water vapour) to be introduced at specific times into the dry nitrogen atmosphere at sub-atmospheric pressures. This procedure will be used in sections 8.6 and 8.7, in order to monitor the influence of subliming water vapour on the Bragg wavelengths of PMMA and TOPAS POFBGs. The vials can then be removed when desired to be reweighed, in order to monitor the reduction in mass due to sublimation, without changing the pressure in the chamber. This procedure avoids the need to backfill the chamber with nitrogen gas to 1atm if a sample had been placed onto the shelf and needed to be collected.

The following paragraphs describe the experiments carried out in order to detect sublimation of water vapour in a freeze dryer. The POFBGs were placed in the vacuum chamber at a set shelf inlet temperature of 20°C, for a minimum of 24hrs to obtain dry conditions in the chamber, prior to starting the tests. The equipment used in this project was described in section 8.4 of this chapter, with schematic diagrams of the locations of the POFBG illustrated in Figure 85 and Figure 88. The pressure was set to 200µbar, since this is within the typical operating pressure range of 133-266µbar (100-200mTorr)[1, 19, 24] that would be used in a standard freeze drying cycle of biological samples.

Samples of distilled water or mannitol 10%w/v were frozen in vials (described in section 5.7.6), weighed using a OHAUS TS400D mass balance and attached to the access port of the freeze dryer. A valve on the access port allows control over gas flow from the vial into the freeze drying chamber, as seen in Figure 96. The Pirani gauge, POFBGs and dew point sensor monitored the presence of sublimed water vapour in the chamber.
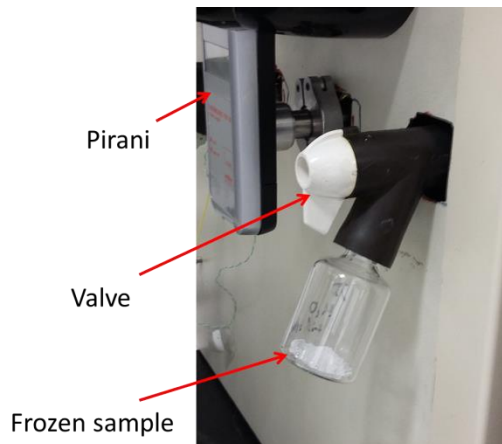
Figure 96 Vial containing a sample of a known mass attached to the access port on the freeze dryer. The valve between the vacuum chamber and the vial was opened to promote sublimation.

8.6.2 POFBGs detecting sublimation from a sample of frozen distilled water

Figure 97 illustrates a typical output from the POFBGs and the Pirani gauge when carrying out an experiment that involves sublimation of water vapour into the chamber; these trends were also observed in Figure 165 to Figure 170 in Appendix H.

In this example (Figure 97), a PMMA POFBG (POF4) showed a red shift in the Bragg wavelength as a result of the introduction of water vapour into the system, which has been observed in literature at 1atm pressure[12]. The vial contained distilled water that had been frozen the previous day in a -21°C freezer and weighed (2.68g) before opening the valve on the access port (Figure 96). Opening the valve reduced the pressure in the vial below the triple point of water and promoted sublimation.

Figure 97 shows that the wavelength and pressure remained stable under low pressure conditions of 200μbar, 20°C inlet shelf temperature and -40°C dew point directly before the sample was introduced. At time 156.5min, the valve was opened and a pressure rise is seen due to the evacuation of gas from the vial into the freeze dryer. At the same time, the thermocouple in the vicinity of the POFBG registered a decrease in temperature of -0.2°C (Figure 169 in Appendix H), as the gas passed across the sensor cooling the region. The combined increase in pressure and the decrease in temperature resulted in an overall increase in Bragg wavelength of POF4 (Figure 97), the red shift was expected based on the work carried out in chapter 6 and 7 of this thesis. The

spike in pressure was observed by the Pirani sensor, chamber pressure gauge, PMMA and TOPAS POFBGs as seen from the graphs in Appendix H for POF4 (Figure 169), POF5 (Figure 170) and POF3 (Figure 168). The pressure spike recovered after 2min, as the vacuum pump returned the pressure in the chamber back to the set point value of 200μbar. The temperature measured by the thermocouple next to the POFBGs was found to have recovered during sublimation.

The graph appears to show the spike in the chamber pressure measured by the freeze dryer's thermocouple gauge had begun earlier than the other sensors; however this is due to limitations in the sampling rate of the commercial VirTis software. The VirTis software could only collect 1 sample every 2min, as this was determined by the manufacturer of the freeze dryer to be suitable for industrial applications.
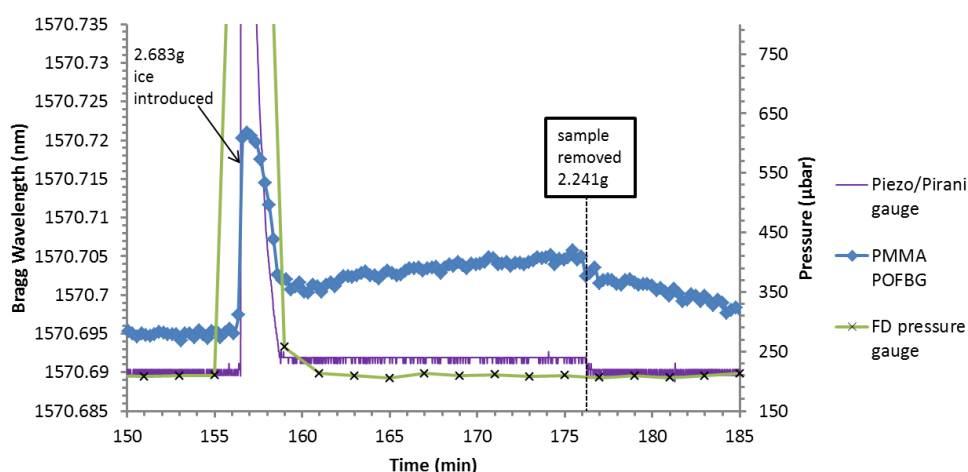
Figure 97 typical output from a POFBG, Pirani gauge and freeze dryer gauge when a sample is introduced to the access port of the freeze dryer. The initial response was a pronounced spike in the freeze drying chamber pressure as the gas in the vial was evacuated. The Bragg wavelength red shifts due to the sublimation of water vapour and Pirani gauge shows a pressure shift due to the changes in the gas composition. The freeze dryer gauge was placed by the manufacturer in an optimised location to measure the chamber pressure and not be influenced by water vapour.

After the chamber pressure recovered to 200μbar (at time 159min), Figure 97 shows an offset in the PMMA POFBG (10pm shift) and the Pirani gauge value (30μbar), as the sensors detect a change in gas composition from the addition of water vapour. The valve was closed at 176min and the sample was taken to the mass balance to be weighed before being placed back into the freezer to avoid melting. The sensors were exposed to 0.442g of water vapour over a 20min period, which had sublimed into the chamber before being collected by the condenser, acting as a water trap in the freeze dryer. As the Bragg wavelength is

relatively consistent over the period, the following gives a reasonable approximation of the flow rate; a value of 1.326g/hr or 0.00036g/s would have been detected by the sensors. A wide range of sublimation rates for pharmaceutical samples were reported in the literature to be achievable depending on the cycle parameters, sample and concentration as they all influence the ice crystal morphology, drying times and resistance to mass flow rate of the subliming water vapour. It has been reported that mass flow rates in the range of <0.24 g/s[112] could be detected using TDLAS, <348.1mg/hr using a freeze drying microbalance[202] and <1.51g/hr/vial using MTM technology[203]. The estimated sublimation rate in this experiment is within the range of the values reported in literature; however they were obtained from samples placed onto the shelf which provided heat transfer to the sample. The POFBGs would need to be compared against these other technologies in future projects, to monitor the mass flow rate of the water vapour in the chamber and particularly if POFBGs could be used to determine this parameter.

During this experiment (Figure 97) the dew point remained constant at -40°C, when compared against the literature, studies report sensors detecting sublimation between -40°C and -60°C dew point[8, 57]. It is likely that the current dew point sensor was not designed to operate within the range required for the detection of gas composition in a freeze dryer, as the lowest detectable dew point for this device is -40°C. Future work would require investigating dew point sensors or chilled mirrors with a wider and lower operating range to compare against the POFBGs.

Figure 97 shows that once the sample was removed (time 176min), a decrease in Bragg wavelength was observed. The pressure reading from the Pirani gauge returned to 200µbar, as the water content in the chamber decreased and the gas composition returned to a purely nitrogen based environment.

8.6.3   POFBGs detecting sublimation from frozen mannitol solution

The procedure described in 8.6.1 was repeated using a 10ml sample of mannitol 10%w/v, frozen in a freezer at -21°C. Figure 98 shows the results obtained when the vial containing the sample was attached to the access port, the valve was opened to allow gas flow for 20min before it was closed and the sample was reweighed. The experiment was repeated 3 times (b, d and f) and the samples were removed at points marked with the letters "c", "e" and "g", to reweigh the sample and determine the quantity of water which had sublimed. As seen

previously, opening the valve caused a pressure spike in the chamber, which was detected by the Pirani gauge, chamber gauge and the POFBG (POF 4). This was followed by an offset in the Pirani gauge reading (30µbar) and the Bragg wavelength of 12pm throughout sublimation.

A drift in the thermocouple temperature was observed (0.3^{o}C) across the entire experiment as seen in Figure 99. As the sensitivity to temperature was determined to be -18 ± 0.3pm/^{o}C in chapter 6, it is possible that the POFBG is reacting to the presence of water vapour due to PMMA having an affinity for water[16, 17].

It is also possible that the POFBG is detecting the movement of gas, which is inducing internal stresses into the fibre. Detection of the movement of the gas would need to be investigated in future projects, particularly as a 14pm offset in the Bragg wavelength was also observed by the humidity insensitive TOPAS POFBG (Figure 100) during sublimation. The offset in the Bragg wavelength of TOPAS POFBG disappeared after the valve was closed to prevent sublimation. When the sample of ice was removed from the system ("c", "e" and "g" in Figure 98), the PMMA POFBG Bragg wavelength was found to decrease towards the value at the start of the experiment.

Figure 100 and Figure 101 show the reactions of TOPAS POFBG (POF 3) and PMMA POFBG (POF 4), to a vial containing no ice "empty vial" that was attached to the system after exposure to subliming water vapour for more than 20min. Initially, a spike in the Bragg wavelength occurred due to the introduction of gas into the chamber, which caused an increase in the chamber pressure (lasting 2min). The Bragg wavelengths were found to have recovered to their values at the start of the experiment (at 150min), 6 min (TOPAS POFBG), 16min (POF4 PMMA POFBG) and 21min (POF5 PMMA POFBG) after opening the valve (at 241min). These recovery times were compared to a vial (with no ice) that was attached to the system after the POFBGs were dried for 24hrs in nitrogen at sub-atmospheric pressure ("d" in Figure 106). The results show that PMMA and TOPAS POFBG Bragg wavelengths recovered within 6min after the valve was opened and air from the vial entered the chamber. These results indicate that exposing the PMMA fibre to water vapour for long durations (>20min) increased the time required for the Bragg wavelength to return to the original value at the start of the experiment. This could have resulted from higher water content in the PMMA fibre after longer exposure times to water vapour and the material's affinity for water, requiring more time to dry the fibre in the chamber after the source was removed.

As the TOPAS POFBG recovered within 6min regardless of the exposure time to water vapour, it is possible that the FBG was reacting to air movement during sublimation or water affected the surface of the fibre. These observations would require further investigation to determine the mechanisms affecting PMMA and TOPAS POFBGs in this environment.

After the final sample was removed at point (g) in Figure 98, a sudden drop in the Bragg wavelength occurs and 20min later it was found to have recovered back to the initial state at the start of the experiment. The delay could be the result of POFBG detecting residual water vapour in the chamber or desorption of water from the fibre, the mechanism would need to be investigated in future projects. During this timeframe the dew point sensor continued to read -40°C dew point, it is believed that the sensor does not have the required specifications to detect the levels of dew point in the chamber, as observed in the previous experiment with frozen distilled water.

The trends described in this section for POF4 and POF3 (data is available in Figure 165 and Figure 166 in Appendix H), were also observed by POF5 (Figure 167 in Appendix H) during the same experiment.
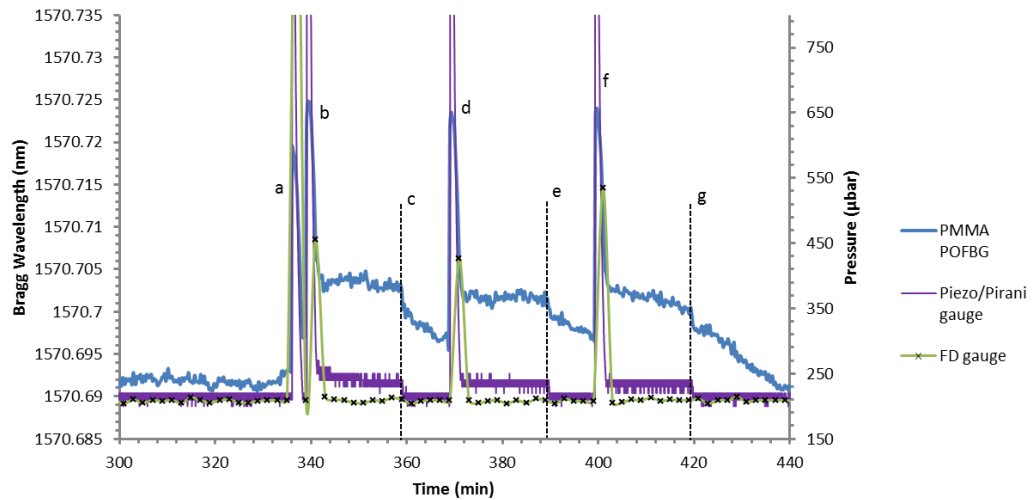
Figure 98 PMMA POFBG (POF 4) wavelength response to sublimation of water vapour from a 10ml mannitol 10%w/v sample, frozen to -21°C. (a) Valve opened, vial containing no sample, (b) valve opened, mannitol mass: 7.16g, (c) valve closed, mannitol mass: 6.47g, (d) valve opened, mannitol mass: 6.47g, (e) valve closed, mannitol mass: 5.99g, (f) valve opened, mannitol mass: 5.99g, (g) valve closed, mannitol mass: 5.56g
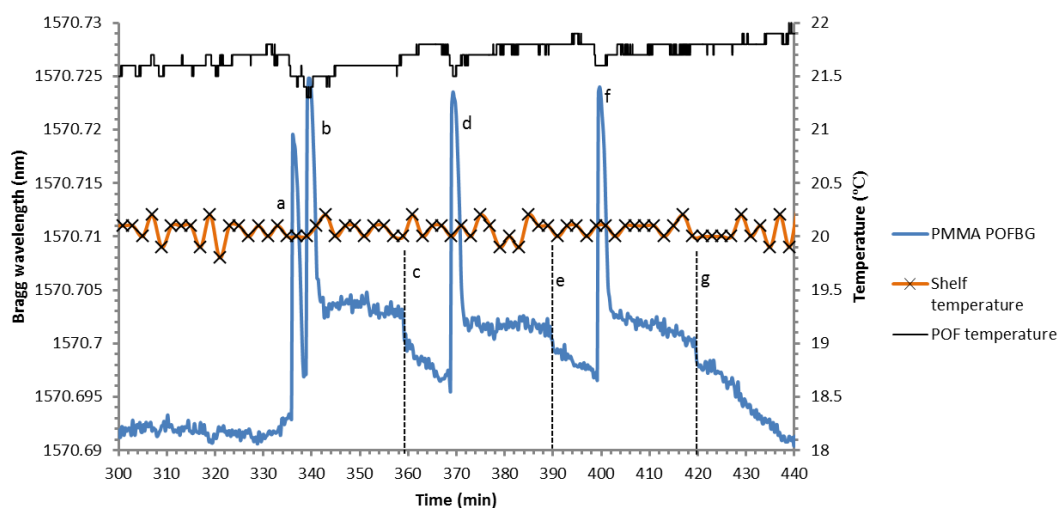
Figure 99 PMMA POFBG (POF 4) wavelength response to sublimation of water vapour from a 10ml mannitol 10%w/v sample, frozen to -21ºC. (a) Valve opened, vial containing no sample, (b) valve opened, mannitol mass: 7.16g, (c) valve closed, mannitol mass: 6.47g, (d) valve opened, mannitol mass: 6.47g, (e) valve closed, mannitol mass: 5.99g, (f) valve opened, mannitol mass: 5.99g, (g) valve closed, mannitol mass: 5.56g
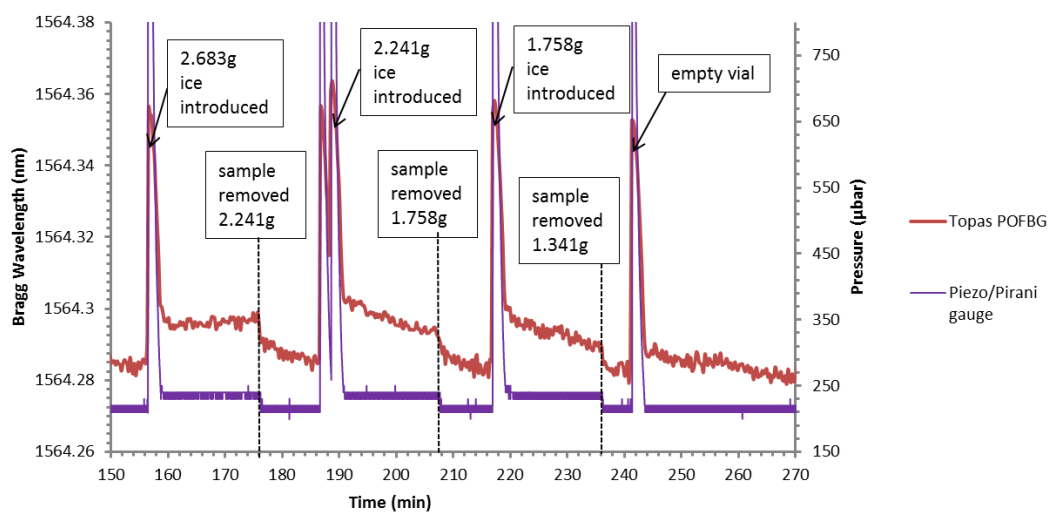
Figure 100 TOPAS POFBG (POF 3) wavelength response to sublimation of water vapour from distilled water frozen to -21ºC. Marked regions indicate where the valve was opened and closed to allow sublimation of water vapour into the chamber and in the last case no ice was present in the vial. Dew point was -40ºC and the temperature deviation measured by the thermocouple in the vicinity of the POF was 0.2ºC.
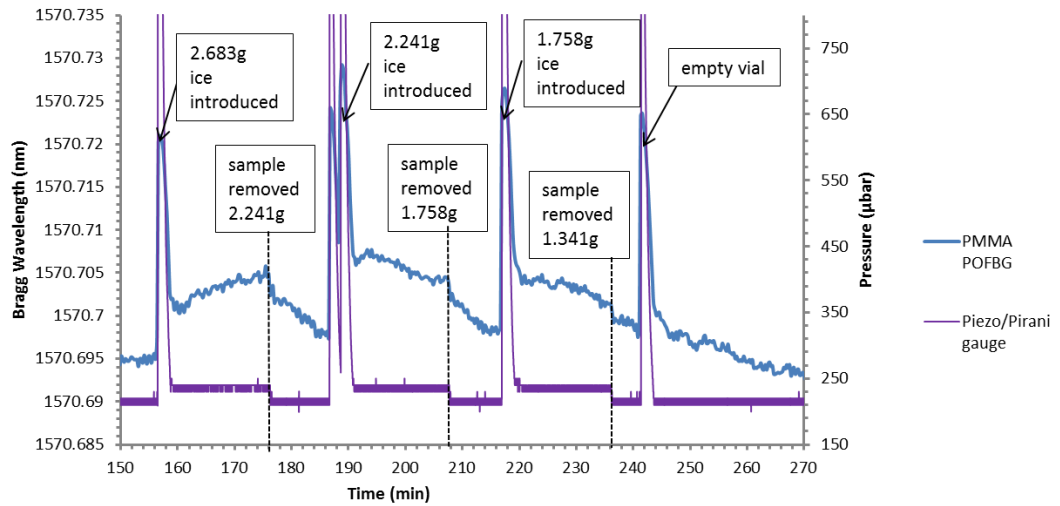
Figure 101 PMMA POFBG (POF 4) wavelength response to sublimation of water vapour from distilled water frozen to -21ºC. Marked regions indicate where the valve was opened and closed to allow sublimation of water vapour into the chamber and in the last case no ice was present in the vial. Dew point was -40ºC and the temperature deviation measured by the thermocouple in the vicinity of the POF was 0.2ºC.

Figure 102 shows the photographs taken of samples that had sublimed over long periods of time in the freeze dryer. It shows sublimation progressing from the edge of the vial towards the central region, top layer towards the base of the vial, as well as the presence of voids in Figure 102(B). Literature has reported atypical heat transfer effects and radiative effects between vials [9, 46, 81] within the freeze dryer, as well as variability in the mass flow rate of the water vapour[112, 203].

Figure 100 and Figure 101 show that the Bragg wavelength did not remain stable throughout the interval when sublimation of water vapour was taking place. Future projects could investigate using other technologies such as TDLAS, to determine if these POFBG sensors are directly detecting changes in mass flow rate or if there are other mechanisms adding to the Bragg wavelength shift.
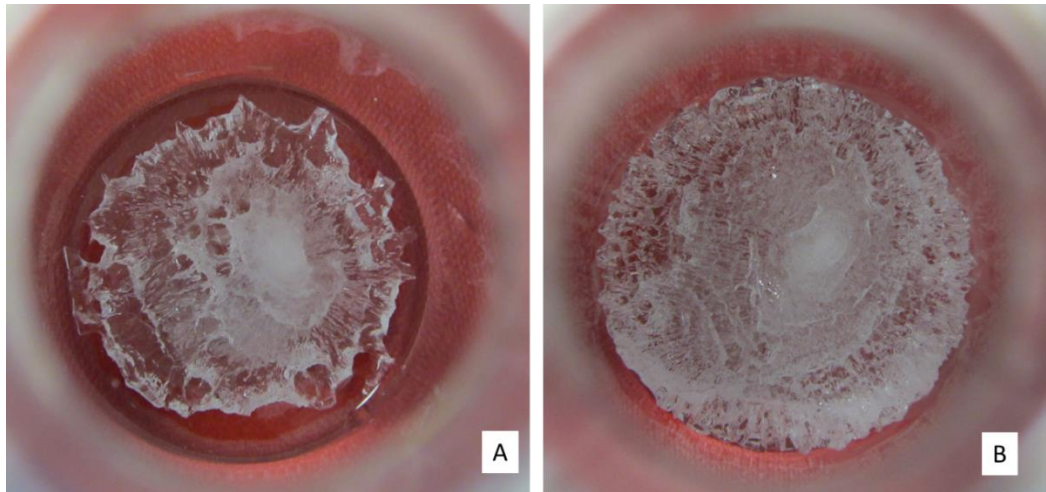
Figure 102 top view photographs looking into the vial at samples of ice, originally 5ml of distilled water frozen to -21ºC, after (A) a sublimation time of 202min at 100μbar, (B) sublimation time of 60min at 200μbar

8.7 POFBGs used to detect sublimation and step changes in pressure

This section compares the response of POFBGs to step changes in pressure carried out in a nitrogen based environment and when water vapour has been introduced into the vacuum chamber. As water has been reported to cause swelling[16, 17] and an increase in the refractive index of PMMA[12], it is anticipated that an increase in the Bragg wavelength would be observed during sublimation, as seen in section 8.6.

The freeze dryer assembly was kept consistent throughout this chapter as has been described in section 8.4. The assembly included the Pirani gauge, POFBGs and dew point sensor, which were used to monitor the gas composition of the chamber for the presence of sublimed water vapour. A K-type thermocouple was placed next to the POFBGs to record the temperature every second during these experiments, detecting temperature drifts due to radiative effects, which were observed in chapter 6.

The POFBGs were positioned on the shelf in the freeze drying chamber as shown in Figure 88 and the IMON512 interrogator was used to monitor the Bragg wavelengths of POF3, POF4 and POF5 (section 5.3) during this experiment.

The POFBGs were dried for more than 25hrs under sub-atmospheric conditions at an inlet shelf temperature of 20°C and the Bragg wavelength was allowed to stabilise (Figure 103) before the step changes in pressure were carried out between 200µbar and 300µbar. Section 8.6.1 describes how water vapour was introduced into the system, by connecting a vial containing a sample of ice to the access port of the freeze dryer (Figure 96).

Figure 103 shows the response of the PMMA POFBG (POF 5) Bragg wavelength to step changes in pressure from 200µbar to 300µbar ("a", "c", "e") and from 300µbar to 200µbar ("b", "d", "f"). These step changes were carried out at 2min intervals in the nitrogen based environment, achieved by having a nitrogen cylinder connected to the freeze dryer inlet. This time interval was chosen to keep the experiment brief in order to reduce the effects of radiative heat transfer from the external environment, which was more noticeable in experiments that took place over several hours (seen in chapter 6). A positive Bragg wavelength shift was observed with increasing pressure, as seen in chapter 7. At this stage a Bragg wavelength shift of 11pm was observed between 200µbar and 300µbar, for a constant temperature in the POFBG region.

The Pirani gauge was programmed to collect in one second intervals a sample and it can be seen from Figure 103 that the device recorded overshoots and undershoots in pressure at points "a", "c" and "e". This shows some limitations in the pressure regulation of the freeze dryer's PID controller, which future projects could address by optimising the performance of the machine for use as a climatic chamber. The POFBG detected the overshoot and undershoot at "e", however as a lower sampling rate was used (1 sample per 15sec) it was not obvious if the overshoot was present in "a" and "c". This sampling rate was determined through experimentation, to be the optimal timeframe for this unit and the software, in order to collect the data required over the long time scales (days). At a higher sampling rate, issues with the data transmission, limitations on the buffer size, file size etc. were observed particularly when collecting the data of 3 POFBGs over these long timeframes. Future projects could investigate different programs and interrogators that could allow the data to be logged over these long timescales (days) at a larger sampling rate.

Point "g" in Figure 103 marks the time that a vial containing no sample was introduced into the system; a pressure spike was observed due to the inrush of air into the chamber, however the dew point remained at -40°C and the temperature remained reasonably stable. The pressure recovered after 2min due to the vacuum pump returning the pressure in the chamber to the set point value of 200μbar. The POFBG Bragg wavelength was also found to have recovered in 6min to the original value at the start of the experiment. This recovery time was also observed in TOPAS and PMMA POFBG (POF3 and POF4), after the fibres were dried for more than 24hrs at 200μbar and 20°C inlet shelf temperature (Figure 106 and Figure 107). This was compared to the recovery time after the fibres were exposed to subliming water vapour in the chamber for 17min ("j" in Figure 104, Figure 105, Figure 106 and Figure 107) and after the valve was closed. The Bragg wavelengths were observed to have recovered to the value at the start of the experiment within 5min (POF3), 24min (POF4) and 27min (POF5). The trends in the times required for the Bragg wavelength to recover were also observed in section 8.6.3. It is hypothesised that the TOPAS POFBG taking the same time to recover after exposure to water and after 24hrs of drying, could be reacting to movement of gas in the chamber or water vapour affecting the surface of the fibre. PMMA POFBGs Bragg wavelengths were shown to take longer to return to the values at the start of the experiment. As PMMA has an affinity for water and was exposed for a long time to water vapour; the material could have adsorbed water into the fibre during sublimation, requiring more time

to dry the polymer in the vacuum chamber. Future work would investigate the mechanisms influencing these fibres and temperature compensation techniques.
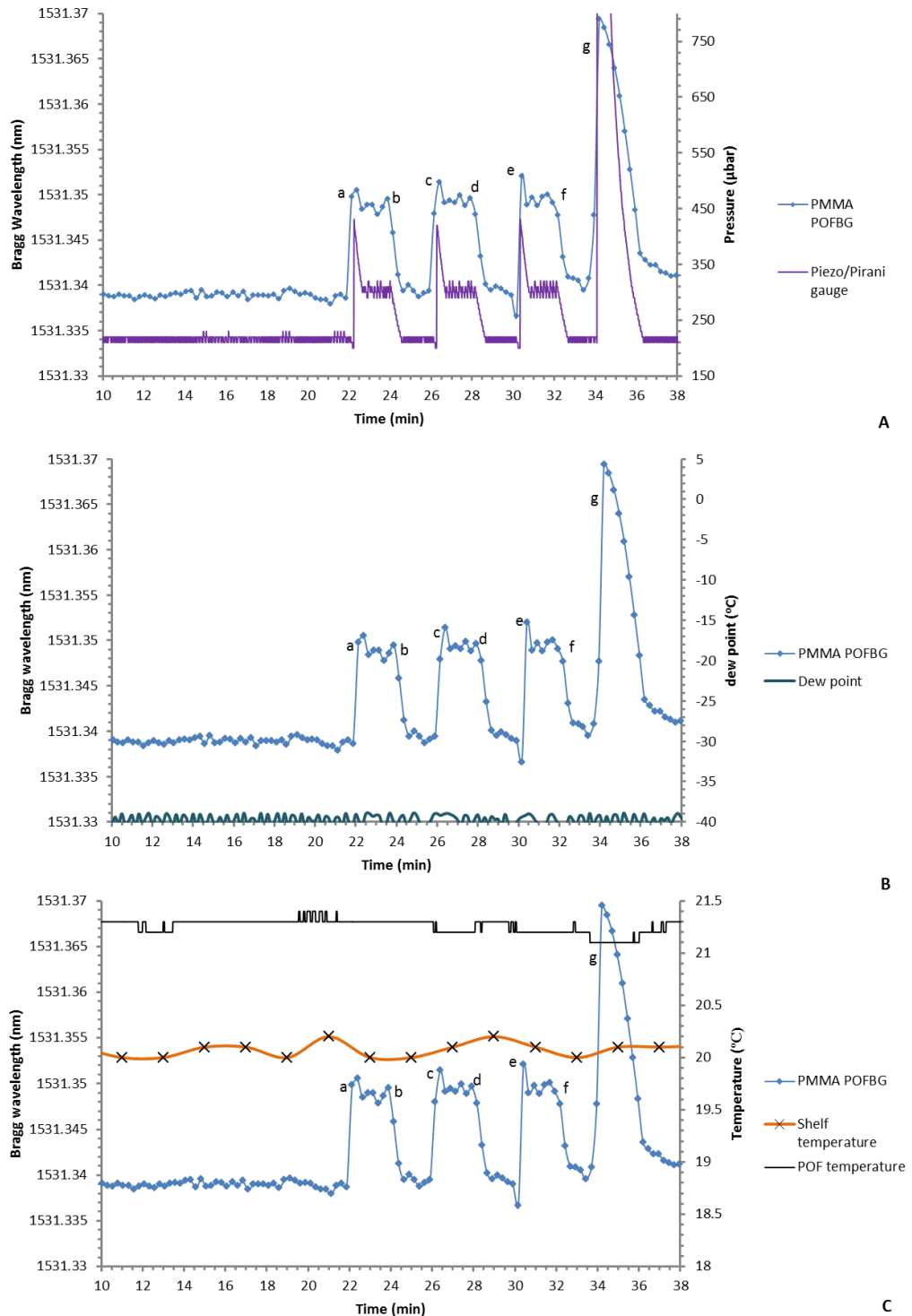
Figure 103 PMMA POFBG (POF5), Bragg wavelength response to changes in (A) pressure (B) dew point, (C) temperature. Step changes in pressure were carried out in a dry nitrogen gas environment under vacuum conditions, from 200μbar to 300μbar ("a", "c" and "e") and from 300μbar to 200μbar ("b", "d" and "f"). Point "g" shows the Bragg response to a vial containing no sample being attached to the access port.

Figure 104 shows the response of PMMA POFBG POF5 to the step changes in pressure between the set points of 200μbar and 300μbar, in a nitrogen based environment ("a", "b", "c"). The trends are the same as observed in Figure 103, with a Bragg wavelength red shift of 9pm occurring for the step change in pressure, at -40°C dew point and a temperature of 21.2°C. This was compared against PMMA POFBG (POF4) in Figure 106 and TOPAS POFBG (POF3) in Figure 107 under the same conditions, and found that the Bragg wavelengths red shifted by 8pm and 26pm respectively. The difference between the response of the TOPAS and PMMA Bragg wavelength, for the same step change in pressure between 200μbar and 300μbar is likely due to the different sensitivities of the polymer. The sensitivities were described in chapter 7 as $2x10^{-4}$ nm/μbar $\pm(0.2x10^{-4})$ for TOPAS POFBG and $7x10^{-5}$ nm/μbar $\pm(0.9x10^{-5})$ for PMMA POFBG. The difference between the sensitivities of the POFBG could be due to a combination of factors, including different types of: materials, properties, thermal treatment process, manufacturing process, dimensions, annealing etc. A control vial (no sample) was attached to the access port of the freeze dryer at points "d" and "e" to observe the behaviour of POFBGs. A pressure spike occurred when the valve was opened as air from the vial rushed into the freeze drying chamber. The Pirani gauge recovered after 3min, as the vacuum pump returned the pressure in the chamber back to the set-point value of 200μbar. The PMMA and TOPAS POFBGs recovered to their original value after ~6min.

At point "f" in Figure 104, Figure 106 and Figure 107, a vial containing 3.192g of ice, was introduced into the system through the access port of the freeze dryer. The sample was prepared the previous day, using distilled water frozen to -21°C. The freeze dryer's inbuilt chamber gauge confirmed that the step changes in pressure were kept between 200μbar and 300μbar in dry nitrogen and during sublimation. The Pirani gauge was used as the reading shifts when the gas composition changes, in this case when water vapour was introduced to the dry nitrogen gas in the chamber.

A pressure spike occurred after the valve was opened, which was detected at "f" by all 3 POFBGs and the Pirani gauge. This was followed by an offset "k" in the Bragg wavelength and Pirani gauge value (Figure 105) due to the PMMA POFBGs affinity for water. The offset remained whilst the valve was opened and the water vapour was allowed to enter into the chamber ("k" to "j"). The offset was found to be 8pm for POF5 (Figure 104) and POF4 (Figure 106) and 11pm for TOPAS POFBG (Figure 107). This response was compared against the Pirani

gauge, which showed that an offset of 30µbar occurred between "k" to "j", due to the introduced water vapour.

The regions marked "g", "h" and "i" indicate step changes in pressure from 200µbar to 300µbar at the same time as subliming water vapour into the freeze drying chamber. The step change in pressure produced a 9pm red shift in the Bragg wavelength for POF5 (Figure 104), 8pm red shift for POF4 (Figure 106) and 19pm for TOPAS POFBG (Figure 107).

This result indicates that water vapour from sublimation causes an offset in the PMMA Bragg wavelength, however it does not influence the POFBGs sensitivity (8-9pm/100µbar) to the step change in pressure.

This was compared against TOPAS POFBG, which showed an offset in the Bragg wavelength of 11pm and that the sensitivity to the step change in pressure decreased from 26pm/100µbar(nitrogen) to 19pm/100µbar in the presence of water vapour for the 3 repeats. This would require further investigation to determine if the sensitivities of POFBGs to pressure are influenced by water vapour. This would allow other potential applications for these devices as sensors to detect water vapour or as pressure sensors in different gas compositions. Future projects would also need to examine temperature compensation techniques and improving the pressure regulation of the freeze dryer.

At "j" the valve was closed, the sample removed and weighed (2.683g). The Pirani gauge value recovered after the vial was removed, as water vapour was no longer detectable in the chamber, the same pattern was observed for the TOPAS POFBG (Figure 107). The PMMA POFBGs recovered 20min after the vial was removed from the access port, this would require further investigation to determine if water is being removed from the POF or if the sensors are still detecting the presence of trace water vapour in the chamber. The behaviour of the TOPAS POFBG would need to be investigated in future projects, as a greater shift was observed, despite the polymer being described in the literature as humidity insensitive[18, 162].
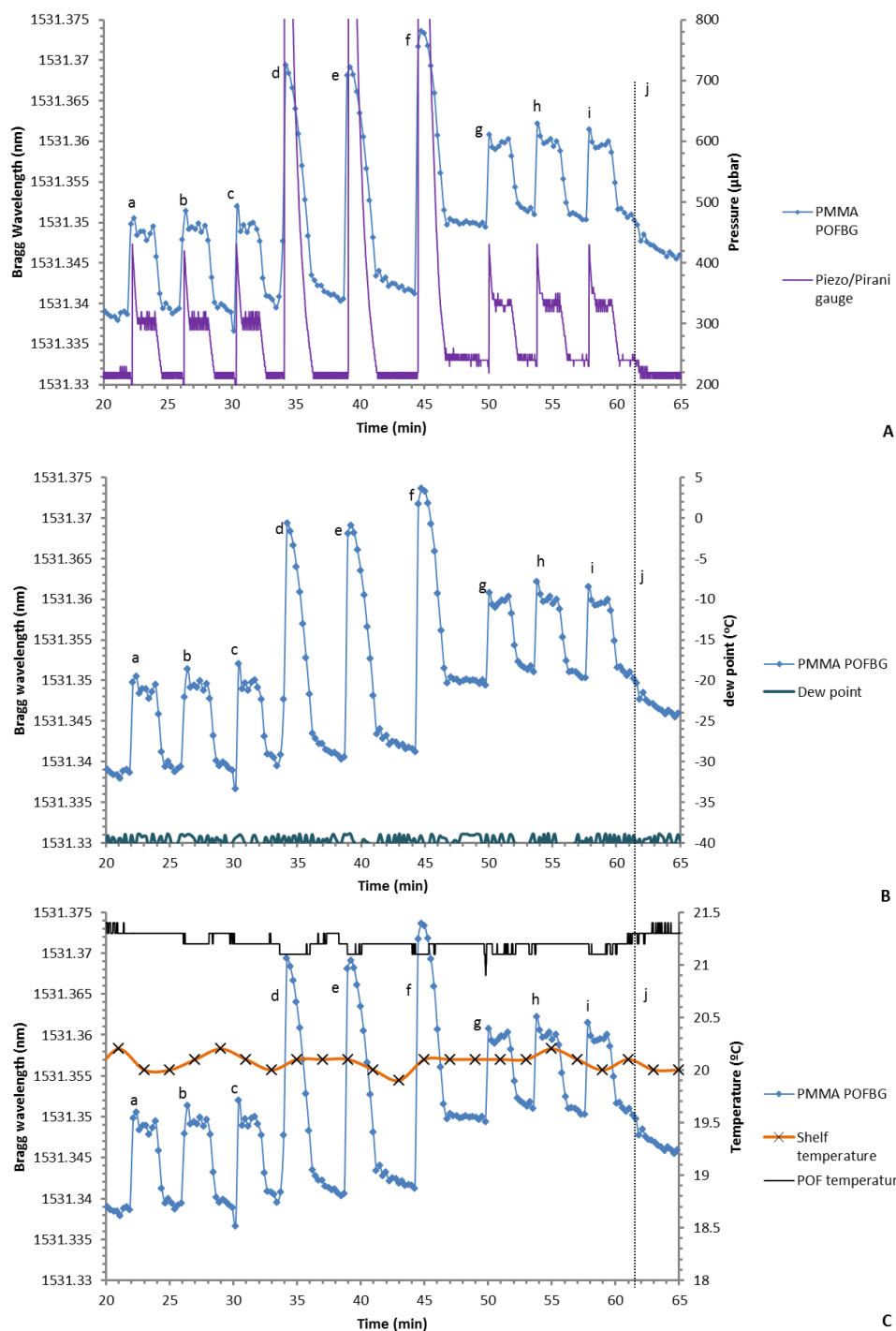
Figure 104 Bragg wavelength response of PMMA (POF5) POFBG to (A) pressure, (B) dew point and (C) temperature. Step changes in pressure in a nitrogen based environment at points "a", "b", "c". Vials containing air were introduced to the access port at points "d" and "e". The vial containing 3.192g of distilled water frozen to -21ºC, was introduced to the access port at point "f". Step changes in pressure were repeated at "g", "h" and "i" during sublimation. Vial was removed at "j" to be weighed (2.683g).
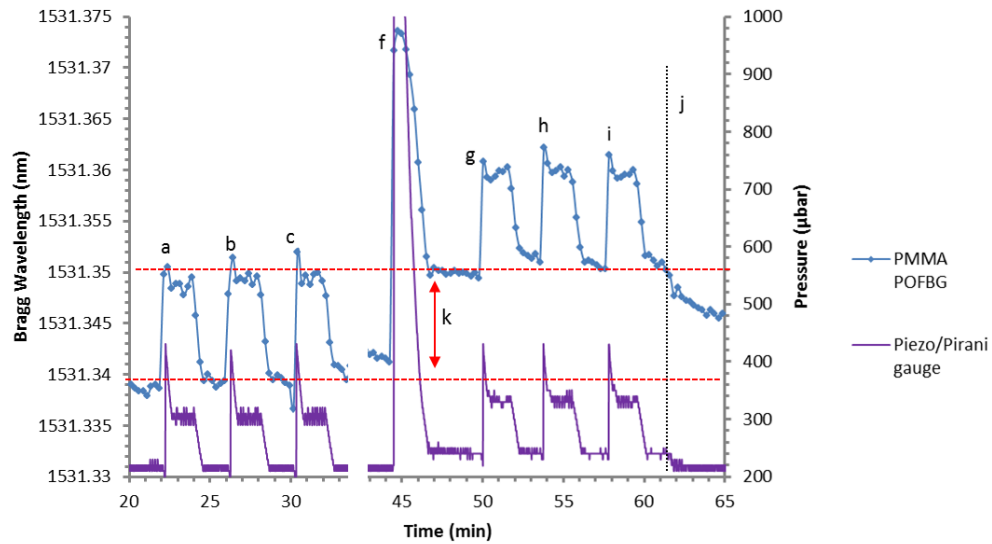
Figure 105 Bragg wavelength response of PMMA (POF5) POFBG to pressure. Step changes in pressure in a nitrogen based environment at points "a", "b", "c". The chamber gauge confirmed step changes in pressure between 200µbar to 300µbar were maintained at "a", "b", "c" and "g", "h" and "i". The vial containing 3.192g of distilled water frozen to -21°C, was introduced to the access port at point "f". A shift in the Bragg wavelength due to sublimation was observed at "k", at the same time as a shift in Pirani gauge reading (30µbar). Vial was removed at "j" to be weighed (2.683g).
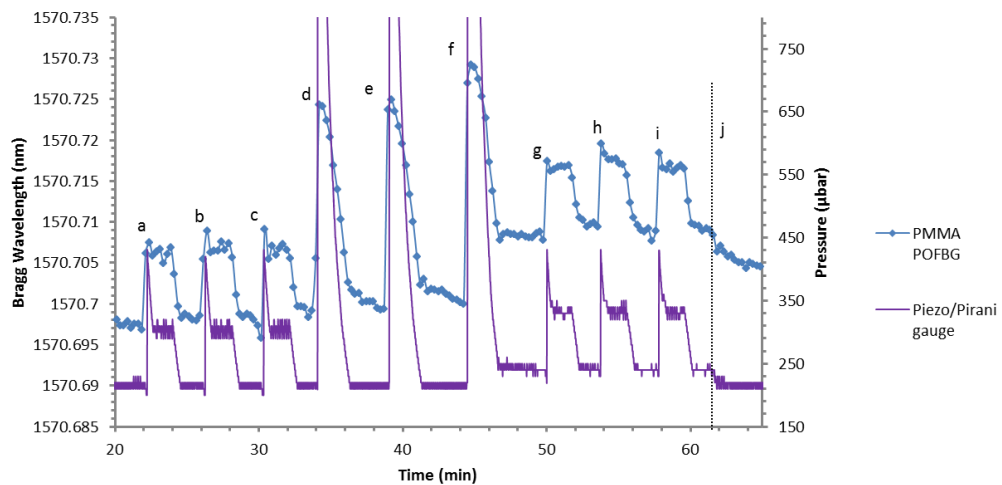
Figure 106 Bragg wavelength response of PMMA (POF4) POFBG to pressure in a vacuum chamber. Step changes in pressure in a nitrogen based environment at points "a", "b", "c". Vials containing air were introduced to the access port at points "d" and "e". The vial containing 3.192g of distilled water frozen to -21°C, was introduced to the access port at point "f". Step changes in pressure were repeated at "g", "h" and "i" during sublimation. Vial was removed at "j" to be weighed (2.683g).
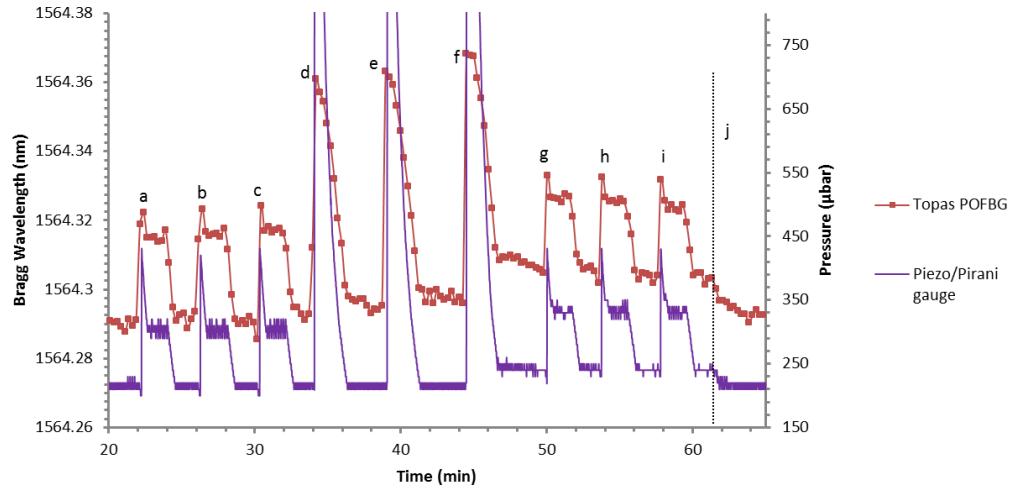
Figure 107 Bragg wavelength response of TOPAS (POF3) POFBG to pressure in a vacuum chamber. Step changes in pressure in a nitrogen based environment at points "a", "b", "c". Vials containing air were introduced to the access port at points "d" and "e". The vial containing 3.192g of distilled water frozen to -21°C, was introduced to the access port at point "f". Step changes in pressure were repeated at "g", "h" and "i" during sublimation. Vial was removed at "j" to be weighed (2.683g).

To determine if the PMMA and TOPAS POFBGs' Bragg wavelength shifts in sections 8.6 and 8.7 are specific to subliming water vapour, an additional experiment was carried out to test if another gas (CO_2) introduced into the chamber can influence the FBG. Quantities of dry ice (0.4g to 1.2g CO_2 pellets) were put into the vial and attached to the access port before opening the valve. A large pressure rise in the chamber occurred that the vacuum pump could not return to 200µbar, as well as changes in the temperature were observed. To try and reduce the CO_2 sublimation rate, the vial was placed in a container with dry ice and the valve of the access port was used to manually throttle the gas into the chamber. Unfortunately it was not possible to control the gas flow into the chamber using this assembly and the chamber pressure could not be returned to the set point value of 200µbar with the assistance of the vacuum pump.

Future work would involve connecting a pressure regulated CO_2 cylinder and the existing nitrogen cylinder, to the gas inlet port of the freeze dryer which is controlled by the solenoid valve and PLC (Figure 84). This assembly would be used in conjunction with temperature compensation techniques, to account for changes in temperature experienced in the chamber. These modifications would allow the gas composition in the chamber to be varied, to observe if other gasses can influence the Bragg wavelength or if the shifts observed in this chapter are specific to subliming water vapour.

8.8 Decreasing the response time of PMMA POFBG by etching the fibre diameter

A PMMA POFBG (POF6) was placed in the Sanyo climatic chamber (at 1atm pressure) as described in section 5.4, to study the effects of varying the size of the POF outer diameter on the response time of the POFBG to changes in temperature and relative humidity. This study used acetone to etch the polymer and reduce the size of the outer diameter. Research into this area is driven by the motivation to improve the response time of these sensors as reaction times are currently in the region of tens of minutes[12] which are too long for most applications. Improving the response time would be beneficial for some industries that require more rapid information on changes in humidity e.g. for the food industry, pharmaceutical industry, agriculture, chemical processing, storage applications, paper manufacturing etc.

The Bragg wavelength and response time of the POFBG to changes in water content is influenced by the fibre geometry and diffusion coefficient[239]. Research has found that some polymers including PMMA, experience different diffusion coefficients for sorption and desorption[17, 153]. Rajan et al reported the water sorption coefficient of PMMA at atmospheric conditions to be 6.4×10^{-9} cm^2/s and desorption coefficient as 9×10^{-9} cm^2/s[17, 239].

Literature also suggests that depending on the manufacturing process and thermal history of the POF, it is possible to obtain different response times for optical fibres which have the same diameter. Literature reported a response time of 30min[12, 15] for a PMMA POFBG with an outer diameter of 195μm[195, 228], tested in a climatic chamber at 22°C when carrying out a step change in humidity from 45%RH to 52%RH[228]. A response time of 1hr was reported for a diameter of 125μm[195], whilst 51min and 31min were observed for two POFs that each had an outer diameter of 190 μm[195].

Etching is a technique used to improve the response times of these POFBGs to humidity in environmental chambers, literature reports that acetone has been used to remove material from PMMA based POFs. In one journal, the diameter of a PMMA POF was etched from 190μm to 135μm and caused a reduction in the response time from 31min to 12min[195]. Another study claims that a response time of 4.5sec[195, 239] was achieved for a step change from 90%RH to 60%RH, after the POFBG (~240–260μm outer diameter with a 12μm core) was etched with a 1:1 ratio of methanol to acetone to achieve an outer diameter of 25μm.

Another method reported by Zhang and Webb [14] was to pre-strain PMMA based POFBG in a climatic chamber, to observe the response times of the FBG whilst carrying out a step change of 10%RH. The chamber temperatures were set to 25°C, 35°C and 50°C during the step change in humidity, and obtained response times of 19min, 13min and 11min respectively.

8.8.1   Method

The Sanyo Gallenkamp climatic chamber was used in this project to control the ambient relative humidity and temperature surrounding the PMMA POFBG. The relative humidity is the ratio between the actual vapour pressure and the saturation pressure of water vapour for a given temperature[102].The saturation vapour pressure of water is known to increase exponentially with temperature[102].

The PMMA POFBG (POF 6) detailed in section 5.4.1, had an FBG inscribed using the detailed method in section 5.2.2 and was UV glued to a silica pigtail using the documented method in section 5.2.4.

The PMMA POFBG has a Bragg wavelength in the 1570nm region and Figure 108 shows the schematic representation of the location of the PMMA POFBG, placed within a housing structure to protect the UV glued joint from air currents within the chamber.
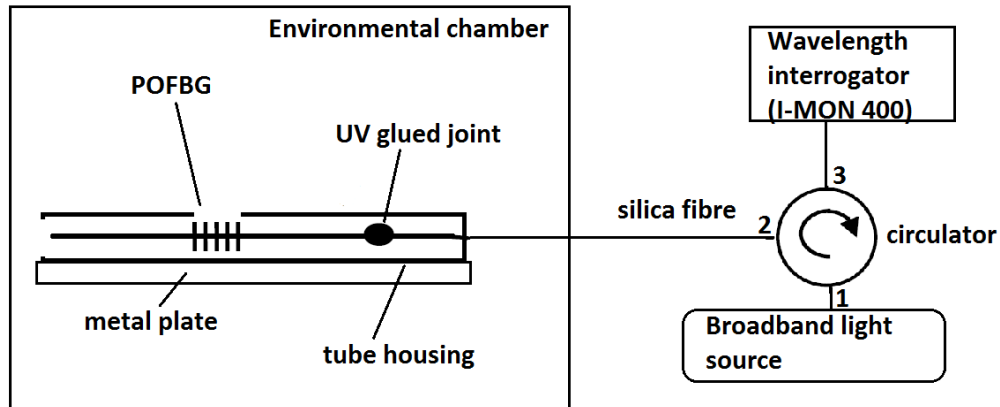
Figure 108 Schematic diagram of the Sanyo Gallenkamp environmental chamber and the sensor which has been fed through the access port.[240]

The response time was calculated according to section 5.6 as the time for the relative wavelength change to reach 90%. In this study, a Thorlabs ASE730 broadband light-source and an IBSEN I-MON 400 system were used to interrogate the POFBG.

The Programmable Logic Controller (PLC) was programmed to maintain a constant temperature in the environmental chamber at atmospheric pressure, whilst the relative humidity (%RH) was varied from 40%RH to 90%RH in steps of 10%RH. The PLC was additionally programmed to record the data from the inbuilt chamber sensors during the course of the cycle as seen in Figure 109. Figure 109 shows that the chamber temperature remained at 24°C during the experiment and the relative humidity was initially maintained at 40%RH for 2hrs to provide sufficient time for the POFBG to stabilise. Subsequently step changes in humidity of 10%RH were carried out and the conditions maintained for 1.5hrs before the process was repeated up to 80%RH. This cycle was programmed to reach 80%RH, as the manufacturer's guide specified that this was the maximum achievable %RH for the requested chamber temperature.

The graph shows a red shift in the Bragg wavelength in response to an increase the humidity of the chamber which is consistent with literature[14, 15, 153].

The fibre initially had a diameter of 120µm before it was etched with acetone for 1min; the diameter was measured using a microscope (section 5.2.1.2) and the POFBG was then placed in the environmental chamber. The fibre was subsequently etched for 30sec before carrying out the next experiment. This process was repeated until a diameter of 96µm was achieved and shown in Table 8-A.
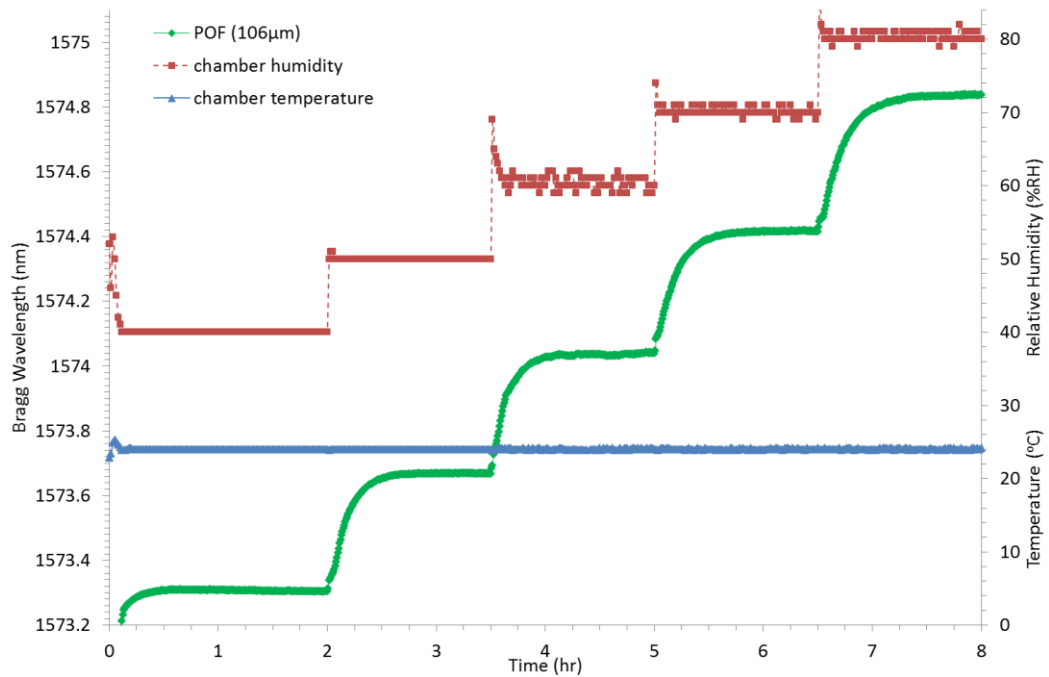
Figure 109 Performance of a PMMA POFBG with a diameter of 106µm for the range 40%RH and 80%RH and at a temperature set point of 24°C.

Table 8-A documents how the reduction in the diameter of the POFBG, influences the response times of the Bragg wavelength to the step changes in relative humidity at 24°C. The table shows a characteristic trend that etching the diameter of this PMMA POFBG, reduces the response time by more than 8min for each 10%RH step change in humidity.

Diameter (µm)	Cumulative etching time (min)	Response time (min)			
		50%RH	60%RH	70%RH	80%RH
120	1.0	30.0	28.8	36.0	38.0
110	1.5	25.5	26.0	28.8	28.0
106	2.0	24.0	21.5	26.0	32.0
101	2.5	19.0	15.0	20.5	29.5
96	3.0	19.0	15.0	20.5	29.5
Maximum improvement in response time (min)		11.0	13.8	15.5	8.5
% improvement in response time		36.7	47.9	43.1	22.3

Table 8-A response times of etched POF for step changes in relative humidity at 24°C[240]

Figure 110 suggests a positive correlation between the fibre diameter and the response time of the POFBG after etching, as generally seen in literature. The graph may suggest that the response time is faster at lower relative humidity values for the same diameter, not previously reported in literature, however this would need to be confirmed in future projects. Future work could also investigate the use of etching POF for applications in freeze drying technology, to observe if the response time to e.g. end of primary drying time detection could be improved.
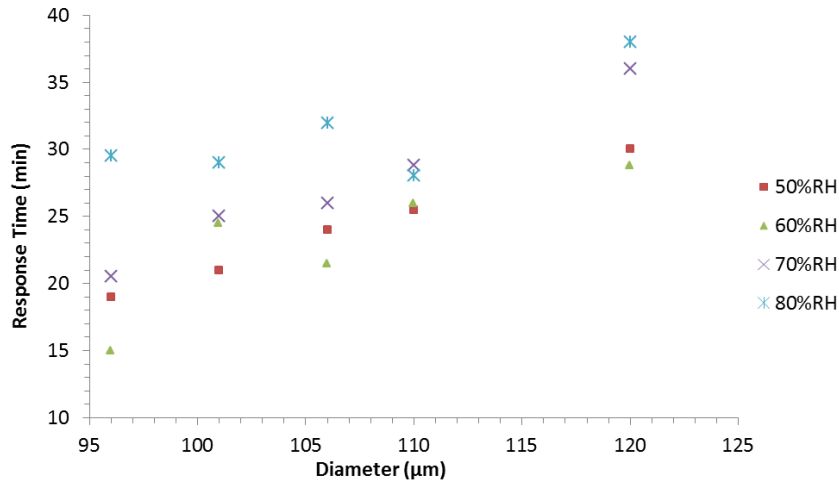
Figure 110 Graph showing the effect of diameter on the response time, where the chamber temperature was set to 24ºC and the relative humidity varied from 40%RH to 80%RH[240]

Figure 111 shows the effect of temperature on the response time of a 96 µm diameter POF to step changes in relative humidity. This fibre had been etched for a total time of 2.5min using acetone. This experiment shows a strong correlation between the temperature and response time of this POFBG. For the given range, increasing the temperature decreases the response time of the sensor. This observation has been seen in literature, and indicated that equilibrium of water in the fibre is achieved faster at higher temperatures[14].
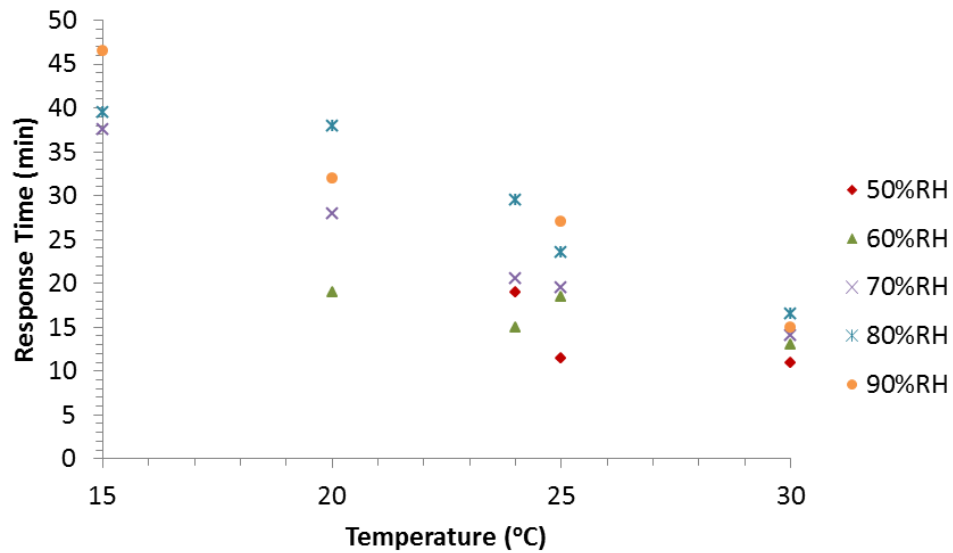
Figure 111 Effect of temperature on the response time of a 96µm POFBG when exposed to step changes in relative humidity from 40%RH to 90%RH.[240]

8.9   Summary and Discussion

This chapter investigated the response of PMMA and TOPAS POFBGs to changes in the water vapour and gas composition in the freeze drying chamber, both at atmospheric and sub-atmospheric conditions. The POFBGs were dried and degassed under sub-atmospheric conditions for more than 24hrs, to ensure dry experimental conditions before water vapour was introduced into the chamber. To this author's knowledge, there are currently no reported publications that discuss the behaviour of POFBGs in freeze dryers or vacuum chambers. This chapter describes the characterisation protocols applied to these sensors in the freeze dryer to determine if they are a viable technology for the detection of sublimation and the end of primary drying.

8.9.1   Water detection in the freeze dryer at atmospheric pressure after backfilling with nitrogen gas

Experiments were carried out to investigate the Bragg wavelength response to a step change in pressure from 2500µbar to 1atm pressure in a dry nitrogen atmosphere (-40°C dew point). Once the backfill stage to 1atm pressure was completed and the gas approached equilibrium, the door was opened to allow water vapour to enter the chamber.

1. Results supporting literature

The results showed red shifts in the Bragg wavelengths of PMMA and TOPAS POFBGs as the chamber pressure increased, which is supported by literature[13, 143, 224] and chapter 7 of this thesis.

2. Results indicating novelty

The work shows novelty as POFBGs were exposed to dry sub-atmospheric conditions and monitored in this region, which has not been reported previously. When water vapour (from the air) entered the dry nitrogen atmosphere (at 1atm pressure), PMMA POFBGs showed significant positive Bragg wavelength shifts greater than 0.79nm. The shifts due to water vapour introduction were several orders of magnitude larger than the shifts (<91pm) as a result of pressure changes from 2500µbar to 1atm in a nitrogen atmosphere, due to PMMA having a documented affinity for water. The results support the observations in literature that water vapour significantly affects the Bragg wavelength of PMMA POFBGs [12, 14, 16, 17], due to a change in the refractive index and swelling of the fibre and shows that this property can be exploited to produce a sensor for low pressure applications.

3. Results requiring further investigations

There were indications in this work to support the observations of POF non-linear sensitivity to sub-atmospheric pressure as seen previously in chapter 7; however shifts in temperature and rapid gas flow were also observed. As discussed in chapter 7, a non-linearity in PMMA and TOPAS POFBG sensitivity with respect to pressure has not previously been observed in literature and would require further investigation. Future work would involve temperature compensation techniques to obtain the Bragg wavelength response due to pressure alone. Shifts in the Bragg wavelength of TOPAS POFBG were also observed when water vapour was introduced into the chamber at 1atm (and sublimation in section 8.6 and 8.7). Future work would involve experiments to determine if other factors such as vapour flow, changes in temperature or water influencing the surface of the polymer are occurring, particularly as TOPAS has been reported to be humidity insensitive[18, 162].

8.9.2 POFBGs used to detect sublimation in a freeze dryer

Experiments involving introducing water vapour through the access port of the freeze dryer at 200μbar were carried out in this chapter. The POFBGs were dried and degassed for a minimum of 24hrs at 200μbar and an inlet shelf temperature of 20°C, prior to starting the experiments.

1. Results which contributed to novelty

The results reveal that PMMA and TOPAS POFBGs initially show a spike in the Bragg wavelength, as air from the vial enters the freeze dryer and increases the pressure in the chamber. The vacuum pump returns the pressure to the set point value of 200μbar after 3min; however an offset in the Bragg wavelength (red shift) and the value indicated by the Pirani gauge remained. This is due to sublimation changing the gas composition in the chamber from nitrogen to water vapour, which can be detected by Pirani gauges in freeze dryers[8, 19, 53]. When the sample of ice or frozen mannitol was removed from the access port, the gas composition returned to a nitrogen gas atmosphere (end of primary drying) and the Pirani gauge and Bragg wavelength were found to have recovered to their original value.

2. Further investigations

The results showed that the Bragg wavelength did not remain stable throughout sublimation; this would require further investigation to determine if water vapour

mass flow rate or other parameters are influencing the FBGs. Literature has reported atypical heat transfer effects and radiative effects between vials [9, 46, 81] within the freeze dryer, as well as variability in the mass flow rate of the sublimed water vapour[112, 203].

8.9.3   POFBGs used to detect sublimation and step changes in pressure

Additional experiments were carried out involving step changes in pressure between 200µbar and 300µbar both in a nitrogen gas atmosphere and during the introduction of water vapour from the access port.

1. Results which contributed to novelty and require further investigation

The results reveal an offset in the Bragg wavelength (red shift) of the PMMA and TOPAS POFBGs when water vapour was introduced to the vacuum chamber. There were also indications that the sensitivity (pm/100µbar) of the PMMA POFBGs Bragg wavelength to this step change in pressure did not change when water vapour was added to the gas composition (nitrogen in the chamber). This would indicate that water vapour from sublimation causes a red shift and offset in the Bragg wavelength however does not influence its sensitivity (pm/100µbar) to the step change in pressure. This was compared against TOPAS POFBG, which showed that the sensitivity to the step change in pressure decreased in the presence of water vapour. This would require further investigation to determine the extent that water vapour influences the sensitivities of POFBGs to pressure, by the use of temperature compensation techniques and improving the pressure regulation of the freeze dryer.

8.9.4   Decreasing the response time of PMMA POFBG by etching the fibre diameter

The last section of this chapter described the effects of etching the outer diameter of the fibre on the response time of a PMMA POFBG to humidity and temperature changes at 1atm.

1. Results supporting literature

The results support literature [195, 228], where reducing the fibre diameter reduced the response time of the FBG to changes in relative humidity in the surrounding environment. The POFBG was also observed to have significantly reduced response times at higher temperatures but higher response times at lower temperatures which might limit applications of these devices.

2. Further investigations

The data indicates that the response time was faster at lower relative humidity values for the same diameter, not previously reported in the literature. This would need to be investigated in future projects and the application of etching POF on the response time of POFBGs in freeze drying applications.

8.10 Future Work

PMMA POFBGs should be used to monitor sublimation from different formulations attached to the access port or placed onto the shelf in the freeze dryer. The freeze drying cycles would be optimised for each formulation, requiring a specific range of pressures and temperatures to maintain product quality. The Bragg wavelength of POFBGs would be monitored during these cycles, to confirm that sublimation and end of primary drying is being correctly identified. As formulations contain many different constituents, future projects would test whether any of these components cause damage to the POFBGs during freeze drying. An example is acetone, which is known in literature to cause damage to acrylic[241], and is part of an organic solvents group that are used occasionally in formulations to increase the sublimation rate, improve stability and decrease reconstitution time[30]. Depending on the outcomes of these experiments and the cost of manufacturing the sensors, different POF materials could be used to determine the optimum material to monitor sublimation of these specific formulations or if applicable, the PMMA POFBG sensor could be replaced after each cycle.

Other POF materials such as polycarbonate (PC)[242], polystyrene (PS), mPOF[243] should be placed in the freeze dryer to test their ability to detect sublimation and determine if they can achieve a greater sensitivity than PMMA. Investigations should determine how changes in the polymer composition, structure (step index vs microstructured), thermal treatment and manufacturing process of the POF influences the sensitivity of the sensors to pressure, temperature and sublimation.

As the target market of the sensor is the pharmaceutical industry, future work would require exposing POFBGs to different sterilisation methods e.g. gamma radiation[244] and eventually testing them in full scale production model freeze dryers.

Whilst carrying out the backfill procedure and the sublimation experiments in this chapter, TOPAS POFBGs were observed to exhibit a red shift when water vapour was introduced into the chamber in dry sub-atmospheric and atmospheric conditions. The mechanism that causes this Bragg wavelength shift would require further investigation, particularly as literature refers to this polymer as being as humidity insensitive[18, 162].

PMMA POFBGs were observed to show varying Bragg wavelength during sublimation, potentially indicating the detection of varying sublimation rate or shifts in temperature. This would require implementation of temperature compensation techniques and verification against other established technologies that monitor mass flow rate, such as TDLAS, MTM and freeze drying mass balance.

The dew point sensor did not register a change in the dew point during sublimation, likely as based on reports in literature [8, 57] the dew point in the chamber is significantly lower than -40°C, the limit of its range. Future projects would involve using a -60°C dew point sensor or chilled mirror, to accurately track the changes in the gas composition in the chamber during sublimation.

Once the vials containing subliming samples were removed from the access port of the freeze dryer, the Bragg wavelength of the PMMA POFBGs took up to 20min to return to the initial wavelength value. This would require further investigation to determine if the delay in the shift of the Bragg wavelength is due to detection of residual water vapour in the chamber, temperature drifts or desorption of water from the fibre.

Changes in the length along central axis of the fibres within the chamber could be investigated, using interrogators that are capable of measuring the reflection time and more importantly detect changes between the reflection return times at different Bragg wavelengths from multiple FBGs on the fibre. Additional experiments should measure changes in polarisation, from torsion or motion of the fibres in the freeze dryer, to provide additional information on how sublimation is influencing the POF.

Modelling of the sorption and desorption of water into the fibre should be investigated, particularly as this chapter shows an initial very rapid Bragg wavelength response to changes in water vapour concentration at dry atmospheric and sub-atmospheric conditions.

Radiative effects and heat transfer from the shelf are influential factors in freeze drying and could influence the Bragg wavelength whilst monitoring sublimation. Future work would investigate different temperature compensation techniques,

such as multiple FBGs on the same fibre to compensate for the effects of temperature, in order to return the correct Bragg wavelength shift as a result of sublimation alone.

Finally, future projects would examine using FBGs that operate in the 800nm spectral region (8dB/m at 830nm)[143], as this region has significantly lower attenuation than the 1550nm region(50dB/m at 1530nm) [178, 183].

8.11 Conclusion

All aims and objectives stated at the start of this chapter have been achieved, including:

- Observe the effects on PMMA and TOPAS POFBGs after backfilling the chamber from sub-atmospheric conditions (2500µbar) to 1atm pressure with dry nitrogen gas.
- Investigate the response of POFBGs to water vapour entering the freeze drying chamber, which contains dry nitrogen gas at 1atm pressure.
- Determine that POFBGs could be used to detect sublimation under sub-atmospheric conditions (using frozen mannitol and water samples).
- Investigate the effects of etching the fibre diameter on reducing the response time to changes in humidity and temperature

The response of PMMA and TOPAS POFBGs to changes in the gas composition in the freeze drying chamber through the introduction of water vapour, both at atmospheric and sub-atmospheric conditions has been determined. Many experiments were carried out to characterise different POFBG sensors and have shown that they can be used to accurately monitor sublimation during freeze drying and determine the end of primary drying for their target market within the pharmaceutical industry.

Currently no reported publications have discussed the behaviour of POFBGs in freeze dryers and this chapter describes in great detail their response to water vapour in the chamber.

The PMMA and TOPAS POFBGs were shown to red shift in response to an increase in pressure and humidity at atmospheric pressure when the door was opened. This shows an additional potential application for detecting leaks in the system or providing information on humidity transfer throughout the dry nitrogen environment.

The POFBGs showed a red shift in the Bragg wavelength when subliming water vapour was introduced through the access port into the system, i.e. a dry

nitrogen atmosphere. A shift in the reading of the Pirani gauge was also observed, a device documented in literature as being used in industry to monitor and detect the end of primary drying of frozen samples. These characterisation results have shown the potential for POFBG sensors to be trialled for freeze drying applications and this thesis will report on the utilisation of these devices in a practical demonstration by monitoring the freeze drying of mannitol and native collagen in the next chapter.

9.1   Overview

This chapter will discuss the detection of the end of primary drying of mannitol and collagen samples using step index TOPAS and PMMA POFBGs. The goal is to investigate the use of POFBG sensors as a novel alternative approach to established technologies for detecting sublimation in freeze drying applications. This chapter builds on the characterisation results of these sensors from the previous three chapters, to track temperature, pressure and sublimation performance in the freeze dryer.

The first area of discussion will be the monitoring of primary drying by both the Pirani gauge and POFBGs sensors of mannitol solutions, a commonly used bulking agent in formulations in the pharmaceutical industry.

The chapter will conclude with a "real life trial": the freeze drying of collagen samples to form scaffolds for tissue engineering applications, whilst using POFBGs to determine the end of primary drying time and comparing their performance to established technologies.

9.2   Aim

This chapter will document the use of POFBGs inscribed in SM PMMA and MM TOPAS fibres (section 5.3) to detect sublimation of water vapour from native collagen and mannitol under vacuum conditions.

As previously discussed the goal of this project was to determine if POFBG technology could be used in the pharmaceutical industry to detect sublimation in a freeze dryer, which was shown in the previous chapter to be highly likely. In this chapter the sensors will be first used to monitor freeze drying of a standard formulation excipient (mannitol) and thereafter a biological sample (collagen). Mannitol was chosen as it is commonly used as a bulking agent in freeze drying, it provides structural support for elegant cake structures, particularly if micro collapse of an amorphous phase occurs[65]. It also has a high eutectic temperature of -1.5°C to allow both conventional and aggressive high temperature cycles to be carried out[65].

As literature reports that terminating primary drying time early can affect product quality[19, 233], the POFBGs will be tested to determine if they can consistently

detect the end of primary drying time of these samples. This research will provide an insight into the potential application of these sensors in the pharmaceutical and biomedical industries.

As the longest and most costly stage in the freeze drying process, the optimisation of the primary drying stage to increase productivity has been extensively researched. There are several commercially available single-vial and batch measurement sensors (e.g. thermocouples, TDLAS), sold to monitor sublimation during a manufacturing process.

This experiment will use and compare the performance of PMMA POFBGs (due to their affinity for water vapour) and a TOPAS POFBG (which is humidity insensitive[12]) to detect sublimation. It is expected that PMMA POFBGs will show a significant Bragg wavelength shift in the presence of water vapour, whereas the TOPAS POFBGs would show limited shifts and react mainly to changes in the ambient temperature.

The pressure and temperature sensitivities of the POFBGs, determined in the previous chapters, will be used where necessary to identify temperature effects caused by heat transfer issues or changes in pressure.

The objectives of this chapter are:
- Determine whether changes in the Bragg wavelength of PMMA and TOPAS POFBGs occur during primary drying of 3 mannitol samples (5ml each).
- Determine whether changes in the Bragg wavelength profile are observed when comparing mannitol and water samples, i.e. increased resistance (see section 9.4) to sublimation influencing drying behaviour[8, 57, 245]
- Determine if POFBGs could monitor sublimation of water vapour from native collagen and whether the end of primary drying could be detected. Samples of native collagen kindly provided by Mr Haris Choudhery were prepared, frozen and freeze dried. The motivation behind the selection of collagen is its implementation in tissue engineering as scaffolds for e.g. tissue/bone regeneration. This procedure was investigated in section 9.5.
- Determine whether the POFBGs can detect the end of primary drying in a highly challenging low flow rate experiment i.e. 2 ml of collagen sample using a low temperature freeze drying cycle.

9.3   Method

The protocols described in sections 5.7 and 5.7.1 were used to investigate the effect of water vapour on PMMA and TOPAS POFBGs (section 5.3). The aim of this chapter was to determine if POFBGs could be used to detect water vapour subliming from frozen samples of a formulation excipient (mannitol) and a biological sample (native collagen) during freeze drying.

Several sensors were attached to the freeze drying unit in Figure 112 according to the specifications in section 5.7, to monitor dew point (SF52), pressure (TM101) and temperature. The dew point sensor and Pirani gauge are instruments that can detect changes in the gas composition of the chamber [8, 53, 77]. A thermocouple will be inserted into each of the mannitol solutions, to track the processes of freezing, solidification, as well as detect the end of primary drying, which is determined by that technology as when the sample temperature rises towards the shelf temperature (section 3.4). The POFBGs will be baselined against these three different types of sensors, as they are established technologies and commonly used to monitor sublimation in a freeze dryer [8, 53, 77].

A customised feedthrough connector (section 5.7.1), was used to pass the K-type thermocouple into the vacuum chamber as seen in Figure 112, it was connected to a TM-947SD data logger that recorded the temperature in the immediate region of the POFs.
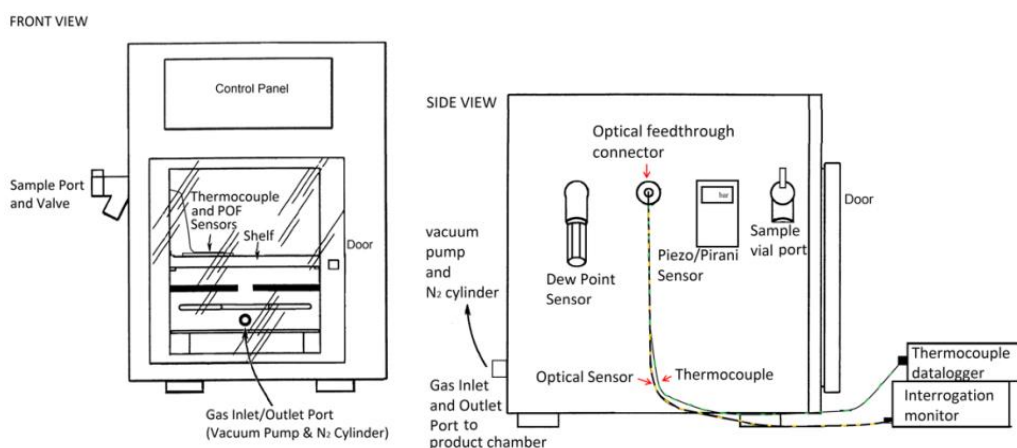
Figure 112 Assembly of the sensors in the freeze dryer to monitor water vapour inside the chamber

The TOPAS and PMMA POFBGs were placed into a protective housing structure and onto the temperature regulated shelf (Figure 112 and Figure 113). Figure 113 shows the arrangement of the FBGs "POF4" and "POF5" (section 5.3), which

were inscribed in the PMMA POF. These POFBGs were separated by 1cm and were manufactured according to the protocols described in section 5.2.

The POFBGs were coupled to a 2x2 1550nm Corning single mode (SM) 50:50 silica coupler (9/125μm), which was connected to a FC/APC silica optical cable. Figure 113 shows that the FC/APC silica optical cable was fed through the vacuum chamber wall using a custom built feedthrough and connected to the interrogator (section 5.7.1). The I-MON 512 USB evaluation software v1.1 was used to analyse the FBG spectrum and calculate the Bragg wavelength using a peak tracking algorithms at a sampling rate of 1 sample per 15sec.

Different freeze drying cycles were used for mannitol and collagen to achieve the objectives described in the aim; the cycles will be described accordingly in each subsection.
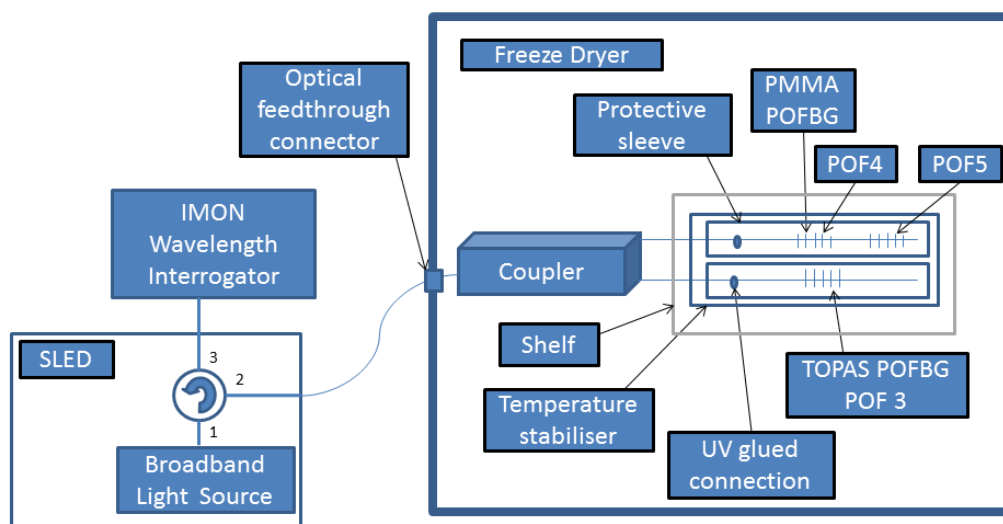
Figure 113 schematic diagram of the POFBG assembly used in this chapter.

9.4 Freeze drying of mannitol solutions

9.4.1 Method

Three samples of 10%w/v D-mannitol (5ml volume, fill depth 0.4mm) were prepared according to section 5.7.6 to be freeze dried in the Virtis Advantage 2.0 (Figure 114).

This excipient was chosen as it is a commonly used bulking agent in pharmaceutical formulations[19, 24, 51, 246] and its performance in the freeze drying environment is well documented[65, 245-248]. It has also been used to baseline and compare the performance of different end of primary drying technologies[8, 57, 249].

Figure 114 POFBG sensor positioned on the shelf next to 3 vials containing 5ml 10%w/v mannitol. K-type thermocouples were inserted into the centre of the vial to monitor product temperature during freeze drying

The samples were placed onto a 20°C shelf and at a rate of -1°C/min cooled to an inlet shelf temperature of -30°C. The samples were frozen at an inlet shelf temperature of -30°C for 3hrs ("Freezing" in Figure 115), before the temperature was increased to -20°C at a rate of 1°C/min. Primary drying (Figure 115) was carried out at an inlet shelf temperature of -20°C for 14hrs and at a chamber pressure of 200μbar. The final stage involved increasing the shelf temperature to 20°C at a rate of 1°C/min and holding the temperature for 3hrs during secondary drying (Figure 115).

Figure 115(C) shows the typical output from the PMMA and TOPAS POFBGs that were exposed to the freeze drying cycle with mannitol samples present in the chamber. The Pirani gauge, dew point sensor and thermocouples were used to monitor primary drying during this work, to compare against the performance of the POFBGs. These sensors were assembled in the freeze dryer unit as described in section 9.3.

The freeze drying cycle was repeated with 3 vials containing 5ml of distilled water. The results from the sensors (section 9.3) will be compared for both experiments (distilled water and mannitol 10%w/v), to determine if the presence of mannitol within the frozen matrix affects the sublimation rate. It would be expected that during primary drying, the sublimation front moves through the frozen mannitol matrix towards the bottom of the sample. During this process a dry cake is left above the sublimation front with voids and channels throughout the dry matrix. This dry cake becomes a significant source of resistance to the water vapour flow from the sublimation front (product resistance, see section 3.3.5.3), which is not present in the frozen distilled water sample. The Bragg wavelength of the POFBGs will be monitored to determine if the effect of product resistance on sublimation rate could be detected.

An additional cycle containing no samples (control cycle) was run to obtain a baseline for the sensors operating in a dry nitrogen atmosphere.

The profiles from the sensors and Bragg wavelengths collected during these cycles will be compared to determine the influence of changes in pressure, temperature and humidity in the chamber on the POFBGs. It is hypothesised that the PMMA POFBGs having an affinity for water vapour, would express a red shift in the Bragg wavelength during sublimation (distilled water and mannitol samples), when compared to dry nitrogen conditions (control cycle).
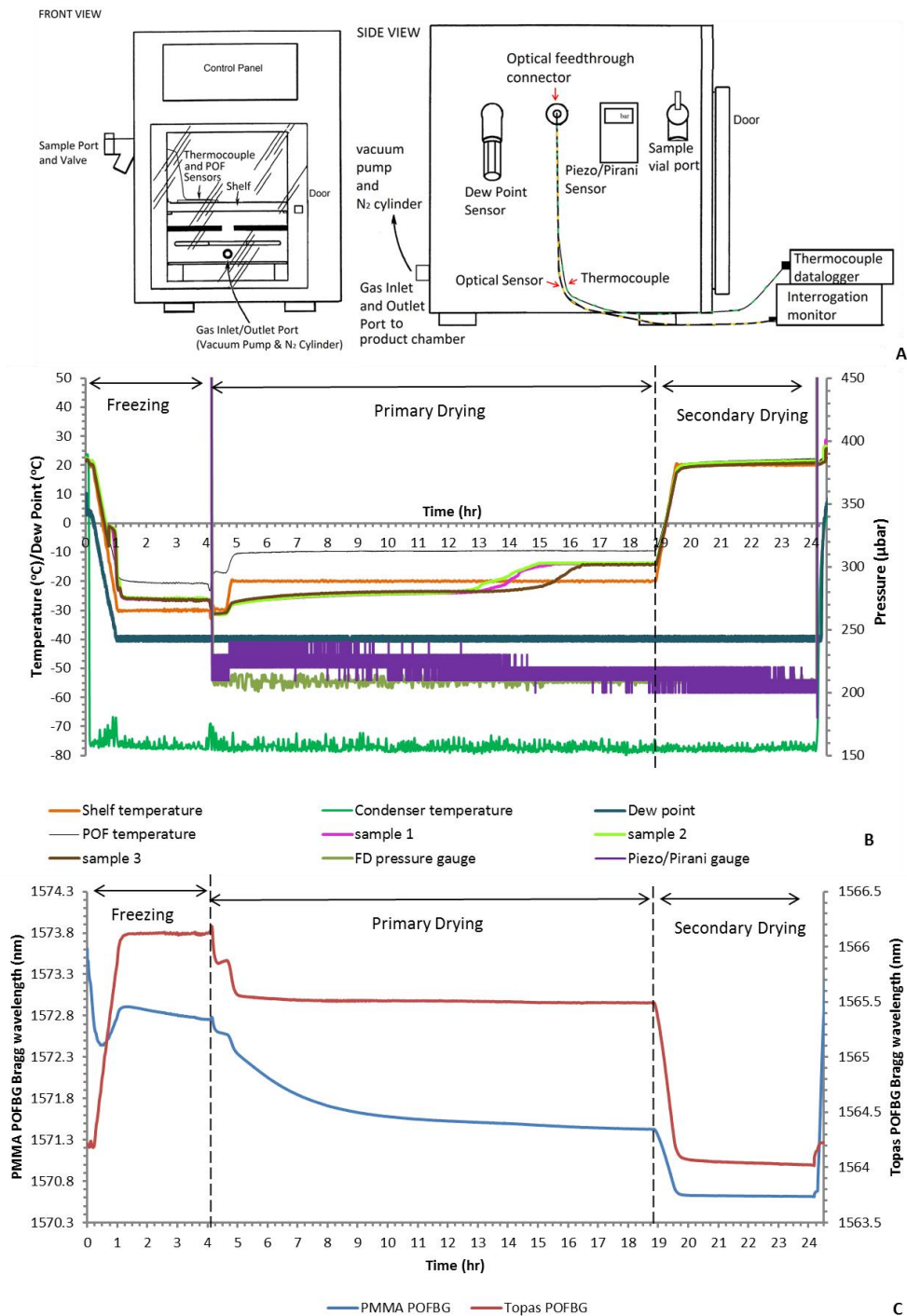
Figure 115 representative freeze drying cycle of 10%w/v mannitol with PMMA and TOPAS based POFBG tracking the progress of the cycle. (A) Schematic representation of the purpose built freeze drying experimental unit (B) Cycle uploaded to the freeze dyer controller, where Pirani was found to have responded the changes in gas composition due to sublimation (maximum offset of 40µbar) and thermocouples monitor product temperature. (C) Wavelength output of the POFBG sensors.

9.4.2 Results

Figure 116 shows the Bragg wavelength and temperature profile of the PMMA POFBG (POF4) during the primary drying stage (Figure 115), of cycles that freeze dried samples of mannitol and distilled water. The profile of the "control cycle" is also available to compare the performance of the sensors in a dry nitrogen atmosphere against an atmosphere containing sublimed water vapour. In each of these cycles, during the primary drying stage, the chamber gauge registered a constant pressure of 200µbar and the dew point sensor remained at -40°C dew point.

The thermocouples reveal that over this timeframe the temperature drifts due to radiative heat effects from the external environment (discussed in chapter 6). This would have influenced the Bragg wavelength; however for the same programmed freeze drying cycle, there appears to be a Bragg wavelength red shift when the PMMA POFBG is exposed to sublimation of water vapour. The Bragg wavelength profile also varied depending on the type of sample being freeze dried (mannitol or distilled water) and this will be examined in the following pages.
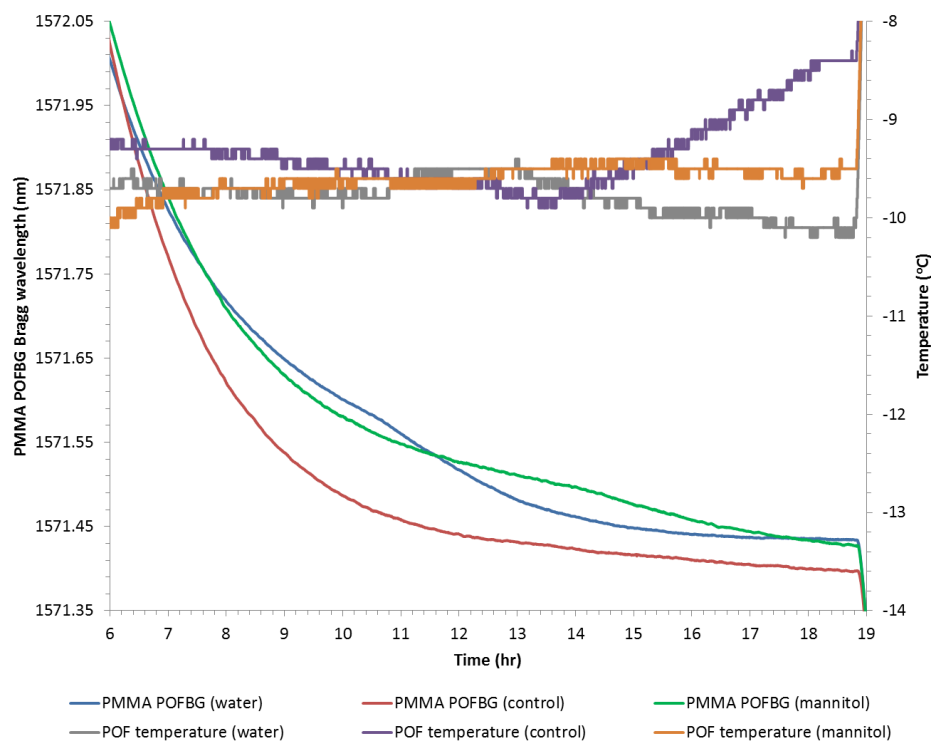
Figure 116 PMMA POFBG (POF4) Bragg wavelength shift during primary drying and temperature profile in the vicinity of the POFBG

The pressure reading from the Pirani gauge during primary drying of ice (distilled water samples) is seen in Figure 117(A) and frozen mannitol in Figure 117(B). When ice was present in the chamber a 40µbar shift was observed, at 9hrs into the cycle the reading began to decrease until it reached the chamber pressure set point of 200µbar (at 11hrs). At this stage sublimation had terminated (according to this device) and the gas composition had recovered to a nitrogen based atmosphere.

When mannitol samples were freeze dried (Figure 117(B)), the pressure reading increased until it achieved an offset of 40µbar, however at 7hrs it appeared to gradually decrease towards the chamber pressure gauge value. The end of sublimation according to this Pirani gauge was achieved at 14hrs into the cycle. As expected, the mannitol samples, having a higher product resistance (section 3.3.5.3) to water vapour flow, finished primary drying later than the water samples (for the same volume and freeze drying cycle). A steady decrease in the mass flow rate from a 5%w/w mannitol run, measured using a TDLAS was reported for a constant temperature, to be associated with an increase in the product resistance[57] (dry cake layer). The product resistance is likely influencing the reading of the Pirani sensor; future work could investigate this effect using other equipment like MTM, TDLAS and more sensitive Pirani gauges.
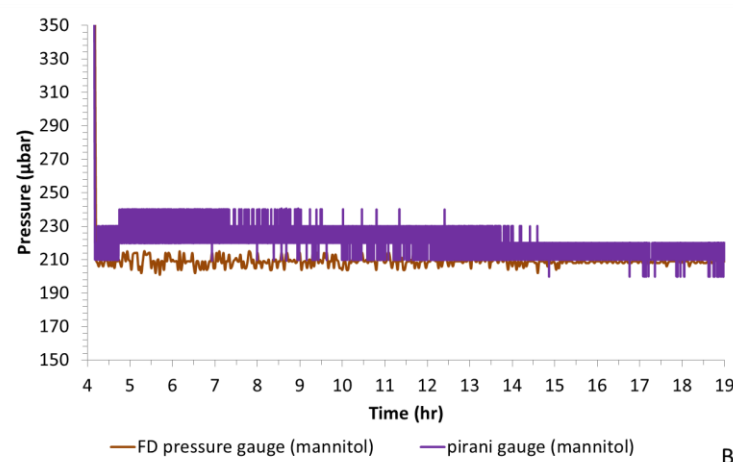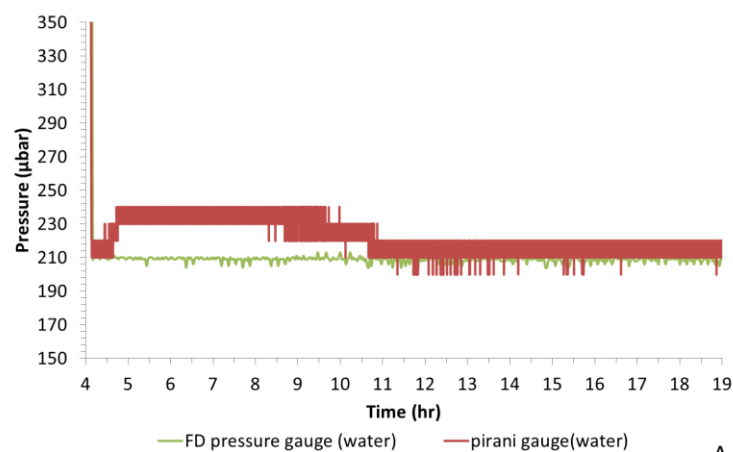
Figure 117 Pirani gauge reading during primary drying of three samples (each 5ml) of (A)distilled water, (B) 10%w/v mannitol solutions

A K-type thermocouple was placed into each vial containing either water (Figure 118A) or mannitol (Figure 118B), to track the product temperature during primary drying. The thermocouples show sublimation cooling occurring at the start of primary drying, before an increase in the product temperature occurs (red boxes) signalling the end of sublimation. The end of "primary drying time" occurs later for the mannitol samples (between 14.8hrs and 16.2hrs) than the water samples (between 11.5hrs and 11.7hrs), due to higher product resistance to subliming water vapour.
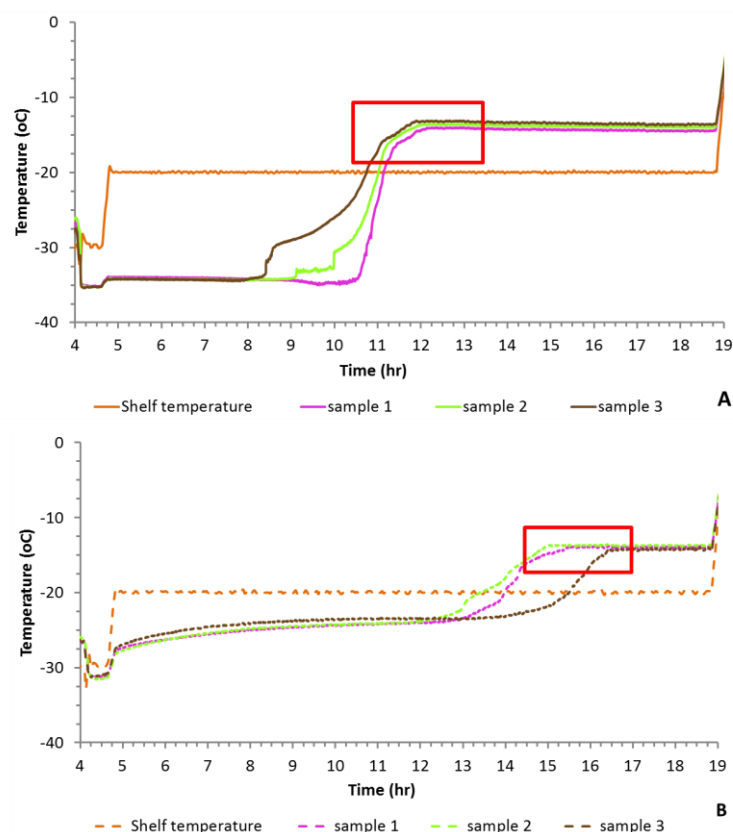
Figure 118 Product temperatures of three samples (each 5ml) during primary drying. Samples consist of (A) distilled water, (B) 10%w/v mannitol solutions. Red boxes indicate the end of primary drying time for the samples.

The variability between the vials could have resulted from differences in the ice crystal morphology within each sample. Literature has reported that the probes facilitate ice nucleation to occur at higher temperatures[67], lead to less super-cooling and larger ice crystals in the product[38]. Nucleation initiation time was also not controlled during the freezing stage (Figure 115) in this freeze drying cycle (seen in Figure 119), which could have caused variability in the ice crystal size[250]. The ice crystal morphology has been documented to influence drying rates[5, 6, 11, 20, 37, 53, 55, 59], with larger interconnected crystals reducing product resistance to sublimation and primary drying times.

Future work could investigate the use of ice fog techniques or ultrasound to control nucleation initiation time[57, 245, 250, 251]. The use of POFBGs to monitor freezing events and product temperature during freeze drying could also be explored.
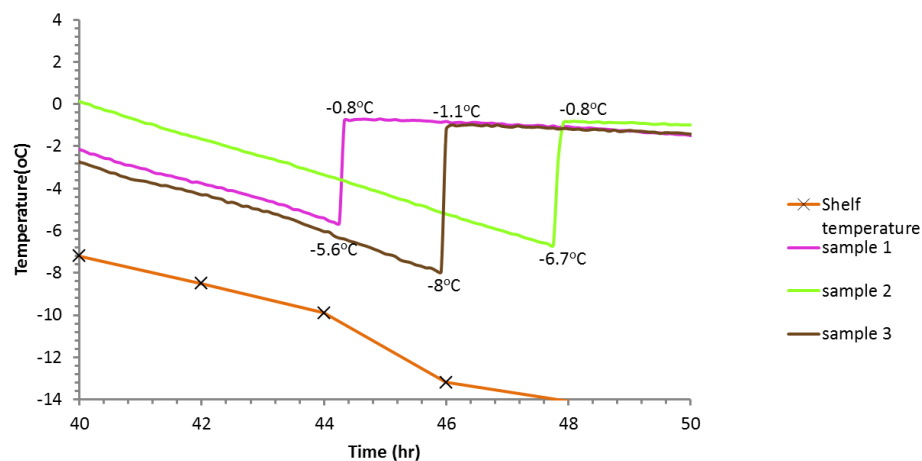
Figure 119 freezing profiles of 10%w/v mannitol solutions

Figure 120 shows the profile of the PMMA POFBG (POF4) Bragg wavelength during a control cycle (dry nitrogen atmosphere) and exposed to water vapour subliming from mannitol samples.

The chamber pressure gauge was confirmed to have remained at the set point value of 200μbar during primary drying in each of these cycles. The graphs of the data from the Pirani gauge are shown in Figure 117 and the product temperatures in Figure 118. When the sensors were exposed to a dry nitrogen atmosphere (no samples in the chamber), the Pirani gauge remained at the set point of 200μbar throughout primary drying. This was the expected result as water vapour was not introduced into the chamber, which would have changed the gas composition and pressure reading.

During this timeframe the dew point sensor continued to read -40°C dew point, it is believed that the sensor does not have the required specifications to detect the levels of dew point present in the chamber (chapter 8).

In the presence of water vapour there is a red shift in the Bragg wavelength of PMMA POFBG (POF4), which increases until it reaches 93pm before gradually decreasing (after 10hrs). At this time a -0.2°C temperature drift is observed in the region of the POFBG. Given that the sensitivity of PMMA POFBG (POF4) to temperature is -19±0.2pm/°C (chapter 6), the red shift is likely due to the polymer's affinity for water influencing the FBG. The gradual decrease in Bragg wavelength after 10hrs could be due to a change in the gas composition or potentially reduced flow rate. This could have resulted from an increase in the product resistance (dry cake layer) to water vapour mass flow as the sublimation front moves through the sample. There is a temperature drift at this time, likely from radiative heat effects (discussed in chapter 6), as these cycles were conducted on different days. This effect is more pronounced towards the end of

primary drying at time 18.6hrs, when a -1.1°C shift was observed between the two cycles (sublimation and control). At this time a 30pm shift is observed, which is partially influenced by the temperature drift. The POFBG could also have been influenced by water vapour present in the chamber or desorption of water from the fibre, the mechanism would require further investigation in future projects. As temperature drifts were observed to have a significant influence over the Bragg wavelength, future work would investigate different temperature compensation techniques to output Bragg wavelength as a function of water vapour alone.
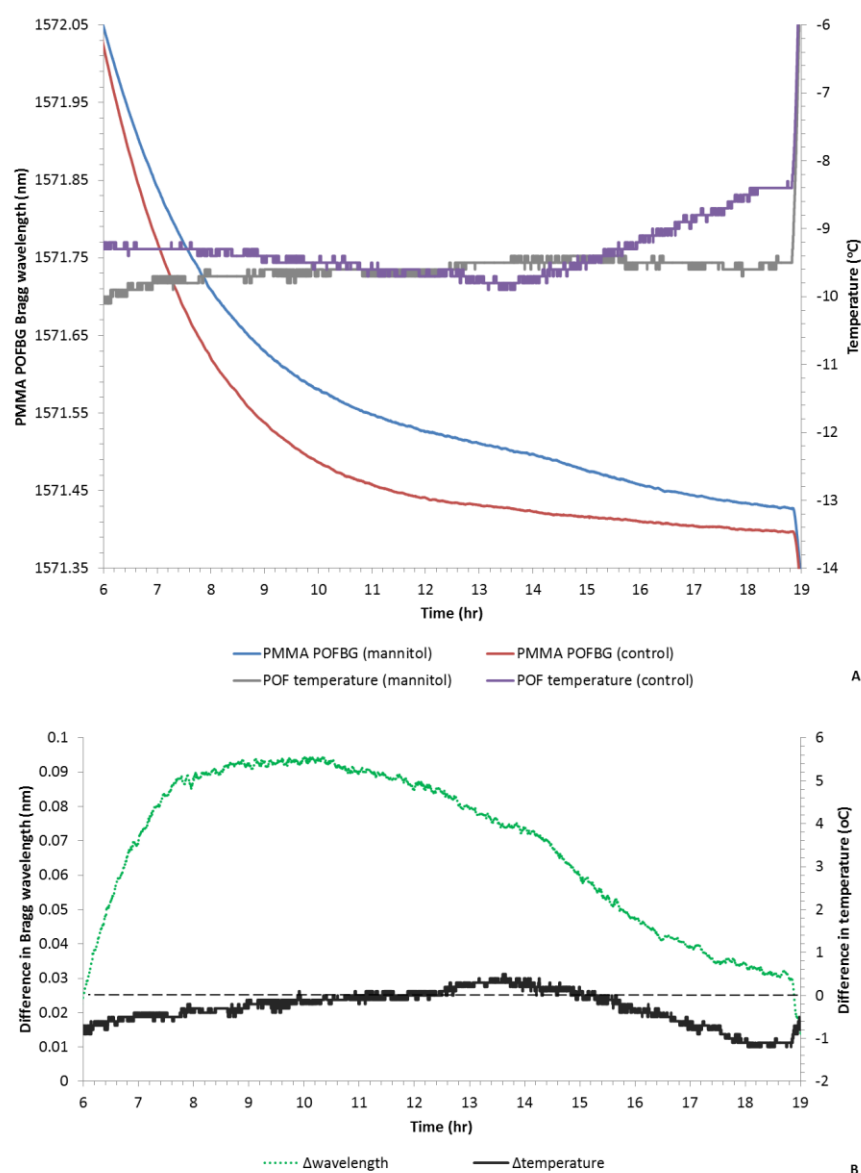
Figure 120 PMMA POFBG (POF4) monitoring the primary drying stage of 10%w/v mannitol solutions. (A) Bragg wavelength response to a control cycle with a dry nitrogen atmosphere (no samples) and a cycle exposed to water vapour from 3 mannitol samples. (B) Graph showing the differences between the Bragg wavelength and temperature of the two cycles (control and water vapour).

Figure 121 shows the Bragg wavelength shift in response to water vapour subliming from three vials containing 5ml samples of distilled water (frozen at -30°C for 3hrs). This is compared to the Bragg wavelength response in a dry nitrogen based atmosphere (control cycle). As observed with the mannitol samples (Figure 120), a red shift in the Bragg wavelength occurred in the presence of subliming water vapour, which supports the trends observed in chapter 8. During this timeframe (primary drying), the dew point remained at -40°C dew point and the chamber pressure gauge constant at the set point value of 200µbar. The product temperature monitored during the course of the freeze drying cycle is available in Figure 118(A) and pressure readings from the Pirani gauge in Figure 117(A).

Figure 121(B) and Figure 120(B) show a difference in the Bragg wavelength profiles of the water and mannitol samples. This trend was also observed by the Pirani gauge and the thermocouples, likely due to the increase in product resistance (mannitol sample) to mass flow rate of water vapour.

In Figure 121(B), the Bragg wavelength shifted by 114pm in the presence of water vapour during primary drying, however at 10.4hrs a rapid decline (compared to Figure 120(B)) occurred as the gas composition changed. The same trend was observed with the Pirani gauge when comparing the water and mannitol sample profiles (Figure 117).

Figure 121 shows temperature drifts during the course of primary drying, likely from the influence of radiative heat effects. In the initial stages of primary drying (up to 10.4hrs), there is a maximum temperature shift of -0.5°C between the cycles (sublimation and control). As the sensitivity of PMMA POFBG (POF4) to temperature is -19±0.2pm/°C (chapter 6), the red shift (up to 114pm) is likely due to the polymer's affinity for water influencing the FBG. In the next time interval (10.4hrs to 14hrs), a decline in the Bragg wavelength from 114pm to 40pm was observed and during the same timeframe a maximum temperature shift of 0.3°C. When comparing these results to the Pirani gauge and thermocouple probes, the sensors indicated that end of primary drying had been achieved during this time frame. This strongly suggests that the POFBG was reacting to the change in the gas composition towards a nitrogen atmosphere, as the mass of subliming water vapour decreased over time. Unfortunately, at the end of the primary drying stage (18.5hrs), a large offset in the temperature from heat transfer issues was observed (up to -1.8°C) and a Bragg wavelength shift of 37pm. Based on the sensitivity of the POFBG to temperature (-19±0.2pm/°C), this indicates that the

offset is the result of temperature drifts and that the end of primary drying could have occurred between 14hrs and 18.5hrs.

These experiments show the potential for the POFBG to be used to monitor sublimation during primary drying. The differences between the Bragg wavelength profiles of both samples would require further investigation, to determine if the POFBGs could be used to determine mass flow rate. This would require further investigation in future projects, as well as development of temperature compensation techniques, to monitor in real time the Bragg wavelength output as a function of water vapour alone.
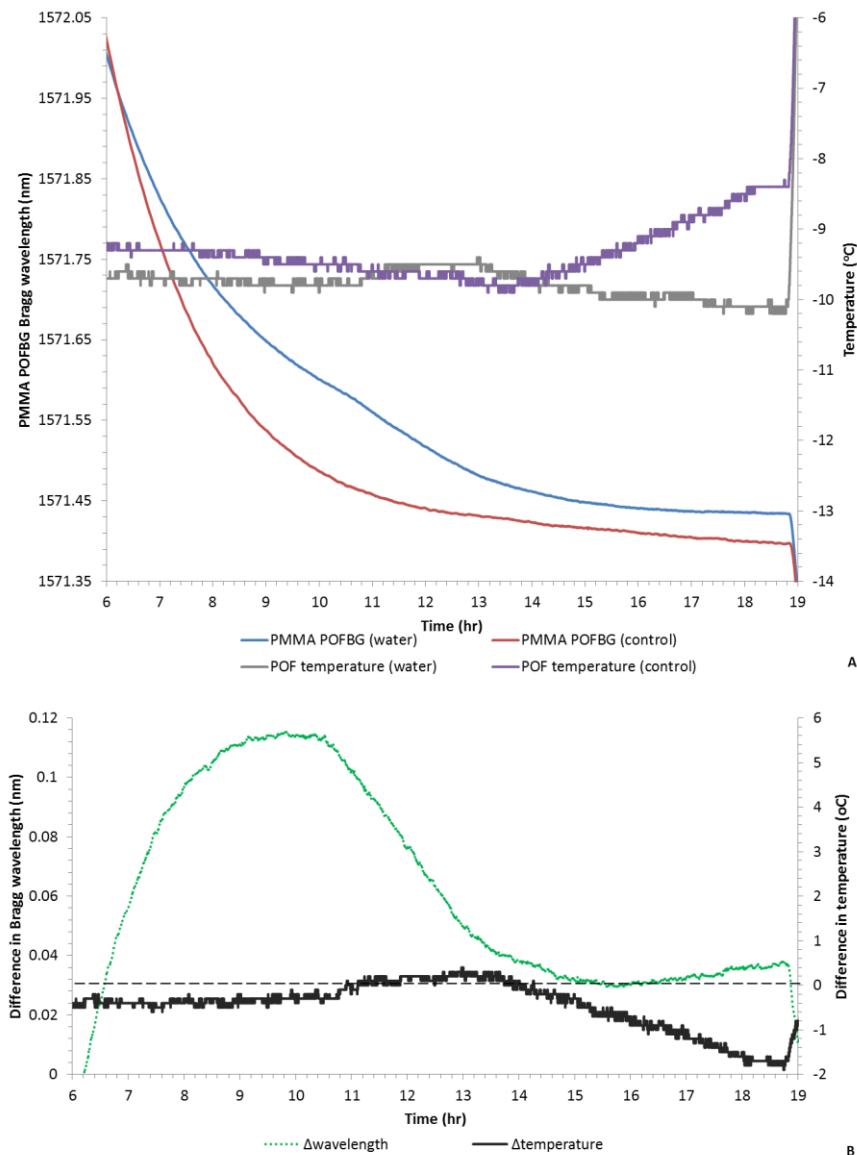
Figure 121 PMMA POFBG (POF4) monitoring primary drying of frozen distilled water. (A) Bragg wavelength response to a control cycle with a dry nitrogen atmosphere (no samples) and a cycle exposed to water vapour from 3 samples of distilled water. (B) Graph showing the differences between the Bragg wavelength and temperature of the two cycles (control and water vapour).

Figure 122 shows the Bragg wavelength response of humidity insensitive TOPAS POFBG (POF3), placed in the same chamber as the PMMA POFBG (POF4) during the sublimation (water vapour) and control (dry nitrogen) cycles. Temperature was monitored in the vicinity of the POFBG and found that radiative heat affected the Bragg wavelength during primary drying. A maximum temperature shift of -0.5^{o}C was observed (up to 11hrs) and a Bragg wavelength shift of 19pm. As sensitivity of TOPAS POFBGs to temperature is -36±0.3pm/^{o}C (chapter 6), it is likely that the Bragg wavelength shift is primarily due to changes in temperature. The radiative effects were also observed at the end of the primary drying stage (18.5hrs), with a -1.8^{o}C temperature shift and a 43pm red shift in the Bragg wavelength. As the sensitivity to temperature is -36±0.3pm/^{o}C, there could be other mechanisms influencing the POFBG, which would require development of temperature compensation techniques and further investigations. These trends were also observed in Bragg wavelength values obtained from TOPAS POFBG (POF3) during the freeze drying of mannitol (Figure 171 in Appendix I).
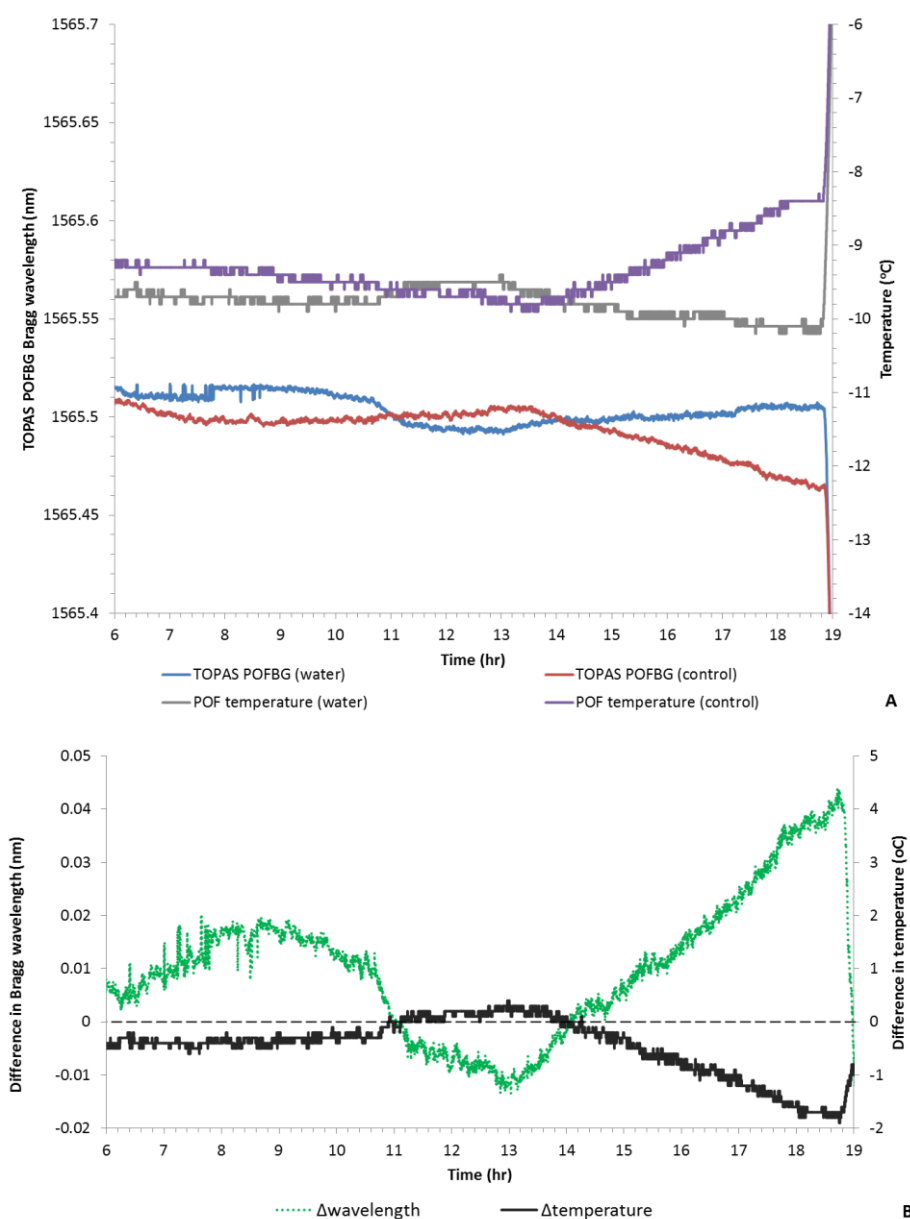
Figure 122 TOPAS POFBG (POF3) monitoring primary drying of frozen distilled water. (A) Bragg wavelength response to a control cycle with a dry nitrogen atmosphere (no samples) and a cycle exposed to water vapour from 3 samples of distilled water. (B) Graph showing the differences between the Bragg wavelength and temperature of the two cycles (control and water vapour).

These experiments show that PMMA POFBG can monitor sublimation during primary drying, however temperature compensation techniques would need to be developed to obtain in real-time, the Bragg wavelength output as a function of water vapour alone. This study used conditions that would create a greater challenge for the POFBGs to detect water vapour and more comparable freeze drying cycles to those programmed for pharmaceutical formulations.

This study used a significantly lower sample number (3 vials) and volume (15ml total volume) than would be expected in industrial and research scale freeze

dryers. In literature, laboratory scale freeze driers (e.g. Lyostar II) have reported to contain up to 240vials[8, 57] when comparing the performance of different sensors and their ability to detect sublimation. This volume was not possible with the benchtop scale freeze drier unit used in this project; however the small volume showed the sensors can be used to monitor the cycle in challenging conditions. Future projects would investigate POFBGs in laboratory scale driers (few hundreds of vials)[19] before scaling up to production scale freeze driers (up to 100000vials)[19]. Different freeze drying cycles and more complex samples would be investigated in future projects, which could form combinations of crystalline and amorphous structures in the frozen matrix.

9.5   Freeze drying of native collagen

In the work reported in the previous chapters the POFBG sensors had been characterised in the vacuum chamber to determine their response profiles to CPP's, including temperature, pressure and humidity. This section will use this information, to monitor the freeze drying of collagen and determine the end of primary drying time.

Collagen is the most abundant protein in mammals, it provides mechanical and structural support to tissues and organs in the body [252]. Collagen has been used in many clinical applications as it has desirable bio-inductive, mechanical and biodegradable properties[253]. An area of interest is the use of collagen in the field of regenerative medicine, where the protein is used in several medical applications [252], such as drug delivery, skin substitutes [31, 254], suturing and as a tissue engineering substrate.

An emerging field for the use of collagen based composites is the production of scaffolds, to be used in surgical procedures to replace tissues damaged through disease, injury or trauma[255].

Surgical treatment typically involves transplanting a tissue collected from a site in the body of the patient (autograft) to replace the missing damaged tissue (e.g. bone), or a transplant/allograft from a donor[255]. These techniques pose challenges, in particular the risk of the patient's immune system rejecting the allograft, higher risk of infection, increased treatment cost and determining whether sufficient tissue was harvested to replace the affected area[255]. To address these issues, tissue engineering investigates an alternative option of developing highly porous biological substitutes (scaffolds) that can regenerate the patients tissues that had been previously damaged[255].

The architecture of the biocompatible scaffold is critical to encourage new tissue growth. The porosity is a critical parameter, as it influences cell migration into the scaffold[256] and the vascular network growth required to provide nutrients and remove waste from the area[254, 255]. To provide control over the pore size, a freeze drying protocol can be implemented to create the desired dimension by controlling the formation of ice crystals, which sublime during primary drying to leave a porous scaffold[31, 256-258].

The pore size varies depending on the application. To promote bone growth, osteoblast cells require scaffolds with pore sizes greater than 100µm, whereas blood vessels endothelial cells require a scaffold with a pore size of 20-80µm[254].

9.5.1 Method

Native collagen samples sourced in-house from rat tails were prepared according to section 5.7.6 by Mr Haris Choudhery and stored in wells (2.5mg/ml) before being gelatinized and frozen overnight at -80°C. Figure 123 shows the freeze drying unit containing the native collagen samples, which was assembled with sensors according to section 9.3.

The first experiment consisted of 7 wells placed onto the shelf in the freeze dryer, each containing 2ml of native collagen samples (2.5mg/ml). The cycle was then repeated with 1 well having the same volume and concentration.

The 35mm wells (2mm fill depth) were loaded into the Virtis Advantage freeze dryer directly onto a -40°C inlet shelf temperature[257, 258] and held at that temperature for 2hours (Figure 124 B(a*)). A slow shelf ramp of 10°C/hr was applied to achieve a shelf temperature of 0°C[258] and the samples were dried for 17hours at 200µbar as shown in Figure 124 B(c*).

Small sample volumes (2ml) in the wells were chosen to pose an additional challenge for the POFBGs than in the previous experiments, as they were now required to monitor trace quantities of subliming water vapour at lower temperatures. The sublimation of the sample(s) was monitored using the -40°C dew point sensor and the Pirani gauge, which were compared against the performance of the new POFBG technology. Once the drying stage was completed the samples were removed and prepared in order to obtain micrographs of the scaffolds using the Scanning Electron Microscope (SEM). Figure 124(C) shows the typical output from the PMMA and TOPAS POFBGs that were exposed to the freeze drying cycle, which had samples present in the chamber. The same trends in the Bragg wavelength were observed for both cycles that contained collagen samples (7 samples (Figure 124) and 1 sample).

The cycle was repeated in a dry nitrogen atmosphere (control cycle), without samples present in the chamber. The output from this cycle would be used to compare the profiles of the sensors and Bragg wavelengths to changes in pressure, temperature and humidity in the chamber. It is hypothesised that the PMMA POFBGs having an affinity for water, would express a shift in the Bragg wavelength when water vapour was present in the chamber (from sublimation), when compared to dry nitrogen conditions (control cycle).

(a)　(b)
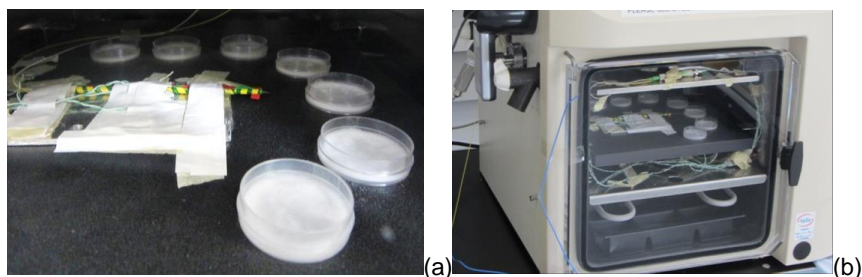
Figure 123 (a) POFBG sensor positioned on the shelf next to seven wells each containing a 2ml volume of frozen native collagen samples, (b) freeze dryer unit with the sensors attached to the access ports, POFBGs on the shelf next to the collagen samples
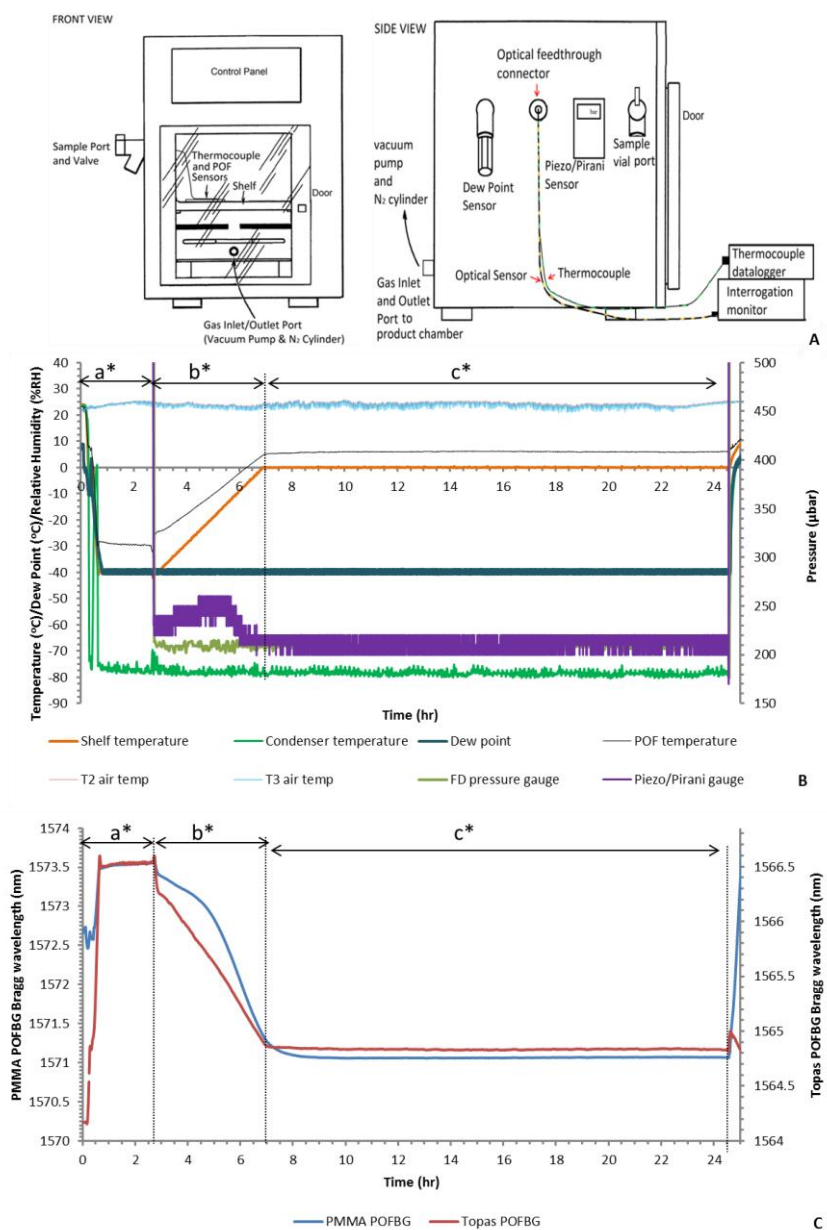
Figure 124 Freeze drying cycle of native collagen (7 samples) with PMMA and TOPAS based POFBG tracking the progress of the cycle. (A) Schematic representation of the purpose built freeze drying experimental unit (B) Cycle uploaded to the freeze dyer controller, where Pirani

9.5.2   Freeze drying 7 native collagen samples (14ml total volume)

During the freezing stage (a*) in Figure 124, the Bragg wavelengths of PMMA and TOPAS POFBGs were influenced by changes in the chamber humidity, temperature and a pressure drop to 200mbar (protocol to seal the chamber). Initially the shelf temperature was precooled from room temperature (23°C) to -40°C before placing the samples on the shelf. This stage was carried out to avoid melting the pre-frozen samples (2mm fill depth) once transferred to the shelf. The chamber was sealed by reducing the pressure to 200mbar and the dew point reduced from 9°C to -40°C. At this stage the freeze drying cycle programmed into the PLC (section 9.5.1), began the freezing stage (Figure 124 (a*)) and held the shelf temperature for 2hrs at -40°C before starting the primary drying stage. As a result the Bragg wavelengths shifted by 2.36nm and 0.93nm for TOPAS and PMMA POFBG respectively. As TOPAS POFBG (POF3) has a sensitivity of -36.0±0.3pm/°C (chapter 6), it is likely that the majority of the shift was due to the -63°C drop in the inlet shelf temperature. As PMMA POFBG (POF4) has a sensitivity of -19.0±0.2pm/°C (chapter 6), temperature significantly influenced the Bragg wavelength; however some cross-sensitivity due to changes in humidity is also likely to have occurred. Chapter 6 describes the protocol used to obtain these sensitivities for a shelf temperature operating range between 20°C to -20°C. Future work would involve optimising the freeze drying unit in order to characterise and obtain the sensitivities of the POFBG sensors for the full working range of the freeze dryer.

As observed in the previous chapters, heat transfer issues [9, 57] can be seen during the cycle. There are several barriers to heat transfer[19, 46], including a temperature gradient between the interior (set point) and surface of the shelf, incomplete contact of the aluminium sheet, vial[19, 46] and POFBGs with the shelf. These heat transfer effects are seen during stage (a*) in Figure 124(B), which shows an offset in the temperature of the POFBGs compared to the inlet shelf temperature.

Figure 124 (b*) and (c*) are the areas where the primary drying stage of the collagen samples is occurring. As the inlet shelf temperature was ramped from -40°C to 0°C in Figure 124(b*), a blue shift in the Bragg wavelength was observed by PMMA and TOPAS POFBGs, likely due to the dominance of the negative thermo-optic coefficient. The pressure was also reduced to 200µbar to promote

sublimation, which would have additionally influenced the Bragg wavelength. In Figure 124(b*) the Pirani gauge displays an offset of 50µbar due to the change in the surrounding gas composition, as sublimation introduces water vapour into the chamber. The Pirani gauge detects the end of primary drying time when the gas composition returns to a predominantly nitrogen based atmosphere and as a result the reading drops to match the freeze dryer gauge pressure (time 6.4hrs in Figure 124(b*)).

During primary drying (sublimation) in Figure 124(b*) and (c*) the dew point remained constant at -40°C, this trend was also observed in the previous chapters. Literature reports that these devices detect sublimation occurring between -40°C and -60°C dew point[8, 57]. As the lowest detectable dew point for this device is -40°C, it is likely that the current dew point sensor was not designed to detect the trace changes in the gas composition in a freeze dryer. Future work would require investigating dew point sensors or chilled mirrors with a wider and lower operating range to compare against the POFBGs.

In order to analyse the behaviour of the Pirani gauge and POFBG during primary drying, the outputs of the sensors were plotted in Figure 125. The plot for TOPAS POFBG is shown in Figure 177 and available in Appendix I.
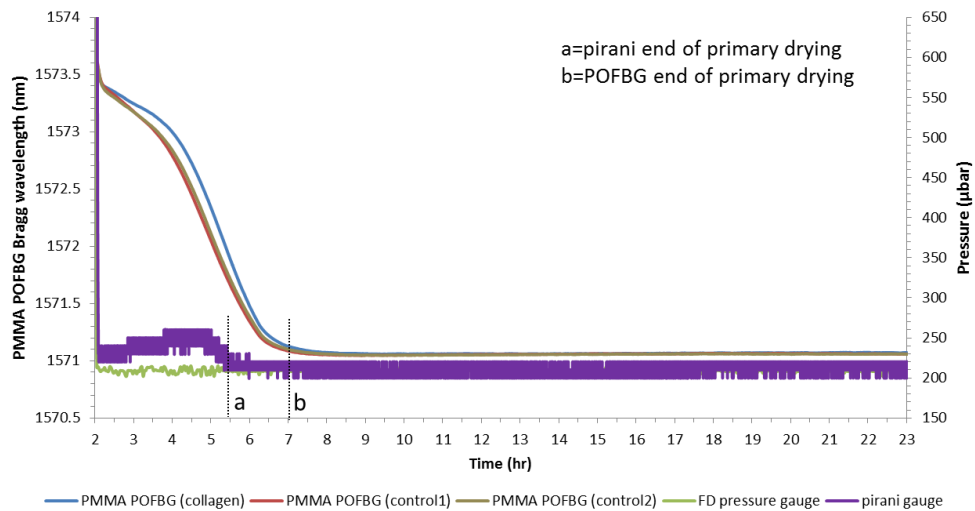
Figure 125 Pirani gauge and PMMA POFBG (POF4) sensor monitoring primary drying of 7 collagen samples. The PMMA POFBG profile was compared against two control cycles (in a dry nitrogen atmosphere) to determine the end of primary drying time. The end of primary drying time has been detected at (a) by the Pirani gauge and (b) by PMMA POFBG.

Figure 125 shows an offset of the pressure reading by the Pirani gauge from the set point pressure value of 200µbar, due to the presence of water vapour in the chamber. The offset increased to a maximum value of 50µbar between 4hrs to 5hrs,

before recovering as the gas composition returned to a nitrogen based environment at time 5.6hrs (Figure 125(a)).

The PMMA POFBG (POF4) was used to monitor three cycles with the same freeze drying program uploaded to the freeze dryer's PLC (section 9.5.1). One run had 7 collagen samples placed into the chamber for freeze drying and the Bragg wavelength was monitored throughout this cycle. The next two cycles repeated the freeze drying program, but in a dry nitrogen atmosphere, these results would act as controls to determine if water vapour influenced the POFBG. During the "control cycles" the Pirani gauge was found to have remained stable at the pressure set point of 200µbar during primary drying. This was the expected result, as there were no samples present in the chamber to introduce water vapour into the atmosphere, change the gas composition and lead to a shift the Pirani gauge value.

Figure 125 shows that the PMMA POFBG (POF4) produced a red shift in the Bragg wavelength when water vapour was introduced into the atmosphere (from the collagen samples), compared to the dry nitrogen atmosphere profiles (controls). During all three cycles the freeze dryer's internal pressure gauge indicated that the pressure remained constant at 200µbar during the primary drying stage. Figure 126(A) shows the Bragg wavelength profiles for the control and water vapour cycle (collagen samples), a red shift in the Bragg wavelength occurred in the presence of water vapour (d*). This is the expected outcome that supports the observed results in the previous chapter. PMMA POFBGs have an affinity for water vapour that leads to an increase in the Bragg wavelength, which is a trend supported by literature[12, 14, 16, 17].
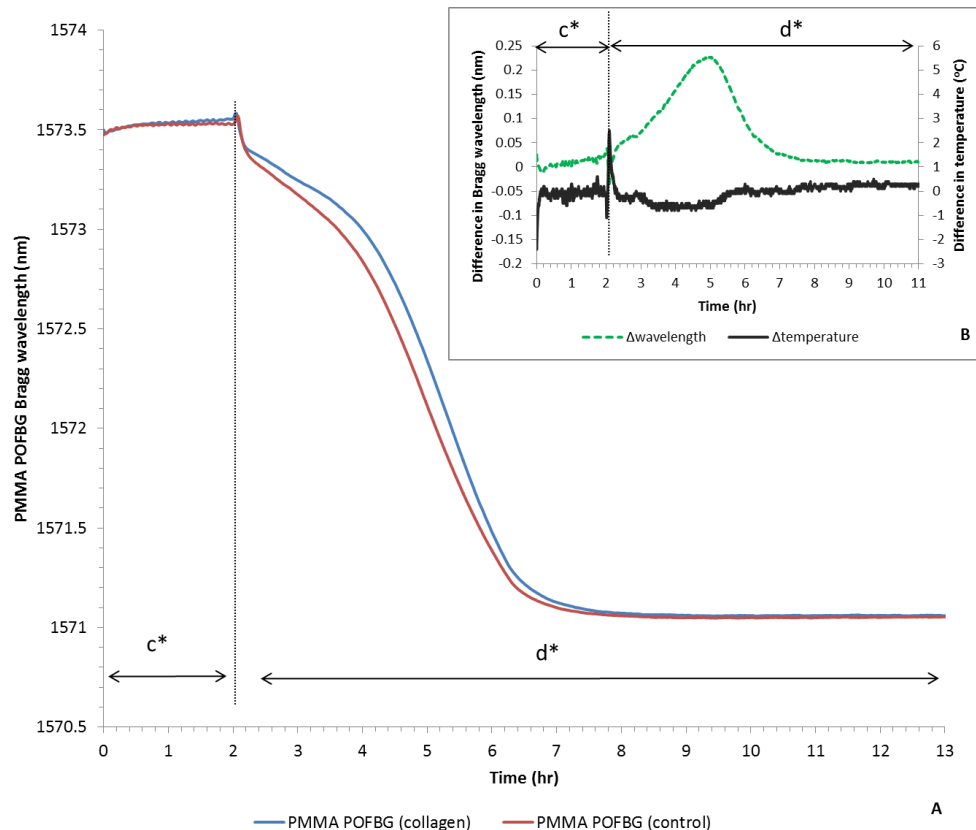
Figure 126 PMMA POFBG sensor (POF4) monitoring the freezing stage (c*) and primary drying stage (d*) of the programmed freeze drying cycle. (A) Bragg wavelength response to a control cycle with a dry nitrogen atmosphere (no samples) and a cycle exposed to water vapour from 7 freeze drying collagen samples. (B) Graph showing the differences between the Bragg wavelength and temperature of the two cycles (control and water vapour).

Figure 126(B) shows the difference between the Bragg wavelength and temperature profiles of the two cycles in (A), i.e. control and water vapour cycle (collagen samples). This graph was plotted to determine that the Bragg wavelength shift seen in Figure 125 was not the result of changes in temperature due to radiative heat effects, but rather due to the presence of water vapour.

Figure 126(B) shows a spike in the temperature occurred at the end of the freezing stage (c*). This is due to limitations in the control system of the freeze dryer that postpones shelf temperature control during the drop in pressure stage to 200µbar, leading to greater differences between repeats in cycles at this phase. This spike was found to quickly recover at the start of primary drying (d*) once the set point pressure of 200µbar was achieved.

Figure 126(B) displays a maximum offset of -0.8°C between the temperature profiles of the control and water vapour cycle during primary drying (d*). Additionally a Bragg wavelength shift of 226pm was observed between 4hrs to 5.5hrs during primary drying (d*) in the presence of water vapour. During the same time interval, Figure

125(a) shows that the Pirani gauge recorded a maximum offset of 50μbar in the pressure reading from the chamber set point, due to a change in the gas composition from the introduction of water vapour.

As PMMA POFBG (POF4) was determined to have a temperature sensitivity of -19.0±0.2pm/°C (chapter 6), the data suggests that the PMMA POFBG is detecting the sublimation of water vapour from the samples. Figure 125 suggests that the POFBGs determined the end of primary drying time (b) to be later than the Pirani gauge (a). This could be a combination of the POFBG detecting residual water vapour in the chamber that the Pirani gauge is not able to detect combined with a delay due to the removal of adsorbed water in the fibre. This would require further investigation using TDLAS or MTM technology, to determine the water vapour composition in the chamber.

These trends were also observed by PMMA POFBG (POF5) during the same experiment, the results are available in Figure 178 and Figure 179 in Appendix I. Figure 127 illustrates the results from the TOPAS POFBG (POF3) sensor during the freeze drying cycle. During primary drying (d*), TOPAS POFBG (POF3) experienced a 55pm red shift in the Bragg wavelength in the presence of water vapour. Figure 127(B) shows the difference in the temperature profile between the two cycles and found a temperature shift of -0.8°C. The sensitivity of TOPAS POFBG (POF3) to temperature is -36±0.3pm/°C (chapter 6). This suggests that the majority of the red shift is due to drifts in temperature from heat transfer issues and radiative heat effects; however water vapour or mass flow could also be influencing the POFBG (chapter 8). Literature has reported TOPAS POFBG to be at least 50 times less sensitive to water than PMMA at atmospheric pressure[12]. These results would require further investigation to determine the mechanism influencing TOPAS POFBGs, as a response to water vapour of this order of magnitude has not been documented in literature (at atmospheric conditions).
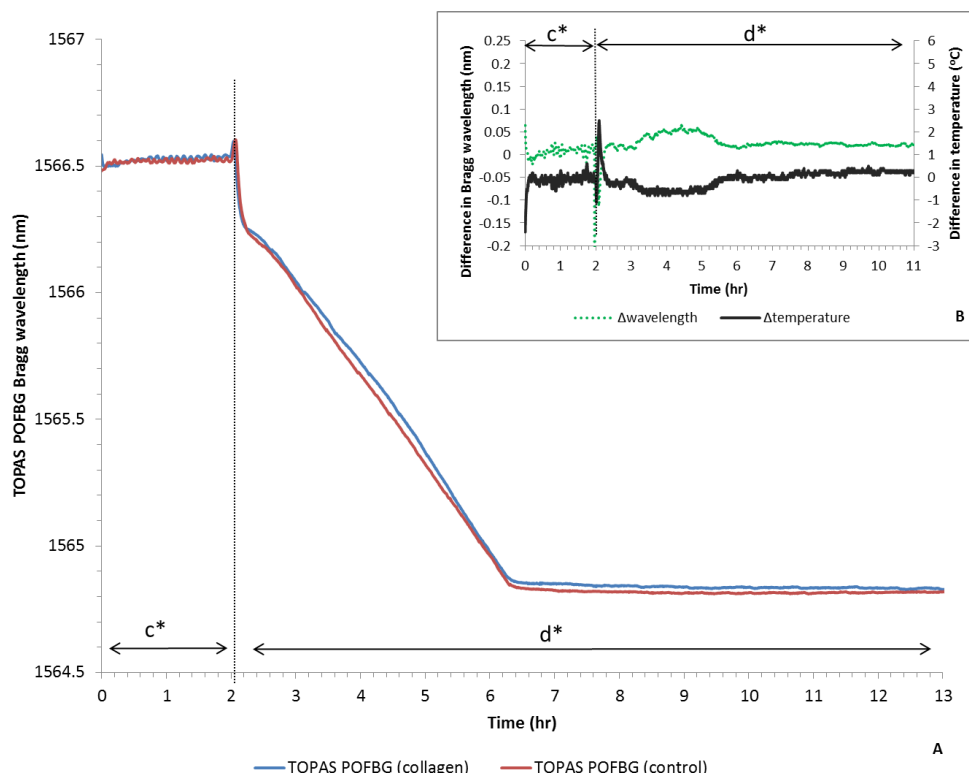
Figure 127 TOPAS POFBG sensor (POF3) monitoring the freezing stage (c*) and primary drying stage (d*) of the programmed freeze drying cycle. (A) Bragg wavelength response to a control cycle with a dry nitrogen atmosphere (no samples) and a cycle exposed to water vapour from 7 freeze drying collagen samples. (B) Graph showing the differences between the Bragg wavelength and temperature of the two cycles (control and water vapour).

9.5.3 Freeze drying a 2ml native collagen sample

Figure 128 shows the outputs from the Pirani gauge and PMMA POFBG (POF4) when a single 2ml sample of native collagen (2.5mg/ml), was freeze dried using the protocol described in section 9.5.1. The same cycle was used to freeze dry the 2ml sample of native collagen as was used for the 7 samples of native collagen (14ml total volume). The plot for TOPAS POFBG is shown in Figure 180 in Appendix I. The graph (Figure 128) shows the same characteristic profile and trends as observed in the previous experiment (section 9.5.2), where a red shift in the Bragg wavelength occurred in the presence of water vapour. The graph indicates the end of primary drying to be 6.2 hrs, however as this is beyond the measuring range of the Pirani it cannot be independently confirmed at this time. The same trend was observed by PMMA POFBG (POF5) in Figure 181 in Appendix I. Figure 128 documented the performance of the Pirani gauge during the cycle, but appears not to have detected the sublimation of water vapour from the 2ml sample (2.5mg/ml native collagen). This process was repeated with another 2ml sample (2.5mg/ml

native collagen), but once more the Pirani gauge did not register an offset in the pressure value from the chamber pressure (set point of 200µbar).

It is possible that the PMMA POFBGs (POF4 and POF5) could be detecting the trace volumes of water vapour subliming from the sample, which are within the noise range for this particular Pirani gauge. Future work would involve verifying and calibrating the POFBGs against other established technologies that monitor sublimation, such as TDLAS, MTM and freeze drying mass balance.
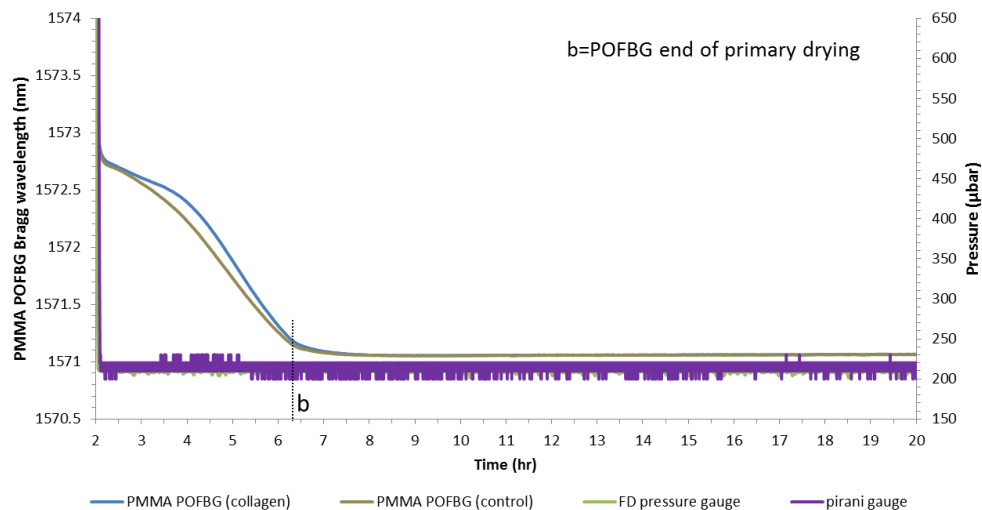
Figure 128 Pirani gauge and PMMA POFBG (POF4) sensor monitoring primary drying of 1 collagen sample (2ml total volume) in a well. The PMMA POFBG profile was compared against a control cycle (in a dry nitrogen atmosphere) to determine the end of primary drying time. The end of primary drying time has been detected at (b) by PMMA POFBG.

Figure 129 compares the shift in Bragg wavelength response of the PMMA POFBG (POF4) between the dry nitrogen atmosphere (control) cycle and water vapour cycle (2ml collagen sample).

During the freezing (c*) and primary drying stage (d*) the dew point sensor remained at a constant -40°C dew point, as seen previously. The graph shows that in the presence of water vapour from sublimation during primary drying (d*), a red shift in the Bragg wavelength occurred. This trend was also observed in the previous experiment (7 collagen based samples).

A Bragg wavelength shift of 175pm and a maximum temperature shift of -0.5°C were measured during the primary drying stage (d*). The sensitivity to temperature of PMMA POFBG (POF4) is -19.0±0.2pm/°C (chapter 6). During primary drying (d*) the chamber pressure gauge and Pirani gauge remained at the pressure set point of 200µbar. This suggests that the red shift in the Bragg wavelength is the result of water vapour in the chamber influencing the Bragg wavelength.

A spike in the temperature in the vicinity of the POFBGs occurred at the end of the freezing stage (c*), which recovered at the start of primary drying. This trend was also observed in the previous experiments, due to limitations in the control system during the pressure reduction stage to 200µbar (to promote sublimation).
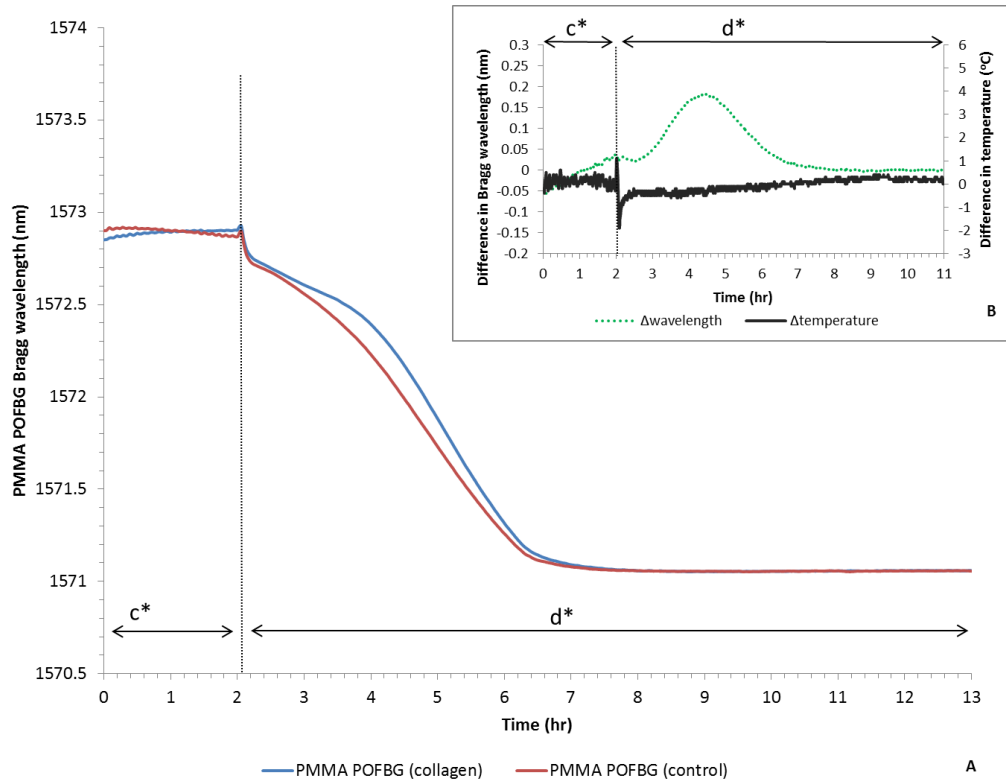

Figure 129 PMMA POFBG sensor (POF4) monitoring the freezing stage (c) and primary drying stage (d*) of the programmed freeze drying cycle. (A) Bragg wavelength response to a control cycle with a dry nitrogen atmosphere (no samples) and a cycle exposed to water vapour from a 2ml freeze drying collagen sample (2.5mg/ml). (B) Graph showing the differences between the Bragg wavelength and temperature of the two cycles (control and water vapour).*

Figure 130 shows the PMMA POFBG (POF5) Bragg wavelength shift in response to water vapour (freeze drying a single 2ml collagen sample (2.5mg/ml)) and a "control" cycle with a dry nitrogen based atmosphere. Both cycles used the same freeze drying protocol described in section 9.5.1.

PMMA POFBG (POF5) experiences the same trends as seen with POF4, where the affinity for water vapour caused a red shift in the Bragg wavelength. In this case a 180pm shift was observed by POF5 for the same temperature, pressure and humidity conditions as POF4. During primary drying (d*), the pressure remained at 200µbar and a maximum temperature shift of -0.5°C was recorded. The sensitivity to temperature of PMMA POFBG (POF5) is -18.0±0.2pm/°C (chapter 6). It is likely that the red shift in the Bragg wavelength is the result of water vapour in the chamber, as

water vapour was reported to cause swelling[16, 17] and an increase in the refractive index of PMMA[12] at atmospheric pressure.

There are occasional spikes in the Bragg wavelength as the freeze dryer PLC ramps the shelf temperature from -40°C to 0°C (from 2hrs to 6hrs). This could be the result of the IMON interrogator detecting several modes being reflected from the grating at these temperatures, or limitations in the peak tracking software. These patterns were observed on multiple occasions as the temperature of the POF increased or decreased in this region. This would require optimisation of the software and POFBG manufacturing process, to maintain consistency in the materials, geometry etc. for batch production and commercial applications.
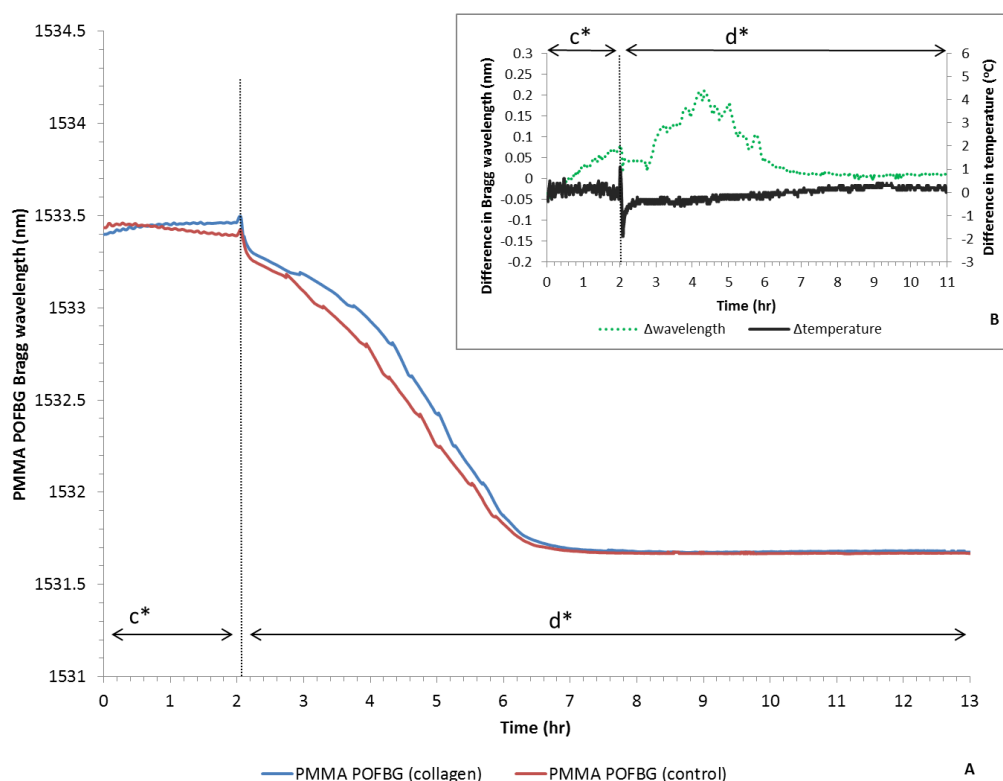

Figure 130 PMMA POFBG sensor (POF5) monitoring the freezing stage (c*) and primary drying stage (d*) of the programmed freeze drying cycle. (A) Bragg wavelength response to a control cycle with a dry nitrogen atmosphere (no samples) and a cycle exposed to water vapour from a 2ml freeze drying collagen sample (2.5mg/ml). (B) Graph showing the differences between the Bragg wavelength and temperature of the two cycles (control and water vapour).

Figure 131 shows the response of TOPAS POFBG (POF3) to the freeze drying process of a single 2ml sample of collagen (2.5mg/ml). The pressure was monitored using the Pirani gauge and chamber pressure gauge, which showed that the readings remained at 200µbar during primary drying (d*). A maximum temperature shift of -0.5°C was observed during "d*", between the control cycle (nitrogen atmosphere) and the water vapour cycle (collagen sample). A red shift in the Bragg

wavelength of 20pm was also observed during this timeframe. As the TOPAS POFBG (POF3) has a temperature sensitivity of -36±0.3pm/°C (chapter6), it is likely that the red shift is the result of the drift in temperature. Future work would need to study the potential mechanisms influencing the TOPAS POFBGs, to determine whether they are influenced by water vapour or a vapour flow rate that induces stresses or movement. This would require further investigation, as in the previous experiments TOPAS POFBG sensors observed red shifts in the Bragg wavelength that could not be accounted for by temperature alone.
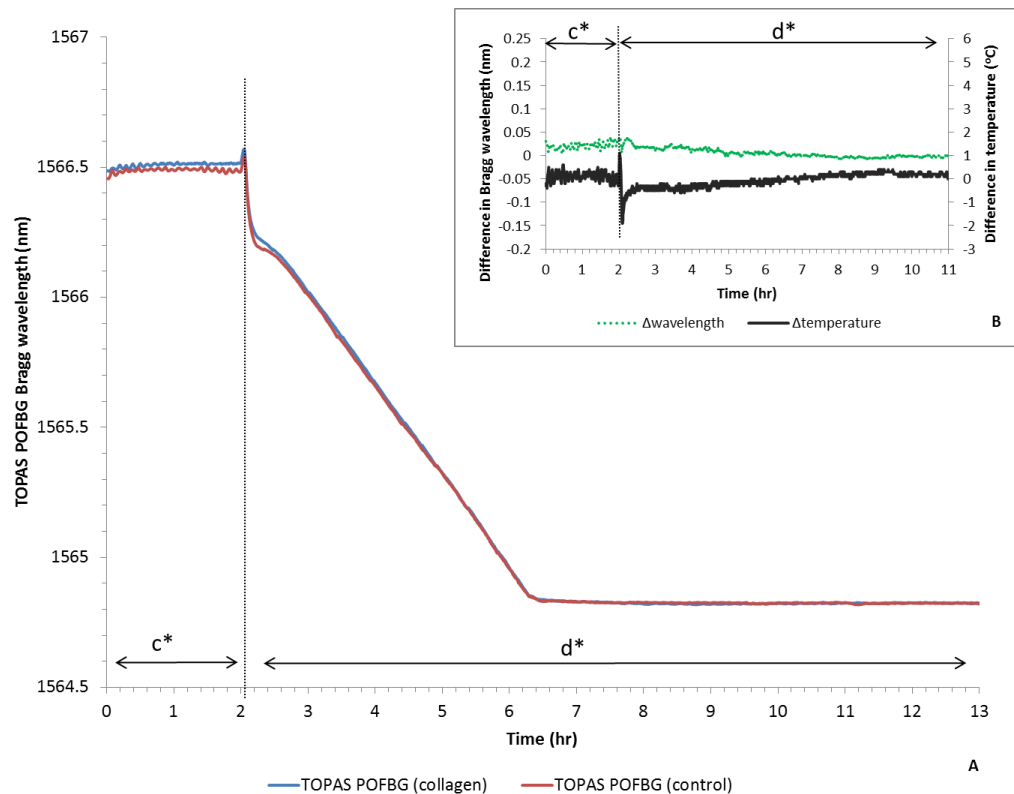
Figure 131 TOPAS POFBG sensor (POF3) monitoring the freezing stage (c*) and primary drying stage (d*) of the programmed freeze drying cycle. (A) Bragg wavelength response to a control cycle with a dry nitrogen atmosphere (no samples) and a cycle exposed to water vapour from a 2ml freeze drying collagen sample (2.5mg/ml). (B) Graph showing the differences between the Bragg wavelength and temperature of the two cycles (control and water vapour).

The results show the potential application of POFBG technology for use in freeze drying applications to detect sublimation and the end of primary drying time. The sensor was likely able to track the presence of water vapour subliming from frozen samples of collagen in the chamber. The device also appeared to show higher sensitivity to low flow rates of water vapour in the chamber than the Pirani gauge and dew point sensors used in this work, however this would require verification in future projects. Future work would involve implementing temperature compensation techniques into the POFBG design, to obtain the Bragg wavelength response due to

water vapour alone. The next research stages would compare POFBGs against other technologies with greater sensitivity to water vapour (e.g. TDLAS) than the Pirani gauge and dew point sensors used in this project. For commercial applications in the medical and pharmaceutical industry, the device would need to be exposed to different sterilisation methods e.g. gamma radiation[244] and eventually tested in full scale freeze dryers using in industry.

The POFBG technology has numerous advantages for use in freeze drying applications, including:

- A batch measurement technique for detection of sublimation
- Non-invasive
- Sensitivity to low flow rate and volumes of water vapour subliming from a sample, which are required to detect end of primary drying time
- It has the potential to be a more cost-effective solution and offer a rapid payback time, compared to the commercial batch measurement techniques used in the freeze drying industry e.g. TDLAS is ~$100K USD and has additional costs (e.g. maintenance and modifications to freeze dryer).
- Does not require large modifications to the freeze dryer unit in order to implement the sensor as with other batch measurement techniques (e.g. TDLAS).

9.5.4   Scanning Electron Microscopy

The final morphology or structural architecture of biological samples and freeze dried cakes are commonly investigated using microscopy (e.g. scanning electron microscope (SEM)[19, 57, 65]).

This section will discuss the micrographs obtained of the freeze dried collagen samples that were exposed to different freeze drying procedures, as this could influence the morphology of the scaffolds and their functionality. The micrographs were acquired with the assistance of Professor Kameel Sawalha, using a Cambridge Stereoscan '90' Scanning Electron Microscope at an accelerating voltage of 25 kV and Orion 6.60.5 software.

Figure 132 and Figure 133 are representative micrographs of the structure of the freeze dried collagen samples discussed in sections 9.5.2 and 9.5.3 and monitored using POFBGs.

The gelatinized collagen samples (2.5mg/ml) were frozen overnight at -80°C, before being transferred to a -40°C precooled shelf in the freeze dryer. The -40°C shelf

temperature was held for 2hrs (freezing stage), before a ramp of 10°C/hr was applied in order to achieve a shelf temperature of 0°C during primary drying. The images show a matrix of collagen fibres and small pores between the structures (Figure 134). The small pore size was likely influenced by fast freezing the samples directly in a -80°C freezer before beginning lyophilisation. Literature states that a fast cooling rate, increased nucleation rate and low set shelf temperature, creates small ice crystals, hence small pore sizes in the final structure[33, 256-259]. The observations would support the trends reported in literature.
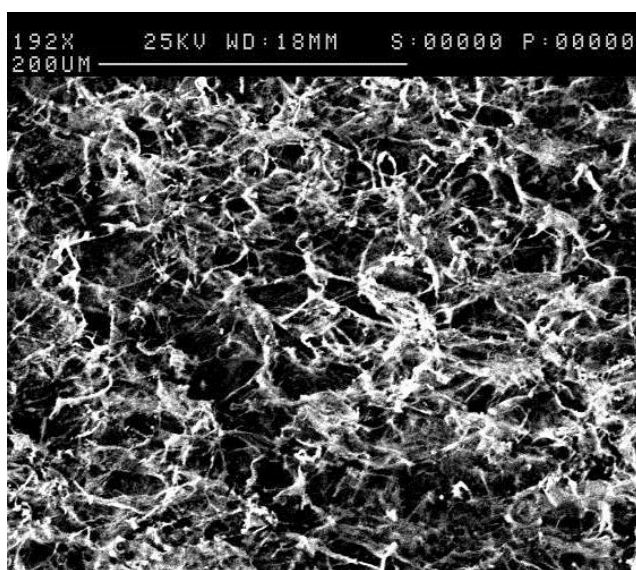
Figure 132 SEM image of the freeze-dried collagen sample
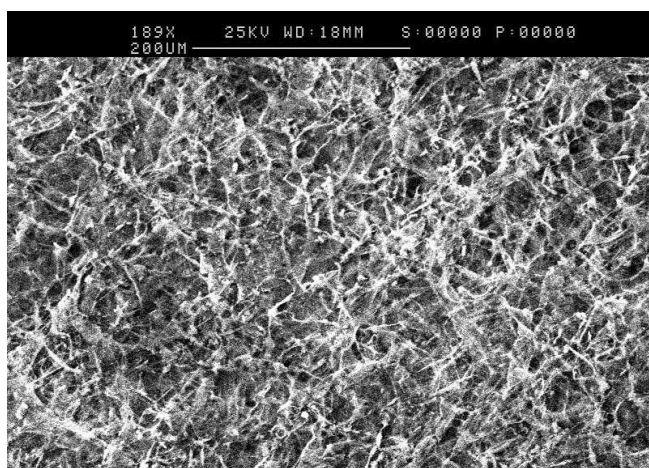
Figure 133 SEM image of the freeze-dried collagen sample
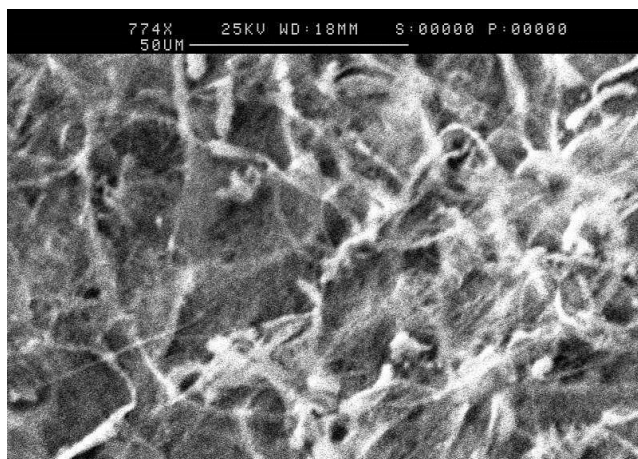
Figure 134 SEM image of the freeze-dried collagen sample

Figure 135 illustrates the results of a freeze dried collagen sample (2.5mg/ml) that had almost the same protocol as Figure 132, Figure 133 and Figure 134, however rather than a ramp of 10°C/hr after the freezing stage; a ramp of 1°C/min was applied in the primary drying stage. The images show the formation of layers of sheets of collagen fibres with a range of pore sizes throughout the internal interconnected structure.
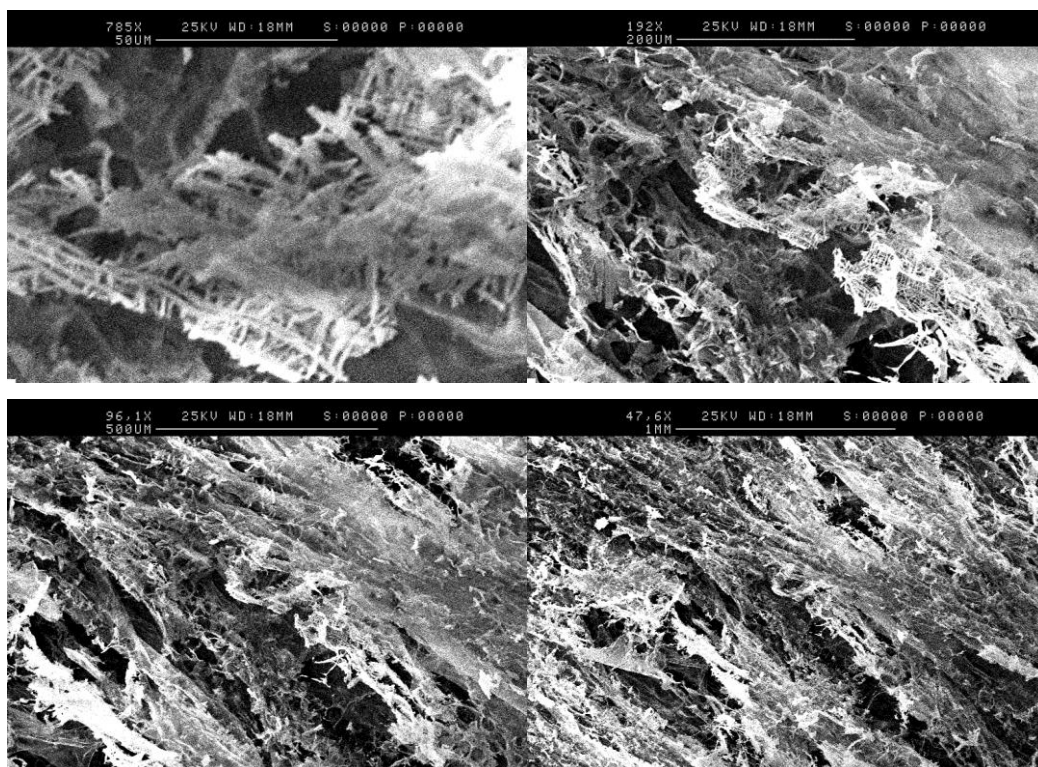
Figure 135 Series of SEM images at increased magnification of a freeze-dried collagen sample

The final experiment (Figure 136) took a sample frozen in a -80°C freezer and placed it onto a -20°C shelf temperature, rather than a -40°C shelf temperature used in the previous experiments. During the freezing stage, the temperature was maintained at -20°C for 2hrs before a ramp of 1°C/min was applied to achieve a shelf temperature of 0°C (primary drying), which was maintained for 17hrs. Figure 136 shows large pores present in the collagen matrix compared to the previous images, from the growth of ice crystals during the freezing stage. As a thermal hold (-20°C for 2hrs) was applied the structure annealed and promoted the growth of large crystals, which sublime during primary drying to leave large pores in the scaffold. This trend of using an annealing stage during freezing to increase to the pore size in collagen scaffolds is documented in literature[258].
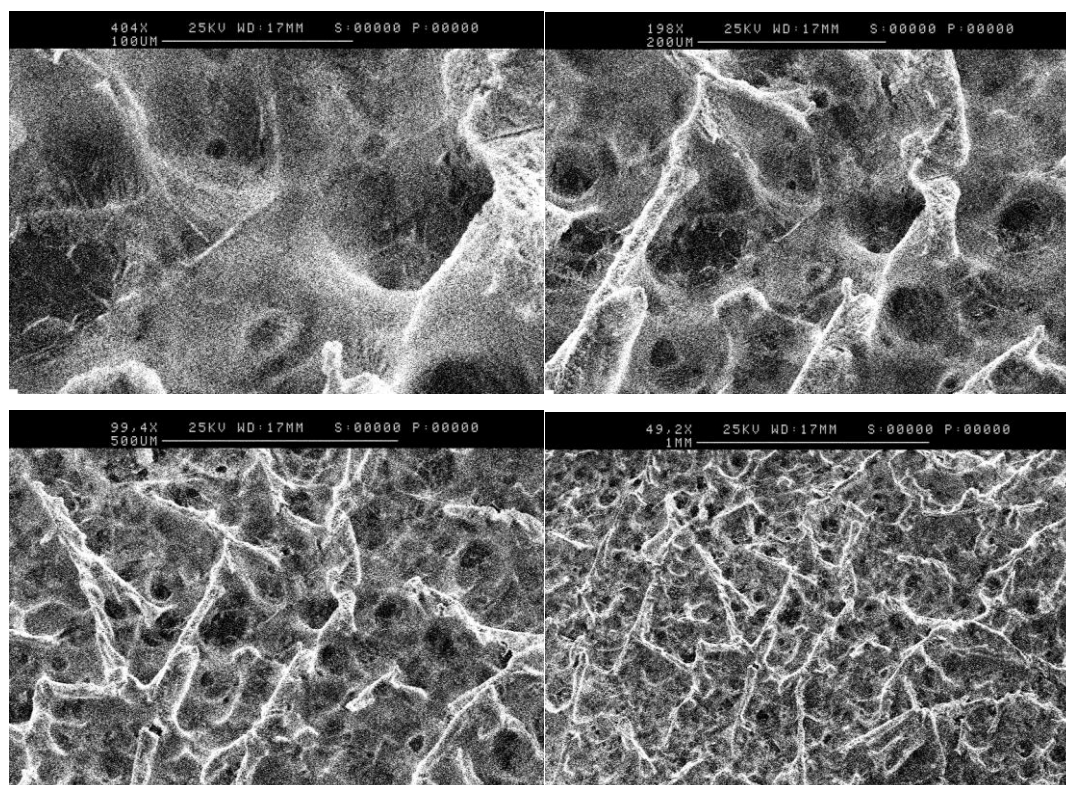
Figure 136 Series of SEM images at increased magnification of a freeze-dried collagen sample

9.6   Future work

This chapter describes the monitoring of the sublimation process of collagen and mannitol samples using PMMA and TOPAS POFBGs. Future projects would use these sensors and other types of POF materials, to monitor the freeze drying cycle of a variety of formulations used in commercial applications. The POFBGs would also be examined, to determine if the formulation constituents have caused damage to the sensors and determine the short term and long term implications of using these devices in a freeze dryer.

To achieve reproducible sensors with the desired characteristics for commercial applications, the manufacturing process of the POFBGs would need to be optimised and scaled-up for batch production.

As the target market for these sensors is the pharmaceutical industry, the reaction of the POFBGs to different sterilisation methods would need to be investigated in detail.

Radiative heat effects have been observed to influence the Bragg wavelength whilst monitoring sublimation. Future work would investigate different temperature compensation techniques, such as multiple FBGs on the same fibre, coating techniques etc. to compensate for the effects of temperature, in order to return the correct Bragg wavelength shift as a result of sublimation.

There was evidence to support the high sensitivity of PMMA POFBGs to small volumes of subliming water vapour into the chamber (2ml sample volume over several hours). In this case the Pirani gauge was unable to detect sublimation and the end of primary drying time as the flow rate fell within the noise range of that sensor. Future work would involve verifying and calibrating the POFBGs against other established technologies that monitor sublimation, such as TDLAS, MTM and freeze drying mass balance. The sample-thief technique could also be used to obtain a vial from the shelf at set time intervals for analysis (e.g. using Karl Fisher) to determine residual moisture content during primary drying.

The dew point sensor used in this project remained at -40°C and did not show an offset in the dew point reading during sublimation (primary drying). It is likely that the sensor in this project did not possess the correct specifications to detect the changes in gas composition in a freeze dryer. As literature [8, 57] reports that the dew point in the chamber is significantly lower than -40°C, future projects would involve using a calibrated -60°C dew point sensor or chilled mirror to baseline the POFBGs against.

9.7   Conclusion

This chapter investigated the application of POFBG technology with the goal to detect in the freeze dryer sublimation and the end of primary drying of a popular product constituent and a biological sample, used in the pharmaceutical and biomedical industries. Trials conducted using the POFBG sensors show the potential for these devices to be used to detect sublimation and the end of primary drying of mannitol, which is commonly used in the pharmaceutical industry as a bulking agent and collagen scaffolds for tissue engineering. Future work would involve verification against other established technologies such as TDLAS, MTM and a -60°C dew point sensor. The next trials would also involve investigating the sensors in research and industrial scale freeze dryers, where significantly larger sample volumes are freeze dried (>240 vials) than were in this project.

These trials were carried out after the previous chapters had characterised the sensors against critical CPPs known to vary in the vacuum chamber. These parameters included pressure, temperature and changes in the gas composition due to the introduction of water vapour into the chamber.

Chapters 8 and 9 conclude that these devices have the potential to detect sublimation and the end of primary drying time, satisfying the aims of this work.

As this chapter investigated only a small selection of materials, future work would involve trials monitoring sublimation of a larger range of pharmaceutical products used in commercial applications. These cycles will allow the sensors to be examined to determine the short and long term outcomes of using these devices in this environment.

As radiative effects were observed throughout these projects, future work would involve developing temperature compensation techniques to obtain a Bragg wavelength output specific to changes in the water vapour composition.

This section will discuss the areas identified within this thesis, which require further investigation. They include suggestions for modifications to the POFBG sensors and freeze dryer unit, before additional experiments in the chambers would be conducted to determine the commercial prospects of these devices.

10.1   POFBG manufacturing process

The next stages would involve additional studies and modifications to the design to tailor the device for commercial applications in the pharmaceutical industry with the following aims:

- Investigate the effect of different sterilisation techniques e.g. gamma radiation[244] on the operation of POFBGs.

- Test the sensors in a variety of models of full scale commercial production freeze dryers to determine any limiting factors to that application.

- Modifications to the housing structure and packaging of the FBGs, to optimise the size of the final sensor for commercial applications.

- Test FBGs that can operate in the 800nm spectral region (8dB/m at 830nm)[143], as this region has significantly lower attenuation than the 1550nm region(50dB/m at 1530nm) [178, 183].

- Using data obtained from the earlier aims, investigate the viability of POFBG sensors as a Process Analytical Technology (PAT) tool and carry out modifications to the design to ensure compatibility with existing freeze dryers for commercial applications.

Note:

PAT is an initiative introduced by the Food and Drug Administration (FDA) to design, analyse and control CPPs throughout the pharmaceutical manufacturing processes[7, 8, 76], to obtain the desired product quality.

Future work would involve modifications to the manufacturing process of POFBGs, to increase the fabrication success rate and the strength and stability of the spectra for commercial applications, by:

- Research to optimise the production of polymer optical fibres achieving reproducible consistent performance, particularly doped few and single mode fibres (e.g. dopants, drawing process, annealing, inscription etc.)
- Production of POF pigtails with demountable connectors as an alternative to POF spliced using UV curable glue to a silica pigtail

10.2 Development of POFBGs for vacuum chambers

Additional experiments on POFBG technology in vacuum chambers would be required, to characterise these devices as well as to optimise the design of the final sensor for the freeze drying industry.

10.2.1 Investigating changes in the properties of POF in the freeze dryer

The detailed mechanisms that affect the POF and POFBGs in the freeze drying chamber require identification and analysis.
The studies would involve placing the sensors within the freeze dryer or other pressure vessel and investigating the following:

- The effects of annealing POFs and POFBGs on the pressure sensitivity, thermo-optic and thermal expansion coefficients.
- Testing other POF materials such as polycarbonate (PC), polystyrene (PS), PMMA and TOPAS mPOF in vacuum conditions. This would provide information on their sensitivities to pressure, temperature or subliming water vapour. These materials would also be studied to develop sensors that comply with PAT requirements (e.g. sterilise in place requirements).
- Investigate how changes in the polymer composition, structure (step index vs microstructured), thermal treatment and manufacturing process of the POF influences the sensitivity of the sensors to pressure, temperature and sublimation.
- Investigate if etching the POFs influences the response time of the sensors in the freeze dryer
- Investigate the long term effects on these viscoelastic materials when exposed to vacuum conditions and during freeze drying cycles (i.e. creep, hysteresis, stress relaxation, sensor lifetime etc.)

10.2.2 Effect of pressure on POFBGs

- The non-linear sensitivities of PMMA and TOPAS POFBGs to pressure under sub-atmospheric conditions described in this thesis would require further investigation.
- Characterise the sensors in both sub-atmospheric and in high pressure climatic chambers to determine the scale of the non-linear relationship to pressure.

10.2.3 Effect of temperature on POFBGs

- Due in particular to the influence of radiative heat effects on POFBGs, the development and inclusion of appropriate temperature compensation techniques are needed. This would ideally remove all the additional signals (see the section 4.3 of the factors that affect the Bragg wavelength i.e. pressure and temp influence) from the output of the sensor apart from the humidity response (due to sublimation). This may be achieved through a number of methods, some examples include:
  - Multiple FBGs on the same POF where some are shielded (with packages, coatings etc.) from certain stimuli. An example of a temperature compensation technique applied to silica optical fibre sensor is shown in Figure 137.
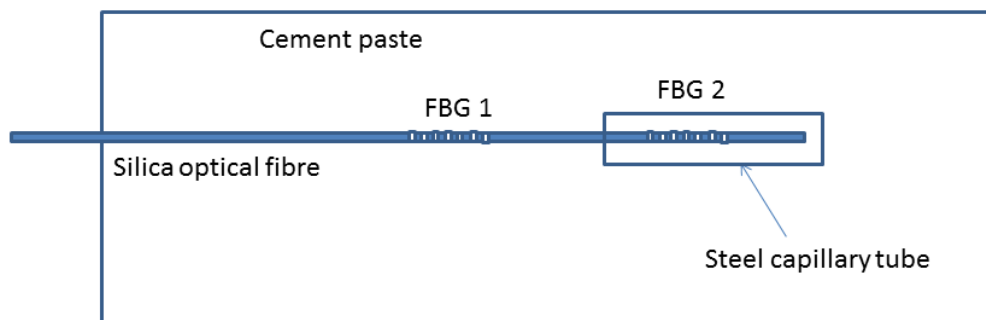
Figure 137 Example of Fibre Bragg Gratings inscribed in a silica optical fibre that are embedded in a cement specimen, where FBG1 senses both strain and temperature and FBG2 senses only temperature [260, 261]

  - Developing lookup tables of compensation values for variations in the additional stimuli.

- As freeze drying cycles can involve inlet shelf temperatures of <-20°C, the POFBGs would need to be characterised at these conditions for commercial applications

- The POFBGs could be placed directly into pharmaceutical or biological samples to determine if product temperature can be accurately monitored during freeze drying.
- Use a series of POFBGs to map the temperature differences within the freeze dryer e.g. to determine changes in heat transfer across the shelf.

10.2.4 Influence of sublimation of water vapour on POFBGs

- PMMA POFBGs would be used to monitor sublimation from different standard formulations attached to the access port or placed directly onto the shelf in the freeze dryer. This will allow direct comparisons to be made of these profiles captured by classical sensors and POFBG's.
- Freeze drying different formulations with POFBGs present in the chamber. This could determine if any of the volatile compounds that escape during freeze drying are compatible with or could cause damage to the sensor.
- The red shift in the Bragg wavelength of TOPAS POFBG in the presence of subliming water vapour would require further investigation, as literature reports this material to be humidity insensitive[18, 162].
- Modelling of sorption and desorption of water from POFs within the freeze drying environment, to determine the exact mechanism by which the rapid changes in humidity affect the fibre.
- Compare the performance of POFBGs against other established technologies such as TDLAS, MTM, -60°C dew point sensor, chilled mirror and freeze drying mass balance. These types of sensors could allow:
  - Calibration against established technologies
  - To determine if POFBGs can be used to accurately detect changes in the mass flow rate during primary drying
  - To determine if POFBGs can detect trace quantities of water vapour in the chamber and that lowest value.
- Experiments to detect changes in the fibre length, polarisation, torsion or motion during the sublimation of water vapour

10.3   Freeze dryer modifications

Investment in modifying the freeze drying vessel used in this project, would expand the range of experiments that can be carried out on POFBGs and reduce sources of noise in the data by:

- Optimising the feedthrough connector to allow multiple sensors into the chamber whilst minimising air leaks.

- Installing a new PLC (including PID controller option) would allow more customised cycles to be programmed for characterisation of the POFBGs i.e. across a wider temperature and pressure range than offered by the Freeze Dryer's current system.

- The use of a modified PLC and PID controller along with additional components in the machine (e.g. analogue solenoid valve), would allow a reduction in the magnitude of the ringing of CPPs (pressure and temperature).

- The modified PLC unit would allow simultaneous logging of the data from the sensors with all signals referenced to the PLC's internal clock. By connecting the sensors (including POFBGs) to the PLC unit, the user could investigate the response time of POFBGs to step changes in CPPs. Programming the PLC to respond to patterns in the data could be used to detect end of primary drying time and automatically start secondary drying.

11   Conclusions

This chapter summarises the advancements achieved in this project and previously discussed in this thesis, in relation to the use of POFBG sensors to monitor CPPs in the freeze-drying environment and detection of sublimation during the primary drying stage.

The primary drying stage is the longest and most costly stage in the freeze-drying cycle. As a result, extensive research has been dedicated to optimising this stage, to reduce production costs and increase productivity. This often involves the use of different types of sensors some of which are part of commercial freeze-drying units (e.g. thermocouples, TDLAS), to determine the end of primary drying time during the manufacturing process.

The initial objectives of this thesis were to determine if POFBG technology could survive and function in the freeze-drying chamber, which has not been previously reported in literature. As that stage proved successful, the next logical step involved characterising the sensors against common CPPs that POFBGs could be exposed to in this environment. After characterisation, the sensors were used in 'real life' tests to determine if sublimation and end of primary drying time of pharmaceutical and biological samples could be identified.

A primary area of interest for this research project was to determine if POFBG technology could have applications in the freeze-drying industry and have the potential to be a cost effective batch measurement solution for the pharmaceutical industry in particular.

The objectives of the thesis were:

- Develop a housing structure that could successfully protect the POFBG sensors (SM PMMA and MM TOPAS POFBG) in the freeze drying environment
- Determine the response of POFBGs to typical temperatures within the freeze dryer at sub-atmospheric pressure and dry conditions of -40°C dew point
- Characterise the sensors at sub-atmospheric pressure conditions (in the 200μbar region) in a dry nitrogen environment (-40°C dew point)
- Investigate potential long term implications of exposing POFBGs to sub-atmospheric conditions (40days)
- Compare the performance of the fabricated PMMA and TOPAS POFBG in the freeze drying environment. PMMA has an affinity for water vapour and was used

to determine if sublimation could be monitored during primary drying. In literature, TOPAS was determined to be insensitive to humidity at atmospheric conditions and was selected to serve as a control for these experiments.

- Observe the effects of backfilling the chamber from sub-atmospheric conditions (2500μbar) to 1atm with dry nitrogen gas on POFBGs (dried for 24hrs at 2500μbar).
- Investigate the response of POFBGs in dry nitrogen gas at 1atm pressure, to the introduction of water vapour when the chamber door was opened.
- Determine if POFBGs could be used to detect sublimation under sub-atmospheric conditions (using frozen mannitol and water samples). The following experiments were carried out at sub-atmospheric pressure:
    - POFBGs were used to monitor water vapour that was introduced at controlled times through the access port of the freeze dryer, whilst maintaining a constant pressure and inlet shelf temperature
    - POFBGs were subjected to step changes in pressure in a dry nitrogen atmosphere and compared against step changes in pressure when water vapour was introduced through the access port
    - POFBGs monitored during a freeze-drying cycle, samples of mannitol or water that were placed onto the shelf, to determine if the sublimation of water vapour could be detected
- Determine if POFBGs could be used to monitor sublimation and detect end of primary drying time of native collagen, which has applications for tissue engineering.

The listed objectives were achieved in this thesis and the conclusions from the research will be outlined in the following paragraphs.

Housing structure

Initial trials involved placing anemometers within the freeze drying chamber to determine the strength of the wind speeds that the POFBGs would have to endure. Some experienced catastrophic failure during the initial stages of freeze drying, during the initial step change in pressure from 1atm to 200μbar to promote sublimation. Some anemometers survived for a sufficient amount of time to provide information on flow rate during the step change in pressure. The anemometers and literature revealed that during the freeze drying process wind speeds greater than

20m/s could be experienced within this environment, however during primary drying much lower speeds were commonplace.

POFBG sensors were placed into different housing configurations and inserted into the machine to develop a suitable device that would allow the POFBGs to be protected and characterised against controlled CPPs within the freeze dryer. The final design involved placing the POFBGs into customised protective sleeves that were attached to a temperature stabilising metal sheet. This configuration proved successful in protecting the POFBGs within the enclosure, whilst allowing exposure to the atmosphere in order to track changes in gas composition in the chamber (i.e. the introduction of water vapour).

Temperature characterisation

SM PMMA and MM TOPAS POFBGs were characterised at sub-atmospheric pressure (200µbar) in a nitrogen based atmosphere at -40°C dew point. The Bragg wavelengths of all the POFBGs red shifted as the inlet shelf temperature decreased from 20°C to -20°C and the temperature in the vicinity of the POFBG dropped. Literature reports that at 1atm pressure and in a controlled humid environment, the Bragg wavelength of the POFBGs increases with a decrease in temperature due to the dominance of the negative thermo-optic coefficient.

The POFBGs and thermocouples were also used to study the influence of radiative heat effects (e.g. solar gain) on the sensors in the vacuum chamber and map the temperature profile across the shelf as these factors have a direct influence on sublimation rate.

It was determined that drifts in temperature from radiative heat effects can be caused by a variety of external factors including solar gain and increase in the room temperature. The drifts in the temperature within the vacuum chamber were monitored by the thermocouples and the POFBGs across the day, despite the shelf inlet temperature remaining stable about the set point value. Future work would involve incorporating temperature compensation techniques into the POFBG design to remove the influence of temperature on the Bragg wavelength for commercial applications.

Pressure characterisation

After determining the sensitivities of the POFBGs to temperature variations in the vacuum chamber with dry nitrogen conditions, it was necessary to characterise the sensors to changes in pressure. The fibres were dried in the vacuum chamber for a minimum of 24hrs before being subjected to pressure step changes between 200μbar and 2500μbar, as this was the maximum operating range for this customised unit.

The results revealed that the Bragg wavelengths of TOPAS and PMMA POFBGs decreased as the chamber pressure was reduced, for a constant shelf inlet temperature and in dry nitrogen conditions. The experiments also revealed that the fibres experienced non-linear tendencies within the 200μbar to 2500μbar region (n=3) at -40°C dew point, particularly when compared to literature that reported sensitivities in high pressure chamber vessels.

The POFBG temperature was measured using a thermocouple, as literature reports that radiative effects influence the temperature in the vacuum chamber. The temperature studies described in this thesis revealed that the radiative heat effects influenced the Bragg wavelength of POFBGs and therefore required constant monitoring during the pressure studies.

Despite observing drifts in the Bragg wavelength due to radiative heat effects, their magnitude was deemed insufficient to account for the increased POFBG sensitivity to pressure in the vacuum chamber. It was hypothesised that the drying process of the fibre coupled with the pressure region investigated could have influenced the strain-optic tensor components; however this would require further investigation as the exact mechanism is not fully understood.

The effect of exposing POFBGs to sub-atmospheric pressures for 40 days was investigated and revealed that a reversible blue shift in the Bragg wavelength occurred. This area would require further trials to determine the long term viability of using POFBGs in freeze drying applications.

Influence of sublimation of water vapour on POFBGs

After characterising the TOPAS and PMMA POFBGs to changes in temperature and pressure in the freeze-drying chamber, the next stage involved exposing the sensors to changes in the water vapour gas composition.

This involved carrying out experiments in both atmospheric and sub-atmospheric conditions, where water vapour was introduced into the freeze dryer at controlled

times, after the fibres had been previously dried in the chamber for a minimum of 24hrs.

The results revealed that both PMMA and TOPAS POFBGs red shifted in response to an increase in pressure (in dry nitrogen atmosphere) and an increase in humidity at atmospheric pressure when the door was opened. They show a potential application for detecting leaks in the system or providing information on any humidity transfer through the dry nitrogen environment.

The POFBGs were placed into the chamber filled with a dry nitrogen atmosphere at sub-atmospheric pressures and then exposed to the sublimation of water vapour at controlled times, from samples of frozen mannitol and distilled water. The Bragg wavelengths were observed to red shift in the presence of subliming water vapour in the chamber. At the same time a shift in the pressure reading of the Pirani gauge was also observed, which is a device documented in literature to be commonly used to monitor sublimation in a freeze dryer and end of primary drying time.

These results show the potential for POFBGs to be used to monitor sublimation during freeze drying applications and determine the end of primary drying time for their target market within the pharmaceutical industry.

<u>POFBGs used to monitor freeze drying of mannitol and native collagen samples</u>

Once the PMMA and TOPAS POFBGs were characterised against typical CPPs in the freeze dryer i.e. temperature, pressure, sublimation of water vapour, a practical demonstration of their ability to monitor freeze drying could be carried out.

This involved using POFBG technology to monitor sublimation of a popular constituent and biological sample, used in the pharmaceutical and biomedical industries. These trials involved monitoring the sublimation of mannitol, which is commonly used in the pharmaceutical industry as a bulking agent and collagen as a scaffold material for tissue engineering applications.

These trials showed that the POFBGs have the potential to be used for detecting sublimation and the end of primary drying time, satisfying the aims of this project. Future work would involve developing temperature compensation techniques, to obtain a Bragg wavelength output specific to changes in water vapour concentration and using the sensors to monitor a larger range of pharmaceutical products used in commercial applications.

References

1. Gross JH. Mass spectrometry : a textbook: Berlin ; New York: Springer, 2004.; 2004.
2. Harris NS. Modern vacuum practice: London : McGraw-Hill, 1989.; 1989.
3. Aulton ME. Aulton's Pharmaceutics: The Design and Manufacture of Medicines. . third ed: Churchill Livingstone Elsevier; 2007. p. 435-40.
4. Meister E, Sasic S, Gieseler H. Freeze-dry microscopy: impact of nucleation temperature and excipient concentration on collapse temperature data. AAPS PharmSciTech. 2009;10(2):582-8.
5. Martin Christ. Smart freeze Drying: Basic Principles, optimum procedures and applications2010 [cited 2017 20/2/2017]:[1-54 pp.]. Available from: https://www.martinchrist.de/fileadmin/user_upload/christ/04_anwendungen/lyophil isation/Smart_FD_Basics_Apps_en.pdf.
6. Rey L, May JC. Freeze-drying/lyophilization of pharmaceutical and biological products May JC, Rey L, editors. New York Marcel Dekker Inc; 1999.
7. Mayeresse Y, Veillon R, Sibille PH, Nomine C. Freeze-drying process monitoring using a cold plasma ionization device. PDA journal of pharmaceutical science and technology / PDA. 2007;61(3):160-74.
8. Patel SM, Doen T, Pikal MJ. Determination of end point of primary drying in freeze-drying process control. AAPS PharmSciTech. 2010;11(1):73-84.
9. Rambhatla S, Pikal MJ. Heat and mass transfer scale-up issues during freeze-drying, I: atypical radiation and the edge vial effect. AAPS PharmSciTech. 2003;4(2):E14.
10. Ratti C. Hot air and freeze-drying of high-value foods: a review. Journal of Food Engineering. 2001;49(4):311-9.
11. Kasper JC, Friess W. The freezing step in lyophilization: physico-chemical fundamentals, freezing methods and consequences on process performance and quality attributes of biopharmaceuticals. European journal of pharmaceutics and biopharmaceutics : official journal of Arbeitsgemeinschaft fur Pharmazeutische Verfahrenstechnik eV. 2011;78(2):248-63.
12. Webb DJ. Polymer Fibre Bragg Grating Sensors and their Applications. In: Rajan G, Iniewski K, editors. Optical fiber sensors : advanced techniques and applications: Boca Raton : CRC Press 2015.
13. Bhowmik K, Ambikairajah E, Peng G-D, Luo Y, Rajan G. High-sensitivity polymer fibre Bragg grating sensor for biomedical applications. 2016 IEEE Sensors Applications Symposium (SAS). 2016:1.
14. Zhang W, Webb DJ. Humidity responsivity of poly(methyl methacrylate)-based optical fiber Bragg grating sensors. Optics Letters. 2014;39(10):3026.
15. Zhang C. Fibre Bragg gratings in polymer optical fibre for applications in sensing [Doctoral dissertation]. UK: Aston University; 2012.
16. Shen J, Chen CC, Sauer JA. Polymer paper: Effects of sorbed water on properties of low and high molecular weight PMMA: 1. Deformation and fracture behaviour. Polymer. 1985;26:511-8.
17. Turner DT. Polymer paper: Polymethyl methacrylate plus water: sorption kinetics and volumetric changes. Polymer. 1982;23:197-202.
18. Yuan W, Khan L, Webb DJ, Kalli K, Rasmussen HK, Stefani A, et al. Humidity insensitive TOPAS polymer fiber Bragg grating sensor. Optics Express. 2011;19(20):19731-9.
19. Costantino HR, Pikal MJ. Lyophilization of biopharmaceuticals USA: american association of pharmaceutical scientists; 2004.

20. Aschenbrenner M, Foerst P, Kulozik U. Freeze-drying of Probiotics. In: Foerst P, Santivarangkna C, editors. Advances in Probiotic Technology: CRC Press; 2015. p. 213-41.
21. Franks F. Freeze-drying of bioproducts: putting principles into practice. European Journal of Pharmaceutics and Biopharmaceutics. 1998;45(3):221-9.
22. Tang XC, Nail SL, Pikal MJ. Freeze-drying process design by manometric temperature measurement: design of a smart freeze-dryer. Pharmaceutical research. 2005;22(4):685-700.
23. Jinsong L. Physical Characterization of Pharmaceutical Formulations in Frozen and Freeze-Dried Solid States: Techniques and Applications in Freeze-Drying Development. Pharmaceutical Development & Technology. 2006;11(1):3-28.
24. Pikal MJ. Freeze Drying. In: SWARBRICK J, editor. Encyclopedia of Pharmaceutical Technology. 3 ed ed. New York: Informa Healthcare; 2007.
25. Petzold G, Aguilera JM. Ice Morphology: Fundamentals and Technological Applications in Foods. Food biophysics. 2009(4).
26. Fissore D, Pisano R, Barresi AA. Applying quality-by-design to develop a coffee freeze-drying process. Journal of Food Engineering. 2014;123:179-87.
27. Liapis AI, Sadikoglu H. Dynamic Pressure Rise in the Drying Chamber as a Remote Sensing Method for Monitoring the Temperature of the Product During the Primary Drying Stage of Freeze Drying. DRYING TECHNOLOGY. 1998;16(6):1153-71.
28. Oetjen G-W, Haseley P. Freeze-Drying volume 2. Germany: John Wiley & Sons; 2008.
29. Greensmith M. Practical dehydration. : Cambridge, England : Woodhead Pub., 1998. 2nd ed.; 1998.
30. Hua T, Liu B, Zhang H. Freeze-drying of pharmaceutical and food products. Cambridge: Woodhead Publishing Ltd; 2010. xvi + 257 pp. p.
31. Offeddu GS, Ashworth JC, Cameron RE, Oyen ML. Multi-scale mechanical response of freeze-dried collagen scaffolds for tissue engineering applications. Journal of the Mechanical Behavior of Biomedical Materials. 2015;42:19-25.
32. Davidenko N, Campbell JJ, Thian ES, Watson CJ, Cameron RE. Collagen–hyaluronic acid scaffolds for adipose tissue engineering. Acta Biomaterialia. 2010;6(10):3957-68.
33. Pawelec KM, Husmann A, Best SM, Cameron RE. Understanding anisotropy and architecture in ice-templated biopolymer scaffolds. Materials Science and Engineering: C. 2014;37:141-7.
34. Rindler V, Lüneberger S, Schwindke P, Heschel I, Rau G. Freeze-Drying of Red Blood Cells at Ultra-Low Temperatures. Cryobiology. 1999;38(1):2-15.
35. Rey L, May JC. Freeze-drying/lyophilization of pharmaceutical and biological products 3rd ed. May JC, Rey L, editors. London: Informa Healthcare; 2010.
36. Varshney D, Singh M. Lyophilized Biologics and Vaccines Modality-Based Aproaches. Varshney D, Singh M, editors. New York: Springer; 2015.
37. Siew A. Freeze Drying Protein Formulations. Common challenges and key considerations when developing a freeze-drying cycle for protein pharmaceuticals. Pharmaceutical Technology Europe. 2014;38(5).
38. Salvatore AV, Valeria R, Antonello AB. Dynamic Parameters Estimation Method: Advanced Manometric Temperature Measurement Approach for Freeze-Drying Monitoring of Pharmaceutical Solutions. Industrial & Engineering Chemistry Research. 2008;47(21):8445-57.
39. King CJ. Freeze-Drying of Foods. London: Butterworths; 1971.
40. Goldblith SA, Rey L, Rothmayr WW. Freeze drying and advanced food technology: Academic Press; 1975.
41. Niazi SK. Handbook of Pharmaceutical Manufacturing Formulations: Sterile Products 2nd ed. London: CRC Press; 2004.

42. Oetjen GW, Haseley P, Klutsch H, Leineweber M, inventors; Steris Gmbh, assignee. Method for controlling a freeze drying process US 6163979 A. Germany2000.
43. Jameel F, Kessler WJ. Real-Time Monotoring and Controlling of Lyophilization Process Parameters through Process Analytical Technology Tools. In: Undey C, Low D, Menezes JC, Koch M, editors. PAT Applied in Biopharmaceutical Process Development And Manufacturing: An Enabling Tool for Quality-by-Design. USA: CRC Press; 2011.
44. Sattler K, Feindt HJ. Thermal Separation Process principles and design. Federal Republic of Germany: VCH Verlagsgesellschaft Weiheim and VCH Publishers USA; 1995.
45. Nazari K. Some studies using LyoDEA as an in-line process analytical technology for freeze-drying. De Montfort University: De Montfort University; 2012.
46. Pikal MJ, Roy ML, Shah S. Mass and heat transfer in vial freeze-drying of pharmaceuticals: role of the vial. Journal Of Pharmaceutical Sciences. 1984;73(9):1224-37.
47. Visioli A. Practical PID control. London: Springer-Verlag 2006.
48. IPEC-Americas. International Pharmaceutical Excipients Council of the Americas FAQs. Available from: http://ipecamericas.org/about/faqs.
49. Biopharmatechnology. Glossary n.d. [cited 2016 10 Oct]. Available from: http://biopharma.co.uk/intelligent-freeze-drying/knowledge-zone/glossary/.
50. Baheti A, Kumar L, Bansal AK. Excipients used in lyophilization of small molecules. Journal of Excipients & Food Chemicals. 2010;1(1):41-54.
51. McNally EJ, Hastedt JE. Protein formulation and delivery, second edition. New York: Informa Healthcare USA c2008.; 2008.
52. Searles JA, Carpenter JF, Randolph TW. Annealing to optimize the primary drying rate, reduce freezing-induced drying rate heterogeneity, and determine T(g)' in pharmaceutical lyophilization. J Pharm Sci. 2001;90(7):872-87.
53. Tang X, Pikal MJ. Design of freeze-drying processes for pharmaceuticals: practical advice. Pharmaceutical research. 2004;21(2):191-200.
54. Franks F, Auffret T. Freeze-drying of pharmaceuticals and biopharmaceuticals.: Cambridge : RSC Pub., c2007.; 2007.
55. Searles JA, Carpenter JF, Randolph TW. The ice nucleation temperature determines the primary drying rate of lyophilization for samples frozen on a temperature-controlled shelf. Journal of Pharmaceutical Sciences. 2001;90:860-71.
56. British Pharmacopoeia Commission Office. British Pharmacopoeia Volume V-Appendix V N. Osmolality. London: Stationery Office; 2013.
57. Schneid SC. Investigation of Novel Process Analytical Technology (PAT) Tools for Use in Freeze-Drying Processes [Doctoral dissertation]. Germany: Friedrich-Alexander University of Erlangen - Nuremberg 2009.
58. BTL. Lyotherm2 Thermal Analysis for Freeze Drying n.d. [cited 2017 20/1]. Available from: http://www.spincotech.com/llp/brochures/btl/Lyotherm.pdf.
59. Hottot A, Vessot S, Andrieu J. Freeze drying of pharmaceuticals in vials: Influence of freezing protocol and sample configuration on ice morphology and freeze-dried cake texture. Chemical Engineering and Processing: Process Intensification. 2007;46(7):666-74.
60. Hui YH. Handbook of Fruits and Fruit Processing. USA: Blackwell Publishing; 2006.
61. Rahman S. Handbook of food preservation. Boca Raton: CRC Press; 2007.
62. Bhatnagar BS, Bogner RH, Pikal MJ. Protein Stability During Freezing: Separation of Stresses and Mechanisms of Protein Stabilization. Pharmaceutical Development & Technology. 2007;12(5):505-23.

63. Scott KL, Lecak J, Acker JP. Biopreservation of Red Blood Cells: Past, Present, and Future. Transfusion Medicine Reviews. 2005;19(2):127-42.
64. Loser Messtechnik. Loser Manual Micro-Osmometer Type 6. 2008.
65. Ekenlebie EP. Pharmaceutical process optimisation of bulk lyophilisates : implications of powder handling [Doctoral dissertation]. UK: Aston University; 2015.
66. Chen R, Slater NK, Gatlin LA, Kramer T, Shalaev EY. Comparative rates of freeze-drying for lactose and sucrose solutions as measured by photographic recording, product temperature, and heat flux transducer. Pharmaceutical development and technology. 2008;13(5):367-74.
67. Milton N, Pikal MJ, Roy ML, Nail SL. Evaluation of manometric temperature measurement as a method of monitoring product temperature during lyophilization. PDA journal of pharmaceutical science and technology / PDA. 1997;51(1):7-16.
68. Mascarenhas WJ, Akay HU, Pikal MJ. A computational model for finite element analysis of the freeze-drying process. Computer Methods in Applied Mechanics and Engineering. 1997;148(1):105-24.
69. Kuu WY, Nail SL, Sacha G. Rapid determination of vial heat transfer parameters using tunable diode laser absorption spectroscopy (TDLAS) in response to step-changes in pressure set-point during freeze-drying. Journal Of Pharmaceutical Sciences. 2009;98(3):1136-54.
70. Ghoshdastidar PS. Heat transfer. : New Delhi : Oxford University Press, Second edition.; 2012.
71. Kondepudi D, Prigogine I. Modern Thermodynamics. : From Heat Engines to Dissipative Structures: Hoboken : Wiley, 2014. 2nd ed.; 2014.
72. Incropera FP, Dewitt DP, Lavine AS, Bergman TL. Fundamentals of heat and mass transfer: John Wiley & Sons Inc. 7th ed. ; 2011.
73. Rambhatla S, Tchessalov S, Pikal MJ. Heat and mass transfer scale-up issues during freeze-drying, III: control and characterization of dryer differences via operational qualification tests. AAPS PharmSciTech. 2006;7(2):E39-E.
74. Duncan D. Headspace Moisture Analysis for Determination of Residual Moisture Content in Lyophilized Pharmaceutical Products. Pharmaceutical Technology Europe. 2016;40(4):28-31.
75. Fissore D, Pisano R, Barresi AA. Pharmaceutical Technology: Monitoring of the Secondary Drying in Freeze-Drying of Pharmaceuticals. Journal of Pharmaceutical Sciences. 2011;100:732-42.
76. Rathore AS, Bhambure R, Ghare V. Process analytical technology (PAT) for biopharmaceutical products. Analytical and bioanalytical chemistry. 2010;398(1):137-54.
77. Patel SM, Jameel F, Pikal MJ. The effect of dryer load on freeze drying process design. J Pharm Sci. 2010;99(10):4363-79.
78. Mangold A. TEMPRIS® PAT TOOL Precise Measurement of Product Temperature in Lyophilization by iQ-mobil solutions GmbH. . 5th International Conference on Lyophilization and Freeze Drying Bologna [Internet]. 2012. Available from: http://islyophil.us.cloudlogin.co/wp-content/uploads/2013/05/Bologna_2012_Mangold2.pdf.
79. Morris AS, Langari R. Measurement and Instrumentation - Theory and Application. Elsevier; 2012.
80. Roy ML, Pikal MJ. Process control in freeze drying: determination of the end point of sublimation drying by an electronic moisture sensor. Journal of parenteral science and technology : a publication of the Parenteral Drug Association. 1989;43(2):60-6.

81. Patel SM, Pikal M. Process Analytical Technologies (PAT) in freeze-drying of parenteral products. Pharmaceutical Development & Technology. 2009;14(6):567-87.
82. Brulls M, Folestad S, Sparen A, Rasmuson A. In-situ near-infrared spectroscopy monitoring of the lyophilization process. Pharmaceutical research. 2003;20(3):494-9.
83. De Beer TRM, Vercruysse P, Burggraeve A, Quinten T, Ouyang J, Zhang X, et al. In-line and real-time process monitoring of a freeze drying process using Raman and NIR spectroscopy as complementary process analytical technology (PAT) tools. Journal of Pharmaceutical Sciences. 2009;98:3430-46.
84. Gieseler H. Product Morphology and Drying Behavior delineated by a new Freeze-Drying Microbalance [PhD]. Germany: University of Erlangen-Nuremberg; 2004.
85. Wilson JS. Sensor Technology Handbook. USA: Elsevier; 2005.
86. Carleton fj, Agalloco Jp. Validation of Pharmaceutical Processes. second edition ed. New York: Marcel Dekker Inc; 1999.
87. Newport Omega. Complete Measurement, Control and Automation Handbook and Encyclopedia. UK: Omega engineering Inc; 2008.
88. Shtargot J, Mirza S. Modern Thermocouples and a High-Resolution Delta-Sigma ADC Enable High-Precision Temperature Measurement. Maxim Integrated Products, 2011.
89. Kasper JC, Wiggenhorn M, Resch M, Friess W. Implementation and evaluation of an optical fiber system as novel process monitoring tool during lyophilization. European Journal of Pharmaceutics and Biopharmaceutics. 2013;83(3):449-59.
90. Kasper JC. Lyophilization of Nucleic Acid Nanoparticles Formulation Development, Stabilization Mechanisms, and Process Monitoring Munich, Germany: Ludwig-Maximilians-University; 2012.
91. Friess W, Resch M, Wiggenhorn M, inventorsDryer with monitoring device US 8,919,007 B2. Germany2014.
92. Cusano A, Cutolo A, Albert J. Fiber Bragg grating sensors: recent advancements, industrial applications and market exploitation. Saif Zone, Sharjah, United Arab Emirates: Bentham Science Publishers Ltd.; 2011.
93. Zhang W, Abang A, Webb DJ, Peng GD. An investigation into the wavelength stability of polymer optical fibre Bragg gratings IN: Micro-structured and specialty optical fibres. Kalli, Kyriacos and Mendez, Alexis (eds) 2012;8426.
94. Schneid SC, Gieseler H, Kessler WJ, Luthra SA, Pikal MJ. Optimization of the secondary drying step in freeze drying using TDLAS technology. AAPS PharmSciTech. 2011;12(1):379-87.
95. FDA. Center for Biologics evaluation and Research Guideline for the determination of Residual Moisture in Dried Biological Products. Bethesda: Food and Drug Administration, 1990.
96. Chen Z, Lu C. Humidity Sensors: A Review of Materials and Mechanisms. Sensor Letters. 2005;3(4):274-95.
97. GEA Pharma Systems. GEA Lyophil LYOPLUS Multipurpose measurement device for pharmaceutical freeze dryers2012 20/1/17. Available from: http://www.gea.com/en/binaries/LYOPLUS-measurement-device-pharma-freeze-dryers-flyer-EN_tcm11-16727.pdf.
98. MKS Instruments Inc. Silicone Oil Leakage -Detection in Freeze Dryer Systems. Application Note [Internet]. 2013 20/1/17. Available from: http://www.aiv.it/wp-content/uploads/2015/09/art2-MKS-V2000P-Leakage-AppNote1.pdf.
99. GEA Pharma Systems. LYOPLUS™ PAT for Pharma Freeze Dryers 2016 [cited 2017 20/1]. Available from: http://www.gea.com/en/products/lyoplus-process-analytical-technology.jsp.

100. Eva H. HOF MASS ANALYZER- Quality control for pharmaceutical freeze drying equipment n/d [cited 2017 20/1]. Available from: http://www.hof-sonderanlagen.de/en/home/news/article/hof-massanalyzer-qualitaets-br-ueberwachung-in-pharmazeutischen-gefriertrocknungsanlagen.html.

101. Reihbandt T. Millrock Technology: Some Common Methods Used to Detect the End of Primary Drying. Lyosight [Internet]. 2016 4/10/16. Available from: http://www.millrocktech.com/wp-content/uploads/2016/07/Tech-Note-Common-Methods-to-Detect-the-End-of-Primary-Drying.pdf.

102. National Physical Laboratory. A guide to the Measurement of Humidity. London: Institute of Measurement and Control; 1996.

103. Postolache O, Silva Girao PMBS, Pereira JMD, Ramos HG. Dew Point and Relative-Humidity Smart Measuring System. Instrumentation and Measurement, IEEE Transactions on. 2006;55(6):2259-64.

104. MKS Instruments Inc. The Basics of Pressure Measurement and Capacitance Manometers. Application Note. 2013(Andover (USA)).

105. Millrock Technology Inc. Vacuum Pressure Measurement Gauges. Freeze drying/Lyophilization Tech Note [Internet]. 2007 4/10/16. Available from: http://freezedryinginfo.com/PDF_Files/MillrockVacuumPressureGauges.pdf.

106. Osborn G, Hansen S. Calibration of Lyophilization Pressure Gauges. Pharmaceutical Technology, Wilmington, USA, Advanstar [Internet]. June 2002 1/1/2017. Available from: https://www.mksinst.com/docs/R/Z130.pdf.

107. DUNIWAY STOCKROOM Corp. Instruction Manual thermocouple Gauge Control Units Models TCG-531 & TCG-531/2 Models TCG-06M & TCG-06M/2. USA [Internet]. 1998 1/1/2017. Available from: https://www.duniway.com/images/_pg/manual-TCG531-06M.pdf.

108. Tenedini KJ, Bart Jr. SG, inventors; S.P. Industries, Inc., The Virtis division (Gardiner, NY), assignee. Freeze drying methods employing vapor flow monitoring and/or vacuum pressure control United States2001.

109. Barresi A, Fissore D. Modern drying technology, Volume 3: Product Quality and Formulation. 3. Weinheim, Germany: John Wiley & Sons; 2011.

110. Couriel B. Advances in lyophilization technology. Bulletin of the Parenteral Drug Association. 1977;31(5):227-36.

111. Fissore D, Pisano R, Barresi AA, inventors; Telstar Technologies, S.L., assignee. Method for monitoring primary drying of a freeze-drying process EP 2516948 A22012.

112. Gieseler H, Kessler WJ, Finson M, Davis SJ, Mulhall PA, Bons V, et al. Evaluation of tunable diode laser absorption spectroscopy for in-process water vapor mass flux measurements during freeze drying. Journal Of Pharmaceutical Sciences. 2007;96(7):1776-93.

113. Schneid SC, Gieseler H, Kessler WJ, Pikal MJ. Non-invasive product temperature determination during primary drying using tunable diode laser absorption spectroscopy. J Pharm Sci. 2009;98(9):3406-18.

114. Kessler B. LyoFlux® – TDLAS Water Vapor Mass Flow Monitor. PSI Physical Sciences Inc Andover, MA. n.d.

115. Willemer H. Measurements of temperatures, ice evaporation rates and residual moisture contents in freeze-drying. Developments in biological standardization. 1992;74:123-34; discussion 35-6.

116. Chouvenc P, Vessot S, Andrieu J, Vacus P. Optimization of the Freeze-Drying Cycle: A New Model for Pressure Rise Analysis. Drying Technology. 2004;22(7):1577-601.

117. Adixen Vacuum Technology. A NEW HUMIDITY MONITORING TECHNIQUE which provides a better understanding of freeze-drying process. LYOTRACK Humidity Monitoring for Freeze-Drying Market [Internet]. 2006. Available from: http://www.johnmorris.com.au/files/product/attachments/10428/292177_opt1.pdf.

118. Adixen by Alcatel Vacuum Technology. LYOTRACK humidity monitoring for freeze-drying a complete lyophilization cycle monitoring device [Internet]. n.d. Available from: http://members.upc.cz/labtech4/dokumenty/Alcatel/Lyotrack-brozura.pdf.

119. Hecht J. Understanding fiber optics International ed., 4th ed. USA: Pearson/Prentice Hall 2002.

120. AIRBUS S.A.S. Optical fibre on aircraft -When the light speed serves data transmission. FAST 47 AIRBUS TECHNICAL MAGAZINE 2010.

121. Paschotta R. Field guide to optical fiber technology: Bellingham, WA : SPIE Press, ©2010.; 2010.

122. Alwayn V. Fiber-Optic Technologies2004 12/5/2017. Available from: http://www.ciscopress.com/articles/article.asp?p=170740&seqNum=5.

123. Argyros A. Microstructured Polymer Optical Fibers. Journal of Lightwave Technology, Lightwave Technology, Journal of, J Lightwave Technol. 2009(11):1571.

124. Large MCJ, Argyros A, Cox F, van Eijkelenborg MA, Ponrathnam S, Pujari NS, et al. Microstructured Polymer Optical Fibres: New Opportunities and Challenges. Molecular Crystals & Liquid Crystals. 2006;446(1):219-31.

125. Newport. Hollow Core Photonic Bandgap Crystal Fibers 2017 [cited 2016 1/3/2017]. Available from: https://www.newport.com/f/hollow-core-photonic-bandgap-crystal-fibers.

126. NKT photonics. HC19-1550-01 Hollow Core Photonic Bandgap Fiber n.d. 20/12/2016. Available from: https://www.newport.com/medias/sys_master/images/images/ha5/hdb/87970923 80702/F-AIR-20-1550-Data-Sheet.pdf.

127. FBGS. FBG - FIBER BRAGG GRATING PRINCIPLE 2017 [cited 2017 14/2/2017]. Available from: http://www.fbgs.com/technology/fbg-principle/.

128. Zhang L, Zhang W, Bennion I. In-Fiber Grating Optic Sensors. In: Yin S, Yu FTS, editors. Fiber optic sensors. New York: Marcel Dekker; 2002.

129. Webb D. Fiber Bragg Grating Sensors. In: Santos JL, Farahi F, editors. Handbook of Optical Sensors: CRC Press; 2014. p. 503-32.

130. Smart Fibres. Our technology FBG Sensing System: Smart Fibres Ltd, UK; n.d. [13/05/2017]. Available from: https://www.smartfibres.com/technology.

131. Grice SJ. Optical fibre sensors and their applications in the industrial weighing and aerospace industries. Aston University; 2010.

132. Jaroslav K, Radek K, Radek V, Frantisek U. Design of a Pressure Sensor Based on Optical Fiber Bragg Grating Lateral Deformation. Sensors, Vol 10, Iss 12, Pp 11212-11225 (2010). 2010(12):11212.

133. Stephen JM. Fiber Bragg Grating Sensors for Harsh Environments. Sensors, Vol 12, Iss 2, Pp 1898-1918 (2012). 2012(2):1898.

134. Tennyson RC, Mufti AA, Rizkalla S, Tadros G, Benmokrane B. Structural health monitoring of innovative bridges in Canada with fiber optic sensors. SMART MATERIALS AND STRUCTURES. 2001;10:560-73.

135. Hong C-Y, Zhang Y-F, Zhang M-X, Leung LMG, Liu L-Q. Application of FBG sensors for geotechnical health monitoring, a review of sensor design, implementation methods and packaging techniques. Sensors and Actuators A: Physical. 2016;244:184-97.

136. Zhou Z, Graver TW, Hsu L, Ou J-p. Techniques of Advanced FBG sensors: fabrication, demodulation, encapsulation and their application in the structural health monitoring of bridges. Pacific Science Review. 2003;5:116-21.

137. Vendittozzi C, Sindoni G, Paris C, Marmo PPd, editors. Application of an FBG sensors system for structural health monitoring and high performance trimming on racing yacht. 2011 Fifth International Conference on Sensing Technology; 2011 Nov. 28 2011-Dec. 1 2011.

138. Ye XW, Su YH, Han JP. Structural Health Monitoring of Civil Infrastructure Using Optical Fiber Sensing Technology: A Comprehensive Review. The Scientific World Journal, Vol 2014 (2014). 2014.

139. Mossman GE, inventorOptical fiber based sensor system suitable for monitoring remote aqueous infiltration. USA patent US20110042557 A1. 2011.

140. Technica. Applications USA2016 [cited 2017 7/6/2017]. Available from: http://technicasa.com/application/.

141. Kawasaki BS, Hill KO, Johnson DC, Fujii Y. Narrow-band Bragg reflectors in optical fibers. Optics Letters. 1978;3(2):66.

142. Hill KO, Fujii Y, Johnson DC, Kawasaki BS. Photosensitivity in optical fiber waveguides: Application to reflection filter fabrication. Applied Physics Letters. 1978;32(10):647-9.

143. Johnson IP. Grating devices in polymer optical fibre [Doctoral dissertation]. UK: Aston University; 2012.

144. Meltz G, Morey WW, Glenn WH. Formation of Bragg gratings in optical fibers by a transverse holographic method. Optics Letters. 1989;14(15):823.

145. Kashyap R, Armitage JR, Wyatt R, Davey ST, Williams DL. All-fibre narrowband reflection gratings at 1500 nm. Electronics Letters. 1990;26(11):730.

146. Limberger HG, Fonjallaz P-Y, Lambelet P, Salathe R-P, Zimmer C, Gilgen HH. "Optical low-coherence reflectometry (OLCR) characterization of efficient Bragg gratings in optical fiber" Proc. SPIE 2044, Photosensitivity and Self-Organization in Optical Fibers and Waveguides. 1993;2044:272-83.

147. Malo B, Hill KO, Bilodeau F, Johnson DC, Albert J. Point-by-point fabrication of micro-Bragg gratings in photosensitive fibre using single excimer pulse refractive index modification techniques. Electronics Letters. 1993;29(18):1668.

148. Geernaert T, Kalli K, Koutsides C, Komodromos M, Nasilowski T, Urbanczyk W, et al. Point-by-point fiber Bragg grating inscription in free-standing step-index and photonic crystal fibers using near-IR femtosecond laser. Optics Letters. 2010;35(10):7.

149. Lai Y, Zhou K, Sugden K, Bennion I. Point-by-point inscription of first-order fiber Bragg grating for C-band applications. Optics Express. 2007;15(26):18318-25.

150. Ibsen Photonics. Phase masks 2017 [cited 2017 30/1/2017]. Available from: http://ibsen.com/products/phase-masks/.

151. Qiu Y, Sheng Y, Beaulieu C. Optimal phase mask for fiber Bragg grating fabrication. Journal of Lightwave Technology, Lightwave Technology, Journal of, J Lightwave Technol. 1999(11):2366.

152. Stuart B. Polymer analysis.: Chichester ; New York : J. Wiley; 2002.

153. Harbach NG. Fiber bragg gratings in polymer optical fibers [Doctoral dissertation]. Switzerland: ÉCOLE POLYTECHNIQUE FÉDÉRALE DE LAUSANNE (EPFL); 2008.

154. Xiong Z, Peng GD, Wu B, Chu PL. Highly tunable Bragg gratings in single-mode polymer optical fibers. IEEE Photonics Technology Letters. 1999;11(3):352.

155. Zoubir A, Lopez C, Richardson M, Richardson K. Femtosecond laser fabrication of tubular waveguides in poly(methyl methacrylate). Optics Letters. 2004;29(16):1840.

156. Schnabel W. Polymers and light: fundamentals and technical applications: Weinheim : Wiley-VCH, ©2007.; 2007.

157. Bartlett RJ, Philip-Chandy R, Eldridge P, Merchant DF, Morgan R, Scully PJ. Plastic optical fibre sensors and devices. Transactions of the Institute of Measurement & Control. 2000;22(5):431.

158. Marcou J. Plastic optical fibres : practical applications: Chichester : Wiley, 1997.; 1997.

159. Morse TF. Specialty optical fibers handbook: Oxford : Academic Press; 2007.

160. Appajaiah A. Climatic Stability of Polymer Optical Fibers (POF) Germany: Bundesanstalt für Materialforshung und -prüfung (BAM) 2004.
161. polymers Ta. TOPAS Cyclic Olefin Copolymer 2011 22/3/2017. Available from: http://www.topas.com/sites/default/files/Products_E_170406.pdf.
162. Woyessa G, Fasano A, Stefani A, Markos C, Nielsen K, Rasmussen HK, et al. Humidity insensitive step-index polymer optical fibre Bragg grating sensors. 24th International Conference on Optical Fibre Sensors. 2015;9634.
163. Daum W, Krauser J, Zamzow PE, Ziemann O. POF - polymer optical fibers for data communication: Berlin ; London : Springer, ©2002.; 2002.
164. Sato M, Ishigure T, Koike Y. Thermally stable high-bandwidth graded-index polymer optical fiber. Journal of Lightwave Technology. 2000;18(7):952-8.
165. Chanda M, Roy SK. Plastics Technology Handbook, Fourth Edition. USA: CRC Press; 2006.
166. Large M, Poladian L, Barton G, van Eijkelenborg MA. Microstructured Polymer Optical Fibres. New York: Springer; 2008.
167. Abang A, Webb DJ. Influence of mounting on the hysteresis of polymer fiber Bragg grating strain sensors. Optics Letters. 2013;38(9):1376.
168. Abang A, Webb DJ. Effects of annealing, pre-tension and mounting on the hysteresis of polymer strain sensors. Measurement Science & Technology. 2014;25(1):015102.
169. Yuan W, Stefani A, Bache M, Jacobsen T, Rose B, Herholdt-Rasmussen N, et al. Improved thermal and strain performance of annealed polymer optical fiber Bragg gratings. Optics Communications. 2011;284:176-82.
170. Woyessa G, Nielsen K, Stefani A, Markos C, Bang O. Temperature insensitive hysteresis free highly sensitive polymer optical fiber Bragg grating humidity sensor. Optics Express. 2016;24(2):1206-13.
171. Emslie C. Polymer optical fibres. Journal of Materials Science. 1988(7).
172. Potter BC. Module 3 - Attenuation in Optical Fibers n.d. 20/3/2017. Available from: http://opti500.cian-erc.org/opti500/pdf/sm/Module3%20Optical%20Attenuation.pdf.
173. Peters K. Polymer optical fiber sensors—a review Smart Mater Struct 2011;20(1).
174. Fiberoptics Technology Incorporated. Operating Temperature n.d. [cited 2017 1/1/2017]. Available from: http://www.fiberopticstech.com/technical/operating_temperature.php.
175. Chang X, Li M, Han X. Recent development and applications of polymer optical fiber sensors for strain measurement. Front Optoelectron China. 2009;2(4):362-7.
176. Topas advanced polymers. Data Sheet TOPAS® 5013L-10 2014 [cited 2017 5/1/2017]. Available from: http://www.topas.com/sites/default/files/TDS_5013L-10_english%20units_0.pdf.
177. ZEONEX Cyclo Olefin Polymer (COP). World's Foremost Optical Polymer for Precision-Molded Optics 2017 [cited 2017 1/3/2017]. Available from: http://www.zeonex.com/optics.aspx#techdata.
178. Carroll KE, Zhang C, Webb DJ, Kalli K, Argyros A, Large MC. Thermal response of Bragg gratings in PMMA microstructured optical fibers. Optics Express. 2007;15(14):8844-50.
179. Dobb H, Webb DJ, Kalli K, Argyros A, Large MCJ, Van Eijkelenborg MA. Continuous wave ultraviolet light-induced fiber Bragg gratings in few- and single-mode microstructured polymer optical fibers. Optics Letters. 2005;30(24):3296.
180. Dobb H CK, Webb DJ, Kalli K, Komodromos M, Themistos C, et al. . Grating based devices in polymer optical fibre - art. no. 618901. In: Culshaw B MA, Bartelt H, Jaroszewicz LR,, editor. Optical Sensing II Proceedings of the Society of Photo-Optical Instrumentation Engineers (Spie) 61892006 p 18901(2006).
181. Johnson IP WD, Kalli K, Large MCJ, Argyros A. . Multiplexed FBG sensor recorded in multimode microstructured polymer optical fibre. In: In: Kalli K UW,

editor. Photonic Crystal Fibers Iv Proceedings of SPIE-The International Society for Optical Engineering 7714(2010).

182. Dobb HL. Fibre gratings in novel optical fibres for applications in sensing [Doctoral dissertation]. UK: Aston University; 2007.

183. Webb DJ, Kalli K, Carroll K, Zhang C, Komodromos M, Argyros A, et al., editors. Recent developments of Bragg gratings in PMMA and TOPAS polymer optical fibers2008.

184. Khanarian G, Celanese H. Optical properties of cyclic olefin copolymers. Optical Engineering. 2001;40(6):1024.

185. Corning. Corning® SMF-28® ULL fiber 2014 20/2/2017. Available from: http://www.corning.com/opticalfiber/products/SMF-28_ULL_fiber.aspx.

186. Abdi O, Wong KC, Hassan T, Peters KJ, Kowalsky MJ. Cleaving of solid single mode polymer optical fiber for strain sensor applications. Optics Communications. 2009;282:856-61.

187. Law SH, Harvey JD, Kruhlak RJ, Song M, Wu E, Barton GW, et al. Cleaving of microstructured polymer optical fibres. Optics Communications. 2006(2):193.

188. Mizunami T, Djambova TV, Niiho T, Gupta S. Bragg gratings in multimode and few-mode optical fibers. IEEE/OSA Journal of Lightwave Technology. 2000;18(2):230.

189. COHERENT. All Solid-State Continuous Wave UV Laser for Writing FBGs [cited 2017 11/2/2014]. Available from: http://www.coherent.co.jp/document/whitepaper/fbg/Azure_for_FBGs_Whitepaper.pdf.

190. Rajan G, Ramakrishnan M, Semenova Y, Ambikairajah E, Farrell G, Gang-Ding P. Experimental Study and Analysis of a Polymer Fiber Bragg Grating Embedded in a Composite Material. IEEE/OSA Journal of Lightwave Technology. 2014;32(9):1726.

191. Ye CC, Dulieu-Barton JM, Webb DJ, Zhang C, Peng GD, Chambers AR, et al. Applications of polymer optical fibre grating sensors to condition monitoring of textiles. Journal of Physics: Conference Series. 2009;178(1):1.

192. Abang A, Webb DJ. Demountable connection for polymer optical fiber grating sensors. OPTICAL ENGINEERING -BELLINGHAM- INTERNATIONAL SOCIETY FOR OPTICAL ENGINEERING-. 2012;51(8):080503.

193. Henkel. LOCTITE Product Selector Industrial Adhesive, Sealant and Functional Coating Solutions2014 [cited 2017 20/2/2017]. Available from: http://hybris.cms.henkel.com/medias/sys_master/catalogsync/catalogsync/9030422331422.pdf.

194. Henkel LOCTITE. LOCTITE® AA 3936™ Technical Datasheet2015 20/2/2017. Available from: https://tds.us.henkel.com/NA/UT/HNAUTTDS.nsf/web/0D5B3CDCA611A37A882571870000D74F/$File/AA%203936-EN.pdf.

195. Zhang W, Webb DJ, Peng G. Investigation Into Time Response of Polymer Fiber Bragg Grating Based Humidity Sensors. IEEE/OSA Journal of Lightwave Technology. 2012;30(8):1090.

196. Gallenkamp S. Environmental Chamber -Instruction Manual. 1994 [cited 2017. Available from: http://www.severnsaleslabequip.com/manual-PDFs/E%20Environmental%20Chambers/sanyo-hcc065-manual-eng.pdf.

197. Ibsen Photonics. I-MON 256 and 512 USB Product Specification. Document No: 9ACFHC82013 10/3/2014. Available from: http://ibsen.com/products/interrogation-monitors/i-mon-usb/i-mon-256-512-usb/.

198. Ibsen Photonics. I-MON Series E-USB Interrogation monitors for FBG sensor systems. IMON Series EUSB Product Sheet v2 [Internet]. n.d. 20/2/2017 [cited 2017. Available from: http://www.forc-photonics.ru/data/files/product-sheet-I-MON-Series-E-USB-v2-web.pdf.

199. Ibsen Photonics. I-MON USB Interrogation Monitors for FBG sensor systemsn.d. 21/2/2017. Available from: http://ibsen.com/wp-content/uploads/Ibsen-Product-Sheets-I-MON-USB.pdf.

200. Photonics I. I-MON 256 USB / 512 USB n.d. [cited 2017 13/2/2017]. Available from: http://ibsen.com/products/interrogation-monitors/i-mon-usb/i-mon-256-512-usb/.

201. Testo. Testo 410-1 - Compact Vane Anemometer 2017 [cited 2017 1/1/2017]. Available from: http://www.testolimited.com/testo-410-1-compact-vane-anemometer.

202. Xiang J, Hey JM, Liedtke V, Wang DQ. Investigation of freeze–drying sublimation rates using a freeze–drying microbalance technique. International Journal of Pharmaceutics. 2004;279(1–2):95-105.

203. Tang XC, Nail SL, Pikal MJ. Evaluation of manometric temperature measurement (MTM), a process analytical technology tool in freeze drying, part III: heat and mass transfer measurement. AAPS PharmSciTech. 2006;7(4):97-.

204. Oerlikon leybold vacuum. Thermovac TM101 Operating Instructions2010 22/2/2017. Available from: http://www.idealvac.com/files/manuals/Oerlikon-Thermovac_TM101.pdf.

205. Liu HY, Peng GD, Chu PL. Thermal tuning of polymer optical fiber Bragg gratings. IEEE Photonics Technology Letters, Photonics Technology Letters, IEEE, IEEE Photon Technol Lett. 2001(8):824.

206. Liu HB, Liu HY, Peng GD, Chu PL. Strain and temperature sensor using a combination of polymer and silica fibre Bragg gratings. Optics Communications. 2003;219:139-42.

207. Zhang C, Zhang W, Webb DJ, Peng GD. Optical fibre temperature and humidity sensor. Electronics Letters. Apr 29 2010;46(643-U63).

208. Zhang W, Webb DJ, Gang-Ding P. Enhancing the sensitivity of poly(methyl methacrylate) based optical fiber Bragg grating temperature sensors. Optics Letters. 2015;40(17):4046.

209. Markos C, Stefani A, Nielsen K, Rasmussen HK, Yuan W, Bang O. High-Tg TOPAS microstructured polymer optical fiber for fiber Bragg grating strain sensing at 110 degrees. Optics Express. 2013;21(4):4758-65.

210. Johnson IP, Yuan W, Stefani A, Nielsen K, Rasmussen HK, Khan L, et al. Optical fibre Bragg grating recorded in TOPAS cyclic olefin copolymer. Electronics Letters. 2011;47(4):271-2.

211. Woyessa G, Fasano A, Stefani A, Markos C, Nielsen K, Rasmussen HK, et al. Single mode step-index polymer optical fiber for humidity insensitive high temperature fiber Bragg grating sensors. Optics Express. 2016;24(2):1253-60.

212. Yuan W, Wang D, Yan P, Yang S. PMMA DC surface flashover in vacuum after thermal treatment. 2007 Annual Report - Conference on Electrical Insulation and Dielectric Phenomena, Electrical Insulation and Dielectric Phenomena, 2007 CEIDP 2007 Annual Report - Conferen. 2007:567.

213. Thomas D. NASA Outgassing Data for Selecting Spacecraft Materials Online 2016 [cited 2017 15/3/2017]. Available from: https://outgassing.nasa.gov/.

214. Chen CC, Shen J, Sauer JA. Polymer paper: Effects of sorbed water on properties of low and high molecular weight PMMA: 11. Fatigue performance. Polymer. 1985;26:89-96.

215. Takaaki I, Miki H, Masataka S, Yasuhiro K. Graded-index plastic optical fiber with high mechanical properties enabling easy network installations. I. Journal of Applied Polymer Science. 2004;91(1):404.

216. Ishigure T, Hirai M, Sato M, Koike Y. Graded-Index Plastic Optical Fiber with High Mechanical Properties Enabling Easy Network Installations. II. JOURNAL OF APPLIED POLYMER SCIENCE. 2004;91:410-6.

217. SP Scientific. AdVantage 2.0 BenchTop Freeze Dryer / Lyophilizer n.d. [cited 2016 12/12/2016]. Available from: http://www.spscientific.com/Products/Commercial_Freeze_Dryers_/_Lyophilizersrs/VirTis/Bench_Top_Lyophilizers/AdVantage_2_0_BenchTop_Freeze_Dryer/.

218. Moors AJ, Pugh RS, Becker PR. NIST Special Publication 1195 Operation of the Millrock Quanta Series Freeze Dryer PC/PLC: Production of Freeze Dried Standard Reference and Control Materials (SRMs/CMs) at the NIST Reference Material Production FacilityJuly 2016 12/11/16. Available from: http://ws680.nist.gov/publication/get_pdf.cfm?pub_id=914761.

219. Liu L, Zhang H, Zhao Q, Liu Y, Li F. Temperature-independent FBG pressure sensor with high sensitivity. Optical Fiber Technology. 2007;13(1):78-80.

220. Xu MG, Reekie L, Chow YT, Dakin JP. Optical in-fibre grating high pressure sensor. Electronics Letters. 1993;29(4):398-9.

221. Wang Y, Wang M, Huang X. High-sensitivity fiber Bragg grating transverse force sensor based on centroid measurement of polarization-dependent loss. MEASUREMENT SCIENCE AND TECHNOLOGY. 2010;21(6):065304.

222. Johnson IP, Webb DJ, Kalli K. Hydrostatic pressure sensing using a polymer optical fibre Bragg gratings [8351-74]. Third Asia Pacific Optical Sensors Conference Proceedings of SPIE: Washington, SPIE; 2012. p. 835106.

223. Bremer K, Reinsch T, Leen G, Roth B, Lochmann S, Lewis E. Pressure, temperature and refractive index determination of fluids using a single fibre optic point sensor. Sensors & Actuators: A Physical. 2017;256:84-8.

224. Bhowmik K, Peng G-D, Luo Y, Ambikairajah E, Lovric V, Walsh WR, et al. Experimental Study and Analysis of Hydrostatic Pressure Sensitivity of Polymer Fibre Bragg Gratings. IEEE/OSA Journal of Lightwave Technology. 2015;33(12):2456.

225. Chiggiato P. Outgassing. TS-MME Coatings, Chemistry and Surfaces CERN CH-1211 Geneva 23 [Internet]. 2006 12/3/2017 [cited 2017 12/3/2017]. Available from: https://cas.web.cern.ch/cas/Spain-2006/PDFs/Chiggiato-1.pdf.

226. Danielson P. Desorbing Water in Vacuum Systems: Bakeout or UV? 2001 [cited 2017 21/3/2017]. Available from: http://www.normandale.edu/departments/stem-and-education/vacuum-and-thin-film-technology/vacuum-lab/articles/desorbing-water-in-vacuum-systems-.

227. TOPAS advanced polymers. TOPAS Cyclic Olefin Copolymer (COC)2006 [cited 2017 15/3/2017]. Available from: http://www-eng.lbl.gov/~shuman/NEXT/CURRENT_DESIGN/TP/FO/COC_topas_product-brochure_english.pdf.

228. Zhang C, Chen X, Webb DJ, Peng GD. Water detection in jet fuel using a polymer optical fibre Bragg grating. 20th International Conference on Optical Fibre Sensors; 2009 October 14; Edinburgh, United Kingdom: SPIE.

229. Zhang W, Webb DJ, editors. Polymer optical fiber grating as water activity sensor 2014: Bellingham Washington, SPIE.

230. Zhang W, Webb D, Peng G. Polymer optical fiber Bragg grating acting as an intrinsic biochemical concentration sensor. Optics Letters. 2012;37(8):1370-2.

231. Watanabe T, Ooba N, Hida Y, Hikita M. Influence of humidity on refractive index of polymers for optical waveguide and its temperature dependence. Applied Physics Letters. 1998;72(13).

232. Ishiyama C, Higo Y. Effects of Humidity on Young's Modulus in Poly(methyl methacrylate). JOURNAL OF POLYMER SCIENCE PART B POLYMER PHYSICS. 2002;40:460-5.

233. Labconco Corporation. A guide to freeze drying for the laboratory2010 1/5/2017 [cited 2017 1/5/2017]. Available from: https://archive-resources.coleparmer.com/MoreInfo/Labconco_guide_freeze_dry_in_lab.pdf.

234. polymers Ta. Packaging2011 22/3/2017. Available from: http://www.topas.com/sites/default/files/files/Packaging_E_2014-06.pdf.
235. British Plastics Federation. Drying of Polymer (including Dehumidifying Dryers, Rotary Wheel Dryers, Low Pressure Dryers, Vacuum Dryers) 2017 [cited 2017 23/3/2017]. Available from: http://www.bpf.co.uk/Plastipedia/Processes/Drying_of_Polymer.aspx.
236. Xiao-ming T, Jian-ming Y, Hwa-yaw T. Photosensitive polymer optical fibres and gratings. Transactions of the Institute of Measurement & Control. 2007;29(3/4):255-70.
237. Wang T, Wang Q, Luo Y, Qiu W, Peng G-D, Zhu B, et al. Enhancing photosensitivity in near UV/vis band by doping 9-vinylanthracene in polymer optical fiber. Optics Communications. 2013;307:5-8.
238. Nestor Jr. CW. Diffusion from Solid Cylinders1980 2/3/2017. Available from: http://web.ornl.gov/info/reports/1980/3445605662271.pdf.
239. Rajan G, Noor YM, Liu B, Ambikairaja E, Webb DJ, Peng G-D. A fast response intrinsic humidity sensor based on an etched singlemode polymer fiber Bragg grating. Sensors & Actuators: A Physical. 2013;203:107-11.
240. Donohoe SB, Peng GD, Webb DJ. Improving the response time of polymer optical fibre Bragg grating water activity sensors. In: Koike Y, Ziemann O, editors. Proceedings of the 24th International Conference on Plastic Optical Fibres, POF2015; Nuremberg, Germany: Technische Hochschule Nürnberg Georg Simon Ohm; 2015. p. 364-70.
241. Millrock Technology. Tech Notes solvent compatibility 2009 [cited 2017 28/3/2017]. Available from: http://www.freezedryinginfo.com/TechNotes.html.
242. Fasano A, Woyessa G, Stajanca P, Markos C, Stefani A, Nielsen K, et al. Fabrication and characterization of polycarbonate microstructured polymer optical fibers for high-temperature-resistant fiber Bragg grating strain sensors Optical Materials Express. 2016;6(2):649-59.
243. Fasano A, Woyessa G, Stajanca P, Markos C, Stefani A, Nielsen K, et al. Production and Characterization of Polycarbonate Microstructured Polymer Optical Fiber Bragg Grating Sensor. In Proceedings of the 24th International Conference on Plastic Optical Fibers. 2015.
244. O'Keeffe S, Lewis E. Polymer optical fibre for in situ monitoring of gamma radiation processes. International journal on smart sensing and intelligent systems. 2009;2(3).
245. Rambhatla S, Ramot R, Bhugra C, Pikal MJ. Heat and mass transfer scale-up issues during freeze drying: II. Control and characterization of the degree of supercooling. AAPS PharmSciTech. 2004;5(4):e58-e.
246. Kim AI, Akers MJ, Nail SL. The physical state of mannitol after freeze-drying: effects of mannitol concentration, freezing rate, and a noncrystallizing cosolute. J Pharm Sci. 1998;87(8):931-5.
247. Roth C, Winter G, Lee G. Continuous measurement of drying rate of crystalline and amorphous systems during freeze-drying using an in situ microbalance technique. J Pharm Sci. 2001;90(9):1345-55.
248. Cavatur RK, Vemuri NM, Pyne A, Chrzan Z, Toledo-Velasquez D, Suryanarayanan R. Crystallization behavior of mannitol in frozen aqueous solutions. Pharmaceutical research. 2002;19(6):894-900.
249. Arshad MS. Application of through-vial impedance spectroscopy as a novel process analytical technology for freeze drying [Doctoral dissertation]. UK: De Montfort University; 2014.
250. Shon M, Mather L. The Importance of Controlling Nucleation Temperature during the Freeze Step. Introduction of ControLyo™ Nucleation On-Demand Technology on the New FTS/SP Scientific™ LyoStar™3 Freeze Dryern.d. 29/5/2017.

Available from: https://www.labrepco.com/data/userfiles/files/The-Importance-of-Controlling-Nucleation-Temperature.pdf.

251. Hottot A, Andrieu J, Nakagawa K. Effect of ultrasound-controlled nucleation on structural and morphological properties of freeze-dried mannitol solutions. Chemical Engineering Research & Design: Transactions of the Institution of Chemical Engineers Part A. 2008;86(2):193-200.

252. Oliveira SM, Ringshia RA, Legeros RZ, Clark E, Yost MJ, Terracio L, et al. An improved collagen scaffold for skeletal regeneration. Journal Of Biomedical Materials Research Part A. 2010;94(2):371-9.

253. Chan EC, Kuo S-M, Kong AM, Morrison WA, Dusting GJ, Mitchell GM, et al. Three Dimensional Collagen Scaffold Promotes Intrinsic Vascularisation for Tissue Engineering Applications. PLoS ONE. 2016(2).

254. Biopharmatechnology. Using freeze drying to control collagen bioscaffolds 2012. Available from: http://biopharma.co.uk/intelligent-freeze-drying/using-freeze-drying-to-control-collagen-bioscaffolds/.

255. O'Brien FJ. Biomaterials & scaffolds for tissue engineering. Materials Today. 2011;14(3):88-95.

256. O'Brien FJ, Harley BA, Yannas IV, Gibson L. Influence of freezing rate on pore structure in freeze-dried collagen-GAG scaffolds. Biomaterials. 2004;25(6):1077-86.

257. Schoof H, Apel J, Heschel I, Rau G. Control of pore structure and size in freeze-dried collagen sponges. Journal of Biomedical Materials Research. 2001;58(4):352-7.

258. Pawelec KM, Husmann A, Best SM, Cameron RE. A design protocol for tailoring ice-templated scaffold structure. Journal of the Royal Society Interface. 2014;11(92):20130958.

259. O'Brien FJ, Harley BA, Yannas IV, Gibson LJ. The effect of pore size on cell adhesion in collagen-GAG scaffolds. Biomaterials. 2005;26(4):433-41.

260. Zhou Z, Ou J. Techniques of temperature compensation for FBG strain sensors used in long-term structural monitoring [5851-31]. PROCEEDINGS- SPIE THE INTERNATIONAL SOCIETY FOR OPTICAL ENGINEERING. 2005;5851:167-72.

261. Zubel MG, Sugden K, Webb DJ, Sáez-Rodríguez D, Nielsen K, Bang O. Embedding silica and polymer fibre Bragg gratings (FBG) in plastic 3D-printed sensing patches IN: Micro-Structured and Specialty Optical Fibres IV. Kalli, Kyriacos and Mendez, Alexis (eds) SPIE Proceedings. 2016.

262. Möhlmann D, Thomsen K. Properties of cryobrines on Mars. Icarus. 2011;212(1):123-30.

263. Maxim Integrated. Using Thermistors in Temperature Tracking Power Supplies. Maxim Integrated Products, 2001.

ITEM	DESCRIPTION	P/N	QTY
1	COMPRESSOR	414098	2
2	CHARGING VALVE	406574	4
3	AIR CONDENSER ASM.	416269	1
4	DRYER	404730	1
5	HEAT EXCHANGER	362848	1
6	SHELF	401692	1
7	CONDENSER	350827	1
8	SOLENOID VALVE ASM (S) #2940E5 2-WAY SOL VALVES	399746	1
9	TEMP. CONTROL	116806	1
10	CAPILLARY .031	275602	25'
11	CAPILLARY .040	380362	10'
12	CAPILLARY .040	380362	6'
13	CAPILLARY .052	381369	10'
14	FAN	416153	1
15	INSULATION KIT (HEAT EXCHANGER)	415941	1
16	INSULATION KIT (SOLENOID VALVE ASM.)	414241	1
17	DRYER	418157	1

CHARGING INSTRUCTIONS:
1. EVACUATE SYSTEM TO 5 MICRONS.
2. HEAT SHELF WHILE EVACUATING SYSTEM.

CHARGING INFORMATION		
	LO-STAGE	HI-STAGE
REFRIGERANT	SUVA 95	R417A
	100 PSIG	13 OZ
OIL	P.O.E	

NOTE:
1. SOFT SOLDER 18" OF CAPILLARY TO SUCTION LINE FOR HEAT EXCHANGE. AN ADDITIONAL 18" SHOULD BE FREE BEFORE ENTERING THE SHELF HEAT EXCHANGER. MORE THAN 18 FREE INCHES MAY BE NEEDED DUE TO SOME COMPONENT LAYOUTS.

	REVISIONS			The Virtis Company			ADVANTAGE		
NO.	LOG #	DATE	BY						
1	618	04/05/02	CJL		TOLERANCES	ITK #	SCALE	DRAWN BY R. ROTTINGER	
2	914	9/20/02	CJL				FULL	APPROVED BY	
3	1229	04/11/03	RFR		FRACTIONAL	TITLE	'EL' REFRIGERATION DIAGRAM		
					ANGULAR	DATE 02/07/02	DRAWING N	163-159-B	

Diagram kindly provided by Biopharma Technology Limited

Methods

The freezing point profiles were measured using two thermistors connected to either an Arduino Mega or Arduino platinum microcontroller (DIY sandbox). Both Arduino boards have a 10bit (1024 discrete levels or digital units) analogue-to-digital converter (ADC) and were connected to a laptop. The Arduino platinum was additionally equipped with an on-board storage unit (micro-SD), which was programmed to store the data recorded during the freezing stage.

A 1ml volume of the solution was pipetted into a 1.5ml micro-centrifuge reaction vial and either a 1.65kohm (at 25^0C) or 100kohm (at 25^0C) thermistor was inserted into the solution. At this stage the logger was activated, the vial was placed into a holder (aluminium or polystyrene) and onto the shelf in the Forma Scientific -86^0C freezer (thermostat registering -68^oC). Once the profile was collected the vial was removed, thawed and the thermistor cleaned before repeating the experiment.

The 1ml sample was either distilled water (freezing point 0.0^0C [5]), 0.9% or 23.3% w/v sodium chloride saline solutions. The 0.9% w/v sodium chloride solutions were obtained from a 300mosm/kg BP intravenous infusion solution at pH 5 (MacoPharma (UK) Ltd, Macoflex 100ml), with a documented freezing point of 0.558^oC[56].

The 23.3% w/v sodium chloride (ACROS Organics) corresponds to the eutectic composition (%) and a eutectic temperature of -22.15^oC (251K) [262]. To minimise variation and errors between the vials, a stock volume of 500ml was produced using a calibrated volumetric flask (E-MIL BORO A, 500±0.25ml in 20^0C, BS1792) and a mass balance. The mass of the salt was weighed using a calibrated scientific mass balance (Sartorius Q stat (High Voltage Ionizer) from Satorius Weighing Technology, to produce the 23.3% w/v sodium chloride solutions. The solution was mixed and allowed to equilibrate, before aliquoting the stock into the individual vials for the experiment.

Control system of the temperature data logger

Several software routines were created and uploaded by Sandra B. Donohoe onto the Arduino boards with different objectives in mind. The feedback loop is summarised in Figure 138, and the output of the system is controlled by the microcontroller.
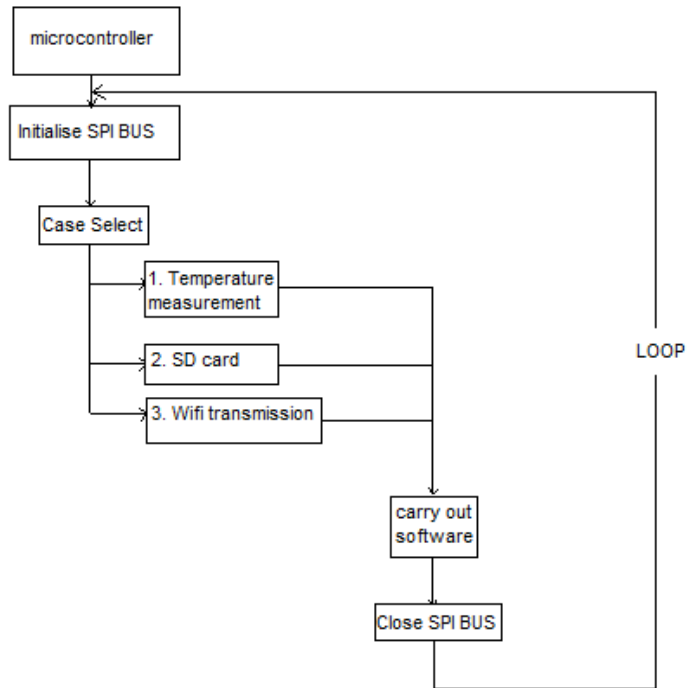
Figure 138 Flow chart of control system. The SPI bus is initiated and a case select function determines which process will be carried out before closing the SPI Bus.

When the system is activated with the use of a switch or turning on the power, the Serial Peripheral Interface (SPI) bus is activated. The SPI bus is a synchronous serial data link, which allows bi-directional (full duplex) transmission of data between Master (microcontroller) and Slave (e.g. ADC chip). The data frame is initiated by the master.

In the case of multiple slave devices, the master can select which device is to be activated through a chip select command ($\overline{SS}$). The system is depicted in Figure 139. The master can select one of three cases, to collect the temperature, store a value onto the SD card or transmit data wirelessly.
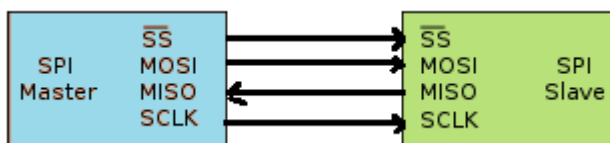
Figure 139 SPI bus interface between the master and the slave. SS is the chip select function, MOSI is the "Master out Slave in" command, MISO is the "Master in Slave out" command and SCLK is the clock.

The program used to collect temperature measurements is summarised Figure 140. The initial stage involves the controller obtaining an input from the user, through the use of a toggle switch. When the switch is in the "off" position, a red LED is turned

on to make the user aware that no data is currently being logged. When the switch is in the "on" position, a green LED is turned on and a file is created and opened on the SD card. The logger then begins to record the time and digital units (each corresponding to a temperature) and store the data in the new file. At the same time data is transmitted to the serial monitor for real-time data collection. When the logger is then turned "off" the data transmission to the file is stopped and the file closed.
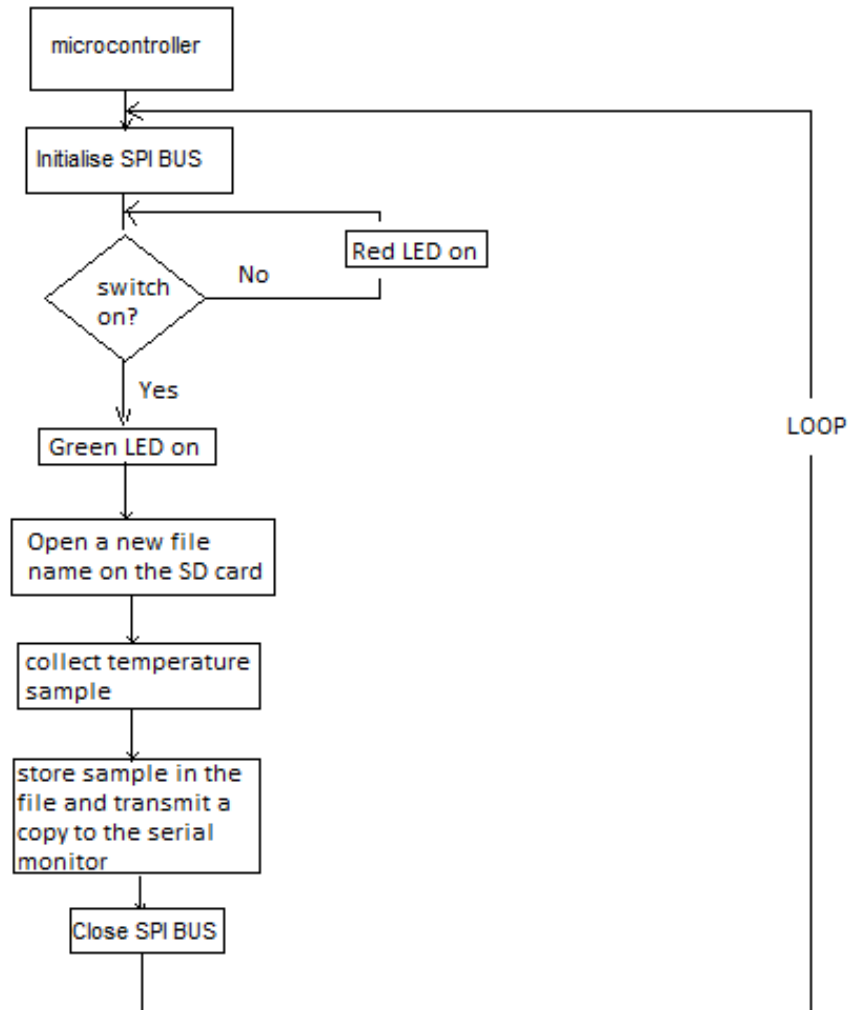
Figure 140 Flow chart shows the process of collecting and storing a digital unit from the ADC connected to the sensor. The value is then stored onto the SD card and transmitted to the laptop prior to closing the bus interface.

Figure 141(a) shows the circuit diagram that was used in the experiments and the schematic diagram of the final unit in Figure 141(b). Figure 142 shows that as the NTC thermistor cools, the resistance change with respect to temperature (and voltage drop) increases and becomes more non-linear. To reduce the non-linear effects A Positive Temperature Coefficient (PTC) resistor was added in series to the NTC thermistor. A 2.2kohm resistor was placed in series with the glass bead

thermistor TH-B12 (rated 1.65kohm at 25^{0}C); whereas a 100kohm resistor was placed in series with an epoxy coated thermistor from RS components (rated 100kohm at 25^{0}C).

A 5V voltage reference source (*TS2950CT-5.0, Maplin*) was selected to keep the voltage entering the circuit consistently at 5V. A 22uF capacitor was selected to steady and reduce fluctuations in the power supply. The data was collected at a sampling rate of 1 sample every 30ms, stored onto the SD card as a comma separated variable file format and simultaneously transmitted to the laptop.
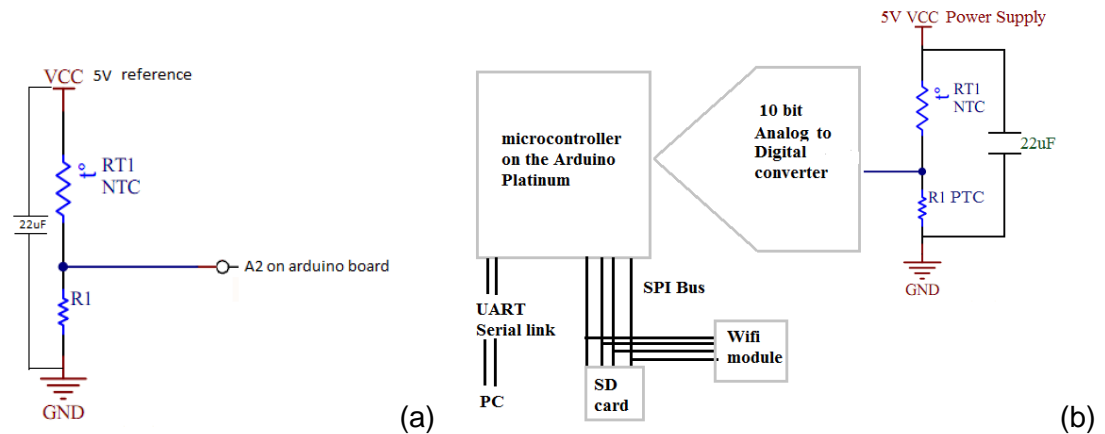
Figure 141 (a) Voltage divider circuit diagram (b) block diagram of the logging device and the analogue linearization circuit

Figure 142 Schematic representation of the non-linear relationship between resistance and temperature of a NTC thermistor. (Nominal resistance at room temperature R$_{25c}$ =10kΩ, thermistor's material constant β=3965K). [263]

Temperature calculation protocol

The Steinheart equation and the negative temperature coefficient (NTC) thermistor coefficients provided by the manufacturer were used to calculate the temperatures

of each solution's freezing profile. The circuit diagrams of the cost effective temperature data logger are available in Figure 141 and the freezing profiles were measured by the ADC's on the Arduino boards.

The Steinhart-Heart equation is a widely accepted model used to determine the temperature in the vicinity of the thermistor, due to the relationship between the changes in the resistance of the semiconductors with respect to temperature. The model is useful over the entire working range of the thermistor and provides a closer approximation to the actual temperature than simpler equations.

The temperature was approximated using the following method:

- *Calculate the voltage drop that is created due to the change in temperature using the value measured by the logger's ADC:*

$$voltage\ drop = \frac{digital\ value}{1024}\ x\ 5V$$

- *To calculate the resistance of the thermistor the following equation was rearranged:*

$$voltage\ drop = \frac{Resistance\ of\ the\ load\ resistor\ (R_1)}{total\ resistance}\ x\ Voltage\ input$$

$$voltage\ drop = \frac{R_1}{R_1 + R_T}\ x\ Vin$$

Where:

R_T=thermistor resistance

R_1=100200Ω rated at 25 ^{0}C

Vin= 5Volts

The following equation can be deduced:

$$R_T = \frac{100200\Omega * 5V}{voltage\ drop} - 100200\Omega$$

- *This calculated thermistor resistance is then be placed into the Steinhart-Hart equation using the coefficients provided by the manufacturer (T is measured in Kelvin):*

$$\frac{1}{T} = A + Bln(Rt) + C\ ln(Rt)^3$$

Where:

A= 1.00063869534204E^{-03}

B= 1.91817108209891E^{-04}

C=9.50095643768765E^{-08}

Appendix C   Freezing profiles of solutions

This section documents the freezing profiles of saline solutions that were recorded using the data logger discussed in Appendix B.

(a) 23.3% w/v sodium chloride solution profiles measured using the Arduino Platinum and 1.65kohm Thermistor
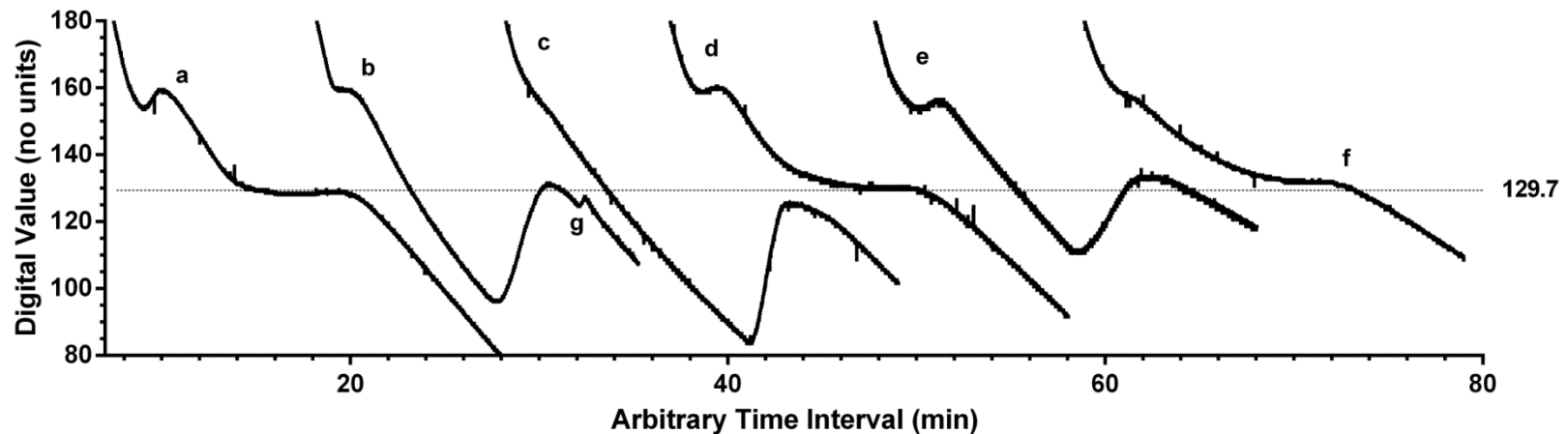
Figure 143 1ml samples of 23.3% w/v sodium chloride frozen in micro-centrifuge reaction vials at different time intervals. The average digital value 129.7 corresponds to the eutectic point 251K [262]. A voltage divider circuit was used in the experiments, consisting of a 1.65kohm thermistor (rated at 25ºC), a 5V regulated supply and 2.2kohm resistor. The output data from the circuit (digital value) was logged at a sampling rate of 30ms, using a 10bit ADC on the Arduino Platinum. n=6. The plastic vials were placed into a housing structure that had been positioned on top of a shelf in the -68ºC freezer. The electromagnetic interference induced into the circuit (e.g. 50Hz) produced 1-2digital units noise about the average digital value 129.7. The lines marked "a", "b", "d" and "e" show tendencies of local nucleation sites formed around the sensor as the solution cooled. The line marked "f" drops in temperature like the rest of the samples, however does not display a rise in temperature prior to freezing. Line "c" shows the characteristic tendencies of cooling sample, including supercooling, heat of fusion and finally solidification once the latent heat is removed. Point "g" is likely caused from movement of the sensor during ice crystal growth.

(b) Distilled water profiles measured using the Arduino Platinum and 100kohm thermistor
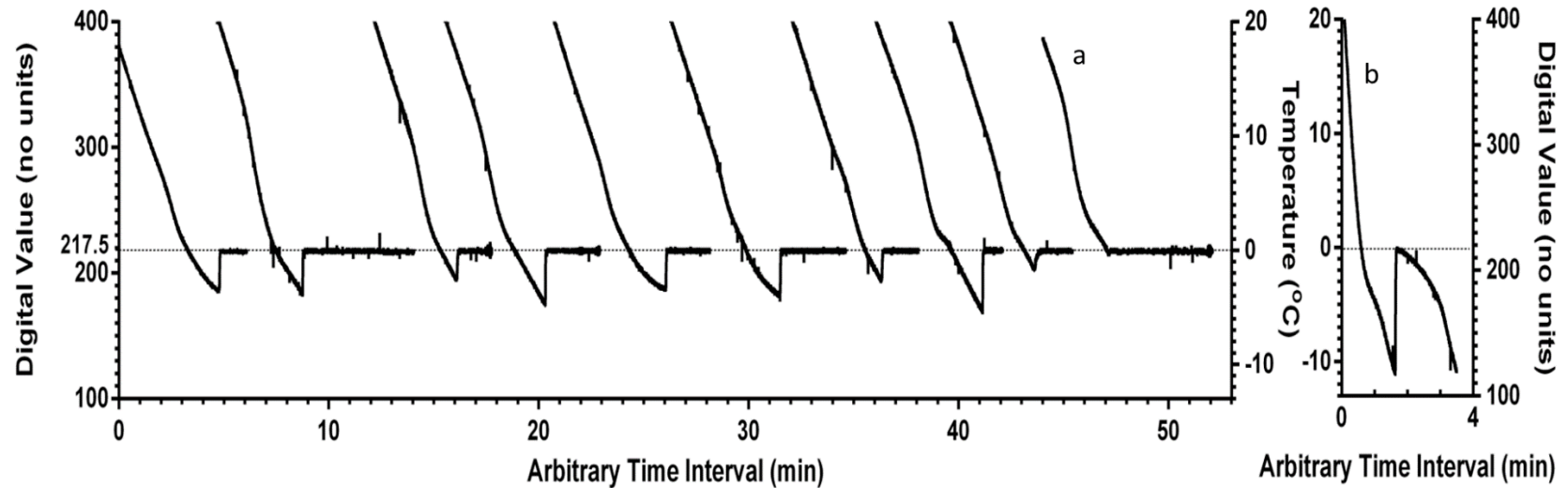
Figure 144 1ml samples of distilled water frozen in micro-centrifuge reaction vials at different time intervals on the shelf of a -68°C freezer. The average digital value 217.5 corresponds to 0°C, known as the equilibrium freezing point of water [11]. Temperature was calculated using the Steinhart-Hart equation and the constants for the thermistor. A voltage divider circuit was used in the experiments, consisting of a100kohm thermistor (rated at 25ºC), a 5V regulated supply and 100kohm resistor. The output data from the circuit (digital value) was logged at a sampling rate of 30ms, using a 10bit ADC on the Arduino Platinum. n=11. The vials were placed into a housing structure that had been positioned on top of a shelf in the freezer. The sample marked "b" (n=1) was placed into a metal housing (cooling rate of 45 °C/min) and solutions "a" n=10 were placed in a polystyrene housing (cooling rate of 6°C/min). Sample "a" showed a minimal degree of supercooling when compared to the other solutions. The electromagnetic interference induced into the circuit, produced 3digital units (or ≈ ±0.25°C) noise about the average digital value 217.5 at freezing.

(c) Distilled water profiles measured using the Arduino Mega and 100kohm thermistor
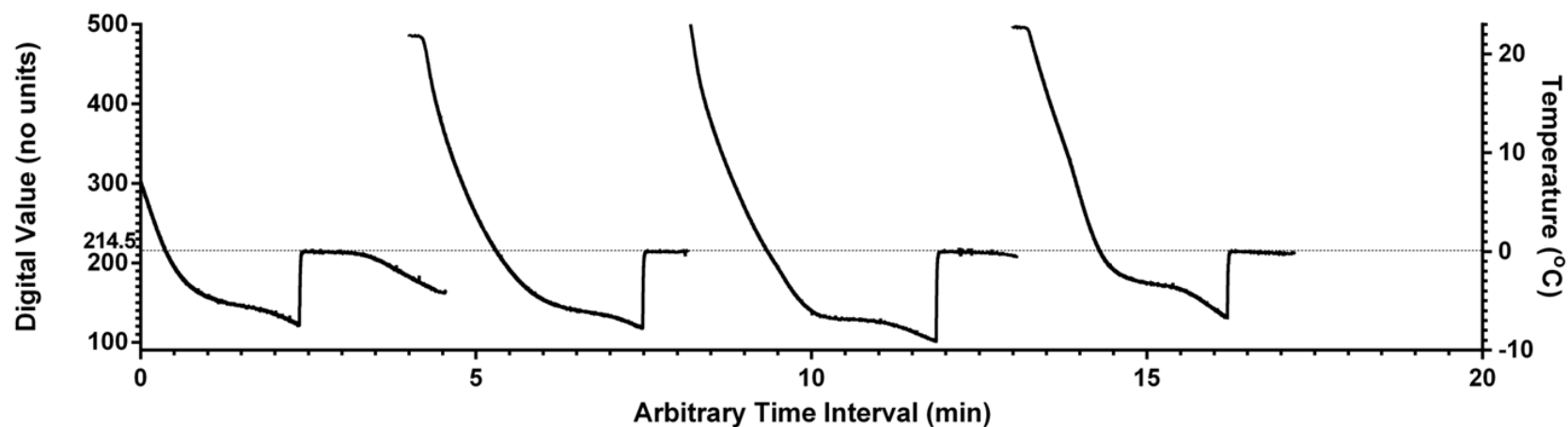
Figure 145 1ml samples of distilled water frozen in micro-centrifuge reaction vials at different time intervals on the shelf of a -68ºC freezer. The average digital value 214.5 corresponds to 0ºC, known as the equilibrium freezing point of water [11]. Temperature was calculated using the Steinhart-Hart equation and the constants for the thermistor listed in Appendix B. A voltage divider circuit was used in the experiments, consisting of a 100kohm thermistor (rated at 25ºC), a 5V regulated supply and 100kohm resistor. The output data from the circuit (digital value) was logged at a sampling rate of 30ms, using a 10bit ADC on the Arduino Mega. n=4. The plastic vials were placed into a housing structure that had been positioned on top of a shelf in the freezer. The electromagnetic interference induced into the circuit, produced 3digital units (or ≈ ±0.25ºC) noise about the average digital value 214.5.

(d) 0.9% w/v sodium chloride solution profiles measured using the Arduino Platinum and 1.65kohm thermistor
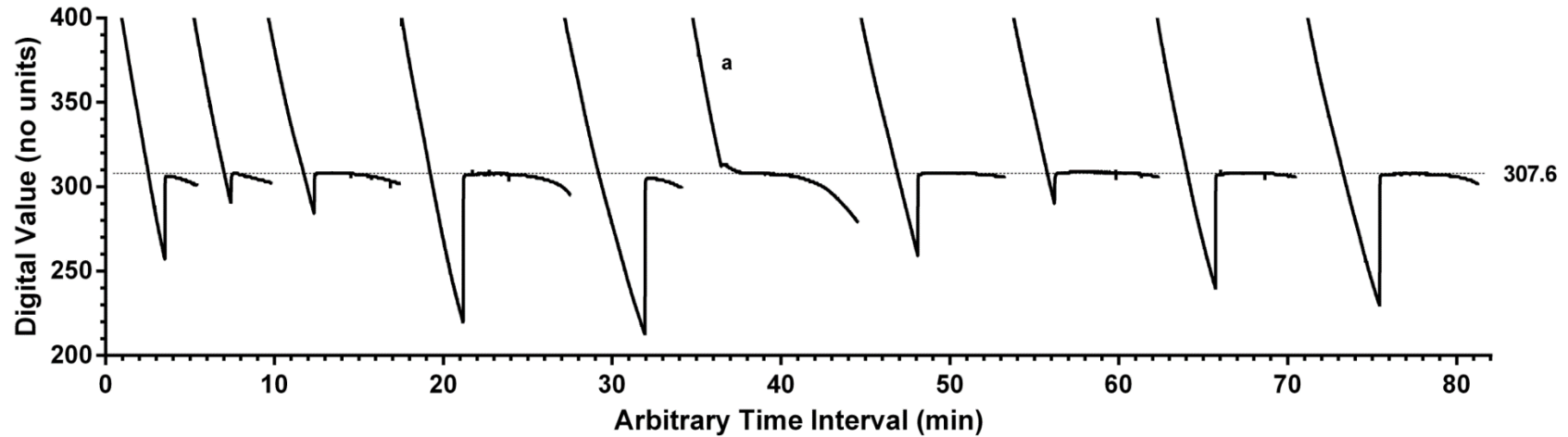
Figure 146 1ml samples of 0.9% w/v sodium chloride solution (300mosm/Kg H20) frozen in micro-centrifuge reaction vials at different time intervals on the shelf of a -68⁰C freezer. The average digital value 307.6 corresponds to 0.558⁰C, known as the freezing point of 300mosm/Kg [56]. A voltage divider circuit was used in the experiments, consisting of a 1.65kohm thermistor (rated at 25°C), a 5V regulated supply and 2.2kohm resistor. The output data from the circuit (digital value) was logged at a sampling rate of 30ms, using a 10bit ADC on the Arduino Platinum. n=10. The plastic vials were placed into a polystyrene housing structure that had been positioned on top of a shelf in the freezer. The electromagnetic interference induced into the circuit, produced 1digital unit of noise about the digital value that corresponds to the freezing point of each frozen sample. The line marked "a" drops in temperature like the rest of the samples, however does not display a rise in temperature prior to freezing

Method

A windmill sensor (3.4.2.3) was used in this project to monitor sublimation and the end of primary drying time. The assembly is illustrated in Figure 147, where the anemometer was placed between the product and condenser chambers in order to baffle water vapour through the blades.

A LAC-EA3000 Handheld Anemometer was used in this experiment to provide information on rotational velocity. This device was built with a magnet positioned on the rotor part of the anemometer (Figure 147).

A Hall Effect Sensor (SS461C by Honeywell) was selected to detect the position and motion of the fan blade and provide feedback on the rotational speed. They are non-contact position sensors which detect a disturbance or strength in the magnetic field [85]. The Hall Effect Sensor is used to convert the physical parameter of motion to an electrical output which provides an indication on the position of the object.

(a)   (b)
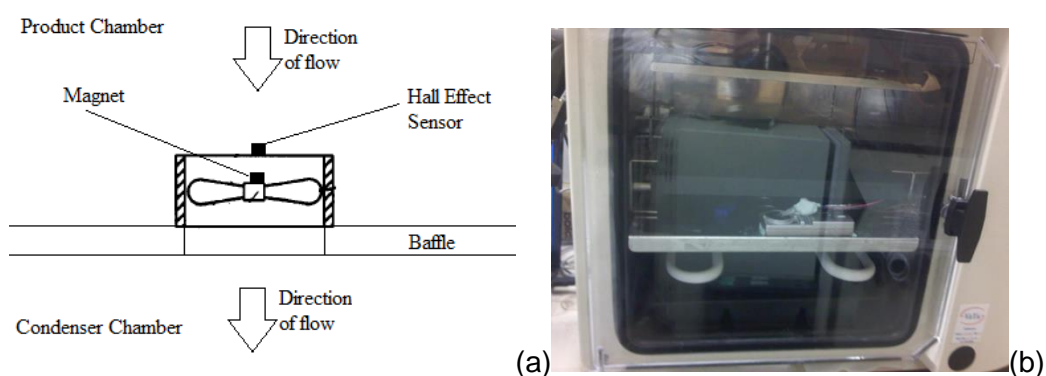
Figure 147 (a) Diagram of the anemometer, magnet and Hall Effect Sensor set-up. (b)Assembly in the freeze dryer

The vapour flow rate through the baffle is logged during the course of the cycle and the end of primary drying is determined by a characteristic decrease in the rotational speed RPM (rev/min). The data was logged over the primary drying phase and an output rotational speed was obtained.

The logging device (Arduino Mega) was placed outside the freeze-dryer and cables were passed into the chamber using a feedthrough connector to the Hall

Effect sensor and anemometer. This avoids damaging the circuit components due to the temperature and vacuum conditions within the chamber.

Distilled water and D-mannitol (Fagron UK) samples (250ml or 500ml) were freeze dried in a steel tray (diameter 27cm, height 2cm), using the freeze drying cycle in Figure 148 and Figure 149. Mannitol (5%w/v and 10%w/v) were prepared using a calibrated scientific mass balance (Sartorius Q stat (High Voltage Ionizer).

K-type thermocouples were inserted into the samples and monitored with a data-logger (OctTemp, MadgeTech), to measure the product temperature throughout the cycle and determine the end of sublimation.

Freezing stage			
Temperature(^{0}C)	Time (min)		Ramp/Hold
-40	360		Hold
Primary Drying			
Temperature(^{0}C)	Time (min)	Vacuum (µbar)	Ramp/Hold
-34	5	1000	Hold
-20	20	1000	Ramp
-15	1350	1000	Hold
Secondary Drying			
Temperature(^{0}C)	Time (min)	Vacuum (µbar)	
10	10	1000	

Figure 148 Freeze drying cycle (samples frozen at -40^{0}C).

Freezing stage			
Temperature(^{0}C)	Time (min)		Ramp/Hold
-30	360		Hold
Primary Drying			
Temperature(^{0}C)	Time (min)	Vacuum (µbar)	Ramp/Hold
-30	5	1000	Hold
-20	20	1000	Ramp
-15	1350	1000	Hold
Secondary Drying			
Temperature(^{0}C)	Time (min)	Vacuum (µbar)	
10	10	1000	

Figure 149 Freeze drying cycle (samples frozen at -30^{0}C).

Protocol for logging rotational speed of the anemometer (rev/min)

This project used a Digital Hall Effect Bipolar Latching Sensor to detect the presence of a magnetic field on the shaft of the rotor. This produces output pulses which correlate directly to the speed of the turning fan and the vapour flow rate. The pulses are detected by the Arduino Mega and the data was then stored (SD card) and transmitted through a Universal Asynchronous Receiver/Transmitter (UART) cable to a laptop. The device uses a Serial Peripheral Interface (SPI) bus system to transmit data from the Master (Arduino board) to the slave (SD card).

The flow chart in Figure 150 summarises the process used to store the time interval required to complete 10 pulses (equivalent to 5 complete revolutions). Using this information of a number of pulses completed in a time frame it is possible to convert the data into a rotational speed in rev/min (RPM) as seen in Equation 13.

$$Rotational\ speed\ (RPM) = \frac{revolution}{time\ (min)}$$

Equation 13

The chart shows that the SPI bus system was initiated when the power to the controller was turned on and the logging begins only when the user has turned the toggle switch into the "ON" position (green LED turns on). At this point a file was produced on the SD card and a timer activated to mark the starting time of the experiment (time=0ms).

The main part of the software routine was written to store the time required to complete 10 pulses as well as the time the data was stored during the experiment. The data was also transmitted to a serial monitor for real-time data collection. When the switch was turned to the "OFF" position the data transmission to the file stopped and the file closed.

The method selected to detect the pulses is through the use of an interrupt sequence, which interrupts the main program in order to execute a priority command within the code, in this case:

- *Add 1 to the register which stores the number of pulses*
- *Change the LED state (1=ON and 0 = OFF)*

When the interrupt sequence finished, the board returns to the point in the code it was at prior to the interrupt.
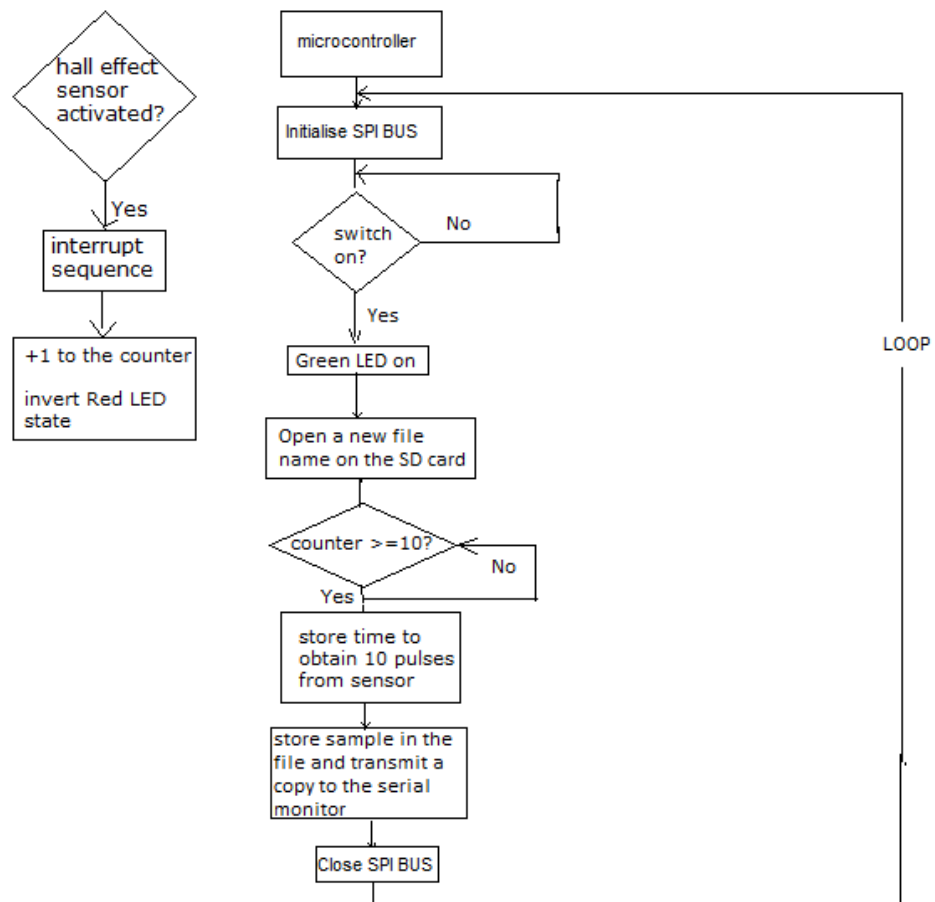
Figure 150 Flow chart developed for storing data on the rotational speed of the blades

The block diagram of the finalised device is illustrated in *Figure 151.*
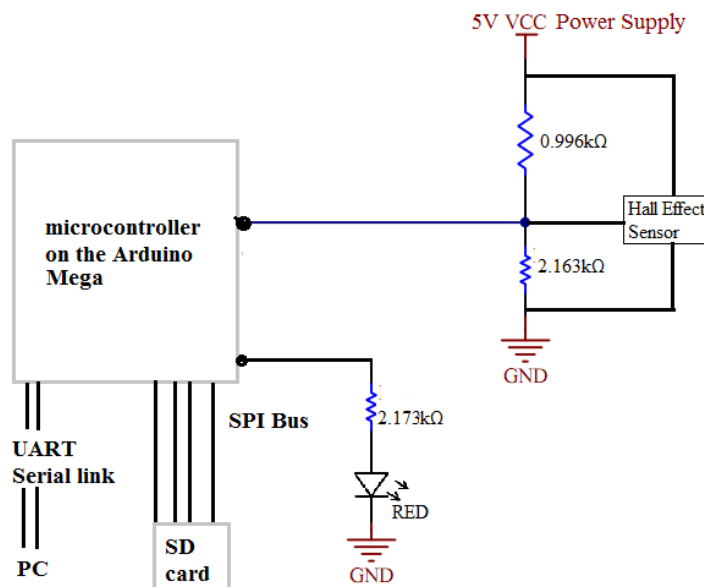
Figure 151 Block diagram of the data logging device and the Hall Effect sensor circuit
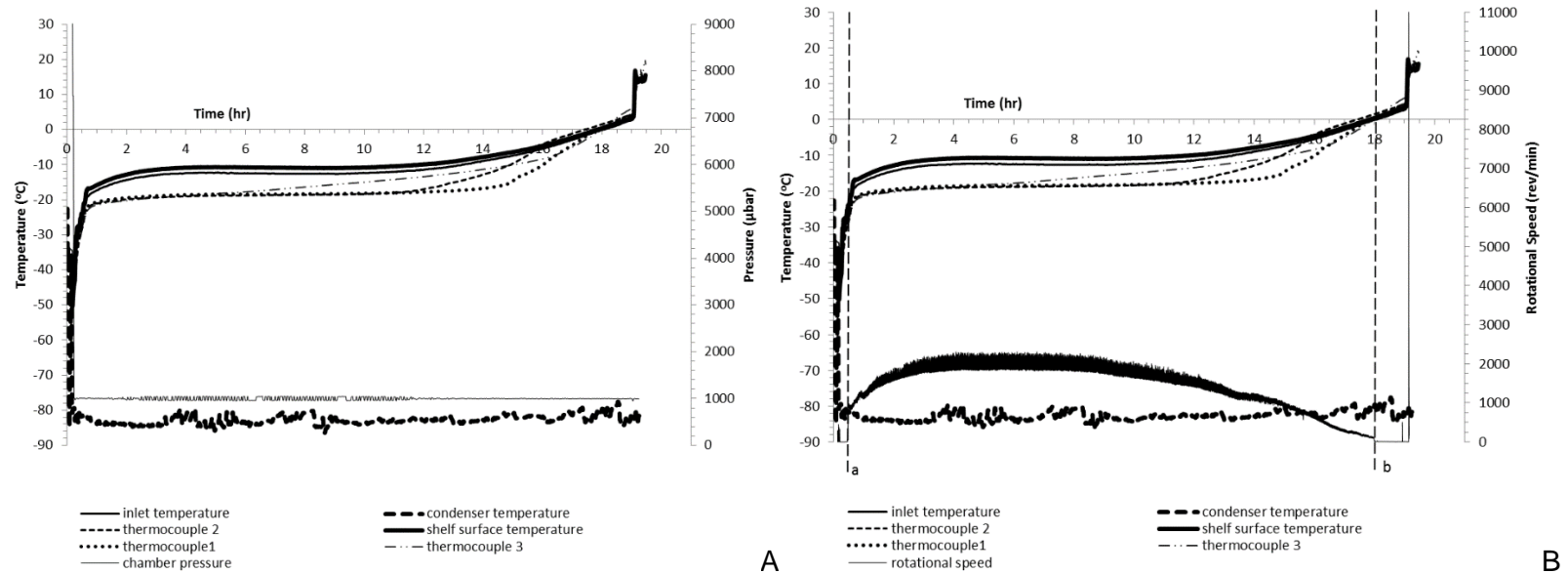
Graph 1 (A) Freeze drying cycle of frozen 250ml 10%w/v mannitol, frozen at -40°C for 6hrs in a 27cm diameter stainless steel tray. The product temperature profiles were measured using K-type thermocouples. Fill depth is 0.44cm. (B) Shows the logged rotational speed of the anemometer sensor over the course of the primary drying cycle shown in graph A. Line "a" shows the beginning of the rotation of the blades. Line "b" shows the time interval when primary drying finished according to the anemometer sensor.
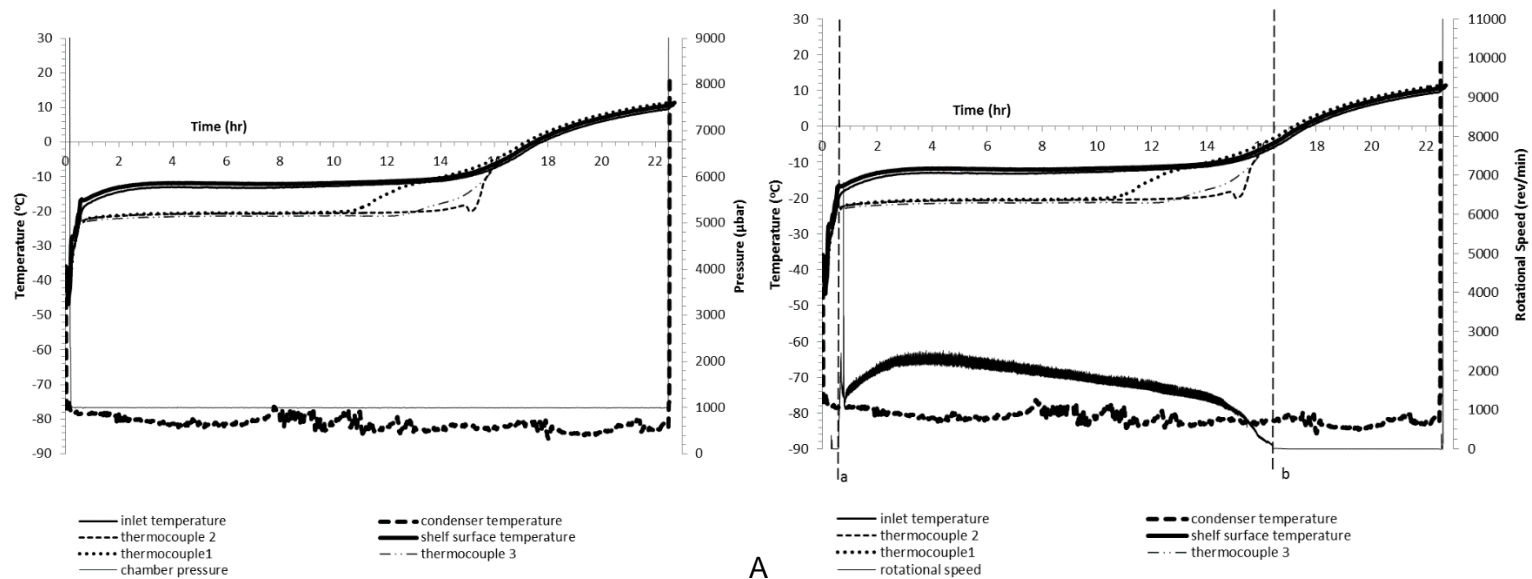
Graph 2 (A) Freeze drying cycle of frozen 250ml 5%w/v mannitol, frozen at -40°C for 6hrs in a 27cm diameter stainless steel tray. The product temperature profiles were measured using K-type thermocouples. Fill depth is 0.44cm. **(B)** Shows the logged rotational speed of the anemometer sensor over the course of the primary drying cycle shown in graph A. Line "a" shows the beginning of the rotation of the blades. Line "b" shows the time interval when primary drying finished according to the anemometer sensor.
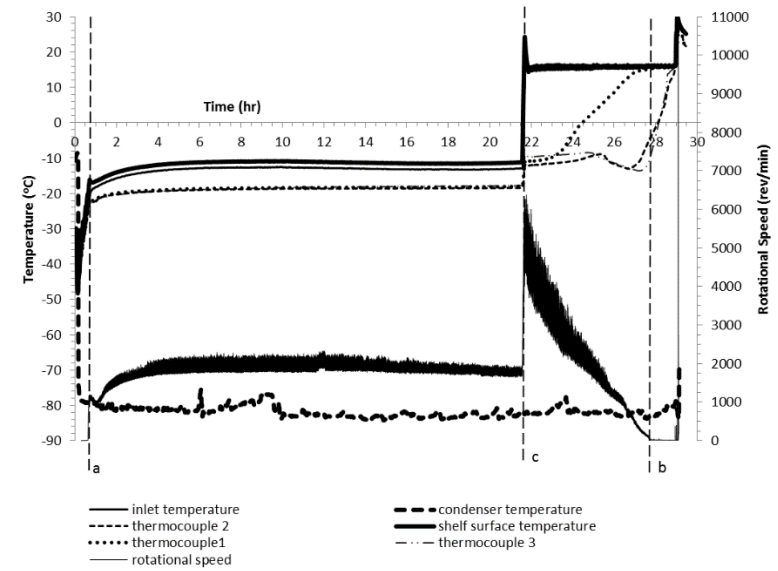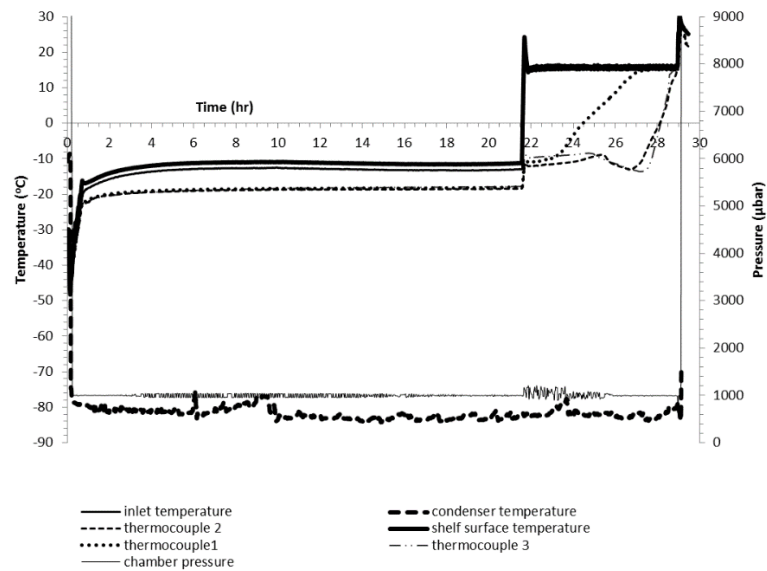
Graph 3 (A) Freeze drying cycle of frozen 500ml 10%w/v mannitol frozen at -40ºC for 6hrs in a 27cm diameter stainless steel tray. The product temperature profiles were measured using K-type thermocouples. Fill depth is 0.88cm. (B) Shows the logged rotational speed of the anemometer sensor over the course of the primary drying cycle shown in graph A. Line "a" shows the beginning of the rotation of the blades. Line "b" shows the time interval when primary drying finished according to the anemometer sensor. Line "c" illustrates a sudden ramp in the shelf and product temperature to 20ºC, leading to large increase in vapour flow rate and an increase in the rotational speed of the anemometer.
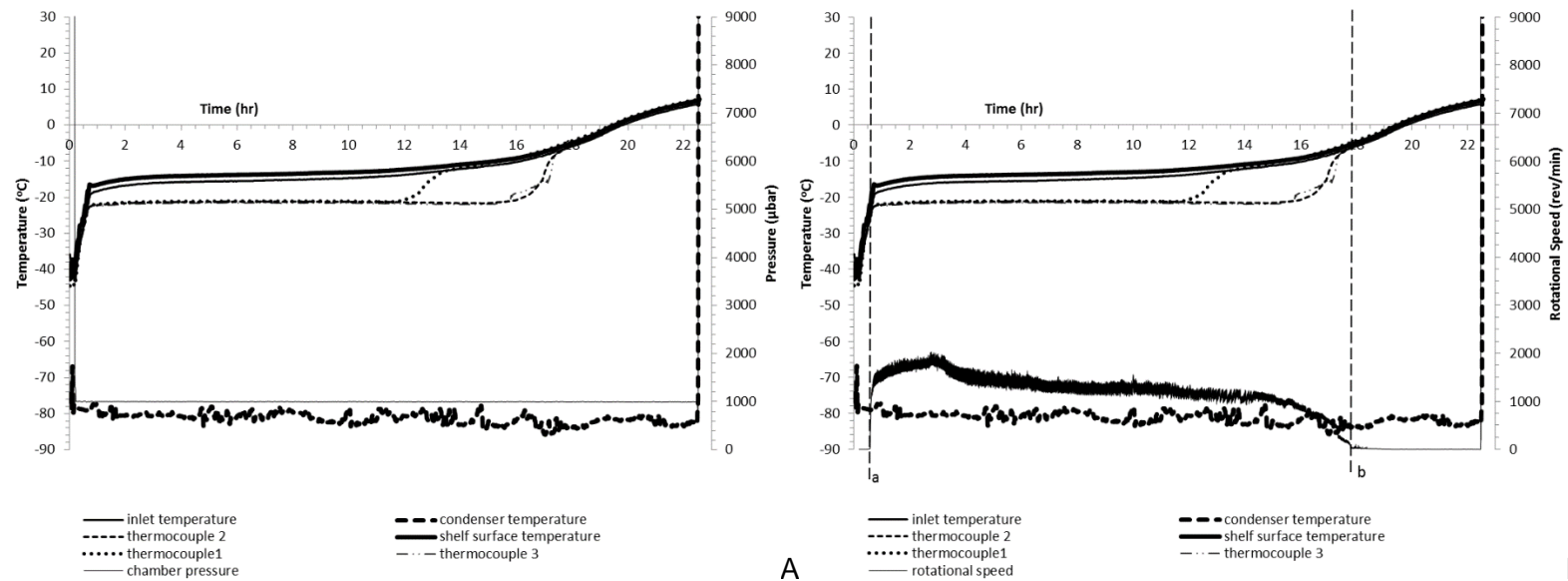
Graph 4 (A) Freeze drying cycle of frozen 250ml distilled water frozen at -30°C for 6hrs in a 27cm diameter stainless steel tray. The product temperature profiles were measured using K-type thermocouples. Fill depth is 0.44cm. (B) Shows the logged rotational speed of the anemometer sensor over the course of the primary drying cycle shown in graph A. Line "a" shows the beginning of the rotation of the blades. Line "b" shows the time interval when primary drying finished according to the anemometer sensor.
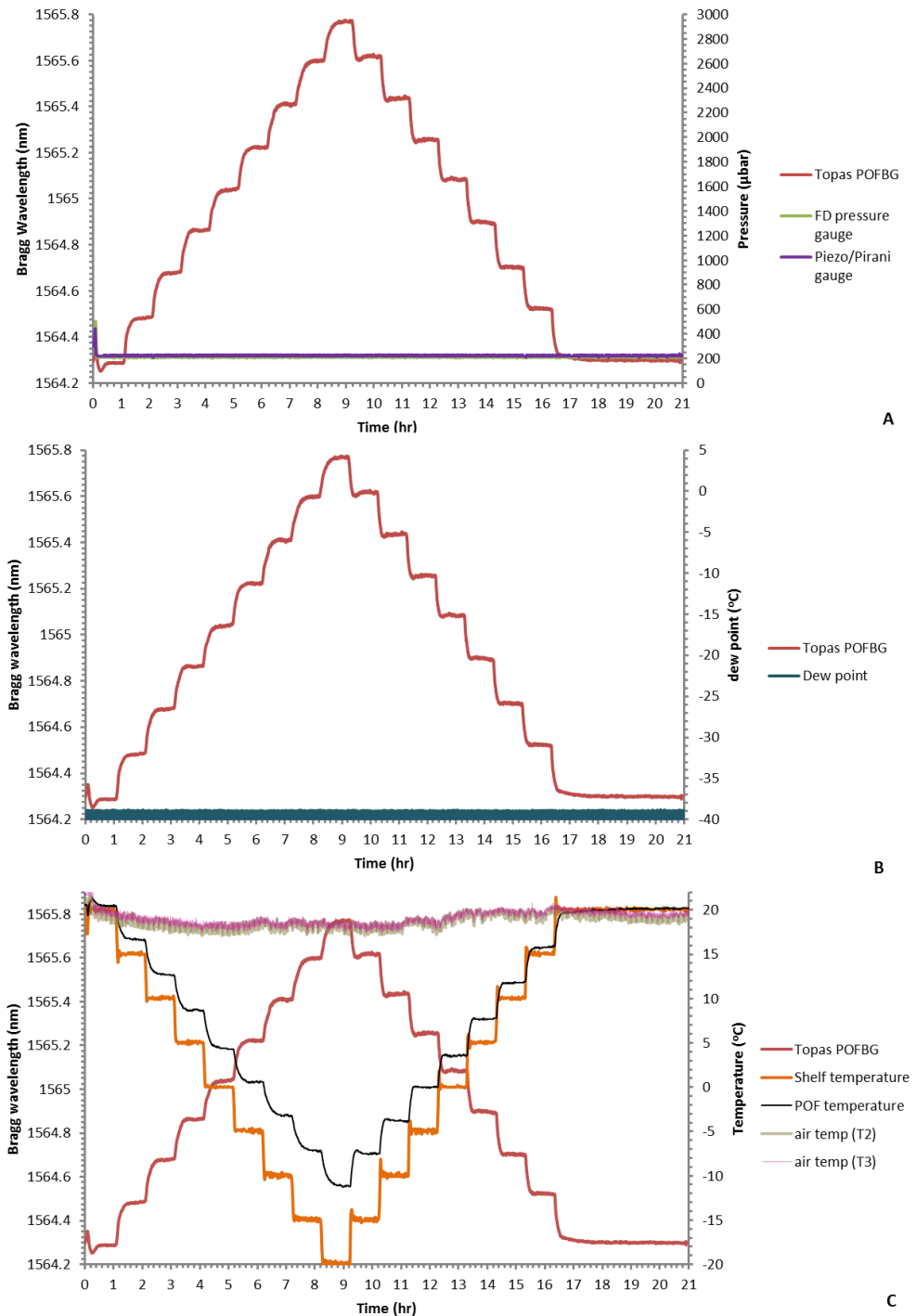
Figure 152 TOPAS POFBG Bragg wavelength against (a) pressure in the chamber, (b) dew point in the chamber, (c) temperature of the shelf, thermocouple temperature in the region next to the POF sensors and air temperature outside the freeze dryer

$y = -0.0179x + 1531.7$
$R^2 = 0.9992$

A

$y = -0.0171x + 1531.7$
$R^2 = 0.9954$

B
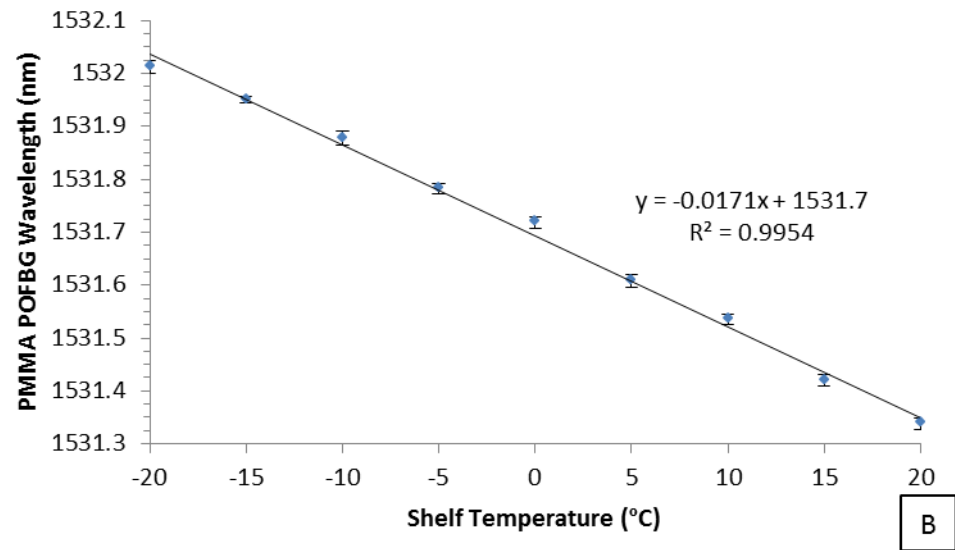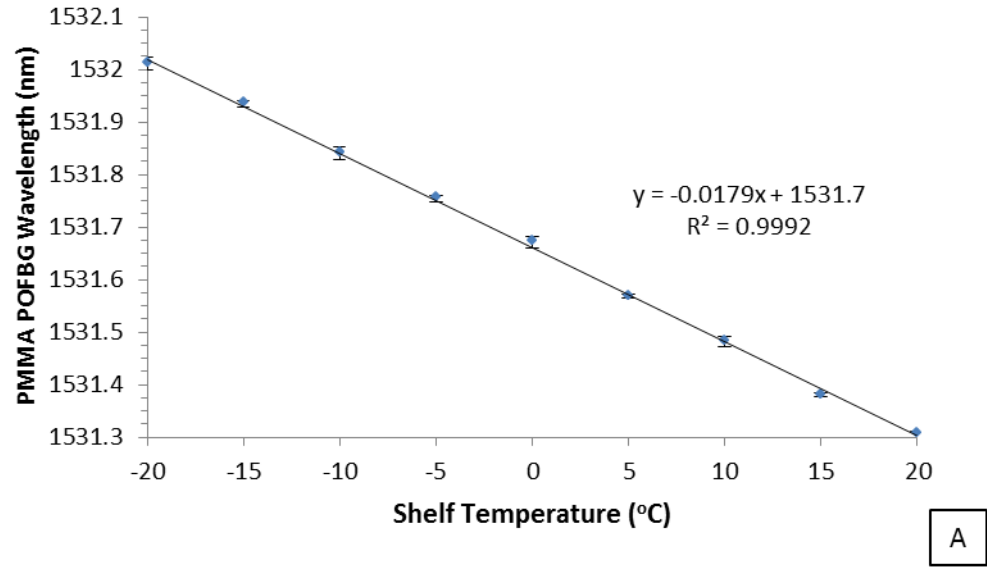
Figure 153 sensitivity of PMMA POFBG (POF5) to temperature in a freeze dryer (n=3), where (A) the temperature is decreased from 20ºC to -20ºC, (b) the temperature is increased from -20ºC to 20ºC
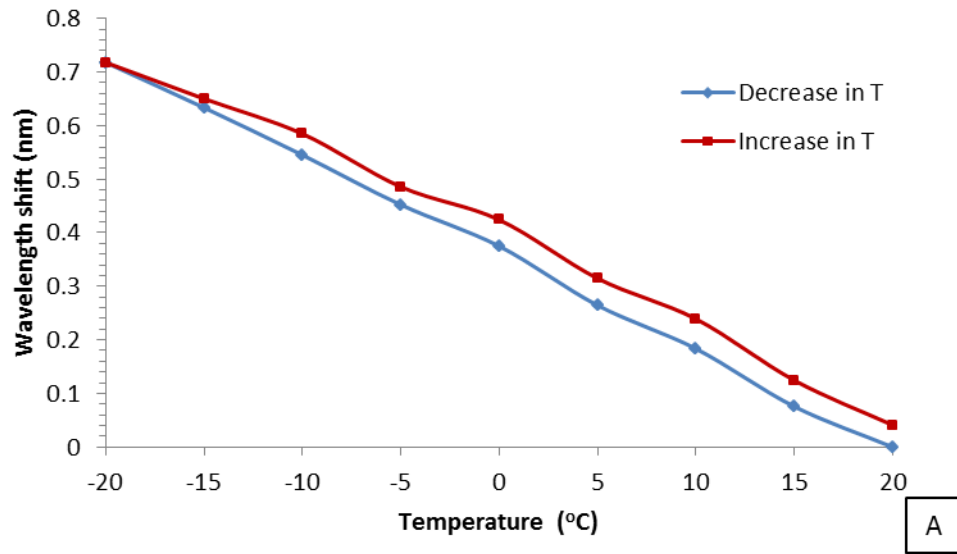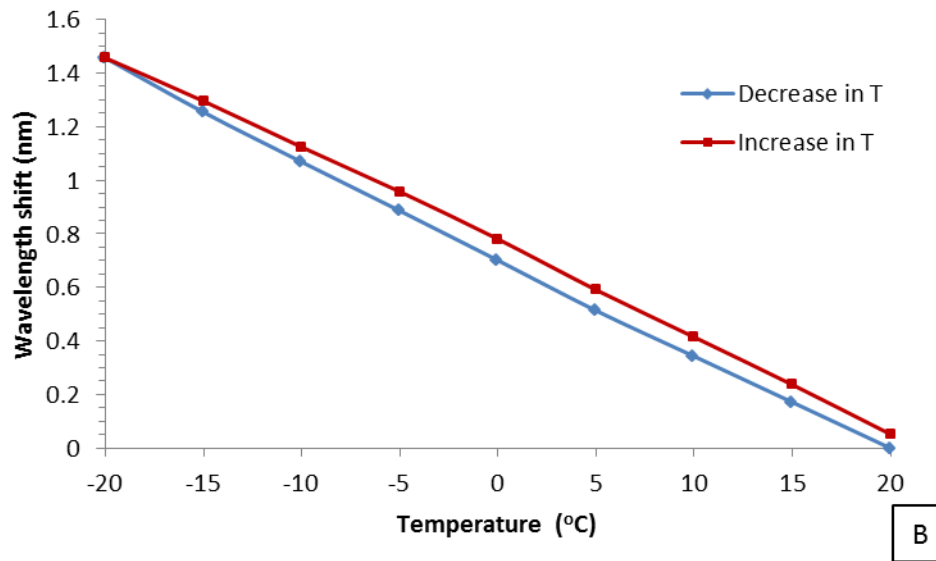
Figure 154 Bragg wavelength shift with respect to temperature in a freeze dryer (a) PMMA POFBG (POF5), (b) TOPAS POFBG (POF3)
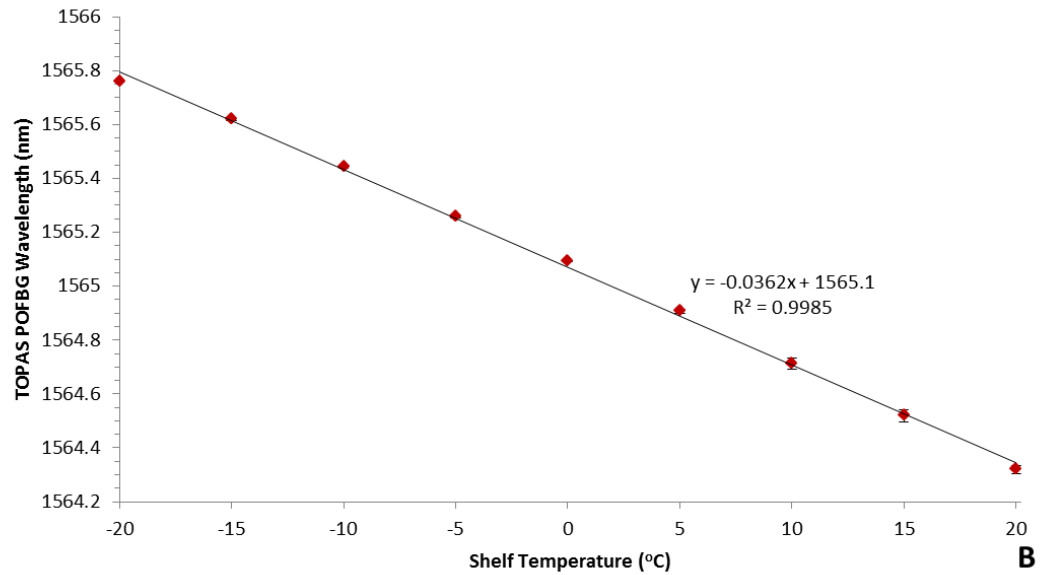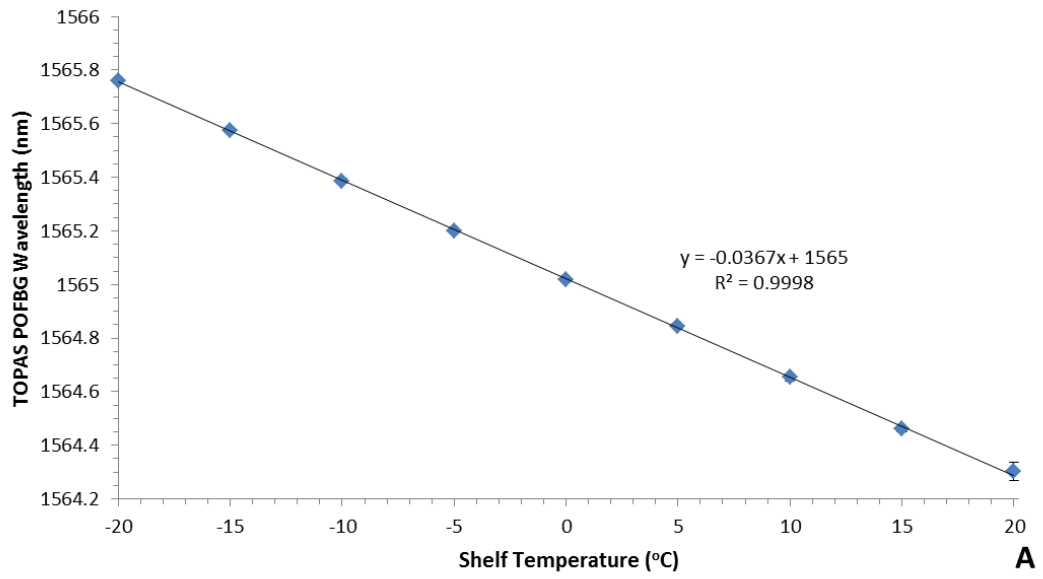
Figure 155 sensitivity of TOPAS POFBG (POF2) to temperature in a freeze dryer (n=3), where (A) the temperature is decreased from 20ºC to -20ºC, (b) the temperature is increased from -20ºC to 20ºC

Pressure cycle used to characterise POFBGs:

Freezing stage			
Shelf Temperature(°C)	Time (min)		Ramp/Hold
+20	5		Hold
Primary Drying			
Shelf Temperature(°C)	Time (min)	Vacuum (µbar)	Ramp/Hold
+20	90	2500	Hold
+20	90	2000	Hold
+20	90	1300	Hold
+20	90	1000	Hold
+20	90	600	Hold
+20	90	500	Hold
+20	90	400	Hold
+20	90	300	Hold
+20	90	200	Hold
+20	90	300	Hold
+20	90	400	Hold
+20	90	500	Hold
+20	90	600	Hold
+20	90	1000	Hold
+20	90	1300	Hold
+20	90	2000	Hold
Secondary Drying			
Temperature(°C)	Time (min)	Vacuum (µbar)	
+20	90	2500	

Table 0-A Pressure cycle loaded to the freeze drying controller. The program keeps a constant shelf temperature and a condenser temperature below -70°C, whilst allowing step changes in pressure and holding those conditions for 90 min
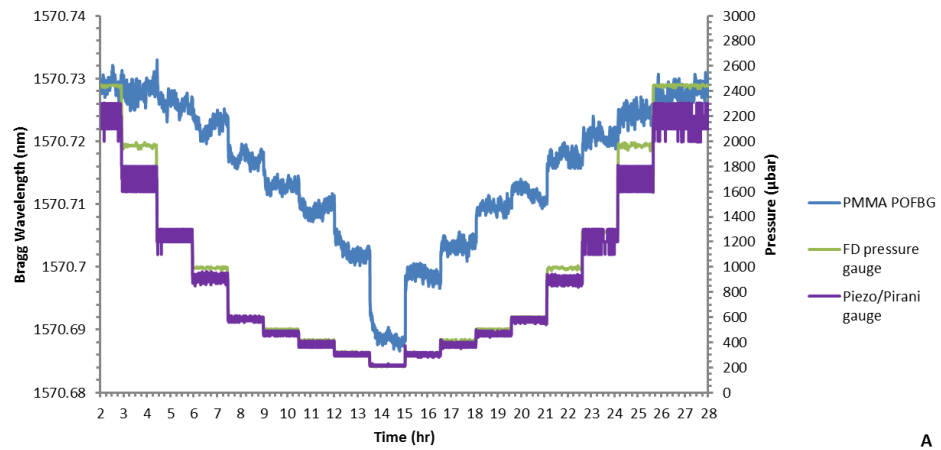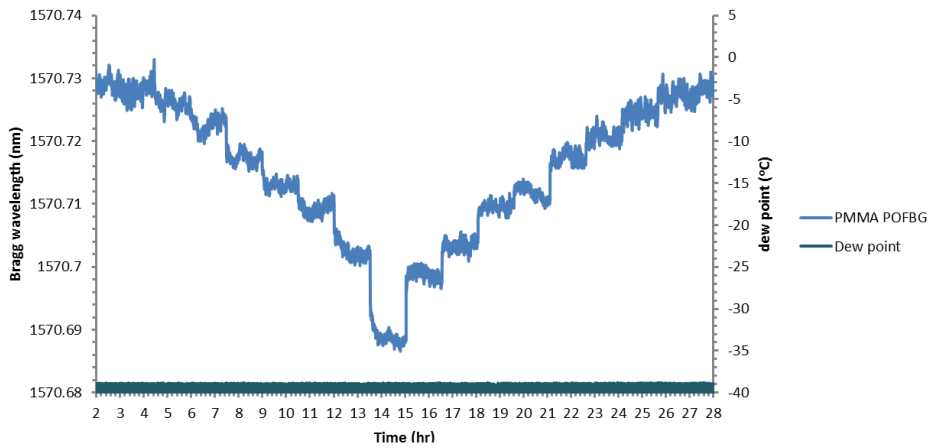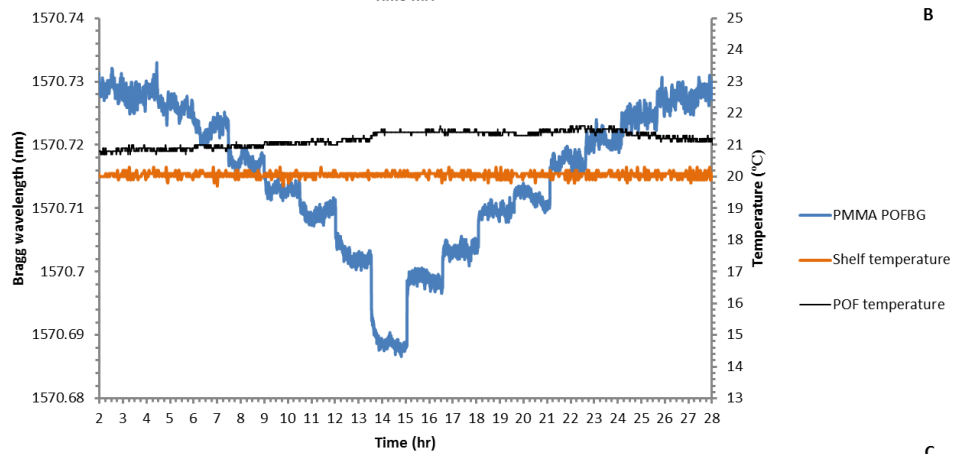
Figure 156 PMMA POFBG (POF4), where Bragg wavelength is plotted against (a) pressure in the chamber, (b) dew point in the chamber, (c) temperature of the shelf and thermocouple temperature in the region next to the POF sensors
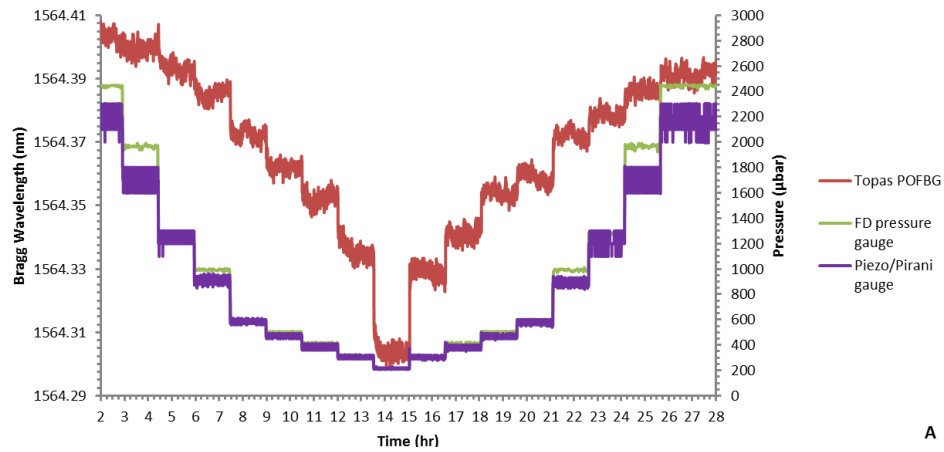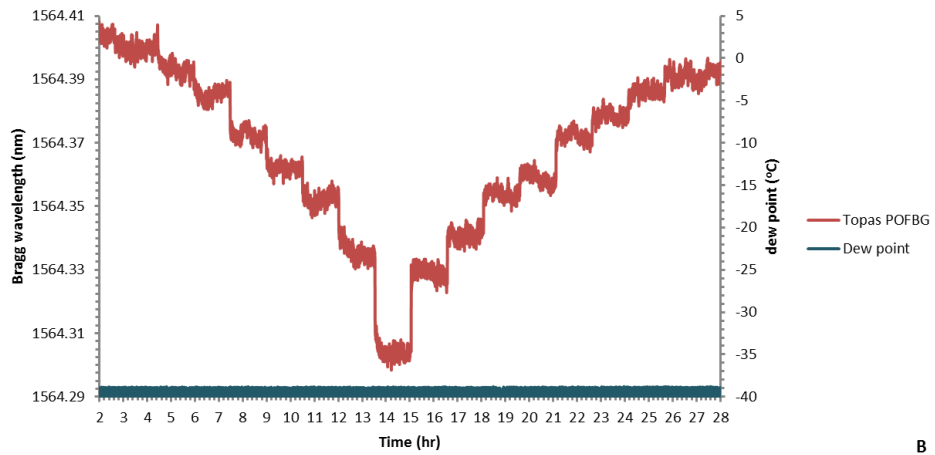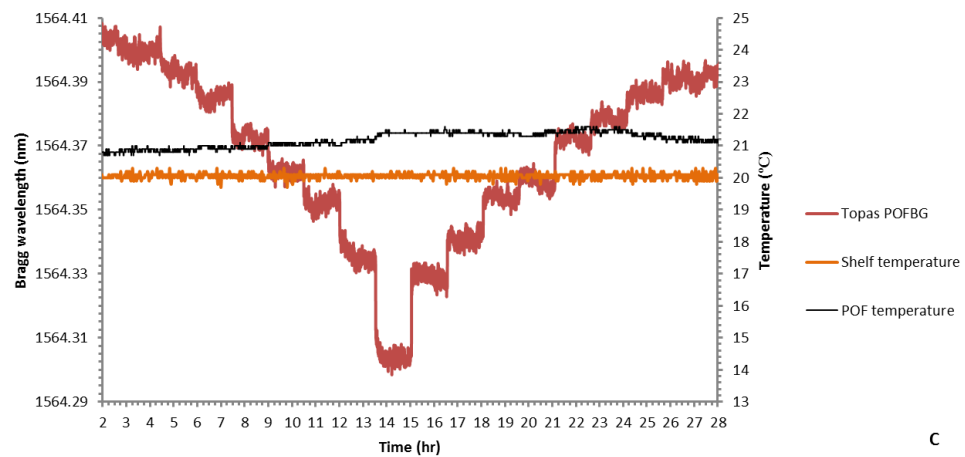
Figure 157 TOPAS POFBG (POF3), where Bragg wavelength is plotted against (a) pressure in the chamber, (b) dew point in the chamber, (c) temperature of the shelf and thermocouple temperature in the region next to the POF sensors
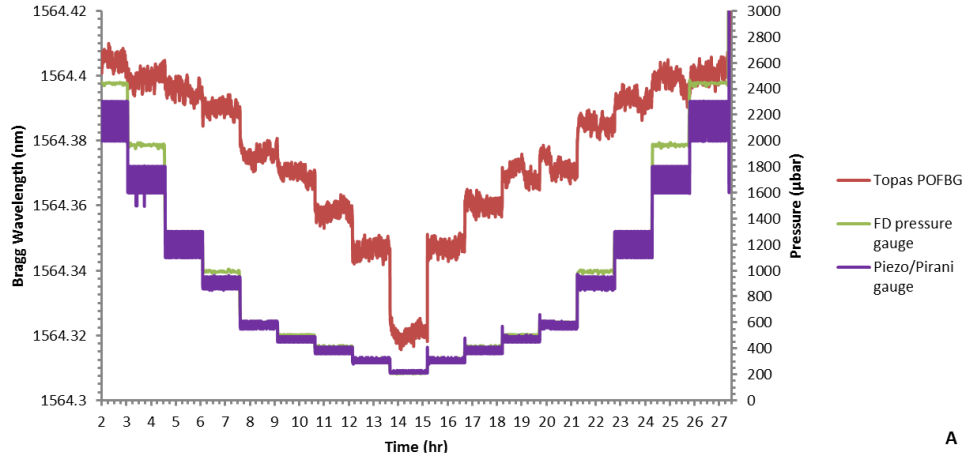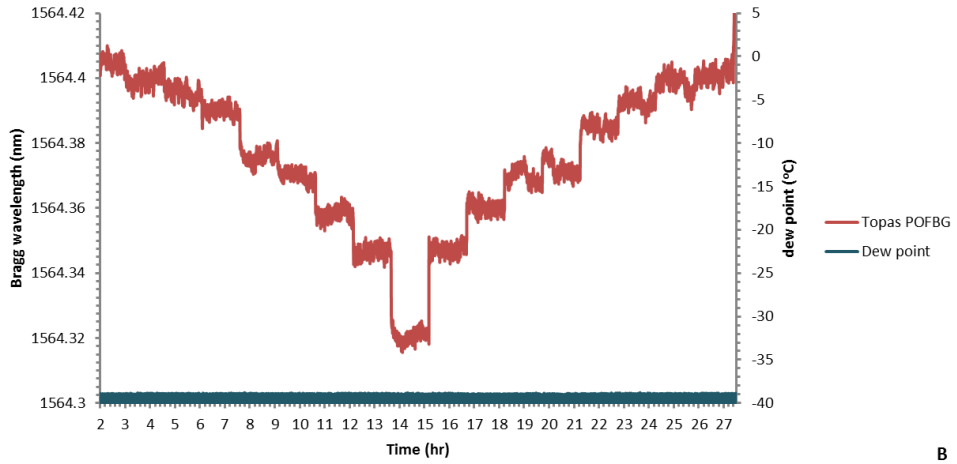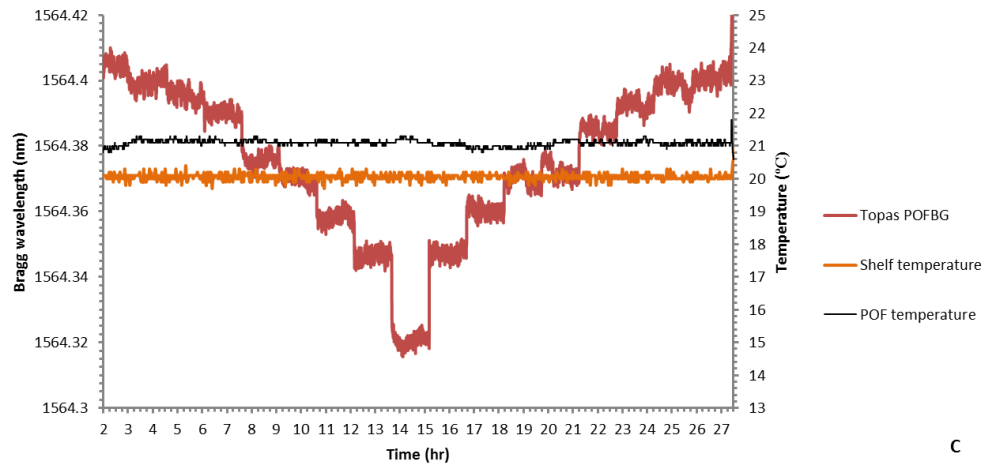
Figure 158 TOPAS POFBG (POF3), where Bragg wavelength is plotted against (a) pressure in the chamber, (b) dew point in the chamber, (c) temperature of the shelf and thermocouple temperature in the region next to the POF sensors
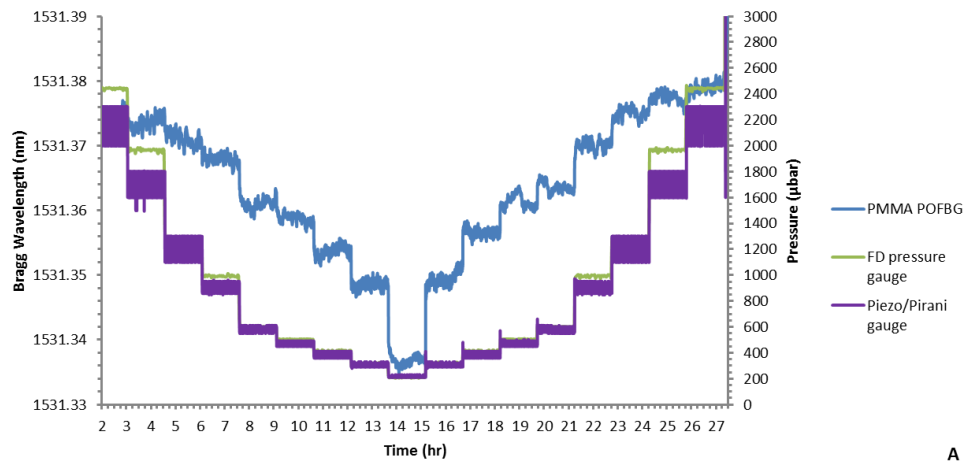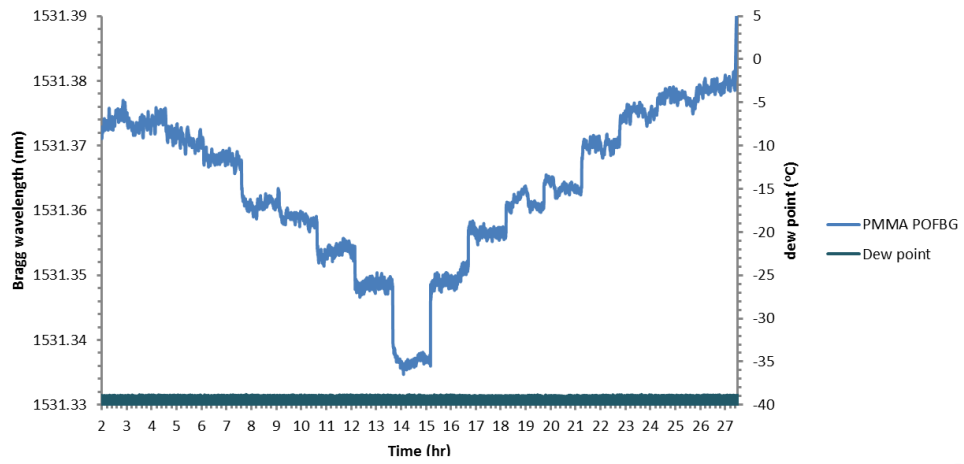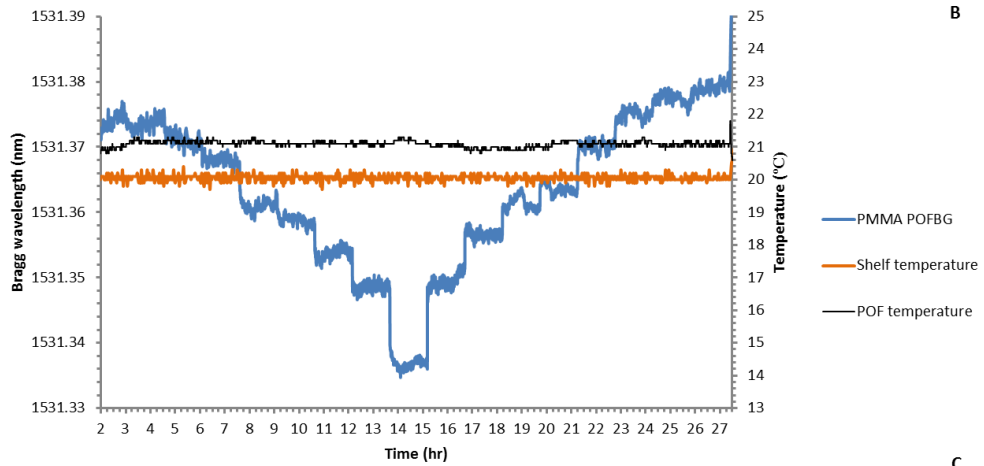
Figure 159 PMMA POFBG (POF5), where Bragg wavelength is plotted against (a) pressure in the chamber, (b) dew point in the chamber, (c) temperature of the shelf and thermocouple temperature in the region next to the POF sensors
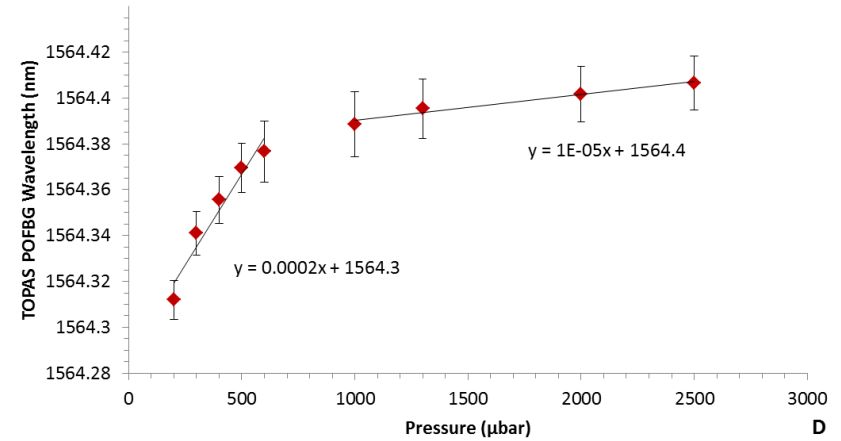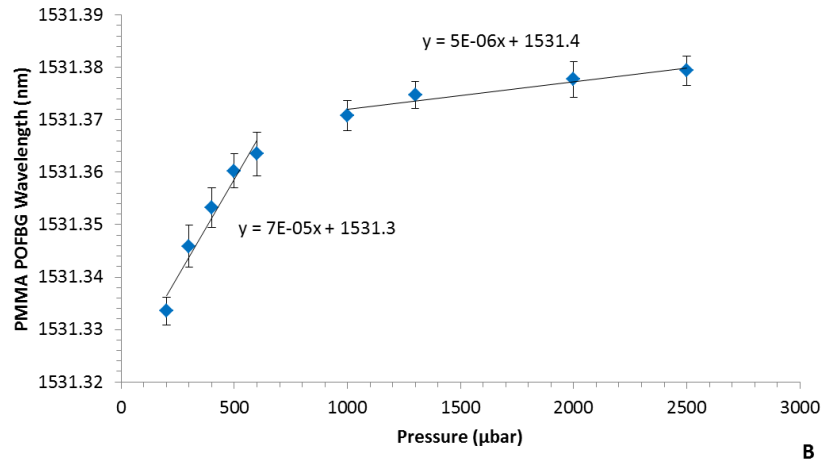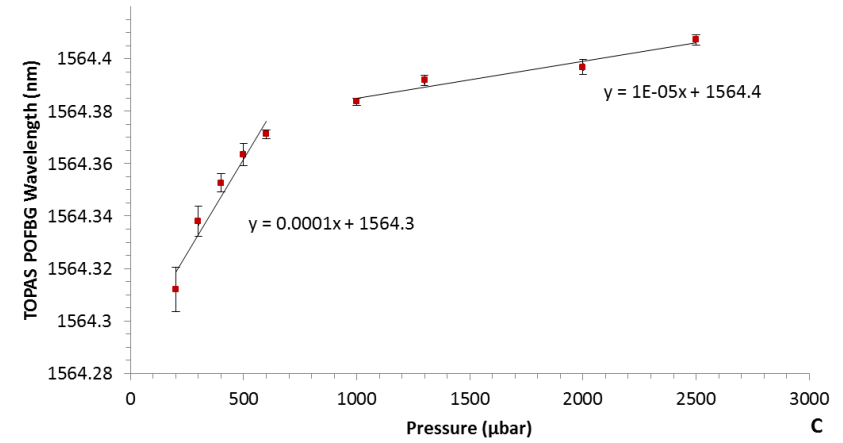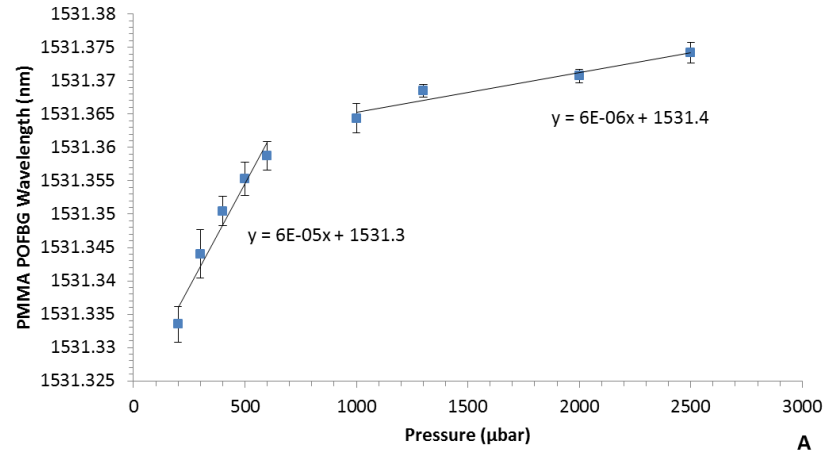
Figure 160 Bragg wavelength shift with respect to chamber pressure (n=3), where (A) the pressure was reduced from 2500μbar to 200μbar for PMMA POFBG (POF5), (b) the chamber pressure was increased from 200μbar to 2500μbar for PMMA POFBG (POF5), (c) the pressure was reduced from 2500μbar to 200μbar for TOPAS POFBG (POF3), (d) the chamber pressure was increased from 200μbar to 2500μbar for TOPAS POFBG (POF3)
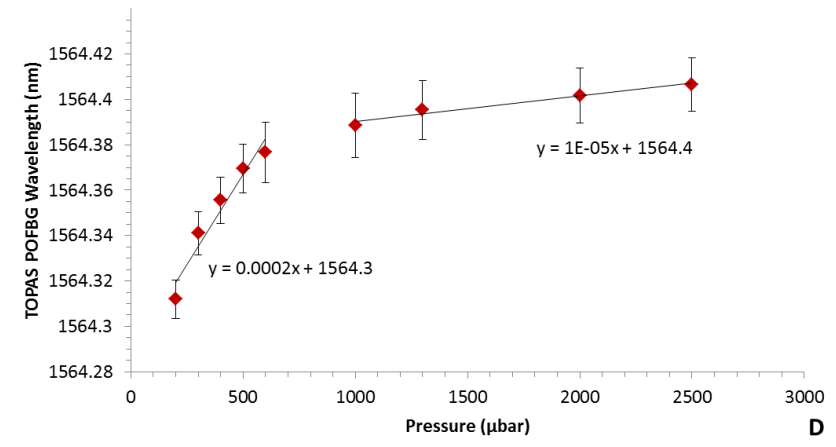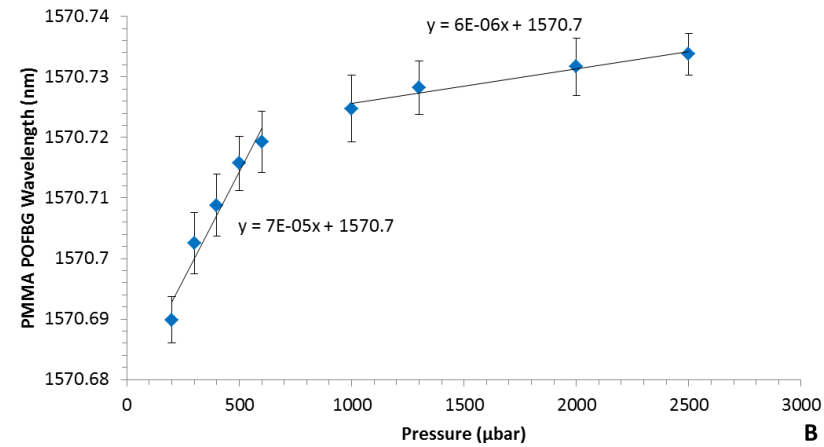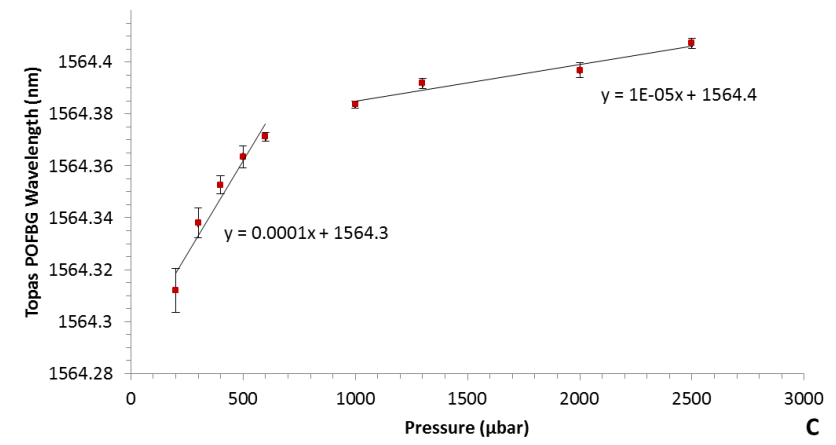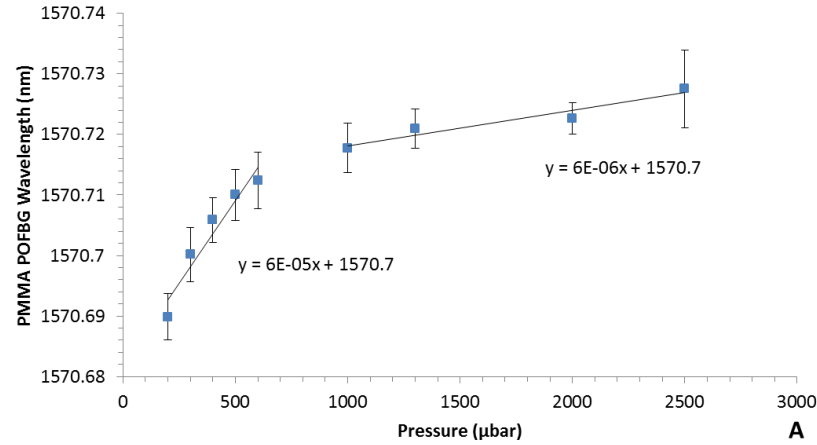
Figure 161 Bragg wavelength shift with respect to chamber pressure (n=3), where (A) the pressure was reduced from 2500µbar to 200µbar for PMMA POFBG (POF4), (b) the chamber pressure was increased from 200µbar to 2500µbar for PMMA POFBG (POF4), (c) the pressure was reduced from 2500µbar to 200µbar for TOPAS POFBG (POF3), (d) the chamber pressure was increased from 200µbar to 2500µbar for TOPAS POFBG (POF3)
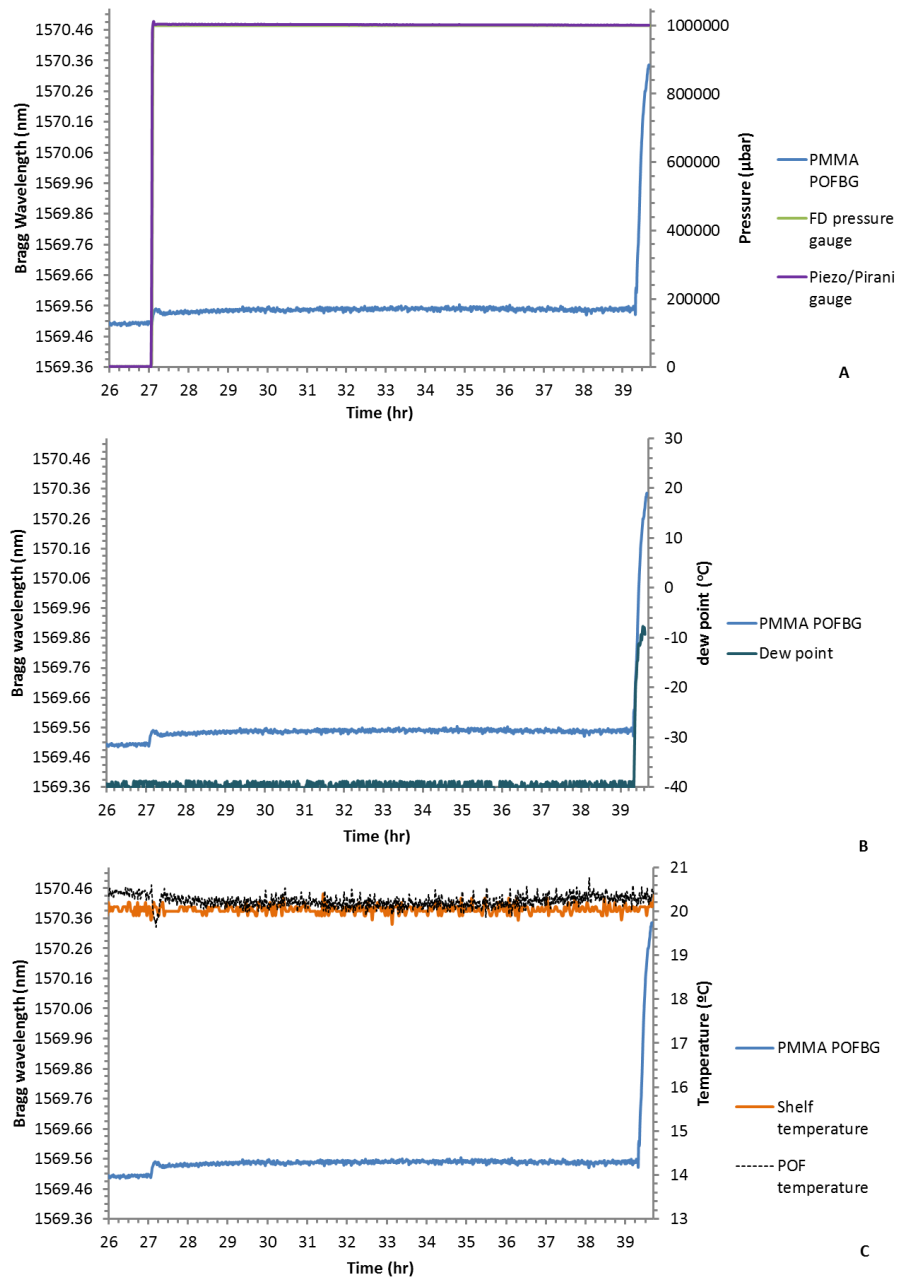
Figure 162 PMMA POFBG (POF 1) Bragg wavelength shift with respect to (a) changes in pressure, at 27hrs the vacuum is released to 1atmosphere and backfilled with dry nitrogen gas, (b) dew point. The dew point remains at -40ºC until 39.4hrs when the freeze dryer door was opened and allowed water vapour into the chamber, (c) temperature in the chamber. The shelf inlet temperature remains at 20ºC, and a drop in POF temperature is observed at 27hrs when the chamber was rapidly filled with nitrogen gas, causing a cooling effect.

Figure 163 TOPAS POFBG (POF 2) Bragg wavelength shift with respect to (a) changes in pressure, at 27hrs the vacuum is released to 1atmosphere and backfilled with dry nitrogen gas, (b) dew point. The dew point remains at -40°C until 39.4hrs when the freeze dryer door was opened and allowed water vapour into the chamber, (c) temperature in the chamber. The shelf inlet temperature remains at 20°C, and a drop in POF temperature is observed at 27hrs when the chamber was rapidly filled with nitrogen gas, causing a cooling effect.
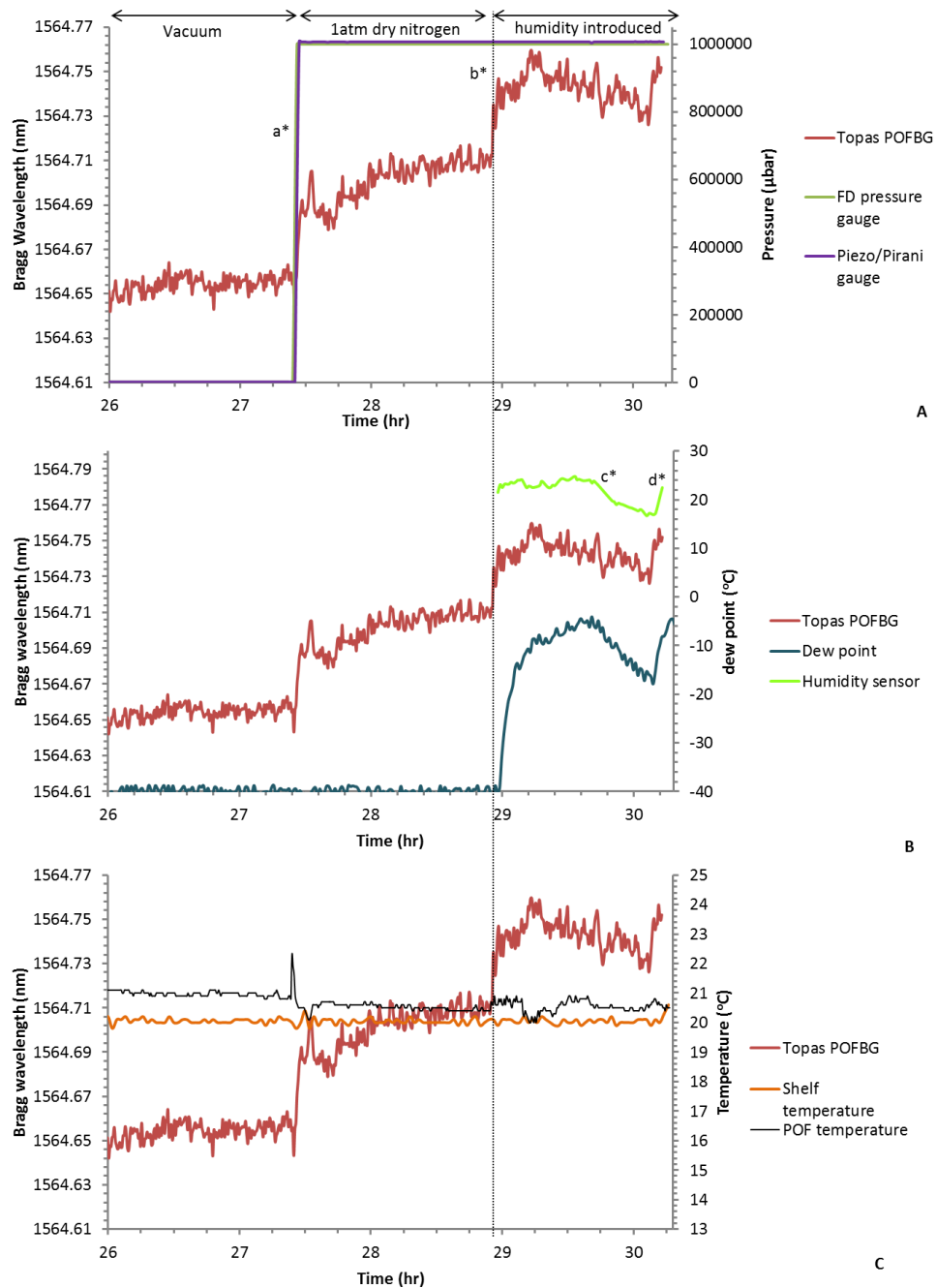
Figure 164 TOPAS POFBG (POF 2) Bragg wavelength shift with respect to (a) changes in pressure, at 27.4 hrs the vacuum is released to 1atmosphere and backfilled with dry nitrogen gas, (b) dew point. The dew point remains at -40ºC until 29hrs when the freeze dryer door was opened and allowed water vapour into the chamber, at 29.6hrs the door was closed and the humidity and dew point decreased (c) temperature in the chamber. The shelf inlet temperature remains at 20ºC, and a drift in the thermocouple temperature is observed.
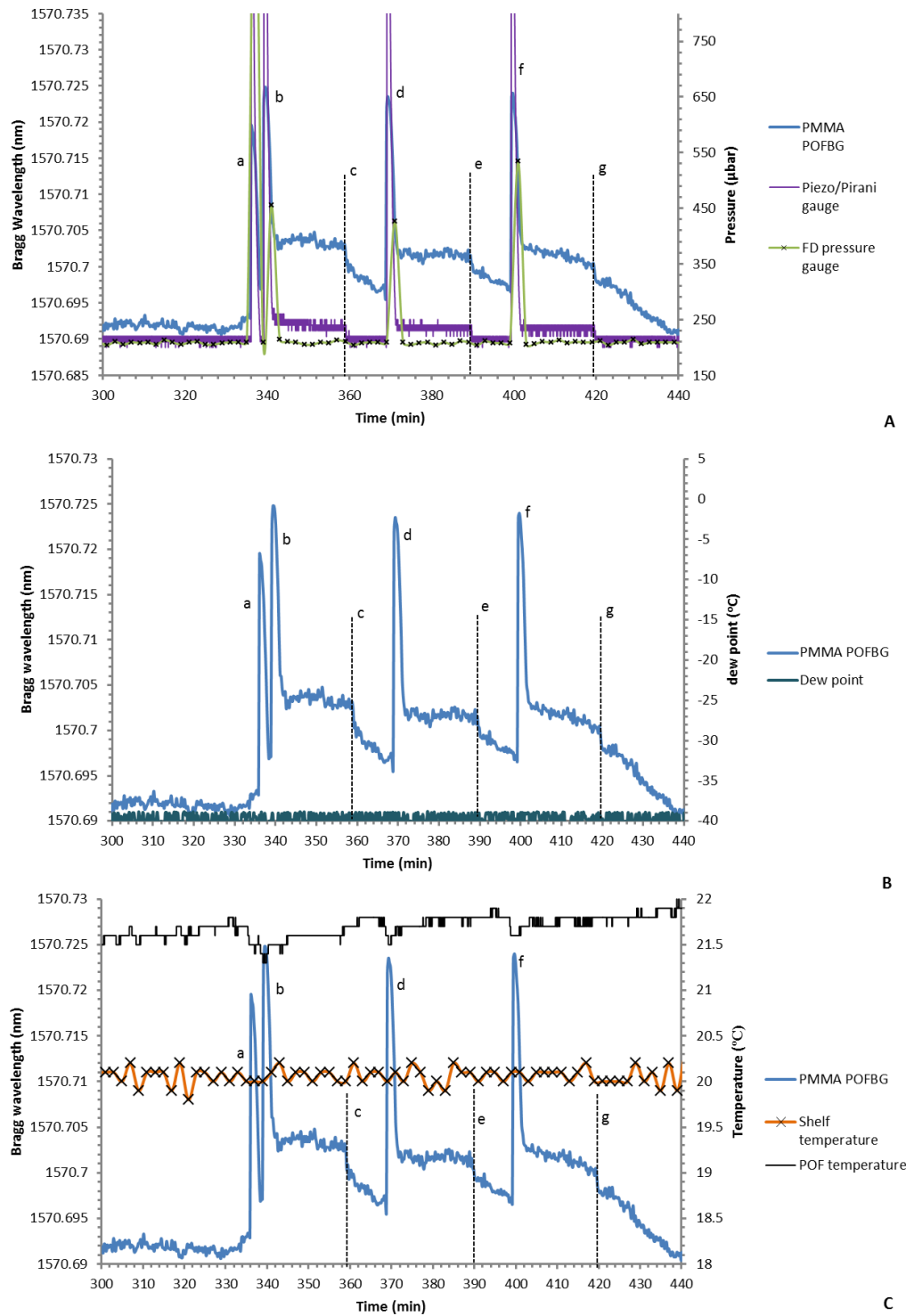
Figure 165 PMMA POFBG (POF 4) wavelength response to sublimation of water vapour from a 10ml mannitol 10%w/v sample (frozen in a -21°C freezer) and attached to the access port of the chamber. Bragg wavelength response with respect to (A) pressure, (B) dew point, (C) temperature, where (a) Valve opened, vial containing no sample, (b) valve opened, mannitol mass: 7.16g, (c) valve closed, mannitol mass: 6.47g, (d) valve opened, mannitol mass: 6.47g, (e) valve closed, mannitol mass: 5.99g, (f) valve opened, mannitol mass: 5.99g, (g) valve closed, mannitol mass: 5.56g
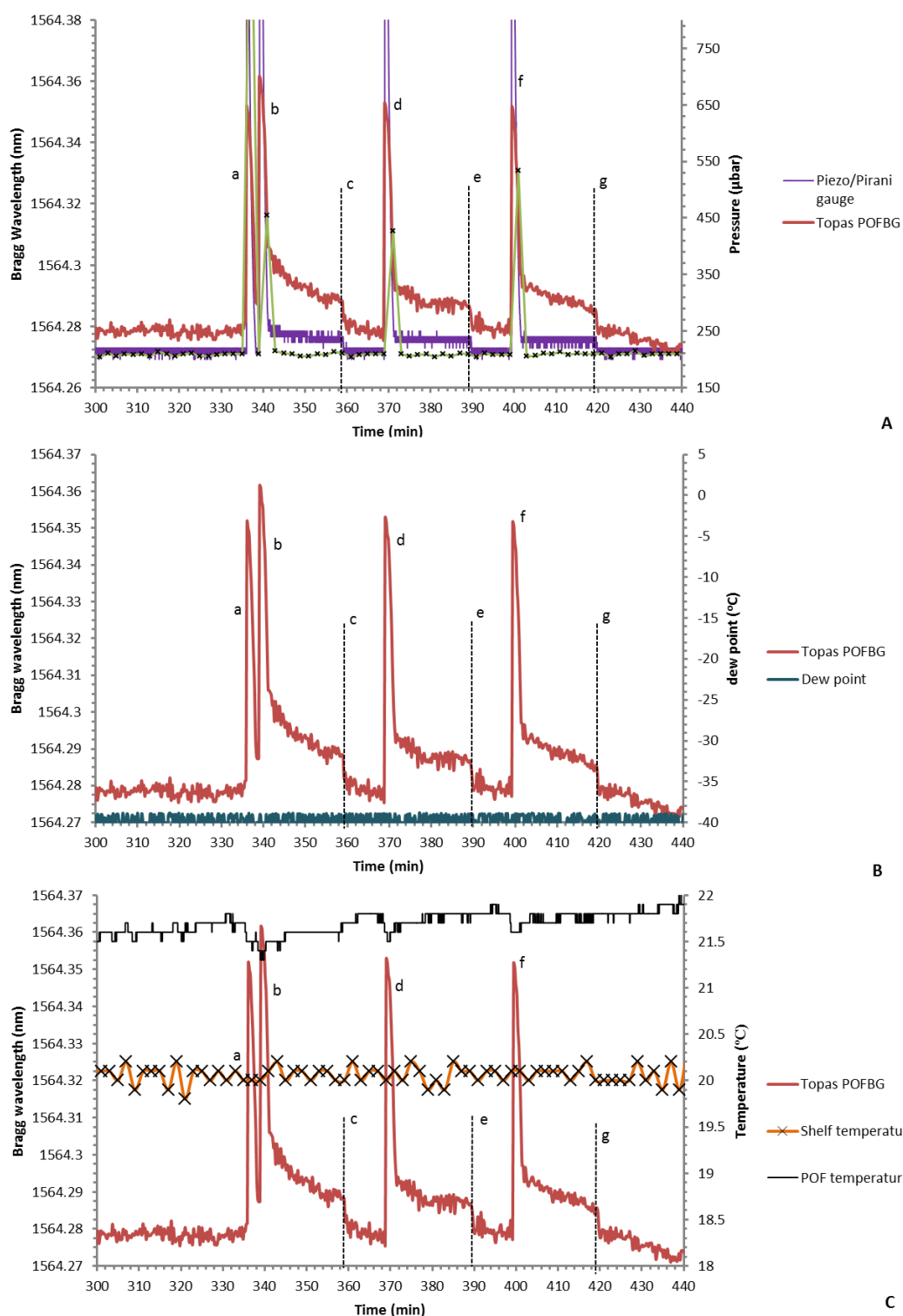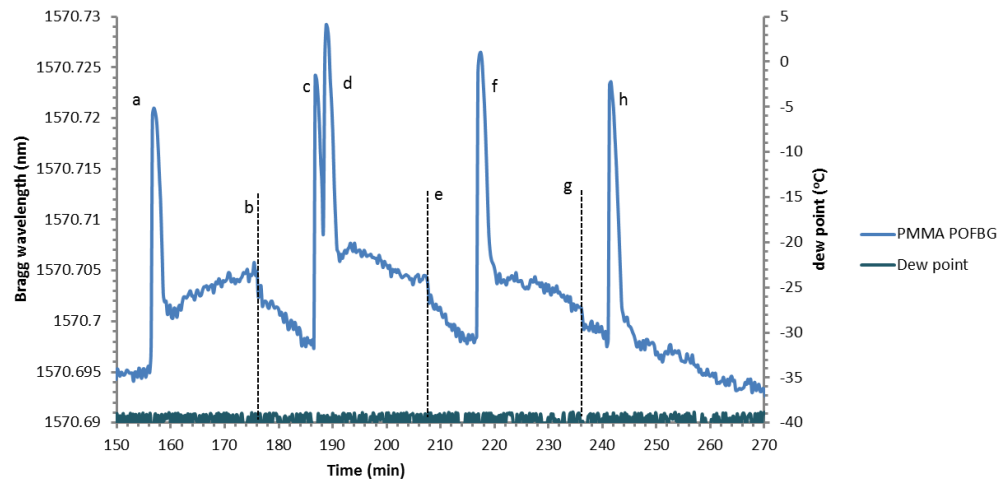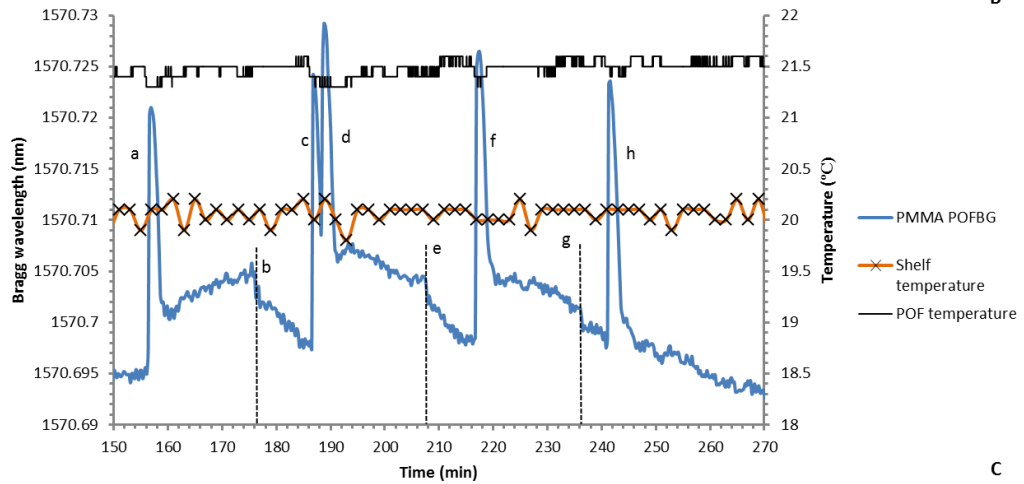
Figure 166 TOPAS POFBG (POF 3) wavelength response to sublimation of water vapour from a 10ml mannitol 10%w/v sample (frozen in a -21ºC freezer) and attached to the access port of the chamber. Bragg wavelength response with respect to (A) pressure, (B) dew point, (C) temperature, where (a) Valve opened, vial containing no sample, (b) valve opened, mannitol mass: 7.16g, (c) valve closed, mannitol mass: 6.47g, (d) valve opened, mannitol mass: 6.47g, (e) valve closed, mannitol mass: 5.99g, (f) valve opened, mannitol mass: 5.99g, (g) valve closed, mannitol mass: 5.56g
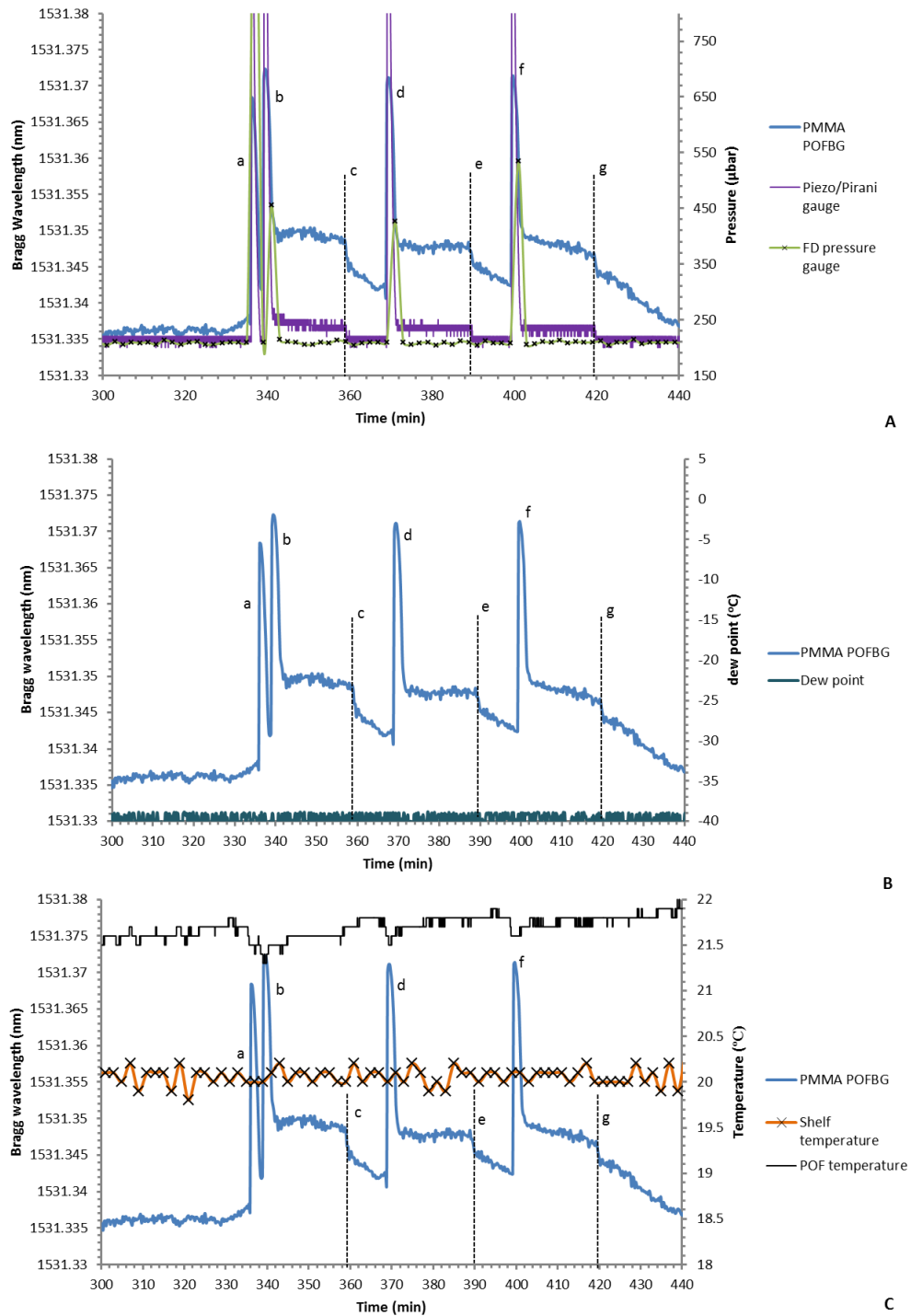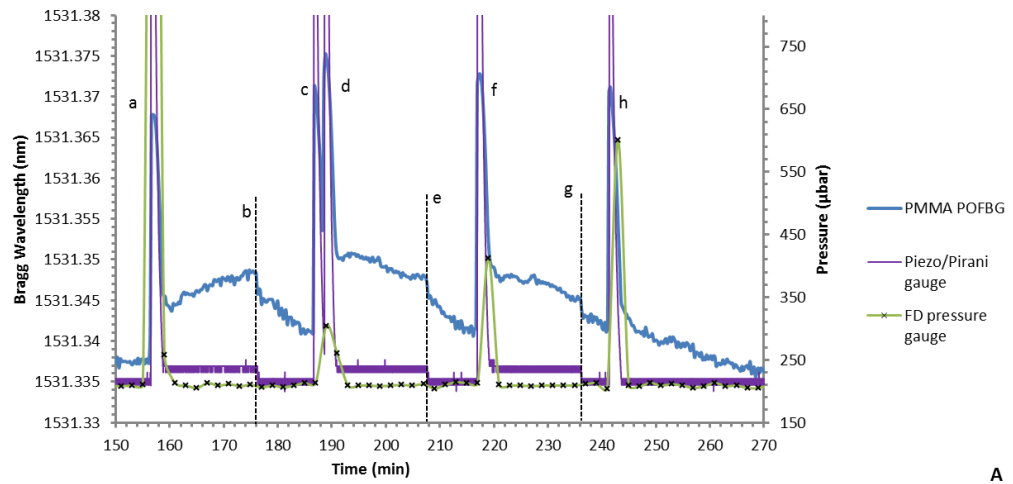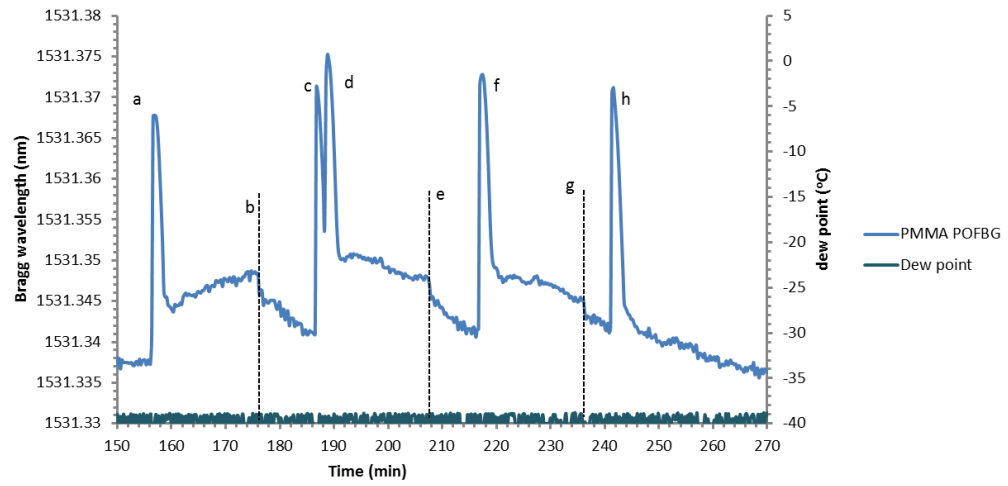
Figure 167 PMMA POFBG (POF 5) wavelength response to sublimation of water vapour from a 10ml mannitol 10%w/v sample (frozen in a -21°C freezer) and attached to the access port of the chamber. Bragg wavelength response with respect to (A) pressure, (B) dew point, (C) temperature, where (a) Valve opened, vial containing no sample, (b) valve opened, mannitol mass: 7.16g, (c) valve closed, mannitol mass: 6.47g, (d) valve opened, mannitol mass: 6.47g, (e) valve closed, mannitol mass: 5.99g, (f) valve opened, mannitol mass: 5.99g, (g) valve closed, mannitol mass: 5.56g
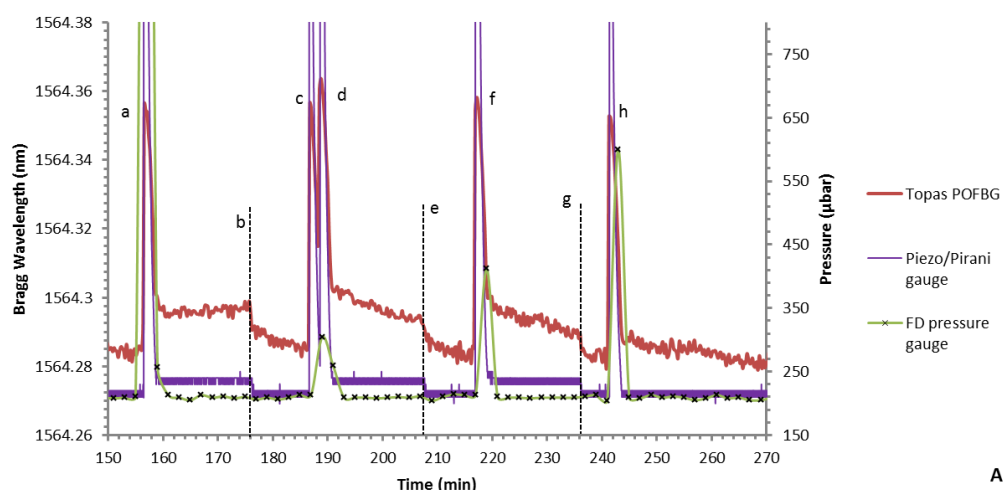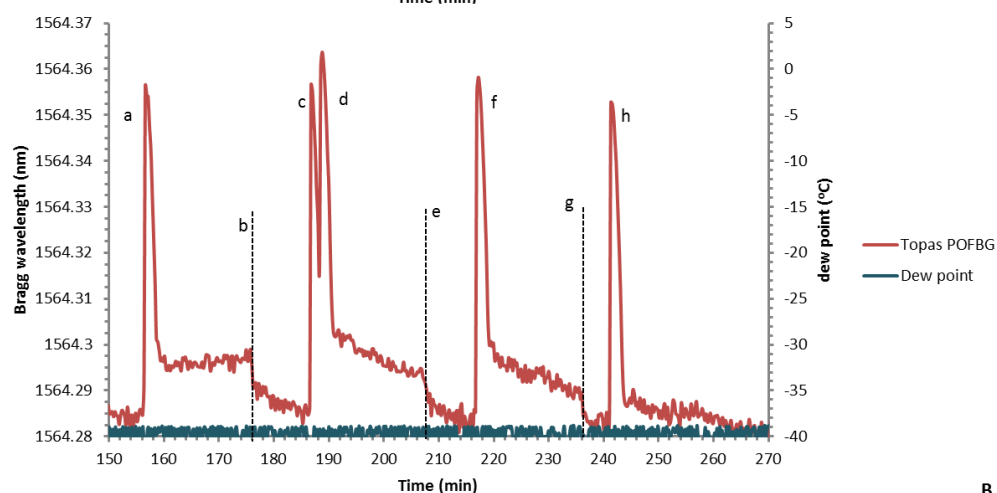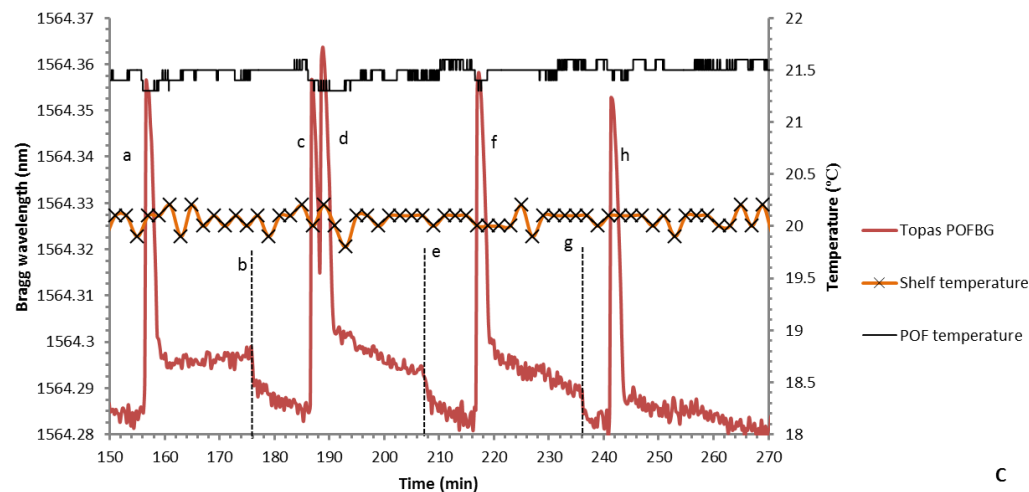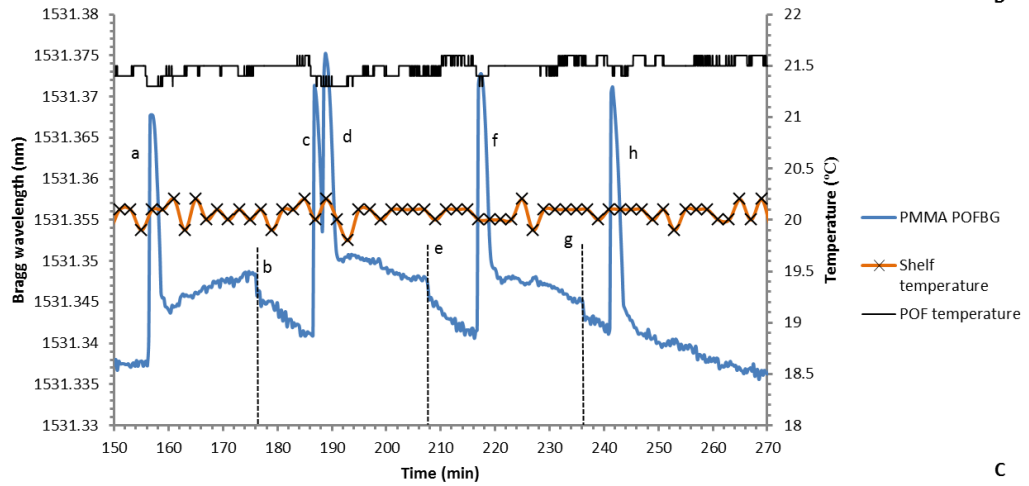
Figure 168 TOPAS POFBG (POF 3) wavelength response to sublimation of water vapour from distilled water sample (frozen in a -21°C freezer) and attached to the access port of the chamber. Bragg wavelength response with respect to (A) pressure, (B) dew point, (C) temperature, where (a) valve opened, ice mass: 2.683g, (b) valve closed, ice mass: 2.241g, (c) Valve opened, vial containing no sample, (d) valve opened, ice mass: 2.241g, (e) valve closed, ice mass: 1.758g, (f) valve opened, ice mass: 1.758g, (g) valve closed, ice mass: 1.341g, (h) Valve opened, vial containing no sample
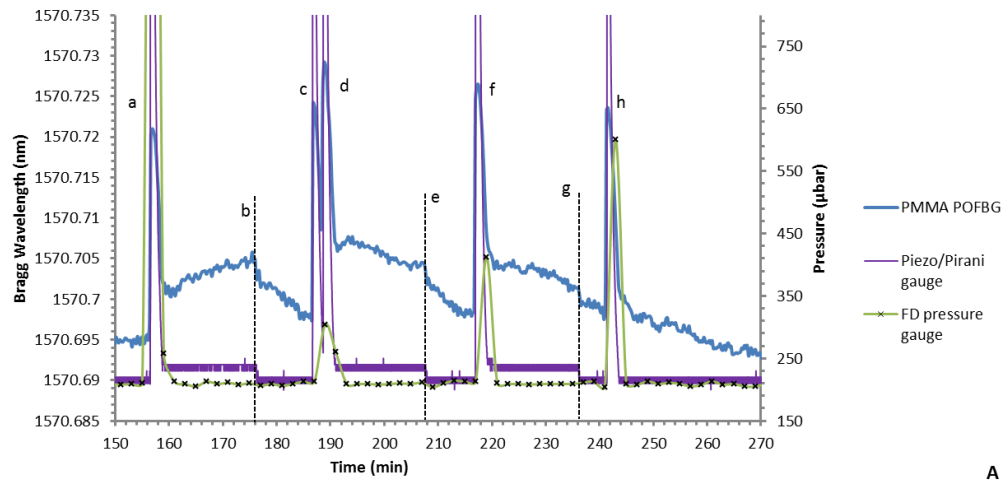
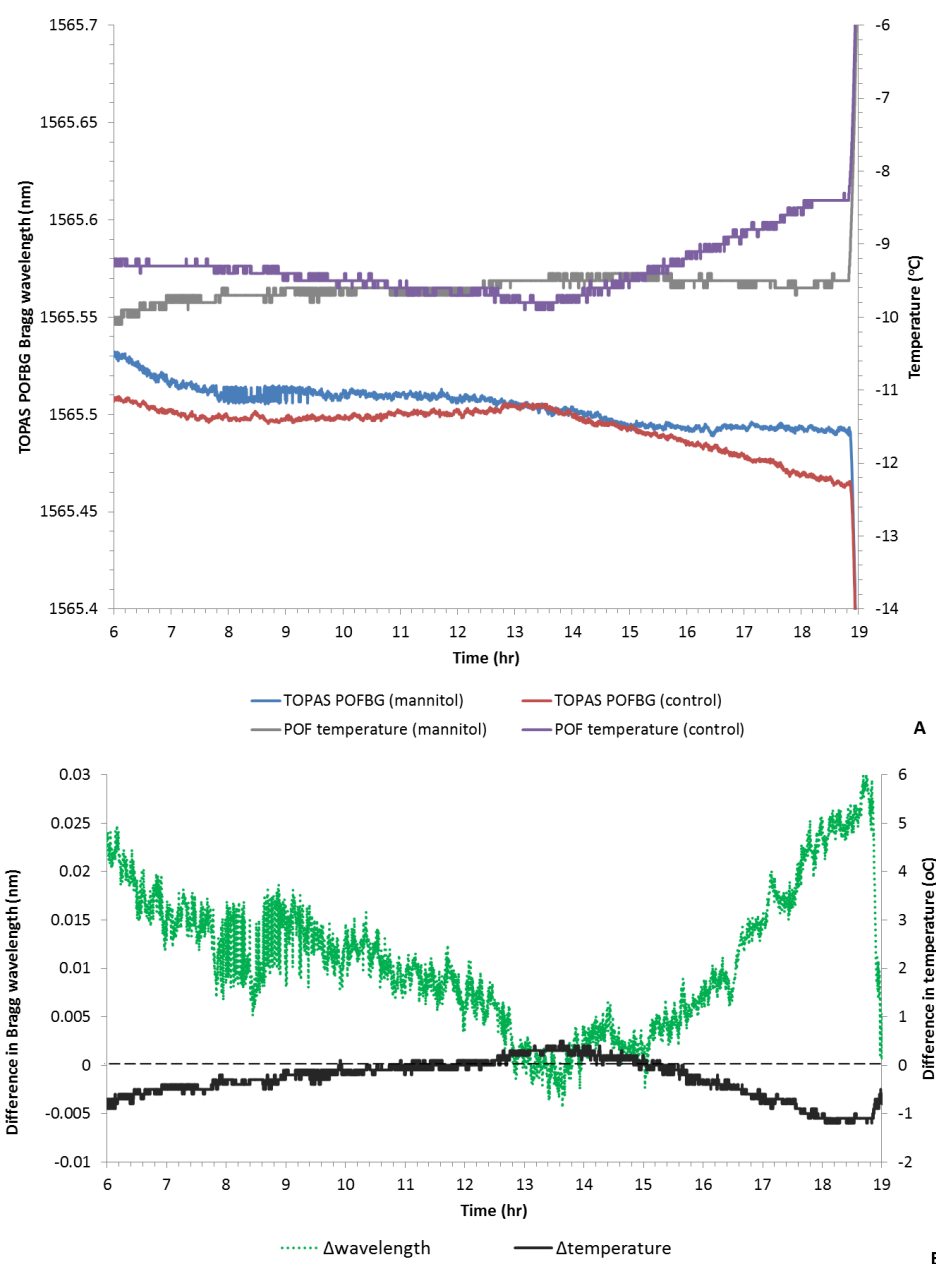*Figure 169 PMMA POFBG (POF 4) wavelength response to sublimation of water vapour from distilled water sample (frozen in a -21°C freezer) and attached to the access port of the chamber. Bragg wavelength response with respect to (A) pressure, (B) dew point, (C) temperature, where (a) valve opened, ice mass: 2.683g, (b) valve closed, ice mass: 2.241g, (c) Valve opened, vial containing no sample, (d) valve opened, ice mass: 2.241g, (e) valve closed, ice mass: 1.758g, (f) valve opened, ice mass: 1.758g, (g) valve closed, ice mass: 1.341g, (h) Valve opened, vial containing no sample*

Figure 170 PMMA POFBG (POF 5) wavelength response to sublimation of water vapour from distilled water sample (frozen in a -21°C freezer) and attached to the access port of the chamber. Bragg wavelength response with respect to (A) pressure, (B) dew point, (C) temperature, where (a) valve opened, ice mass: 2.683g, (b) valve closed, ice mass: 2.241g, (c) Valve opened, vial containing no sample, (d) valve opened, ice mass: 2.241g, (e) valve closed, ice mass: 1.758g, (f) valve opened, ice mass: 1.758g, (g) valve closed, ice mass: 1.341g, (h) Valve opened, vial containing no sample

Figure 171 TOPAS POFBG (POF3) monitoring the primary drying stage of 10%w/v mannitol solutions. (A) Bragg wavelength response to a control cycle with a dry nitrogen atmosphere (no samples) and a cycle exposed to water vapour from 3 mannitol samples. (B) Graph showing the differences between the Bragg wavelength and temperature of the two cycles (control and water vapour).
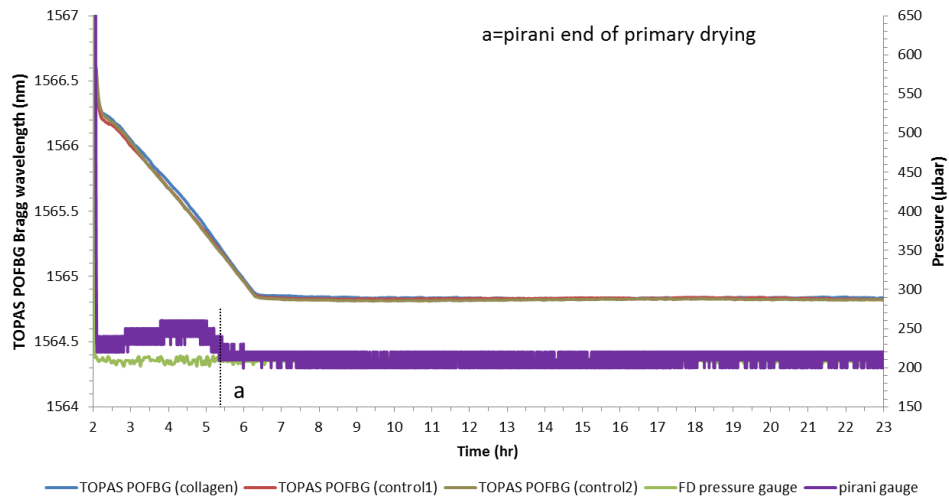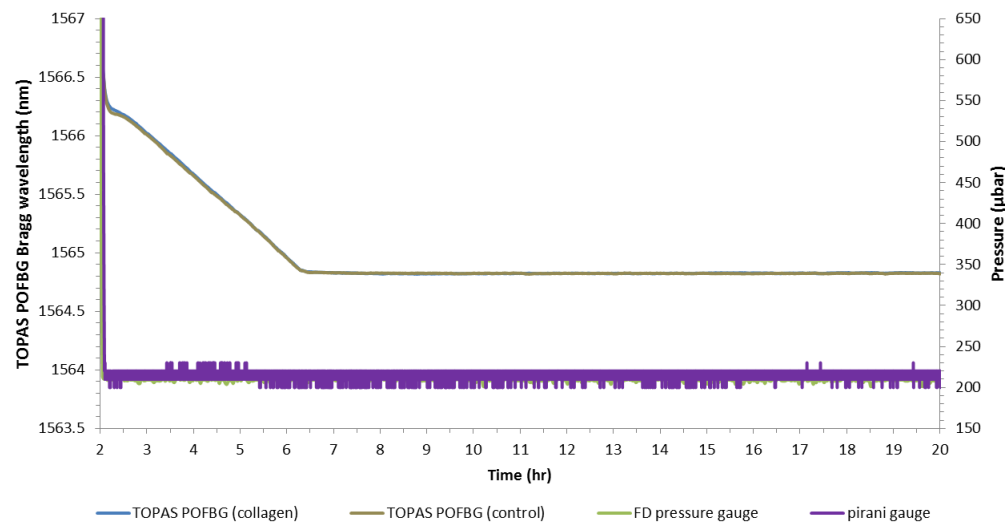
Figure 172 Pirani gauge and TOPAS POFBG (POF3) sensor monitoring primary drying of 7 collagen samples. The TOPAS POFBG profile was compared against two control cycles (in a dry nitrogen atmosphere). The end of primary drying time has been detected at (a) by the Pirani gauge.
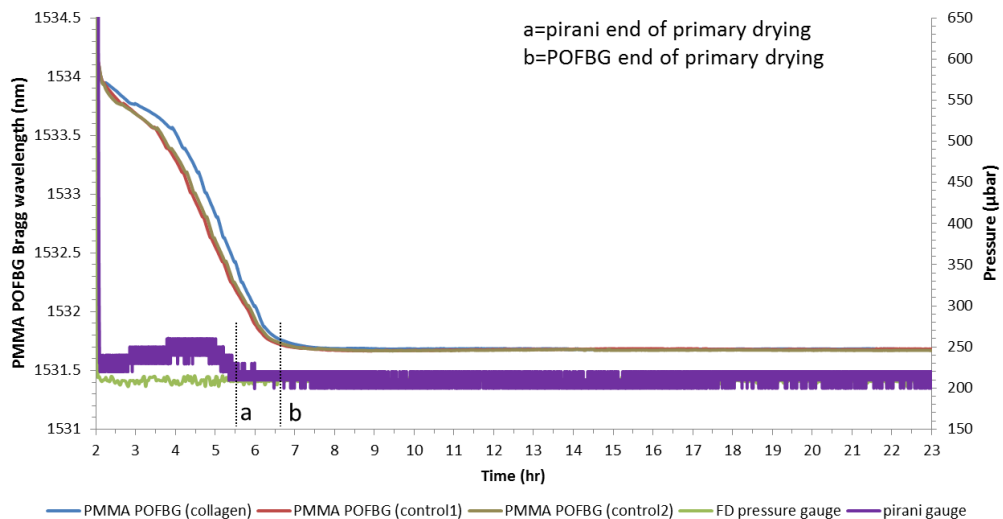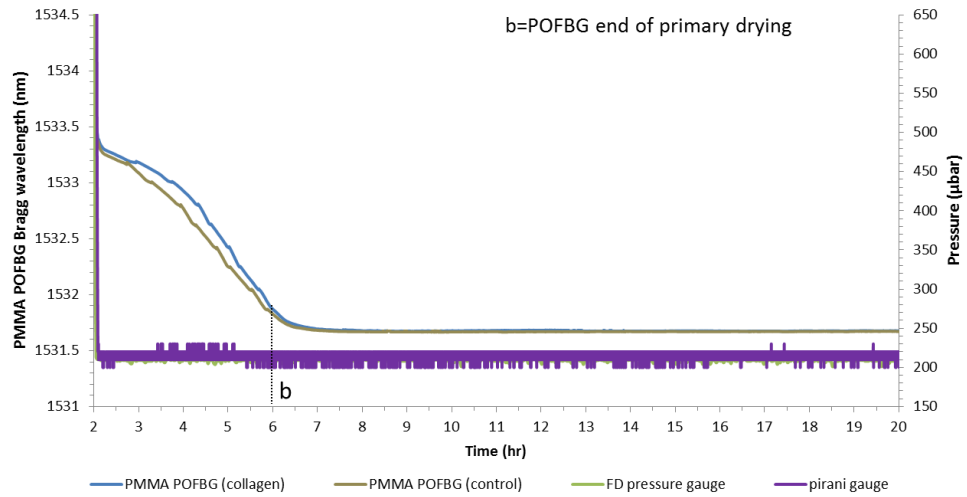

Figure 173 Pirani gauge and PMMA POFBG (POF5) sensor monitoring primary drying of 7 collagen samples. The PMMA POFBG profile was compared against two control cycles (in a dry nitrogen atmosphere) to determine the end of primary drying time. The end of primary drying time has been detected at (a) by the Pirani gauge and (b) by PMMA POFBG.
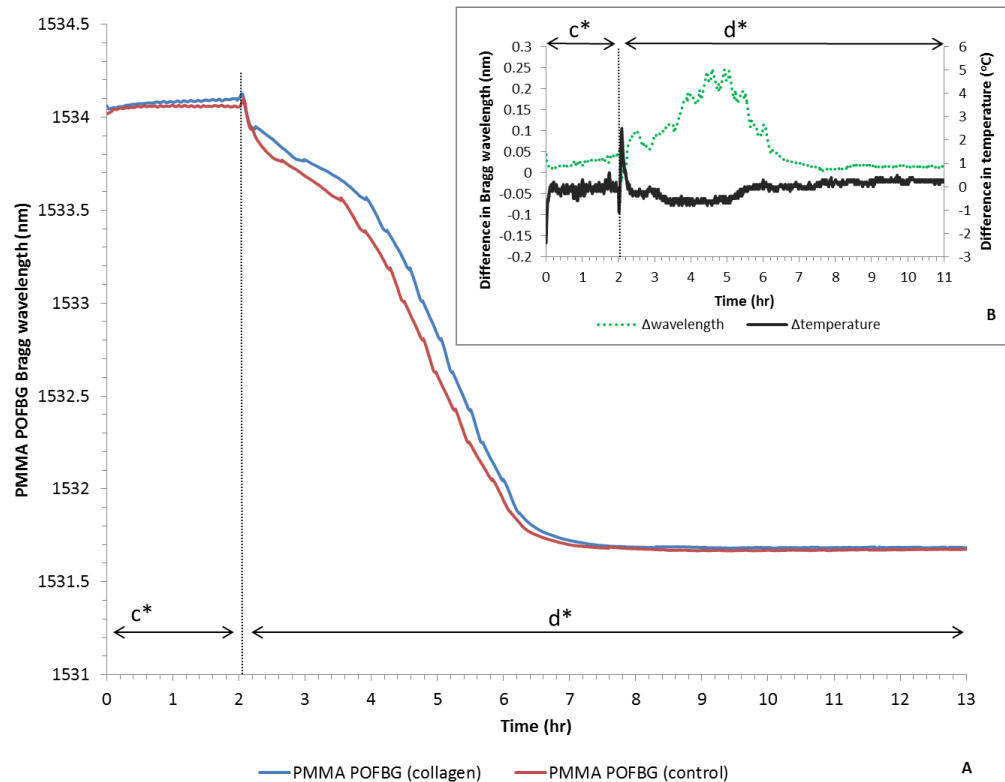
Figure 174 PMMA POFBG sensor (POF5) monitoring the freezing stage (c*) and primary drying stage (d*) of the programmed freeze drying cycle. (A) Bragg wavelength response to a control cycle with a dry nitrogen atmosphere (no samples) and a cycle exposed to water vapour from 7 freeze drying collagen samples. (B) Graph showing the differences between the Bragg wavelength and temperature of the two cycles (control and water vapour).
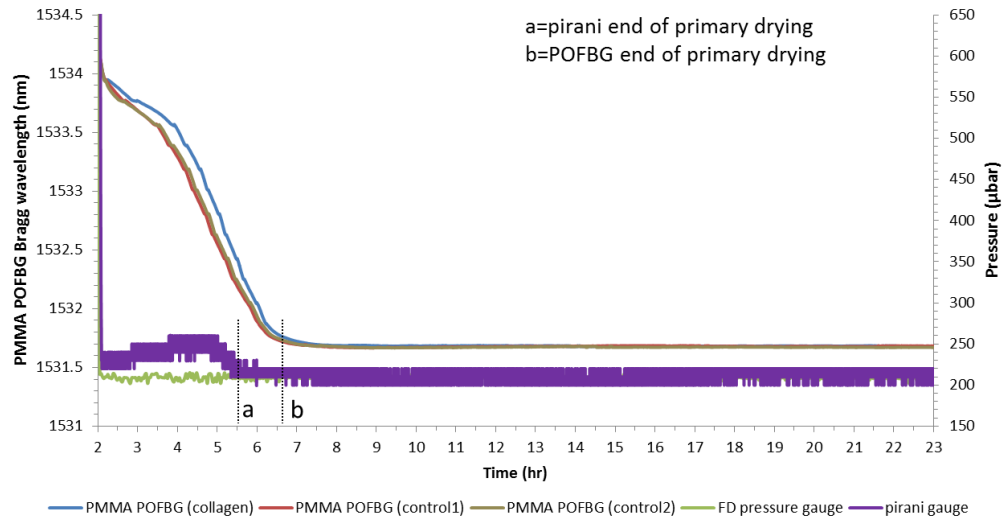

Figure 175 Pirani gauge and TOPAS POFBG (POF3) sensor monitoring primary drying of 1 collagen sample (2ml) in a well. The PMMA POFBG profile was compared against a control cycle (in a dry nitrogen atmosphere) to determine the end of primary drying time. The end of primary drying time has been detected at (b) by PMMA POFBG.
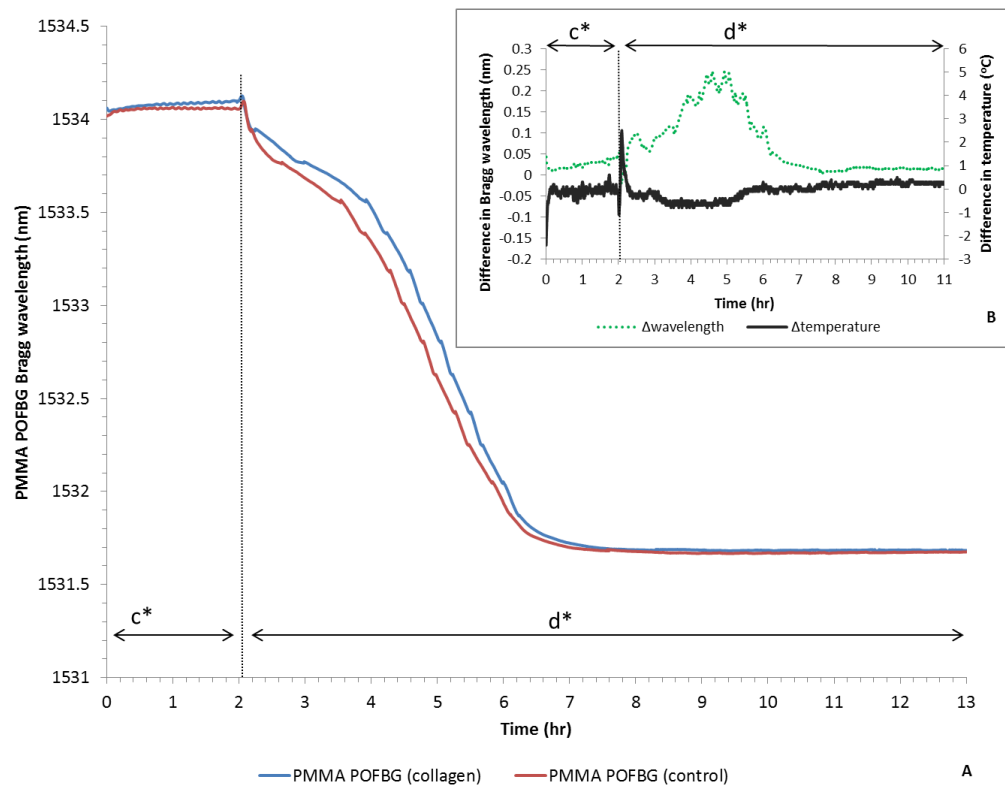
Figure 176 Pirani gauge and PMMA POFBG (POF5) sensor monitoring primary drying of 1 collagen sample (2ml) in a well. The PMMA POFBG profile was compared against a control cycle (in a dry nitrogen atmosphere) to determine the end of primary drying time. The end of primary drying time has been detected at (b) by PMMA POFBG.
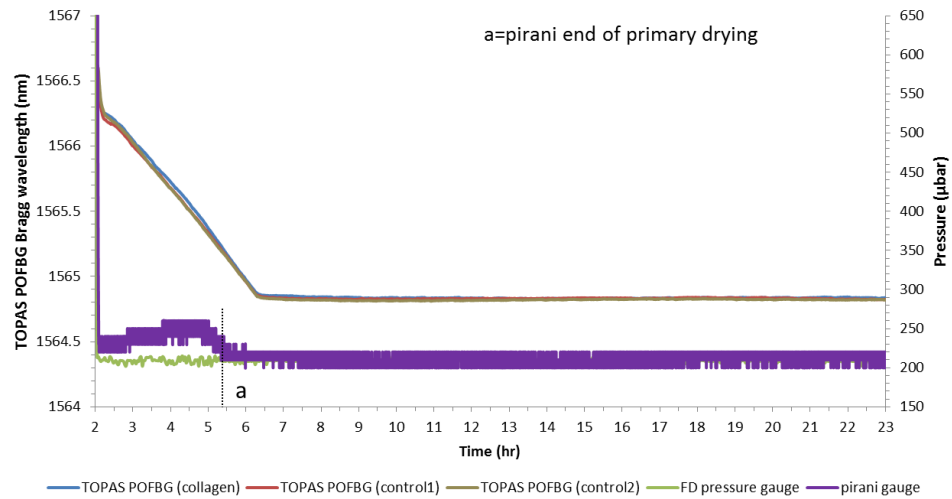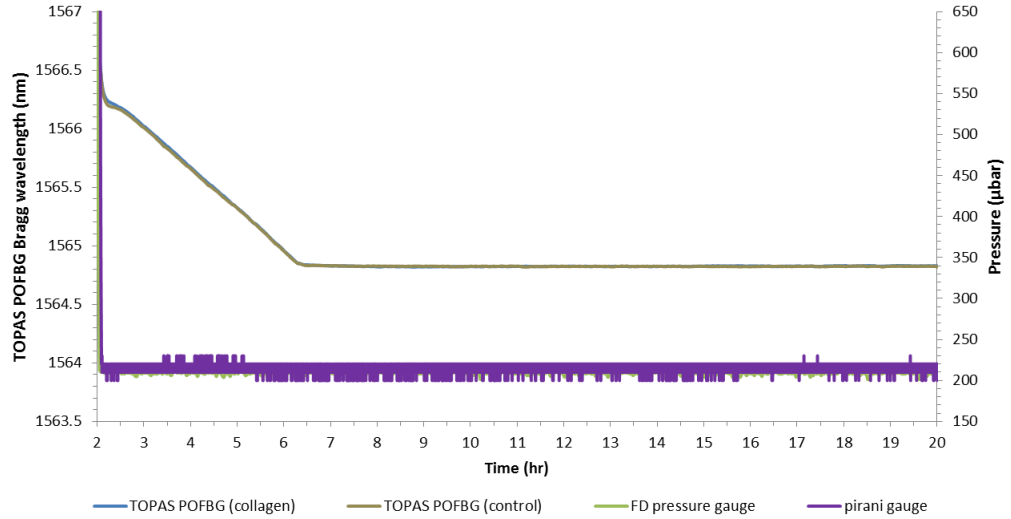

Figure 177 Pirani gauge and TOPAS POFBG (POF3) sensor monitoring primary drying of 7 collagen samples. The TOPAS POFBG profile was compared against two control cycles (in a dry nitrogen atmosphere). The end of primary drying time has been detected at (a) by the Pirani gauge.
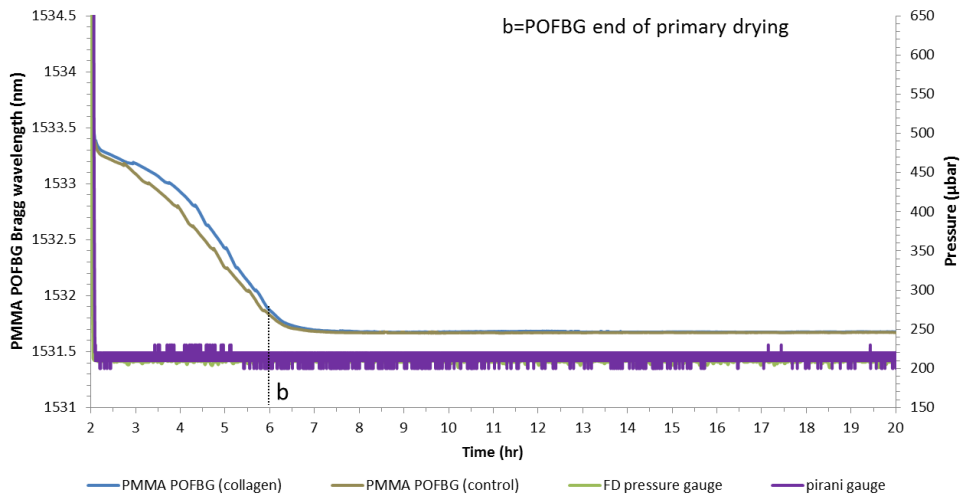
Figure 178 Pirani gauge and PMMA POFBG (POF5) sensor monitoring primary drying of 7 collagen samples. The PMMA POFBG profile was compared against two control cycles (in a dry nitrogen atmosphere) to determine the end of primary drying time. The end of primary drying time has been detected at (a) by the Pirani gauge and (b) by PMMA POFBG.

Figure 179 PMMA POFBG sensor (POF5) monitoring the freezing stage (c*) and primary drying stage (d*) of the programmed freeze drying cycle. (A) Bragg wavelength response to a control cycle with a dry nitrogen atmosphere (no samples) and a cycle exposed to water vapour from 7 freeze drying collagen samples. (B) Graph showing the differences between the Bragg wavelength and temperature of the two cycles (control and water vapour).

Figure 180 Pirani gauge and TOPAS POFBG (POF3) sensor monitoring primary drying of 1 collagen sample (2ml) in a well. The PMMA POFBG profile was compared against a control cycle (in a dry nitrogen atmosphere) to determine the end of primary drying time. The end of primary drying time has been detected at (b) by PMMA POFBG.

Figure 181 Pirani gauge and PMMA POFBG (POF5) sensor monitoring primary drying of 1 collagen sample (2ml) in a well. The PMMA POFBG profile was compared against a control cycle (in a dry nitrogen atmosphere) to determine the end of primary drying time. The end of primary drying time has been detected at (b) by PMMA POFBG.